KU LEUVEN

ARENBERG DOCTORAL SCHOOL
Faculty of Engineering Science

Impact of energy and climate policies on electricity generation

Analysis based on large-scale unit commitment modeling

Kenneth Van den Bergh

Prof. William D'haeseleer, supervisor
Prof. Erik Delarue, co-supervisor

Dissertation presented in partial fulfillment
of the requirements for the degree of
Doctor of Engineering Science (PhD):
Mechanical Engineering

July 2016

Impact of energy and climate policies on electricity generation

Analysis based on large-scale unit commitment modeling

Kenneth VAN DEN BERGH

Examination committee:
Prof. Adhemar Bultheel, chair
Prof. William D'haeseleer, supervisor
Prof. Erik Delarue, co-supervisor
Prof. Geert Deconinck
Prof. Dirk Van Hertem
Prof. Benjamin F. Hobbs
(The Johns Hopkins University, USA)
Prof. Hannes Weigt
(Universität Basel, Switzerland)
Dr. Cindy Bastiaensen
(Elia System Operator, Belgium)

Dissertation presented in partial fulfillment of the requirements for the degree of Doctor of Engineering Science (PhD): Mechanical Engineering

July 2016

Dankwoord

Writing a PhD dissertation is something you do alone (otherwise it is being called plagiarism). Getting a PhD, however, is something you do with the support and help of various people. I would like to take some time to thank these people.

Allereerst zou ik mijn promotoren William en Erik van harte willen bedanken voor de afgelopen vijf jaren, waarvan een jaar als masterthesisstudent (toen ik nog prof. D'haeseleer en prof. Delarue moest zeggen) en vier jaren als doctoraatsstudent. In het leven is het belangrijk om mentors te hebben, zeker als je nog zo onervaren bent als ondergetekende. Mentors zijn mensen naar wie je kan opkijken en van kan leren, wegens hun kennis en de manier waarop ze in het leven staan. Mentors zijn mensen die je vrijheid geven als het mogelijk is, maar je bij les houden als het moet. Ik heb het geluk gehad tijdens mijn doctoraat twee mentoren te hebben gevonden in William en Erik. Daarvoor, mijn oprechte dank.

Dit doctoraatsonderzoek is gefinancierd door Elia System Operator. In nauwe samenwerking met Elia werd er een model van het Europese elektriciteitssysteem ontwikkeld. Ik zou Elia willen bedanken om mij de kans te geven mij vier jaar te verdiepen in de wondere wereld van elektriciteitssystemen en modelleren. Zonder de financiële en inhoudelijke steun van Elia was dit doctoraat er niet geweest. De samenwerking met Elia heeft mij ook de kans gegeven om reeds te proeven van de industrie, wat ik altijd als een grote meerwaarde heb ervaren. Ik wil ook de vele mensen bedanken die ik heb ontmoet binnen Elia voor het delen van hun kennis en de aangename samenwerking, in het bijzonder Cindy Bastiaensen, Viviane Illegems, Dries Couckuyt, Janus De Bondt, Rafael Feito-Kiczak, Fabian Georges, Peter Van Roy en Frank Wellens.

I would also like to sincerely thank all members of the examination committee. The valuable feedback I received significantly improved the quality of this dissertation. Prof. Bultheel, thank you for chairing my examination committee.

Geert and Dirk, thank you for being on this journey with me from the beginning, as members of my supervisory committee. Ben and Hannes, thank you for your enthusiasm and the always interesting discussions we had during conferences, meetings and the defense. Cindy, thank you for being the driving force behind this research project.

A special *dankuwel* goes out to prof. Ben Hobbs for hosting me at The Johns Hopkins University in the Spring of 2015. Ben, I admire your hospitality and your impressive knowledge of power systems. It was a pleasure discussing research (and other things) with you and being part of your research group for this short period. I would also like to thank Elina, Robin, Nicolas, Juliaan, Tony, Anouk and Adrien for all the fun we had during lunch breaks and weekends. My research visit was enabled by a travel grant of FWO (Flemish Research Foundation).

Ik krijg spontaan vooruitlopende heimwee bij de gedachte dat mijn doctoraat afloopt. Niet zozeer naar het geknoei in mijn computercode, maar wel naar de vele fijne collega's/vrienden en momenten die ik achterlaat. Bij deze een woord van dank aan alle collega's om samen een fijne werkplek te maken van TME. Tijs, Arnout en Thomas, bedankt om het zoveel uren met mij uit te houden in de kleine ruimte die onze bureau was. Eric, Ruben en Kristel, bedankt om samen een nieuwe generatie ingenieurs te laten kennismaken met de warmteoverdracht. Kenneth B., Andreas, Kris, Mathias, Juliana, Jeroen, Nico, Sarah en Daniël, bedankt om van onze onderzoeksgroep de tofste te maken van het hele departement. Dries, Dieter, Bram, Damien, Geert, Niels, Pieter, Maarten, Filip, Igor, Muhannad, Cornelia, Nicholas, Emre, Stefan, Thanos, Sepideh, Paul, Bart, Mats, Wim en Vahid, bedankt om me af en toe ook een goal te laten scoren tijdens de voetbalwedstrijdjes op vrijdag of op TME-weekend. Valérie, bedankt om steeds met de glimlach paraat te staan om me verder te helpen met praktische beslommeringen.

Tenslotte zou ik mijn ouders, broer, familie en vrienden willen bedanken. Ons verhaal gaat veel verder terug dan dit boekje, maar ik zou de gelegenheid willen aangrijpen om jullie te bedanken voor de mooie momenten uit het verleden. Ik kijk vol goesting uit naar wat de toekomst ons zal brengen.

Tinne, jou bedanken in woorden is onmogelijk, maar ik ben het je verplicht om toch een poging te wagen. Bedankt voor wie je bent, voor alles wat je doet, altijd recht uit het hart, nooit omdat het moet.

Kenneth
Leuven, juli 2016

Abstract

Electricity generation systems in Europe are undergoing dramatic changes, largely driven by changing energy and climate policies. In this dissertation, three evolutions are dealt with in particular: (1) the deployment of intermittent renewables in electricity systems such as wind and solar photovoltaics, (2) the integration of electricity markets and (3) the mitigation of CO_2 emissions from the electricity sector.

The focus of this dissertation is on the technical and cost-related aspects of electricity generation systems, taking an operational viewpoint (i.e., no investment decisions are studied in this work). The dissertation presents several case studies inspired by realistic and large-scale electricity systems. Concerning the deployment of intermittent renewables, the impact of variable renewable generation on cycling of conventional power plants is studied, as well as the impact of remote renewables–such as offshore wind–on grid congestion. Regarding the integration of electricity markets, this dissertation investigates the benefits of integrating reserve markets and discusses the flow-based market coupling implemented in Central Western European day-ahead markets. Finally, concerning CO_2 emission abatement in the electricity sector, the impact of a CO_2 emission price on the generation of electricity is studied, together with the policy interaction between the European emission trading system and the deployment of renewables.

A unit commitment model has been developed and is used in this dissertation. This model, referred to as the LUSYM model, is a state-of-the-art deterministic unit commitment model, formulated as a tight and compact mixed-integer program and able to solve large-scale electricity systems within reasonable run times. The model includes power plant constraints, renewables curtailment, load curtailment, storage units, transmission grid constraints and reserve constraints. Benchmarking simulations show that the LUSYM model is competitive or outperforms commercial unit commitment packages in terms of optimality of simulation results and/or run times.

All the case studies presented in this dissertation, providing qualitative and quantitative insights, indicate that electricity systems are indeed evolving in the direction envisioned by policy makers (at least when it comes to the deployment of renewables, the integration of electricity markets and the reduction of CO_2 emissions). However, this dissertation also demonstrates that changing energy and climate policies pose new challenges to electricity systems, such as maintaining the system balance with a large share of intermittent generation. In this respect, unit commitment modeling plays an important role in evaluating policies and their impact on electricity generation systems, in order to develop effective and efficient policies.

Beknopte samenvatting

Elektriciteitssystemen in Europa ondergaan drastische veranderingen, hoofdzakelijk gedreven door veranderend energie- en klimaatbeleid. In dit proefschrift worden drie evoluties in het bijzonder behandeld: (1) de integratie van intermitterende hernieuwbare bronnen zoals wind- en zonne-energie, (2) het koppelen van elektriciteitsmarkten en (3) de mitigatie van CO_2-emissies in de elektriciteitssector.

Dit proefschrift focust, vanuit een operationeel standpunt, op de technische en kosten-gerelateerde aspecten van elektriciteitsproductie (investeringsbeslissingen worden niet bestudeerd). Het proefschrift behandelt verschillende gevallenstudies, gebaseerd op realistische en grootschalige elektriciteitssystemen. Betreffende de integratie van intermitterende hernieuwbare bronnen is de impact van variabele hernieuwbare elektriciteitsproductie op het gebruik van conventionele centrales bestudeerd, net zoals de impact van afgelegen hernieuwbare productie-eenheden - zoals windenergie op zee - op netwerkcongesties. Betreffende het koppelen van elektriciteitsmarkten onderzoekt dit proefschrift de voordelen van het koppelen van reservemarkten en bespreekt het de *flow-based* marktkoppeling zoals geïmplementeerd in West-Europese *day-ahead* markten. Tenslotte, betreffende de mitigatie van CO_2-emissies in de elektriciteitssector is de impact van een CO_2-prijs op de productie van elektriciteit onderzocht, samen met de interactie tussen het Europese emissiehandelssysteem en de integratie van hernieuwbare energie.

Een *unit commitment* model is ontwikkeld, onder de naam LUSYM, en gebruikt in dit proefschrift. Dit model is een *state-of-the-art* deterministisch *unit commitment* model, geformuleerd als een efficiënt *mixed-integer* probleem dat grootschalige elektriciteitssystemen kan oplossen met een aanvaardbare rekentijd. Het model omvat beperkingen van elektriciteitscentrales en hernieuwbare productie-eenheden, vraagbeperking, opslageenheden, netwerkbeperkingen en reservebeperkingen. Vergelijkende simulaties tonen aan dat het LUSYM model competitief is of beter doet dan commerciële *unit commitment* modellen in

termen van optimaliteit en/of rekentijd.

Alle besproken gevallenstudies in dit proefschrift verschaffen kwalitatieve en kwantitatieve inzichten en tonen aan dat elektriciteitssystem evolueren in de richting aangegeven door beleidsmakers (tenminste met betrekking tot de integratie van hernieuwbare energie, het koppelen van elektriciteitsmarkten en de mitigatie van CO_2-emissies). Echter, dit proefschrift toont ook aan dat veranderend energie- en klimaatbeleid nieuwe uitdagingen stelt voor het elektriciteitssysteem, zoals het handhaven van het systeemevenwicht met een groot aandeel intermitterende productie. In dit opzicht speelt *unit commitment* modellering een belangrijke rol in het evalueren van beleidsmaatregelen en hun impact op elektriciteitssystemen, met als doel om effectief en efficiënt beleid te ontwikkelen.

Abbreviations

AC	Alternating current
AT	Austria
ATC	Available transfer capacity
BA	Bosnia-Herzegovina
BE	Belgium
BG	Bulgaria
CBCO	Critical branch critical outage
CCGT	Combined-cycle gas turbine
CH	Switzerland
CHP	Combined heat and power (cogeneration)
CWE	Central Western Europe
CZ	Czech Republic
D-2CF	Day-2 congestion forecast
DACF	Day-ahead congestion forecast
DC	Direct current
DCDF	Direct current distribution factors
DE	Germany
DK	Denmark
DSK	Demand shift key
DUC	Deterministic unit commitment
EC	European commission
ED	Economic dispatch
EE	Estonia
ENTSO-E	European network of transmission system operators for electricity
ES	Spain
ETS	Emission trading system
EU	European Union
EUR	Euro

FACTS	Flexible AC transmission systems
FAV	Final adjustment value
FBMC	Flow-based market coupling
FI	Finland
FR	France
FRM	Flow reliability margin
GR	Greece
GSK	Generation shift key
HR	Croatia
HU	Hungary
HVDC	High voltage direct current
IC	Internal combustion engine
IE	Ireland
ISK	Injection shift key
ISO	Independent system operator
IT	Italy
LCOE	Levelized cost of electricity
LCP	Large combustion plant
LMP	Locational marginal price
LT	Lithuania
LU	Luxembourg
LUSYM	Leuven university system model
LV	Latvia
MACC	Marginal abatement cost curve
MDT	Minimum down time
ME	Montenegro
MILP	Mixed-integer linear program
MINLP	Mixed-integer non-linear program
MINP	Mixed-integer non-linear program
MIP	Mixed-integer linear program
MK	Macedonia
MUT	Minimum up time
NEX	Net exchange position
NL	Netherlands
NO	Norway
NRA	National regulatory authority
NTC	Net transfer capacity
NUC	Nuclear generation unit
O&M	Operations and maintenance
OCGT	Open-cycle gas turbine
OPF	Optimal power flow

PBUC	Price-based unit commitment
PDF	Probability density function
PL	Poland
PSDF	Phase shifter distribution factor
PST	Phase shifting transformer
PT	Portugal
PTDF	Power transfer distribution factor
PV	Photovoltaics
PX	Power exchange
RAM	Remaining available margin
RES	Renewables
RO	Romania
RS	Serbia
SCOPF	Security-constrained optimal power flow
SCUC	Security-constrained unit commitment
SI	Slovenia
SK	Slovakia
SPFE	Solar power forecast error
SPP-C	Coal-fired steam power plant
SPP-G	Gas-fired steam power plant
SPP-L	Lignite-fired steam power plant
SUC	Stochastic unit commitment
SW	Sweden
TJ	Turbo jet
TSO	Transmission system operator
UC	Unit commitment
UK	United Kingdom
VOM	Variable operations and maintenance
WPFE	Wind power forecast error

List of symbols

Matrices and vectors are denoted in bold.

Sets

B (index b)	set of bids
C (index c)	set of line contingencies
I (index i)	set of power plants
I^{nsr} (index i^{nsr})	subset of power plants delivering non-spinning reserves
I^{nuc} (index i^{nuc})	subset of nuclear power plants
J (index j)	set of storage units
L (index l)	set of lines (in a nodal network)
K (index k)	set of lines in a zonal network
N (index n)	set of nodes
S (index s)	set of reserve zones
T (index t)	set of time steps
Y (index y)	set of all grid injection categories
Y^{G} (index y^{G})	subset of generation-related categories
Y^{L} (index y^{L})	subset of load-related categories
Z (index z)	set of zones

Parameters

Δt	length of one time step in hours (h)
η_i	rated efficiency of power plant i
η_j^c	charging efficiency of storage unit j
η_j^d	discharging efficiency of storage unit j
$A_{l,n}$	element of incidence matrix of the grid {-1,0,1}
$A_{n,i}^{plant}$	element linking power plant i to node n {0,1}
$\mathbf{A^{plant,N}}$	matrix linking generation units to nodes (N-by-I) {0,1}
$\mathbf{A^{plant,Z}}$	matrix linking generation units to zones (Z-by-I) {0,1}
$A_{n,j}^{stor}$	element linking storage unit j to node n {0,1}
$A_{s,i}^{rsr}$	element linking power plant i to reserve zone s {0,1}
$A_{s,n}^{rsr}$	element linking node n to reserve zone s {0,1}
$\overline{ATC}_l$	positive available transmission capacity of line l (MW)
$\underline{ATC}_l$	negative available transmission capacity of line l (MW)
$AV_{i,t}$	availability of power plant i at time step t {0,1}
$\mathbf{B^{bus}}$	bus admittance matrix (N-by-N)
$\mathbf{B^{bus*}}$	reduced bus admittance matrix (N-1-by-N-1)
$\mathbf{B^{branch}}$	branch admittance matrix (L-by-N)
$\mathbf{B^{branch*}}$	reduced branch admittance matrix (L-by-N-1)
CC	CO_2 emission cost (EUR/tCO_2)
$D_{n,t}$	electricity load at node n at time step t (MW)
$\mathbf{D^N}$	vector with nodal load (N-by-1) (MW)
$\mathbf{D^Z}$	vector with zonal load (Z-by-1) (MW)
EF_i	CO_2 emission factor of power plant i (Δt tCO_2/MWh$_{\mathrm{th}}$)
EM_i	CO_2 emissions of power plant i (t$CO_2/\Delta t$)

$\overline{F}_l$	maximum power flow through line l (MW)
$\underline{F}_l$	minimum power flow through line l (MW)
$\overline{\mathbf{F}}^{\mathbf{N}}$	vector with line capacities in nodal network (L-by-1) (MW)
$\overline{\mathbf{F}}^{\mathbf{Z}}$	vector with line capacities in zonal network (K-by-1) (MW)
F_l^0	zero-imbalance flow through line l (MW)
$\mathbf{F}^{\mathbf{0,Z}}$	vector with base case flows in zonal network (K-by-1) (MW)
F_l^{ref}	reference flow through line l (MW)
FAV_l	final adjustment value on line l (MW)
FC_i	fuel cost of power plant i (ΔtEUR/MWh$_{\text{th}}$)
FRM_l	flow reliability margin on line l (MW)
$GSK_{n,z}$	generation shift key of node n in zone z
$ISF_{l,n}$	injection shift factors
ISF	injection shift factor matrix (L-by-N)
$\mathbf{ISF}^*$	reduced injection shift factor matrix (L-by-N-1)
ISK	matrix with injection shift keys (N-by-Z)
$\mathbf{ISK}^{\mathbf{Y}}$	matrix with injection shift keys of category y (N-by-Z)
LCC_n	load curtailment cost at node n (ΔtEUR/MWh)
MC_i	marginal generation cost of power plant i (ΔtEUR/MWh)
MDT_i	minimum down time of power plant i (Δt)
MUT_i	minimum up time of power plant i (Δt)
NC_i	generation cost at minimum output of power plant i (EUR/Δt)
OP_i	required planned outages of power plant i (Δt)
$\overline{P}_i$	maximum power output of power plant i (MW)
$\underline{P}_i$	minimum power output of power plant i (MW)
PC_j	maximum charging power of storage unit j (MW)
PD_j	maximum discharging power of storage unit j (MW)

$\overline{PE}_j$	maximum energy content of storage unit j (MWh)
$\underline{PE}_j$	minimum energy content of storage unit j (MWh)
$\mathbf{PTDF^N}$	nodal power transfer distribution factor matrix (L-by-N)
$\mathbf{PTDF^{N*}}$	node-to-link power transfer distribution factor matrix (K-by-N)
$\mathbf{PTDF^Z}$	zonal power transfer distribution factor matrix (K-by-Z)
$\mathbf{PTDF^{Y,Z}}$	zonal power transfer distribution factor matrix of category y (K-by-Z)
$Q^P_{b,z}$	price of bid b in zone z (ΔtEUR/MWh)
$Q^Q_{b,z}$	quantity of bid b in zone z (MW)
RAC^{lol}	reserve allocation cost for load curtailment (ΔtEUR/MW)
RAC^{cur}	reserve allocation cost for renewables curtailment (ΔtEUR/MW)
RAM_l	remaining available margin of line l (MW)
RC_i	ramping cost of power plant i (EUR/MW)
RCC_n	renewables curtailment cost at node n (ΔtEUR/MWh)
RD_i	maximum ramp-down rate of power plant i (MW/Δt)
$RES_{n,t}$	available renewable generation at node n at time step t (MW)
RU_i	maximum ramp-up rate of power plant i (MW/Δt)
SD_i	maximum shut-down rate of power plant i (MW/Δt)
SDC_i	shut-down cost of power plant i (EUR/shut-down)
$SR^+_{s,t}$	upward spinning reserve in reserve zone s at time step t (MW)
$SR^-_{s,t}$	downward spinning reserve in reserve zone s at time step t (MW)
SU_i	maximum start-up rate of power plant i (MW/Δt)
SUC_i	start-up cost of power plant i (EUR/start-up)
TC_i	total generation cost of power plant i (ΔtEUR/MWh)

Variables

$\boldsymbol{\theta}$	nodal voltage angles (rad)
$cost_{i,t}^{gen}$	generation cost of power plant i at time step t (EUR/Δt)
$cost_{n,t}^{lc}$	load curtailment cost at node n at time step t (EUR/Δt)
$cost_{i,t}^{ramp}$	ramping cost of power plant i at time step t (EUR/Δt)
$cost_{n,t}^{rc}$	renewables curtailment cost at node n at time step t (EUR/Δt)
$cost_{n,t}^{rsr}$	reserve allocation cost for load and renewables curtailment at node n at time step t (EUR/Δt)
$cost_{i,t}^{start}$	start-up cost of power plant i at time step t (EUR/Δt)
$cost_{i,t}^{stop}$	shut-down cost of power plant i at time step t (EUR/Δt)
$f_{l,t}$	power flow through line l at time step t (MW)
$\mathbf{F^N}$	vector with line power flows in a nodal network (L-by-1) (MW)
$\mathbf{F^Z}$	vector with line power flows in a zonal network (K-by-1) (MW)
$g_{i,t}$	power generation of power plant i above minimum output at time step t (MW)
$gen_{i,t}$	power generation of power plant i at time step t (MW)
$lc_{n,t}$	load curtailment at node n at time step t (MW)
NEX_z	net exchange position of zone z (MW)
$of_{i,t}$	forced outage of power plant i at time step t {0,1}
$op_{i,t}$	planned outage of power plant i at time step t {0,1}
$p_{n,t}$	power injection in the grid at node n at time step t (MW)
$\mathbf{P^N}$	vector with nodal power injections in the grid (N-by-1) (MW)
$\mathbf{P^{Y,N}}$	vector with nodal power injections in the grid of category y (N-by-1) (MW)
$\mathbf{P^Z}$	vector with zonal power injections in the grid (Z-by-1) (MW)

$\mathbf{P^{Y,Z}}$	vector with zonal power injections in the grid of category y (Z-by-1) (MW)
$pc_{j,t}$	charging power of storage unit j at time step t (MW)
$pd_{j,t}$	discharging power of storage unit j at time step t (MW)
$pe_{j,t}$	energy level of storage unit j at time step t (MWh)
$r^{+}_{i,t}$	scheduled upward spinning reserve from power plant i at time step t (MW)
$r^{-}_{i,t}$	scheduled downward spinning reserve from power plant i at time step t (MW)
$r^{cur}_{n,t}$	scheduled reserve from renewables curtailment at node n at time step t (MW)
$r^{lol}_{n,t}$	scheduled reserve from load curtailment at node n at time step t (MW)
$rc_{n,t}$	renewables curtailment at node n at time step t (MW)
$v_{i,t}$	start-up status of power plant i at time step t {0,1}
$w_{i,t}$	shut-down status of power plant i at time step t {0,1}
$x_{b,z}$	accepted share of bid b in zone z
$z_{i,t}$	on/off-status of power plant i at time step t {0,1}

Contents

Abstract iii

Abbreviations vii

List of symbols xi

Contents xvii

1 Introduction 1

1.1 Context 1

1.2 Methodology 4

1.3 Research issues 4

2 Unit commitment model 7

2.1 Introduction to unit commitment modeling 8

2.2 Mathematical formulation of the LUSYM model 11

2.2.1 Unit commitment 11

2.2.2 Power plant outages 19

2.3 Validation of the model 20

2.3.1 Benchmarking with existing unit commitment models . 21

2.3.2 Benchmarking with historical generation data 23

2.4 Summary and conclusions 25

3 Network models in unit commitment 27

3.1 Introduction 28
3.2 DC power flow 30
3.3 Nodal-zonal network reduction 33
3.3.1 Clustering nodes into zones 33
3.3.2 Zonal PTDF matrix 34
3.4 Improved method to calculate injection shift keys 36
3.4.1 Time averaging of injection shift keys 36
3.4.2 Improved injection shift keys 37
3.5 Evaluation of improved injection shift keys 40
3.5.1 Case study - Central European electricity network . . . 40
3.5.2 Time variability of the injection shift keys 42
3.5.3 Flows through the network 43
3.5.4 Zonal generation balances 45
3.5.5 Computational tractability 45
3.6 Summary and conclusions 46

4 Cycling of conventional power plants 49

4.1 Introduction 50
4.2 Cylcing of conventional units 52
4.2.1 Cycling cost 52
4.2.2 Technical cycling limits 53
4.3 System and model description 55
4.3.1 System description 55
4.3.2 Model description 56
4.4 Results and discussion 58

4.4.1 Cycling in a high and low-dynamic portfolio 58
4.4.2 Technical limits of cycling 62
4.4.3 The cost of cycling 63
4.5 Summary and conclusions 67

5 Redispatching with high renewables penetration 69
5.1 Introduction 70
5.2 Redispatch actions and costs 73
5.3 Model description 75
5.3.1 Day-ahead model (unit commitment) 77
5.3.2 Redispatch model 78
5.4 The Belgian power system as case study 80
5.5 Results and discussion 82
5.5.1 Reference scenario: Belgian 2016 power system 82
5.5.2 Impact of loop flows 84
5.5.3 Impact of increasing offshore wind 87
5.5.4 Impact of preventive N-1 security criterion 90
5.6 Summary and conclusions 91

6 Benefits of coordinating reserves among market zones 93
6.1 Introduction 94
6.2 Methodology 96
6.2.1 Framework 96
6.2.2 Model description 98
6.2.3 Case study 103
6.3 Results and discussion 105
6.3.1 Reserve sizing 105
6.3.2 Reserve allocation 107

6.3.3 Reserve activation 109
6.3.4 Discussion 111
6.4 Summary and conclusions 112

7 Flow-based market coupling in Central Western Europe 115
7.1 Introduction 116
7.2 Cross-border capacity allocation 118
7.2.1 Nodal market clearing 120
7.2.2 Available transfer capacity 121
7.2.3 Flow-based market coupling 123
7.3 Flow-based market coupling parameters 124
7.3.1 Zonal power transfer distribution factors 125
7.3.2 Remaining available margin 126
7.3.3 Base case (day-2 congestion forecast) 127
7.3.4 Summary 128
7.4 Summary and conclusions 128

8 CO_2 abatement in the electricity sector 131
8.1 Introduction 132
8.2 System and model description 135
8.2.1 System description 135
8.2.2 Model description 137
8.3 CO_2 emissions in the electricity generation sector 137
8.3.1 CO_2 emission drivers 137
8.3.2 Absolute emission plane 142
8.4 Marginal abatement cost curves 144
8.4.1 Methodology 144
8.4.2 Results 145

8.4.3 Discussion 150
8.5 Interaction between the EU ETS and other policies 154
8.5.1 The European emission trading system 154
8.5.2 Policy interaction: literature overview 155
8.6 Impact curves 157
8.6.1 Methodology 158
8.6.2 Results 160
8.7 Summary and conclusions 165

9 Summary, conclusions and suggestions for further research 169
9.1 Summary and conclusions 169
9.2 Suggestions for further research 172

A Benchmarking case studies 177
A.1 Benchmarking with existing unit commitment models 177
A.2 Benchmarking with historical generation data 179

B Network models 183
B.1 AC power flow 183
B.2 DC power flow 186
B.3 DC power flow with power flow controlling devices 190
B.3.1 Phase shifting transformers 191
B.3.2 High voltage direct current lines 193
B.4 DC power flow with N-1 security 195

C CO_2 emissions in the electricity sector 199
C.1 Fuel switching 199
C.2 Electric vehicles in the electricity sector 203
C.3 Renewables investments triggered by a CO_2 price 204

References **207**

Short curriculum **227**

Publications by the author **229**

Chapter 1

Introduction

Electricity generation systems in Europe are undergoing unseen changes, largely driven by changing energy and climate policies. This dissertation studies the impact of these energy and climate policies on electricity generation in a European context. The presented analyses are based on a newly developed large-scale electricity generation model, i.e., the unit commitment model LUSYM (Leuven University System Model).

This first chapter describes the context and the methodology of the research, and presents the outline of the dissertation.

1.1 Context

Two mutually reinforcing drivers are changing electricity generation systems worldwide and particularly in Europe: policy and technology. Policy makers aim to make electricity generation systems more secure, competitive and environmentally sustainable than before. Technological evolutions make it possible to extract electric energy with different cost structures than before (e.g., the decrease in investment costs for solar photovoltaics), more efficiently than before (e.g., the increase in rated efficiencies of fossil-fuel power plants) and from other sources than before (e.g., the ongoing developments in offshore wind energy far from the shore). Technological evolutions and policy making are interdependent. Policies can trigger, steer and accelerate technological evolutions and, the other way around, technological evolutions can create opportunities for policy makers.

This dissertation focusses on the impact of energy and climate policies on electricity generation systems in the European Union (in particular as of chapter 4, chapters 2-3 deal with the unit commitment model). European energy and climate policies pursue three targets for the electricity sector: (1) a secure electricity system which guarantees security of supply for the end consumers, (2) a competitive electricity system that supplies electric energy effectively and cost-efficiently, and (3) an environmentally sustainable electricity system with a main focus on climate (European Commission, 2016a). Towards these aims, the European Union established the Energy Union in 2015. The Energy Union focuses on five mutually supportive dimensions: energy security, a fully-integrated internal energy market, energy efficiency, decarbonization of the economy, and research and innovation in low-carbon technologies (European Commission, 2015).

As a direct consequence of European energy and climate policies, the European electricity generation sector is changing. Amongst others, the following three important evolutions can be observed.

1) **Deployment of intermittent renewables.** The European Union has set ambitious targets for the deployment of renewable energy, i.e., a 20% share of renewable energy in final energy consumption by 2020 (European Commission, 2016d). This European target is translated in national targets for each member state, giving each member state the freedom to implement its own mechanisms to support investments in renewable energy installations. Since 2014, the 2030 framework for climate and energy is being discussed, featuring a renewable energy target of at least a 27% share in final energy consumption. However, this target would be only binding on a European level and would not be translated into binding member state targets (European Commission, 2014b). Since it is relatively easier to deploy renewables in the electricity sector than in the heating or transport sector, it is projected that the share of renewables in final electricity consumption will surpass 20% by 2020.[1] As a result, the installed capacity of intermittent renewables has increased drastically over the last years. Intermittent generation, such as the generation from wind and solar photovoltaics, can be defined as electricity generation that is variable, limitedly dispatchable and only partially predictable. The intermittent character of renewables makes it more challenging to maintain system balance and obtain a safe and secure system operation.

2) **Integration of electricity markets.** The European Union aims for one single liberalized and integrated electricity market. As a result,

[1] The European Union has set a specific renewables target for the transport sector of 10% renewables share by 2020.

electricity markets in Europa are increasingly coupled. As such, electric energy and/or electric reserve capacity can be exchanged between different market zones. A first major step in the market coupling process was taken in November 2006 with the coupling of the Belgian, Dutch and French day-ahead markets (PowerNext, 2006). Since February 2015, the day-ahead electricity markets of 19 European countries are coupled, covering about 85% of European power consumption (EpexSpot, 2015). More recently, the focus shifted towards integrating intra-day markets and balancing markets (ENTSO-E, 2015b).

3) **Reducing greenhouse gas emissions.** The European Union has also set ambitious greenhouse gas reduction targets, i.e., a 20% reduction in greenhouse gas emissions by 2020 compared to 1990 levels (European Commission, 2016d). This European target is split in a target for the emitters operating under the European emission trading system (EU ETS), amongst which electricity generators, and nationally determined targets for other emitters. The ETS target is a 21% reduction in greenhouse gas emissions by 2020 compared to 2005 levels (the non-ETS target is a 10% reduction in overall EU greenhouse gas emissions by 2020 compared to 2005 levels). More recently, the 2030 framework for climate and energy is being discussed, containing a greenhouse gas reduction target of 40% in domestic EU greenhouse gas emissions by 2030 compared to 1990 levels. Again, this overall target would be split into an ETS target (43% reduction by 2030 compared to 2005 levels) and nationally non-ETS targets (30% reduction EU-wide by 2030 compared to 2005 level) (European Commission, 2014b). The EU ETS, which is in place since 2005, sets a cap to the greenhouse gas emissions from heavy industry, including electricity generators, and more recently aviation within the European Economic Area (i.e., the EU plus Norway, Iceland and Liechtenstein). Emission allowances, which have to be handed in for each ton of emitted CO_2-equivalent can be traded between emitters, resulting in a CO_2 price. In much of the analysis that follows, the main focus is on CO_2 emissions. As such, electricity generators face a CO_2 emission cost equal to the EU ETS CO_2 price. It is an interesting observation that local or national policies concerning heavy CO_2 emitters (e.g., coal-fired power plants) and/or CO_2-free generation (e.g., renewables or nuclear power plants) do not change the overall CO_2 emissions inside the European Union because of the EU ETS emission cap; only the ETS price of emission allowances is affected by national policies.

1.2 Methodology

A large-scale unit commitment model has been developed and is used in this dissertation to study the impact of energy and climate policies on electricity generation in Europe. A unit commitment model is a bottom-up, engineering-based model of the electricity generation sector. This model is a pure operational model (i.e., no investments in generation or transmission capacity are considered) that minimizes the operational system costs, taking technical limitations of the generation portfolio and transmission network into account.

A unit commitment model is an appropriate and eligible modeling tool to study the electricity sector since it captures the techno-economic constraints of electricity generation. Generation and consumption (plus losses) of electric energy have to match on an instantaneous basis, otherwise the system frequency starts deviating from its reference value (i.e., 50 Hz in Europe) and the whole electricity system could collapse if the deviation becomes too large. As such, technical constraints of power plants and transmission networks become important as they limit the actions that system operators or market players can undertake to maintain real-time system balance.

The research presented in this dissertation focusses on:

- The generation of electricity, constrained by network limitations.
- Short-term operational aspects of the electricity generation system. The generation portfolio and transmission system is considered fixed in this dissertation.
- Large-scale and realistic electricity generation systems. The presented case studies are based on real-life electricity systems, often consisting of several hundreds of power plants and thousands of hourly or quarter-hourly time steps.

1.3 Research issues

This dissertation investigates the impact of energy and climate policies on electricity generation in Europe. More specifically, three important evolutions are addressed: 1) the deployment of intermittent renewables, 2) the integration of electricity markets and 3) reducing greenhouse gas emissions. Towards this aim, a unit commitment model is developed and used. The following research issues are dealt with.

0) Unit commitment modeling with network constraints

Chapter 2 presents the large-scale unit commitment model developed in this research, i.e., the LUSYM model. LUSYM is a state-of-the art deterministic unit commitment model, formulated as a tight and compact mixed-integer program. Chapter 2 is based on *K. Van den Bergh, K. Bruninx, E. Delarue, and W. D'haeseleer. LUSYM: a unit commitment model formulated as a mixed-integer linear program. KU Leuven Working Paper, 2015.*

Chapter 3 studies the implementation of network constraints in unit commitment models. In particular, zonal DC power flow representations of the electricity grid are discussed. Chapter 3 is based on *K. Van den Bergh and E. Delarue. An improved method to calculate injection shift keys. Electric Power Systems Research, 134:197-204, 2016* and *K. Van den Bergh, E. Delarue, and W. D'haeseleer. DC power flow in unit commitment models. KU Leuven Working Paper, 2014.*

1) Deployment of intermittent renewables

Chapter 4 studies the impact of intermittent renewables on cycling of conventional power plants. Cycling is changing the power output and/or the on/off-status of a power plant. Intermittent renewables change the type of power plants that cycle and the required amount of cycling. Since power plant cycling entails costs, the deployment of intermittent renewables impacts also generation costs. The addressed research questions are: how do renewables affect the total operational costs, including cycling costs, and how important are cycling costs in the total operational costs? Chapter 4 is based on *K. Van den Bergh and E. Delarue. Cycling of conventional power plants: technical limits and actual costs. Energy Conversion Management, 97:70-77, 2015.*

Chapter 5 studies the impact of offshore wind on redispatching. The deployment of renewables in remote areas can lead to overloadings of transmission lines. Redispatching is adjusting the day-ahead market outcome in order to prevent line overloadings and obtain a safe operational system state. The addressed research questions are: how are redispatching quantities and costs affected by the deployment of remote renewables, and how does redispatching change with loop flows and a N-1 security criterion? Chapter 5 is based on *K. Van den Bergh, D. Couckuyt, E. Delarue, and W. D'haeseleer. Redispatching in an interconnected electricity system with high renewables penetration. Electric Power Systems Research, 127:64-72, 2015.*

2) Integration of electricity markets

Chapter 6 studies the benefits of integrating reserve markets. Spatial smoothing of system imbalances and spatial arbitrage during the allocation and activation

of reserves can lead to cost reductions. However, cross-border transmission limits constrain the coordination among market zones. The addressed research question is: what are the economic benefits of integrating reserve markets, considering limited transfer capability between the markets? Chapter 6 is based on *K. Van den Bergh, R. Broder Hytowitz, K. Bruninx, E. Delarue, W. D'haeseleer, and B. Hobbs. Benefits of coordinating sizing, allocation and activation of reserves among market zones. Submitted for publication, 2016.*

Chapter 7 studies flow-based market coupling. Flow-based market coupling is the methodology used since May 2015 to couple day-ahead electricity markets in Central Western Europe (Belgium, France, Germany and the Netherlands). The addressed research questions are: what are the methodological principles on which flow-based market coupling is based, and how does it relate to other cross-border capacity allocation mechanisms? Chapter 7 is based on *K. Van den Bergh, J. Boury, and E. Delarue. The flow-based market coupling in Central Western Europe: concepts and definitions. The Electricity Journal, 29:24-29, 2016.*

3) Reducing greenhouse gas emissions

Chapter 8 studies the impact of a CO_2 emission price on the electricity generation sector. The marginal abatement cost curve of the electricity sector is discussed. Moreover, policy interactions between the European emission trading system and the deployment of renewables in the electricity sector are quantified by means of impact curves. The addressed research questions are: what is the CO_2 abatement in the electricity sector following from a CO_2 emission price, and how are the CO_2 emissions and the CO_2 emission price affected by the deployment of renewables? Chapter 8 is based on *K. Van den Bergh and E. Delarue. Quantifying CO_2 abatement costs in the power sector. Energy Policy, 80:88-97, 2015* and *E. Delarue and K. Van den Bergh. Carbon mitigation in the electric power sector under cap-and-trade and renewables policies. Energy Policy, 92:34-44, 2016.*

All abbreviations and symbols (sets, parameters and variables) used in the subsequent chapters are listed and explained at the outset of this dissertation.

Chapter 2

Unit commitment model

Chapter based on:

K. Van den Bergh, K. Bruninx, E. Delarue, and W. D'haeseleer. LUSYM: a unit commitment model formulated as a mixed-integer linear program. KU Leuven Working Paper, 2015.[1]

Abstract: This chapter presents a state-of-the-art deterministic unit commitment (UC) model, formulated as a mixed-integer linear program (MIP), and referred to under the name LUSYM (Leuven University System Model). This model has been developed during this PhD research and has been applied in several publications. A UC model determines the optimal scheduling of a given set of power plants to meet the electricity load, taking account of the operational constraints of the electricity system. The presented formulation is tight and compact, and includes power plant constraints, renewables curtailment, load curtailment, storage units, transmission grid constraints and spinning reserves. The model is able to solve large-scale electricity systems within reasonable run times. Run times are reduced by means of a tight and compact formulation, efficient data handling and the use of best-in-class MIP solvers.

Keywords: Unit commitment; mixed-integer linear programming; tight and compact formulation.[2]

[1] The publication on which this chapter is based benefited from discussions with, apart from the co-authors, G. Morales-España (TU Delft).

[2] All abbreviations and symbols used in this chapter are listed and explained at the outset of this dissertation.

2.1 Introduction to unit commitment modeling

The unit commitment (UC) problem can be defined as the scheduling of electric power generating units over a daily to weekly time horizon in order to minimize operational system costs (Hobbs et al., 2001). The unit commitment solution must respect the technical and operational limits of the electricity system, such as power plant constraints and reserve requirements. The unit commitment model gives for each generation unit and each time step the unit commitment (UC) decision, i.e., the on/off-status, and the economic dispatch (ED) decision, i.e., the power output if online.[3] The UC decision is typically taken hours to days before the actual delivery, since most power plants cannot start-up quickly. The ED decision is typically taken minutes to hours before the actual delivery, as changing the power output of an online plant requires less time than bringing a power plant online. The UC decision problem translates into a more complex mathematical formulation than the ED decision, due to the binary nature of the on/off decision.[4]

The UC problem can be addressed from a system perspective or a generator perspective. According to the system perspective, the operational cost for the whole system is minimized while guaranteeing supply-demand balance in the system. One speaks of a Security-Constrained Unit Commitment (SCUC) if also security and transmission constraints are considered. This system perspective corresponds to a vertically integrated environment, in which a regulated monopolist schedules the generation portfolio at minimum operational cost (i.e., cost-based unit commitment), or to an unbundled environment with a centralized and controlled Electricity Pool model (i.e., bid-based unit commitment, e.g., the PJM market). A SCUC can also be used as a proxy for the market outcome of a liberalized market based on a decentralized model with bilateral trading and possibly Power Exchanges (e.g., the European electricity market), under the assumption of perfect competition. According to the generator perspective, the profit of one generator is maximized given its generation portfolio and an electricity price. This type of UC problem is referred to as Price-Based Unit Commitment (PBUC) or Self-Unit Commitment. The generator perspective corresponds to a deregulated market environment in which generators are responsible for the UC decision of their generation portfolio (Delarue, 2009).

UC models are partial equilibrium models, focusing solely on the electricity sector. Interactions between the electricity sector and other sectors in the economy are neglected (e.g., fossil fuel prices are imposed as exogenous

[3]The terms *time instant*, i.e., a specific moment in time, and *time step*, i.e., the time interval between two time instants, are used interchangeably in this dissertation.

[4]Including non-spinning reserves in the economic dispatch decision introduces a binary on/off-decision in the ED problem.

parameters to UC models, neglecting the relation between fossil fuel-fired electricity generation and fossil fuel prices). UC models can be distinguished from other electricity generation models based on the classification parameters proposed by Ventosa et al. (2005):

- Degree of competition: UC models can correspond to a competitive market or a regulated vertically integrated monopoly. Strategic behavior of market players (e.g., an oligopolistic market) is not represented in UC models.
- Time frame: UC models are short-term operational models with a time frame of days to weeks and a time resolution of minutes to hours. No long-term decisions, such as investments in new generation capacity, are usually considered.
- Generation system: The main distinctive characteristic of UC models is the high level of detail with which the generation units are represented, considering each power plant individually with its technical limits.
- Demand flexibility: UC models often use an inelastic demand, which is a fair assumption for short-term analyses. However, an increasing amount of academic literature deals with including demand flexibility in UC modeling, see for instance De Jonghe et al. (2014), Papavasiliou and Oren (2014) and Patteeuw et al. (2015).
- Uncertainty: The various sources of uncertainty in the electricity sector (e.g., power plant outages, renewable forecast errors) can be addressed with a deterministic or a stochastic approach. In a deterministic unit commitment (DUC) model, generation units are scheduled based on expected values of probabilistic input parameters. Possibly, reserves are scheduled to deal with deviations from the expected values. In a stochastic unit commitment (SUC) model, the full probabilistic distribution of uncertain parameters is taken into account. A SUC model is computationally more challenging than a DUC model. A detailed overview of unit commitment under uncertainty is given by Tahanan et al. (2015).
- Transmission constraints: Transmission constraints can be implemented in UC models by means of an AC power flow model, a DC power flow model or a trade-based model. However, often grid constraints are neglected in UC models, assuming the considered electricity system is a copper plate.

The UC problem is a non-convex and non-linear problem. The non-convexity is caused by the binary nature of the on/off-decision and non-linearities occur due to, amongst others, non-linear generation cost curves and non-linear transmission constraints. All this makes the UC problem a difficult problem to solve. Over the course of the last decades, different mathematical methods have been used to

solve the UC problem. Sheble and Fahd (1994), Sen and Kothari (1998), Yamin (2004), Padhy (2004), Farhat and El-Hawary (2009) and Saravanan et al. (2013) give an overview of these different methods, of which the most important are Exhaustive Enumeration (i.e., listing all possible combinations of on/off-states and picking the most optimal one), Priority Listing (i.e., committing generation units in order of increasing marginal generation cost until the electricity load is met), Dynamic Programming (i.e., optimization-based method that searches for the minimum cost solution by solving simpler subproblems), Lagrangian Relaxation (i.e., the Lagrangian of the optimization problem is solved), Mixed-Integer Programming (i.e., optimization-based method to solve a mixed-integer problem by means of the branch-and-bound method), Decommitment Method (i.e., starting with all units online and switching-off units) and more recently meta-heuristic methods such as Fuzzy Systems, Genetic Algorithms, Artificial Neural Networks, Evolutionary Programming, Tabu Search and Ant Colony Search Algorithms.

A mathematical method that gained importance due to drastic improvements in solver performances is mixed-integer programming (MIP) (Hobbs et al., 2001). MIP is an operational research method in which certain variables are restricted to integer values. The advantage of UC MIP is threefold: (1) the MIP solver returns a feasible solution (if feasible solutions exist and can be found by the MIP solver), (2) the level of optimality is known (the MIP solver returns the optimality gap between the MIP solution and the lower bound to the UC problem), and (3) MIPs can handle complex side constraints which can not be implemented in, for instance, priority listing and Lagrangian relaxation. The disadvantage of UC MIP is longer run times, compared to faster methods such as Priority Listing. However, due to improvements in commercial solvers, processing speed and model formulations, UC MIP models are nowadays often used in industry and academia.

This chapter presents a deterministic linearized mixed-integer formulation of the security-constrained unit commitment problem (further referred to as MIP UC).[5] The formulation is implemented in the latest release of GAMS (2016) and solved with the latest release of Cplex MIP solver (IBM, 2016) or Gurobi MIP solver (Gurobi Optimization, 2016).[6] Processing of input and output data happens in Matlab (MathWorks, 2016), using the Matlab-GAMS coupling as described by Ferris et al. (2011). The model is able to solve the unit commitment

[5]The acronyms MIP and MILP refer both to mixed-integer linear programs. Non-linear mixed-integer programs are referred to with the acronym MINP (or MINLP). This chapter deals with linear mixed-integer programs, here referred to with the acronym MIP.

[6]Cplex MIP solver and Gurobi MIP solver are the best-performing (commercial) MIP solvers, in terms of detecting feasibility and run times needed to find the optimal solution (Mittelmann, 2016).

problem for large scale electricity systems (several hundreds of generation units, about hundred time steps) within several hours.[7]

Several academic and commercial UC models exist. Examples of academic UC models are the WILMAR model developed by mainly Scandinavian research institutes (Meibom et al., 2003), the ELMOD model developed at the Dresden University of Technology in Germany (Leuthold et al., 2008a, 2012), and Dispa-SET developed by the EU JRC Institute for Energy and Transport (Hidalgo González et al., 2014). Commercial unit commitment models are Plexos (Energy Exemplar, 2015), Promod (Ventytx Energy, 2015), Antares (Doquet et al., 2008) and Bid3 (Pöyry, 2015). All these UC models differ slightly, depending on the purpose of the model and the setting in which it is developed. Note that this is anything but an exhaustive list of available UC models.

This chapter continues as follows. Section 2.2 describes the MIP formulation of the UC problem in detail. Section 2.3 discusses the validation of the LUSYM model and section 2.4 summarizes.

2.2 Mathematical formulation of the LUSYM model

The LUSYM model can be split in two parts; (1) the unit commitment model itself with hourly or quarter-hourly time resolution and a daily or weekly time horizon (see subsection 2.2.1), and (2) a yearly power plant outages module with daily or weekly time resolution (see subsection 2.2.2). The outage scheduling happens before the unit commitment scheduling.

2.2.1 Unit commitment

A MIP of the UC problem consists of one objective function, i.e., minimize total operational system cost, subject to several system constraints. The mixed-integer formulation of the unit commitment problem is extensively described in the literature. Arroyo and Conejo (2000) present a mixed-integer linear formulation, based on three binary variables per generation unit and per time step (i.e., on/off-state, start-up status and shut-down status). Carrión and Arroyo (2006) present an updated version of the mixed-integer linear formulation, requiring only one binary variable per generation unit and per time step (i.e., on/off-state). Both formulations are equivalent, but the former is tighter. Tightness refers to how good the feasible area of a mixed-integer problem is approximated by the

[7] Simulations run on an Intel®Core™ i7-2620M CPU@2.7GHz, 8 GB RAM. The exact run time heavily depends on the considered instance and optimality gap.

relaxed version of the formulation (the better the feasible area is approximated, the tighter the formulation). An important concept in this regard is the convex hull. The convex hull is defined as the smallest convex feasible region containing all feasible integer points of a MIP (Wolsey, 1998). The relaxed version of a perfectly tight formulation describes the convex hull of the MIP. Another important characteristic of a unit commitment formulation is its compactness. Compactness refers to the number of variables and equations needed to describe the problem (the fewer variables and equations, the compacter the formulation). A mixed-integer problem solves faster the more compact and tight its formulation is. Typically, there is a trade-off between tightness and compactness of the formulation.[8]

Several authors propose a tight and compact formulation of (part of) the MIP UC formulation. Ostrowski et al. (2012) describe a tighter formulation of the generation limits and ramping limits of power plants. Morales-España et al. (2013a) present a formulation which is simultaneously tighter and compacter, with special focus on the generation limits of power plants. Rajan and Takriti (2005) discuss a tight formulation of the minimum up and down times. Morales-España et al. (2013b) focus on a tight and compact formulation of the start-up and shut-down trajectories of power plants. Frangioni et al. (2009) present a tighter formulation of the linear approximation of the production cost curve. Damcı-Kurt et al. (2013) present a tight description of the two-period ramping constraint. Yang et al. (2015) show that splitting up the power output of a generation unit in the minimum output and the output exceeding the minimum output allows a tighter and compacter formulation. Zheng et al. (2015) presents two cuts to tighten the unit commitment formulation, based on a natural understanding of the problem and the generalized flow cover inequality.

The MIP UC formulation presented in this chapter is based on the papers mentioned above. The nomenclature can be found in the list of symbols at the outset of the dissertation.

Objective function

The objective function of the UC model is to minimize total operational system cost, consisting of generation costs, start-up costs, shut-down costs, ramping costs, load curtailment costs, renewables curtailment costs and reserve allocation

[8]The importance of tightness with respect to compactness depends on the considered instance. Moreover, the MIP formulation interacts with the solution process of the MIP solver, leading to changes in run times which are sometimes hard to explain. Therefore it is impossible to draw general recommendations to reduce MIP run times that work for every instance.

costs for load and renewables curtailment:

$$\min \sum_{i,t} \left(cost_{i,t}^{gen} + cost_{i,t}^{start} + cost_{i,t}^{stop} + cost_{i,t}^{ramp} \right) + \sum_{n,t} \left(cost_{n,t}^{lc} + cost_{n,t}^{rc} + cost_{n,t}^{rsr} \right) \tag{2.1}$$

The generation costs include fuel costs, CO_2 emission costs and variable operations and maintenance costs. The generation cost of a power plant is time depending (due to changing fuel and CO_2 emission prices) and output depending (due to the output-dependent generation efficiency). The non-linear cost curve is linearized and time-averaged as follows:[9]

$$cost_{i,t}^{gen} = NC_i \, z_{i,t} + MC_i \, g_{i,t} \qquad \forall i, \forall t \tag{2.2}$$

The start-up and shut-down costs follow from, respectively:[10]

$$cost_{i,t}^{start} = SUC_i \, v_{i,t} \qquad \forall i, \forall t \tag{2.3}$$

$$cost_{i,t}^{stop} = SDC_i \, w_{i,t} \qquad \forall i, \forall t \tag{2.4}$$

The ramping cost follows from:

$$0 \leq cost_{i,t}^{ramp} \geq RC_i \left(g_{i,t} - g_{i,t-1} \right) \tag{2.5}$$

$$0 \leq cost_{i,t}^{ramp} \geq RC_i \left(g_{i,t-1} - g_{i,t} \right) \tag{2.6}$$

The load curtailment cost follows from:

$$cost_{n,t}^{lc} = LCC_n \, lc_{n,t} \qquad \forall n, \forall t \tag{2.7}$$

The renewables curtailment cost follows from:

$$cost_{n,t}^{rc} = RCC_n \, rc_{n,t} \qquad \forall n, \forall t \tag{2.8}$$

[9] The cost curve can be approximated with multiple linear intervals, but this increases run times drastically while accuracy only increases slightly (Arroyo and Conejo, 2000; Frangioni et al., 2009). Moreover, time-dependent cost parameters $NC_{i,t}$ and $MC_{i,t}$ can be imposed to the unit commitment model.

[10] A more advanced formulation of the start-up cost takes account of the off-line time of the power plant and distinguishes between hot starts, warm start and cold starts (Arroyo and Conejo, 2000; Morales-España et al., 2013b).

The reserve allocation cost for load and renewables curtailment follows from:

$$cost^{rsr}_{n,t} = RAC^{lol}\, r^{lol}_{n,t} + RAC^{cur}\, r^{cur}_{n,t} \qquad \forall n, \forall t \tag{2.9}$$

Note that the reserve allocation cost for spinning reserves from conventional units is implicitly taken into account in the generation cost.

Market clearing

The market clearing constraint imposes the supply-demand balance at each node for each time step. The supply-demand balance consists of generation from conventional units, (dis)charging from storage units, generation from renewables, the electricity load and injections in the electricity grid.

$$\sum_i A^{plant}_{n,i}(z_{i,t}\,\underline{P_i} + g_{i,t}) + \sum_j A^{stor}_{n,j}\,(pd_{j,t} - pc_{j,t}) + RES_{n,t} - rc_{n,t} = D_{n,t} - lc_{n,t} + p_{n,t} \qquad \forall n, \forall t \tag{2.10}$$

Renewables and load curtailment

Electricity generation from renewables (and cogeneration units) is mainly driven by other factors than the electricity demand (e.g., weather conditions, subsidies) and is therefore only to a limited extent dispatchable. Renewable generation can be curtailed in the energy market or scheduled as reserves, but renewables curtailment is limited by the available renewable generation:[11]

$$0 \leq rc_{n,t} + r^{cur}_{n,t} \leq RES_{n,t} \qquad \forall n, \forall t \tag{2.11}$$

[11] In today's electricity markets, most of the renewable generation has priority access to the grid, meaning that renewable generators have an incentive to generate as much electricity as possible, regardless of any electricity market signal. As such, generation of renewable electricity sources can be modeled as negative load, resulting in a residual load (i.e., original load minus renewables generation) to be met by centralized and dispatchable units. However, renewable electricity generators are becoming increasingly integrated in the electricity market operation. As such, renewable generation units can be modeled in a similar way as conventional generation units, with the difference that renewable generation units have zero marginal generation costs (or even negative marginal generation costs if subsidized) and time-variable maximum power outputs (depending on the meteorological conditions). In the LUSYM model, renewable generation time series are imposed to the model with the possibility to curtail renewables at a certain cost. A high renewables curtailment cost corresponds to today's electricity markets with priority access for renewables, whereas a zero (or low) renewables curtailment cost corresponds to future electricity markets with active participation of renewables.

Load curtailment (or load shedding) can be scheduled in the energy market or as reserve, and is limited by the load:

$$0 \leq lc_{n,t} + r^{lol}_{n,t} \leq D_{n,t} \qquad \forall n, \forall t \tag{2.12}$$

Finally, renewables and load curtailment are non-negative:

$$rc_{n,t}\,,\, r^{cur}_{n,t}\,,\, lc_{n,t}\,,\, r^{lol}_{n,t} \geq 0 \qquad \forall n, \forall t \tag{2.13}$$

Power plant generation limits

A power plant can only generate power within a certain power range. It is important to highlight that the power plant output is defined as $gen_{i,t} = z_{i,t}\,\underline{P}_i + g_{i,t}$. The lower limit for the power output above the minimum power output is:

$$0 \leq g_{i,t} - r^{-}_{i,t} \qquad \forall i, \forall t \tag{2.14}$$

The upper generation limit for power plants with $\mathrm{MUT_i} \geq 2$ is given by:

$$\begin{gathered} g_{i,t} + r^{+}_{i,t} \leq (\overline{P}_i - \underline{P}_i)\, z_{i,t} - (\overline{P}_i - SU_i)\, v_{i,t} - (\overline{P}_i - SD_i)\, w_{i,t+1} \\ \forall i \in MUT_i \geq 2, \forall t \end{gathered} \tag{2.15}$$

If $\mathrm{MUT_i} = 1$, Eq. (2.15) is replaced by:

$$\begin{gathered} g_{i,t} + r^{+}_{i,t} \leq (\overline{P}_i - \underline{P}_i)\, z_{i,t} - (\overline{P}_i - SU_i)\, v_{i,t} - \max(SU_i - SD_i, 0)\, w_{i,t+1} \\ \forall i \in MUT_i = 1, \forall t \end{gathered} \tag{2.16}$$

$$\begin{gathered} g_{i,t} + r^{+}_{i,t} \leq (\overline{P}_i - \underline{P}_i)\, z_{i,t} - (\overline{P}_i - SD_i)\, w_{i,t+1} - \max(SD_i - SU_i, 0)\, v_{i,t} \\ \forall i \in MUT_i = 1, \forall t \end{gathered} \tag{2.17}$$

Eqs. (2.14)-(2.17) describe the convex hull of the power plant generation limits (Morales-España, 2014).

Additional generation limit constraints can be imposed by considering multiple time steps (Ostrowski et al., 2012), however it is not sure that these constraints result in a speed-up given that they make the formulation tighter but less

compact. These additional constraints are:

$$g_{i,t} + r^{+}_{i,t} \leq (\overline{P}_i - \underline{P}_i)\, z_{i,t+K_i} + \sum_{k=1}^{K_i} (SD_i - \underline{P}_i + (k-1)\, RD_i) w_{i,t+k} - \sum_{k=1}^{K_i} (\overline{P}_i - \underline{P}_i)\, v_{i,t+k} \qquad \forall i, \forall t = 1, ...T - K \tag{2.18}$$

with $K_i = \min\{MUT_i\,;\, (\overline{P}_i - SD_i)/RD_i + 1\,;\, T - t\}$. Eq. (2.18) is only tightening Eq. (2.15) if K $\geq$ 2.

Forced or planned power plant outages can force power plants to stay offline (see subsection 2.2.2).

$$z_{i,t} \leq AV_{i,t} \tag{2.19}$$

Finally, generation and reserve scheduling variables are non-negative or binary.

$$gen_{i,t}\,,\, g_{i,t}\,,\, r^{+}_{i,t}\,,\, r^{-}_{i,t} \geq 0 \qquad \forall i, \forall t \tag{2.20}$$

$$z_{i,t}\,,\, v_{i,t}\,,\, w_{i,t} \in \{0, 1\} \qquad \forall i, \forall t \tag{2.21}$$

Power plant ramping limits

The basic ramping-up and ramping-down constraints are, respectively:

$$g_{i,t} + r^{+}_{i,t} - g_{i,t-1} \leq RU_i\, z_{i,t} + (SU_i - \underline{P}_i - RU_i)\, v_{i,t} \qquad \forall i, \forall t \tag{2.22}$$

$$g_{i,t-1} - g_{i,t} + r^{-}_{i,t} \leq RD_i\, z_{i,t-1} + (SD_i - \underline{P}_i - RD_i)\, w_{i,t} \qquad \forall i, \forall t \tag{2.23}$$

Additional ramping constraints can be imposed by considering more time steps (Ostrowski et al., 2012), however it is again not sure that these additional constraints result in a speed-up as they make the formulation tighter but also less compact. Additional ramping-up constraints are:

$$g_{i,t} + r^{+}_{i,t} - g_{i,t-1} \leq RU_i\, z_{i,t} - (RU_i - SD_i + \underline{P}_i)\, w_{i,t+1} + (SU_i - \underline{P}_i - RU_i)\, v_{i,t} \qquad \forall t, \forall i \in RU_i > SD_i - \underline{P}_i \;\&\; MUT_i \geq 2 \tag{2.24}$$

$$g_{i,t} + r^{+}_{i,t} - g_{i,t-2} \leq 2\, RU_i\, z_{i,t} + (SU_i - \underline{P}_i - RU_i)\, v_{i,t-1} + (SU_i - \underline{P}_i - 2\, RU_i)\, v_{i,t} \qquad \forall t, \forall i \in MUT_i \geq 2 \;\&\; MDT_i \geq 2 \tag{2.25}$$

Analogously, additional ramping-down constraints are:

$$g_{i,t-1} - g_{i,t} + r^{-}_{i,t} \leq RD_i\, z_{i,t} + (SD_i - \underline{P}_i)\, w_{i,t} - RD_i\, v_{i,t} \\ -(RD_i - SU_i + \underline{P}_i)\, v_{i,t-1} \qquad \forall t, \forall i \in RD_i > SU_i - \underline{P}_i \;\&\; MUT_i \geq 2 \tag{2.26}$$

$$g_{i,t-2} - g_{i,t} + r^{-}_{i,t} \leq 2\, RD_i\, z_{i,t} + (SD_i - \underline{P}_i)\, w_{i,t-1} - 2\, RD_i\, (v_{i,t-1} + v_{i,t}) \\ +(SD_i - \underline{P}_i + RD_i)\, w_{i,t} \qquad \forall t, \forall i \in MUT_i \geq 2 \;\&\; MDT_i \geq 2 \tag{2.27}$$

Power plant minimum up and down times

The minimum down time and up time constraints are given by, respectively:

$$1 - z_{i,t} \geq \sum_{t'=t+1-MDT_i}^{t} w_{i,t'} \qquad \forall i, \forall t \tag{2.28}$$

$$z_{i,t} \geq \sum_{t'=t+1-MUT_i}^{t} v_{i,t'} \qquad \forall i, \forall t \tag{2.29}$$

In addition to the above constraints, the following logic relationship between the different power plant statuses is needed:

$$z_{i,t-1} - z_{i,t} + v_{i,t} - w_{i,t} = 0 \qquad \forall i, \forall t \tag{2.30}$$

Eqs. (2.28)-(2.30) describe the convex hull of the minimum up and down time constraints (Rajan and Takriti, 2005).

Spinning reserve constraints

Spinning reserve constraints can be imposed to reserve zones, consisting of one or multiple nodes. Upward spinning reserves can be delivered by online power plants, load curtailment and curtailed renewable generation. Downward spinning reserves can be delivered by online power plants and renewables curtailment. Upward and downward spinning reserve requirements are given by, respectively:

$$\sum_{i} A^{rsr}_{s,i}\, r^{+}_{i,t} + \sum_{n} A^{rsr}_{s,n}\, (r^{lol}_{n,t} + rc_{n,t}) \geq SR^{+}_{s,t} \qquad \forall s, \forall t \tag{2.31}$$

$$\sum_i A^{rsr}_{s,i}\, r^-_{i,t} + \sum_n A^{rsr}_{s,n}\, r^{cur}_{n,t} \geq SR^-_{s,t} \qquad \forall s, \forall t \tag{2.32}$$

Storage unit constraints

Different storage technologies, such as pumped hydro storage and electric batteries, can be implemented in the unit commitment model by the same set of constraints. The energy balance of a storage unit is given by:

$$pe_{j,t} = pe_{j,t-1} + \Delta t\, pc_{j,t}\, \eta^c_j - \frac{\Delta t\, pd_{j,t}}{\eta^d_j} \qquad \forall j, \forall t \tag{2.33}$$

The energy level of a storage unit and its charging and discharging power rates are limited:

$$0 \leq pc_{j,t} \leq PC_j \qquad \forall j, \forall t \tag{2.34}$$

$$0 \leq pd_{j,t} \leq PD_j \qquad \forall j, \forall t \tag{2.35}$$

$$\underline{PE}_j \leq pe_{j,t} \leq \overline{PE}_j \qquad \forall j, \forall t \tag{2.36}$$

Grid constraints

A DC power flow representation of the electricity grid is implemented, including the possibility to add a zero-imbalance flow to the line flows. The DC power flow is a linearized description of the electricity grid characteristics, respecting Kirchhoff's voltage and current laws. Injection shift factors (ISFs) or power transfer distribution factors (PTDFs) give the linear relationship between power injections in the grid and flows through transmission lines (see chapter 3 for the difference between ISF and PTDF).

$$f_{l,t} = \sum_n PTDF_{l,n}\, p_{n,t} + F^0_l \quad \forall l, \forall t \tag{2.37}$$

$$\sum_n p_{n,t} = 0 \qquad \forall t \tag{2.38}$$

$$\underline{F}_l \leq f_{l,t} \leq \overline{F}_l \qquad \forall l, \forall t \tag{2.39}$$

Alternatively, a trade-based grid representation can be used. In a trade-based grid representation, only Kirchhoff's current law is respected. If the trade-based

grid representation is used, Eqs. (2.37)-(2.39) are replaced by:

$$p_{n,t} = \sum_{l} A_{l,n}\, f_{l,t} \qquad \forall n, \forall t \tag{2.40}$$

$$\underline{F}_l \leq f_{l,t} \leq \overline{F}_l \qquad \forall l, \forall t \tag{2.41}$$

Chapter 3 discusses grid constraints in unit commitment modeling in more detail.

Boundary conditions and optimality gap

The UC model is solved in sequential optimization blocks if the total optimization period is too large to optimize at once (e.g., one year can be solved as 52 weekly optimization blocks). Consecutive optimization blocks are linked by means of sequential boundary conditions, meaning that the system state at the end of an optimization is the starting condition for the next optimization block. Consecutive optimization blocks can overlap, in order to obtain a more optimal unit commitment decision.

An optimality gap is imposed to the MIP solver (also referred to as stopping tolerance). The solver will stop the solution process when the optimality gap is reached and return the best solution found so far. For instance, an optimality gap of 1% indicates that the returned solution (i.e., the upper bound of the MIP minimization problem) has an operational system cost that is at most 1% higher than the optimal feasible cost (i.e., the lower bound of the MIP minimization problem). The smaller the optimality gap, the larger run times. In this dissertation, optimality gaps between 0.05% and 1% are used, depending on the case study. The imposed optimality gap is always an order of magnitude smaller than the cost difference between the studied scenarios, in order to draw solid conclusions (e.g., if two scenarios have a cost difference of 1%, the imposed optimality gap is at most 0.1%).

2.2.2 Power plant outages

The unit commitment scheduling is preceded by a power plant outage scheduling. One distinguishes between planned outages (e.g., yearly maintenance) and unplanned or forced outages (e.g., technical failure). Planned outages can be scheduled at moments of low (forecasted) residual load (i.e., load minus renewables generation). The planned outage scheduling problem is formulated as a deterministic mixed-integer linear program, with a time frame of one year

and a time step of one day. Forced outages are randomly distributed during the year. The duration of a planned and forced outage can be imposed to the outage scheduling module (typically, outages are assumed to last for one day).

Objective function

The objective function of the planned outage scheduling is to minimize the maximum generation margin (i.e., the margin between available generation capacity and load). In other words, outages are planned during moments with large generation margins. The planned outage scheduling is performed for each node separately. Since the time step is one day, the daily average load and renewables generation are used in the power plant outage module.

$$\min M \tag{2.42}$$

$$M \geq \sum_i A_{n,i}^{plant}\, op_{i,t}\, \overline{P}_i + RES_{n,t} - D_{n,t} \qquad \forall t \tag{2.43}$$

The binary variable $op_{i,t}$ is zero if power plant i undergoes a planned outage at day t, otherwise $op_{i,t}$ is one.

Total duration of planned outages

The number of days with a planned outage is imposed as follows:

$$\sum_t 1 - op_{i,t} = OP_i \qquad \forall i \tag{2.44}$$

The planned outage schedule $op_{i,t}$ and the forced outage schedule $of_{i,t}$ (which is determined randomly) combine into the power plant availability $AV_{i,t}$ as follows:

$$AV_{i,t} = op_{i,t}\; of_{i,t} \qquad \forall i, \forall t \tag{2.45}$$

2.3 Validation of the model

The LUSYM model is validated in two different ways: (1) by comparing its performance with existing unit commitment models and (2) by comparing its simulation results with historically observed generation data.

2.3.1 Benchmarking with existing unit commitment models

The performance of the unit commitment model, in terms of optimality of simulation results and run times, is compared with three commercial unit commitment models: Promod (Ventytx Energy, 2015), Plexos (Energy Exemplar, 2015) and Antares (Doquet et al., 2008). This benchmarking exercise is repeated every year (from 2013 to 2016) for LUSYM in order to track its progress. The aim of this benchmarking exercise is to give a rough idea about how LUSYM compares with other unit commitment models. The results presented below should be interpreted with care since only one specific benchmarking case is considered.[12]

As benchmarking case, a 2030 scenario of the Central Western European electricity sector (i.e., Belgium, France, Germany, Luxembourg and the Netherlands) is considered (ENTSO-E, 2014). The electricity system contains 552 power plants and 4 pumped storage units (storage scheduling is optimized over the week). The network model consists of 5 nodes and 7 lines, represented by a trade-based network model. One full year is simulated in weekly blocks of 168 hours with an hourly time resolution. No power plant outages and reserve requirements are imposed. Load can be curtailed at a cost of 10,000 EUR/MWh and renewables at a cost of 0 EUR/MWh. All simulations are run on an Intel®Core^{TM} i7-2620M CPU@2.7 GHz with 8 GB RAM. The LUSYM model is solved by Gurobi with a 1% optimality gap (i.e., the returned solution has an operational system cost that is at most 1% higher than the optimal feasible cost). The MIP model contains about 883,000 equations and 642,000 variables of which 318,000 binary variables. A detailed overview of the input data of this benchmarking case can be found in Appendix A.

Fig. 2.1 gives an overview of the performance of the different models, in terms of optimality (i.e., minimization of generation cost) and run times. First, it is clear that the LUSYM model performs similarly to Plexos–which is also a MIP-based model–both in terms of optimality and run times (the difference in operational system costs between Plexos and LUSYM are within the optimality gap). Note that one can only fairly compare simulation results from models run in the same year, due to ongoing software developments. As such, one should compare the run time of Plexos with the run time of the LUSYM 2013 version. LUSYM outperforms the more heuristic-based models Promod and Antares in terms of optimality with about 15%, while the run time is about the same for Promod and considerably shorter for Antares (for the Promod 2013 version and the Antares 2015 version). Antares is able to drastically reduce run times, mainly by relaxing binary constraints in the unit commitment problem.

[12]This benchmarking exercise is performed in collaboration with Elia System Operator. The Promod and Antares simulations were run by Elia System operator.

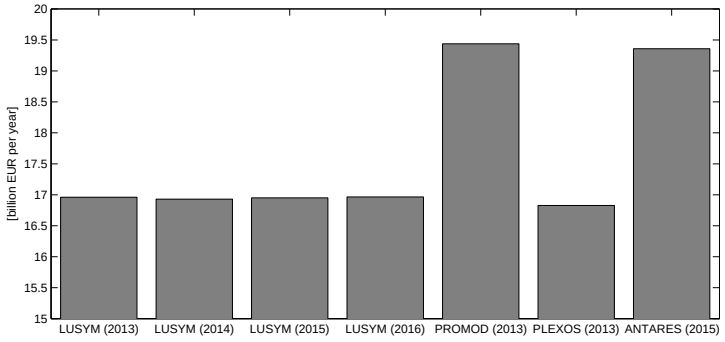

(a) Total operational system cost.

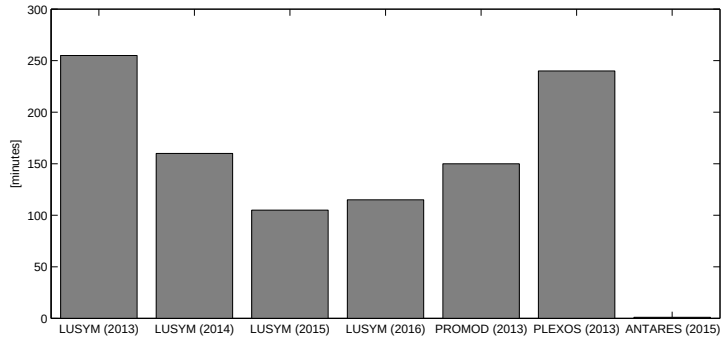

(b) Run times.

Figure 2.1: Comparison of the LUSYM model performance, in terms of optimality of simulation results and run times, with three commercial unit commitment models: Promod, Plexos and Antares.

Promod and Antares underuse the flexibility in the electricity system, such as pumped storage and cross-border transmission, resulting is higher system costs. Second, LUSYM shows a remarkable speed-up over the course of the years (although there is a slight increase in run times comparing the 2015 version with the 2016 version). This speed-up is caused by three factors: (1) improvements in solver performance (the 2013 benchmarking case was solved by Gurobi 5.5, the 2016 case by Gurobi 6.5), (2) a more compact and tight formulation of the unit commitment problem, and (3) a more efficient implementation of the code in Matlab and GAMS (e.g., reading the bulk part of the input data only once into GAMS, instead of for every optimization separately).

2.3.2 Benchmarking with historical generation data

The simulation results of LUSYM are compared with historical generation data for the 2013 European electricity system (ENTSO-E, 2015a). The benchmarking case considers the full ENTSO-E area, consisting of 32 countries: Austria, Belgium, Bosnia-Herzegovina, Bulgaria, Croatia, Czech Republic, Denmark, Estonia, Finland, France, Germany, Greece, Hungary, Ireland, Italy, Latvia, Lithuania, Luxembourg, Macedonia, Montenegro, Netherlands, Norway, Poland, Portugal, Romania, Serbia, Slovakia, Slovenia, Spain, Sweden, Switzerland and the United Kingdom. The generation portfolio contains 2,692 power plants and 23 pumped storage units (storage scheduling is optimized over the day). The network model consists of 32 nodes and 56 lines, represented by a trade-based network model. A full year is considered in daily blocks with an hourly time resolution. No reserve requirements are imposed. Load and renewables can be curtailed at a cost of 3,000 EUR/MWh. The unit commitment model is solved by Cplex with a 1% optimality gap. A detailed overview of the input data of this benchmarking case can be found in Appendix A.

The model is calibrated in order to match simulation results with historically observed generation. Generation from nuclear power plants and lignite-fired power plants is reduced for some countries by increasing the number of planned outages and decreasing the installed capacity.

Fig. 2.2 shows the simulation results and the historical observed generation per country for each generation technology. Although it is not possible to match historical generation perfectly due to inherent simplifications of a deterministic unit commitment model, such as the lack of uncertainty, the LUSYM model is able to reproduce historical generation data acceptably well. The model takes about 17 hours to run on a laptop (Intel®Core^{TM} i7-2620M CPU@2.7 GHz with 8 GB RAM).

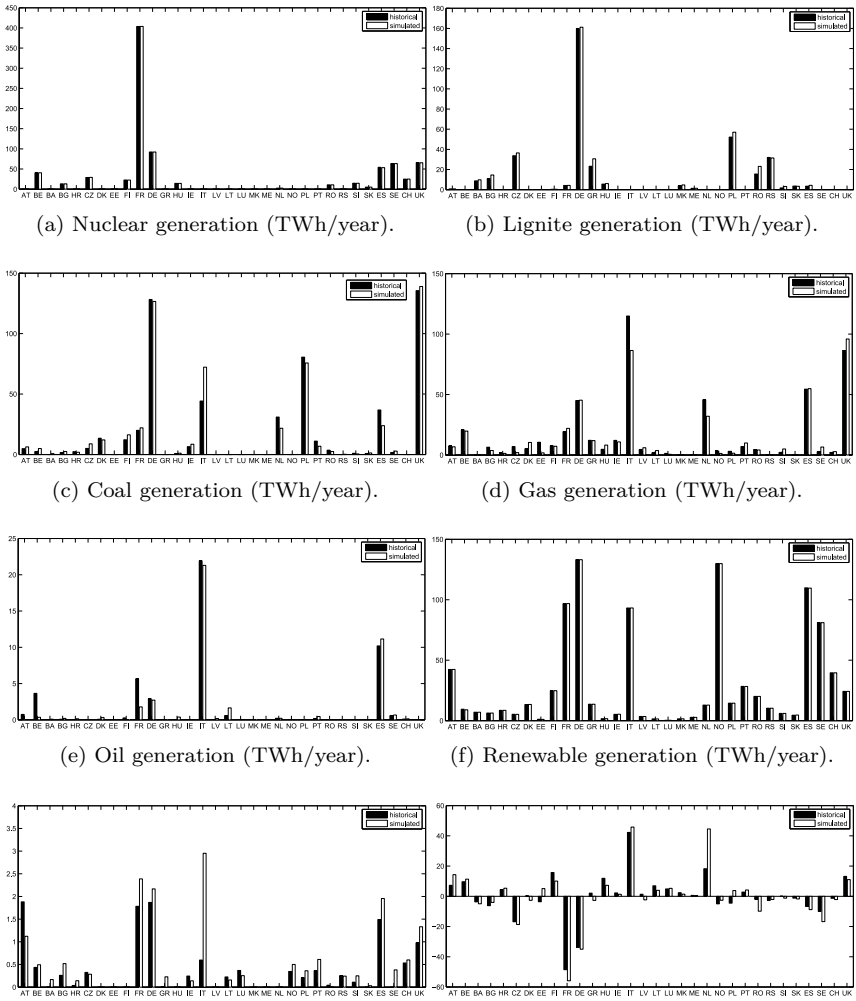

(a) Nuclear generation (TWh/year).

(b) Lignite generation (TWh/year).

(c) Coal generation (TWh/year).

(d) Gas generation (TWh/year).

(e) Oil generation (TWh/year).

(f) Renewable generation (TWh/year).

(g) Net pumped storage consumption (TWh/year).

(h) Net import (TWh/year).

Figure 2.2: The LUSYM model is able to reproduce historical generation data acceptably well (case study of the 2013 European electricity system). The black bars refer to historical data, the white bars refer to simulation results.

2.4 Summary and conclusions

This chapter presents LUSYM, a state-of-the-art mixed-integer linear program (MIP) of a deterministic security-constrained unit commitment model. LUSYM has been developed during this PhD research and has been used to study the impact of energy and climate policies on electricity generation.

The presented formulation is tight and compact, including power plant constraints, renewables curtailment, load curtailment, storage units, transmission grid constraints and spinning reserve constraints. The model also includes a planned outage scheduling module. The model is implemented in GAMS and solved with the latest release from Cplex or Gurobi MIP solver.

Benchmarking simulations show that the model is competitive with existing commercial unit commitment models, in terms of optimality and run times, and that the model is able to reproduce historically observed generation data. The run time of LUSYM is limited by a tight and compact formulation, an efficient implementation and the use of best-in-class MIP solvers.

Chapter 3

Network models in unit commitment

Chapter based on:

K. Van den Bergh and E. Delarue. An improved method to calculate injection shift keys. Electric Power Systems Research, 134:197-204, 2016.

K. Van den Bergh, E. Delarue, and W. D'haeseleer. DC power flow in unit commitment models. KU Leuven Working Paper, 2014.[1]

Abstract: Transmission network constraints become increasingly relevant in generation scheduling models, given the ongoing integration of market zones and the deployment of renewables in remote areas. Typically, a DC power flow is used in generation models. A full nodal network representation is often not possible due to computational limitations. Therefore, reduced zonal network models are needed. Moreover, zonal network models are sometimes preferred to nodal network models for historical and socio-political reasons. For instance, the current European market design is based on a zonal network model. In a zonal model, the number of nodes is limited by grouping nodes into zones. A crucial step in the nodal-zonal network reduction is the calculation of injection shift keys (ISKs). Injection shift keys denote the nodal contribution to the zonal generation balance and are needed to compile different nodes into one equivalent node. This chapter starts off with a detailed discussion on DC power flow and nodal-zonal network reductions. Further on in this chapter, an improved

[1]The publications on which this chapter is based benefited from discussions with, apart from the co-authors, D. Van Hertem (KU Leuven) and P. Van Roy (Elia).

method to calculate injection shift keys is proposed. According to the improved method, the generation and load portfolio is split in different categories, and injection shift keys are determined separately for each category. As such, zonal network representations are obtained that better approach the true physical characteristics of the network. A case study of the central European electricity system indicates that the improved method is able to approximate the nodal network without a considerable increase in computational cost.

Keywords: DC power flow, power transfer distribution factor (PTDF), nodal-zonal network reduction, injection shift key (ISK), generation shift key (GSK), demand shift key (DSK).[2]

3.1 Introduction

A proper representation of transmission networks in electricity system models is becoming increasingly important. Given the integration of different market zones and the deployment of renewables in sometimes remote areas in the network, transmission constraints become more relevant and should hence be taken into account in operational and planning models of the electricity generation sector (Kardakos et al., 2014).

A full non-linear AC power flow would be the most appropriate network representation in electricity generation models such as unit commitment models (Kumar et al., 2004). However, due to the high computational cost of an AC power flow in a unit commitment model, a DC power flow is often preferred (Stott et al., 2009). The DC power flow gives a linear relationship between power injections and power flows by means of power transfer distribution factors (PTDF). The difference in power flows resulting from a DC and an AC model are estimated at about 5% on average for high voltage grids, although power flow deviations for single lines can be larger (Purchala et al., 2005b).[3] In this chapter, a DC power flow representation of the network is discussed.

A full implementation of the network in electricity generation models is not always feasible due to the large size of real-life networks and the concomitant high computational cost. Therefore, reduced network models are needed, representing as good as possible the characteristics of the full network model without jeopardizing the computational tractability. Reduced network models can also be relevant for congestion management purposes in electricity markets

[2]All abbreviations and symbols used in this chapter are listed and explained at the outset of this dissertation.

[3]The 5% difference between DC and AC power flow models refers to the Mean Absolute Percent Error (MAPE) of the calculated line flows.

(Ehrenmann and Smeers, 2005). Policy makers might prefer a reduced network model to a full network implementation for, besides computational reasons, historical and socio-political reasons. For instance, current electricity markets in Europe are based on a strongly reduced model of the electricity network.

A standard network reduction technique is equivalencing of the external network by computing impedances and eliminating unnecessary elements (Ward, 1949; Deckmann et al., 1980a,b; Housos et al., 1980; Tinney and Bright, 1987; Enns and Quada, 1991). Equivalent networks have been used for short circuit analysis as they can reproduce the voltages and currents of the remaining buses. However, equivalent networks are not able to approximate flows of the eliminated branches. Therefore, the usage of equivalent networks is limited in power flow analysis (Oh, 2010). Another network reduction technique consists of grouping nodes in a limited number of zones, hereby reducing the number of nodes in the network (Bart and Andreewsky, 2005; Papaemmanouil and Andersson, 2011). A zone is assumed to be a copper plate, meaning that transmission constraints (and losses) within a zone can be neglected. The remaining transmission lines between zones can be grouped in inter-zonal links. This second network reduction technique is referred to as the nodal-zonal reduction in this chapter.

The nodal-zonal reduction technique starts from a full nodal description and derives a simplified zonal network in three sequential steps. First, nodes with similar electric characteristics are clustered in zones (Oh, 2012; Klos et al., 2014; Biskas et al., 2011; Kang et al., 2013; Shayesteh et al., 2015). Second, nodes within a zone are replaced by an equivalent node with–approximately–the same relationship between power injections in the network and power flows through the remaining inter-zonal lines (Cheng and Overbye, 2005; Purchala et al., 2005a; Oh, 2010; Doquet, 2015). Third, the remaining inter-zonal lines between two zones can be replaced by one equivalent inter-zonal link (Duthaler et al., 2008; Oh, 2012).

This chapter deals with the second step in the nodal-zonal reduction, i.e., grouping nodes in an equivalent node. A commonly used grouping approach is based on injection shift keys (ISKs) (Vukasovic and Skuletic, 2007). ISKs are a mathematical expression of the spatial distribution of electricity generation and load within a zone. Each node within the zone contributes to the equivalent node in accordance with its ISK. ISKs are an important parameter, influencing the nodal-zonal reduction to a great extent. Nevertheless, different formulas can be found in the literature to calculate ISKs. Certain papers consider both generation and load, and determine the ISK as the nodal contribution relative to the zonal balance, see for instance Oh (2010). Other papers consider only generation and determine the ISK as the nodal generation relative to the total generation in the zone, see for instance the flow-based market coupling methodology (Amprion et al., 2014). It is often unclear why a certain ISK

calculation method is preferred. Moreover, ISKs are time-dependent as the spatial distribution of generation and load changes in time. This results in time-averaging errors when a daily or weekly average zonal network model is needed.

The chapter proceeds as follows. Section 3.2 discusses the DC power flow. Section 3.3 presents in detail the nodal-zonal network reduction technique. Section 3.4 discusses the challenges related to injection shift keys and proposes an improved method to calculate them. This improved method is evaluated in section 3.5 based on a case study of the central European electricity network. Section 3.6 concludes.

3.2 DC power flow

The DC power flow is a linearization of the AC power flow equations, based on three assumptions: (i) line resistances are negligible relative to line reactances, (ii) the voltage profile is flat and (iii) the voltage angle differences between neighboring nodes are small (see Appendix B for a description of the AC power flow). Given these assumptions, the static AC power flow equation for active power injections simplifies to:

$$\mathbf{P^N} = \mathbf{B^{bus}}\,\boldsymbol{\theta} \tag{3.1}$$

The active power flow through a transmission line can be written as:

$$\mathbf{F^N} = \mathbf{B^{branch}}\,\boldsymbol{\theta} \tag{3.2}$$

Substituting the voltage angles $\boldsymbol{\theta}$ from Eqs. (3.1)-(3.2) gives the DC power flow equation:

$$\mathbf{F^N} = \mathbf{ISF}\ \mathbf{P^N} \tag{3.3}$$

or in scalar format:

$$F^N_{l,t} = ISF_{l,n}\ P^N_{n,t} \quad \forall\, l, \forall\, t \tag{3.4}$$

with

$$\mathbf{ISF} = \begin{bmatrix} 0 & \mathbf{ISF^*} \end{bmatrix} \tag{3.5}$$

$$\mathbf{ISF^*} = \mathbf{B^{branch*}} \left(\mathbf{B^{bus*}}\right)^{-1} \tag{3.6}$$

Since $\mathbf{B^{bus}}$ is a rank-deficient matrix, Eq. (3.6) can only be solved after removing the reference node. In this example, node 1 is denoted as reference

node. The full LxN-dimension of the injection shift factor matrix (**ISF**) can be restored by inserting a zero column in the reduced ISF matrix (see Eq. (3.5)).

An element in the ISF matrix gives the sensitivity of the active power flow through line l with respect to an additional power injection in node n and with the reference node as sink. Given the properties of linearity and superposition, the sensitivity of line flows to power injections in node n_1 with node n_2 as sink can be written as a linear combination of the ISF-elements with the reference node as sink (Guler et al., 2007):

$$PTDF^{N}_{l,n_1-n_2} = ISF_{l,n_1} - ISF_{l,n_2} \tag{3.7}$$

An element in the nodal power transfer distribution factor matrix ($\mathbf{PTDF^N}$) gives then the sensitivity of the active power flow through line l with respect to an additional power injection in node n_1 and withdrawal at node n_2. The nodal PTDF matrix hence does not depend on the chosen reference node, unlike the ISF matrix. The nodal PTDF matrix depends on the network topology but not on the operating point of the system (although the accuracy of the DC power flow depends on the system operating point, see below) (Baldick, 2003).

The above mentioned equations are valid for every time step. An additional equation is added to the DC power flow equation to ensure a unique solution after removing the reference node from Eq. (3.6). This equation imposes the sum of all power injections to be zero:

$$\sum_{n} P^{N}_{n,t} = 0 \quad \forall\, t \tag{3.8}$$

Consider the simple 4-node network in Fig. 3.1.a. Assuming the same line susceptance for all lines (0.5 p.u.), defining positive flow directions as denoted in Fig. 3.1.a, and taking node 1 as the reference node, the ISF matrix becomes:

$$\mathbf{ISF} = \begin{bmatrix} 0 & -0.25 & -0.75 & -0.5 \\ 0 & -0.25 & 0.25 & -0.5 \\ 0 & -0.25 & 0.25 & 0.5 \\ 0 & 0.75 & 0.25 & 0.5 \end{bmatrix} \tag{3.9}$$

The ISF matrix indicates that a power injection of 1 MW in node 3 (see third column in ISF matrix) with off-take in the reference node (i.e., node 1) results in a line flow of -0.75 MW in line A and 0.25 MW in lines B, C and D.

Appendix B.2 gives a more comprehensive description of the DC power flow, including a step-by-step derivation of the ISF matrix for the simple 4-node

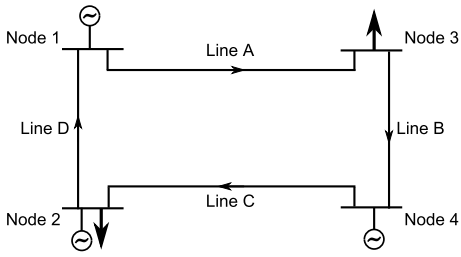

(a) Nodal network.

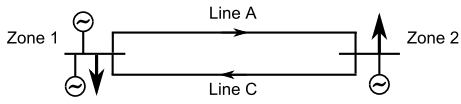

(b) Zonal network.

Figure 3.1: Simple electricity network to illustrate the nodal-zonal network reduction. Generation units are located at node 1 (base load unit), node 2 (peak load unit) and node 4 (base load unit). Load is located at nodes 2 and 3. Zone 1 consists of nodes 1 and 2, zone 2 of nodes 3 and 4.

network. Appendix B.3 describes the DC power flow with power flow controlling devices such as phase shifting transformers and high voltage DC lines. Appendix B.4 discusses the DC power flow with the N-1 security criterion.

The accuracy of the DC power flow depends on the accuracy of the DC power flow assumptions. The higher the voltage level of the considered grid, the more valid the assumption on negligible line resistances is. In the Belgian high voltage grid (70-380 kV), the average resistance/reactance ratio ranges from 10% at 380 kV to 32% at 70 kV. According to Purchala (2005), for resistance/reactance ratios below 50%, the average error is always smaller than 5% and falls below 2% for resistance/reactance ratios below 20%. The second assumption is a flat voltage profile. It is however almost impossible to avoid voltage fluctuations in an electricity grid. For small standard deviations in voltages (less than 0.01 p.u.), the average error made by this assumption is limited to 5%.[4] However, realistic examples of voltage fluctuations in actual power systems show that this assumption is the most critical one and the largest source of DC power flow errors (Purchala et al., 2005b). The third assumption is small voltage angle differences between neighboring nodes. In general, this assumption is correct if the grid is weakly loaded. However, even during peak load, this assumption is justifiable in a strongly meshed grid (e.g., the Belgian grid). For example, a

[4]The error is defined as the relative difference in line flows between the AC and the DC power flow solution, averaged over all lines.

winter peak load of 13 GW in the Belgian high voltage grid leads to a maximum voltage angle difference between neighboring nodes of 6°. In this case, which only occurs on a small number of lines, the error is less than 1%.

In general, one can conclude that for high voltage grids–which are mostly the ones looked at in generation models–the accuracy of DC power flow is around 5%, compared to AC power flow and averaged over all lines. The deviation on single line flows can be much larger. As such, the accuracy of DC power flow is acceptable, but one should always keep the limitations of DC power flow in mind and be careful with drawing conclusions about single lines (Purchala et al., 2005b). Note that the deviation between DC power flow simulations and the real grid flows is probably larger than the error made by using a linear DC grid model instead of a more accurate non-linear AC grid model. Simplifications of the grid topology (e.g., neglecting the grid at lower voltage levels), assumptions on the grid topology (e.g., configuration of substations) and other input data related difficulties cause deviations between AC power flow simulations and reality.

3.3 Nodal-zonal network reduction

The nodal-zonal network reduction starts from a full nodal PTDF matrix and ends up with a simplified zonal PTDF matrix. The nodal-zonal reduction method is illustrated by a simple example (see Fig. 3.1).

3.3.1 Clustering nodes into zones

The first step in reducing the nodal to a zonal PTDF matrix is defining the zones. Nodes should be clustered such that no congestion occurs within a zone, and that nodes within the same zone have a similar impact on the inter-zonal links. A well-known clustering approach is based on locational marginal prices (LMP, also referred to as nodal prices). No congestion occurs between neighboring nodes with the same LMPs and hence these nodes can be grouped in one zone. Another clustering principle is based on nodal PTDFs. Nodes with similar nodal PTDFs are grouped in a zone. The above mentioned clustering approaches are based on electric characteristics of the network. However, in real-life examples, nodes are often clustered into zones based on administrative regions (e.g., one zone per country or province).

Clustering algorithms are not part of this dissertation and it is assumed that the zones are already defined.

In the simple example (see Fig. 3.1), nodes 1-2 are grouped in zone 1 and nodes 3-4 in zone 2. The intra-zonal lines B and D can be removed from the ISF matrix, resulting in the node-to-link PTDF matrix:

$$\mathbf{PTDF^{N*}} = \begin{bmatrix} 0 & -0.25 & -0.75 & -0.5 \\ 0 & -0.25 & 0.25 & 0.5 \end{bmatrix} \tag{3.10}$$

The node-to-link PTDF matrix has as number of rows the number of inter-zonal lines (i.e., lines A and C in the considered example) and as number of columns the number of nodes (i.e., 4 nodes in the considered example). The number of columns in the node-to-link PTDF is reduced from the number of nodes to the number of zones (i.e., 2 zones in the considered example) in the following subsection.

3.3.2 Zonal PTDF matrix

In a second step, the nodes within a zone are replaced by one equivalent node and the zonal PTDF matrix is determined. The zonal PTDF matrix gives the linear relation between the flow on inter-zonal lines and zonal power injections.

The zonal PTDFs are derived from the node-to-link PTDF matrix by means of injection shift keys (ISKs). ISKs indicate the nodal contribution to (a change in) the zonal balance. As such, ISKs contain information about the spatial distribution of generation within a zone.

In this chapter, the ISKs are calculated as the nodal power injection divided by the zonal generation balance:

$$\begin{aligned} ISK_{n,z,t} &= \frac{P^N_{n,t}}{\sum_{n \in z} P^N_{n,t}} \quad \forall\, z, \forall\, n \in z, \forall\, t \\ ISK_{n,z,t} &= 0 \quad \forall\, z, \forall\, n \notin z, \forall\, t \end{aligned} \tag{3.11}$$

The nodal power injection $P^N_{n,t}$ can be positive (injection in the network) or negative (off-take from the network). The sum of each column in the ISK matrix is one. The ISK cannot be determined in case of balanced zones (i.e., $\sum_{n \in z} P^N_{n,t} = 0$).

ISKs have to be known a priori to derive a zonal network, whereas the zonal network is needed to determine the power injections and hence the ISKs. Therefore, ISKs are determined a priori based on expected nodal power injections. In this chapter, the ISKs are based on a nodal simulation. In real-life applications, ISKs are determined based on simplified simulations and/or the expertise of

system operators. However, the use of the nodal simulations to calculate the ISKs is justified since the aim of this chapter is to compare an improved ISK-calculation method with the standard method, which can be done as long as both methods are based on the same assumptions.

The zonal PTDF matrix follows from the matrix multiplication of the node-to-link PTDF matrix with the ISK matrix. This multiplication indicates that the columns of the zonal PTDF matrix are a weighted sum of the columns of the node-to-link PTDF matrix, based on the spatial distribution of generation and load within a zone.

$$\mathbf{PTDF^{Z}} = \mathbf{PTDF^{N*}}\ \mathbf{ISK} \tag{3.12}$$

Consider the simple example of Fig. 3.1 and assume that zone 1 exports 100 MW to zone 2 and nodal power injections are as follows: P_1 = 120 MW, P_2 = -20 MW, P_3 = -150 MW, P_4 = 50 MW. The ISK matrix and the zonal PTDF matrix for the simple example are, respectively:

$$\mathbf{ISK} = \begin{bmatrix} 1.2 & 0 \\ -0.2 & 0 \\ 0 & 1.5 \\ 0 & -0.5 \end{bmatrix} \tag{3.13}$$

$$\mathbf{PTDF^{Z}} = \begin{bmatrix} 0.050 & -0.875 \\ 0.050 & 0.125 \end{bmatrix} \tag{3.14}$$

ISKs can correspond to a change of the system state relative to a so-called base case. One speaks then of an *incremental* ISK matrix. A base case is, for instance, a system state in which each zone is balanced (i.e., no net export or import). An incremental ISK matrix indicates the nodal contribution to a change in the zonal balance. A ISK matrix can also correspond to a single system state (i.e., *absolute* ISK matrix), indicating the nodal contribution to the zonal balance. The zonal PTDF matrix following from incremental ISKs is an incremental PTDF matrix and only valid for the considered base case. The base case causes transmission flows, both within the zones and between the zones. Therefore, a term is added to the zonal DC power flow, corresponding to the inter-zonal flows in the base case. In case of absolute ISKs, the base-case flows are zero.

The zonal DC power flow equation becomes:

$$\mathbf{F^{Z}} = \mathbf{PTDF^{Z}}\ \mathbf{P^{Z}} + \mathbf{F^{0,Z}} \tag{3.15}$$

or in scalar format:

$$F_{k,t}^{Z} = \sum_{z} PTDF_{k,z}^{Z} \, P_{z,t}^{Z} + F_{z}^{0,Z} \quad \forall k, \forall t \tag{3.16}$$

The remainder of this chapter focusses on absolute ISKs, but an analogous reasoning is applicable to incremental ISKs.

3.4 Improved method to calculate injection shift keys

The calculation of the ISK matrix is a crucial but not straightforward step in the nodal-zonal network reduction. This section gives an overview of one of the main difficulties with ISK calculation, i.e., time averaging, and proposes an improved method to solve this issue.

3.4.1 Time averaging of injection shift keys

The nodal-zonal network reduction is typically performed for multiple time steps at once (e.g., on a daily basis). In order to derive one zonal network which is valid for the whole considered time frame, time-independent ISKs are needed. However, ISKs can change from time step to time step as the spatial distribution of generation and load within a zone changes in time. Time averaging of ISK results in a loss of accuracy of the zonal network.

Fig. 3.2 shows for the considered case study of the central European electricity system (see section 3.5.1) the daily average ISKs and the standard deviation for the daily average ISKs. The daily average ISKs can be positive or negative; the absolute values of the daily ISKs are shown in Fig. 3.2.[5] The standard deviation is a measure for the time-variability. Fig. 3.2 indicates that certain nodes have a highly time-variable ISK. Both the average ISK and the standard deviation are expressed in percentage (i.e., ISKs are ratios that can be expressed in percentages).

Time-variability of ISKs is caused by changing nodal or zonal balances, and is intensified if the zonal balance is small compared to the nodal balance, see Eq. (3.11). These effects are illustrated in Fig. 3.3 for one particular node in the

[5] Absolute values are plotted for the sake of clarity. Fig. 3.2 would be-roughly speaking-mirrored (with the y-axis as the mirror line) when the ISK values were used (positive and negative) instead of the absolute values.

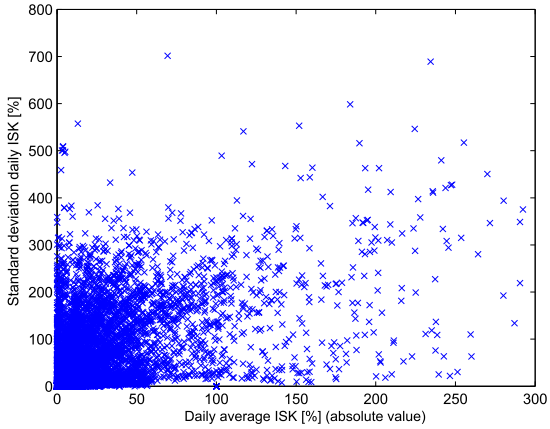

Figure 3.2: Daily average ISK (absolute value) and standard deviation for the simple zonal model (case study of Central Europe). The standard deviation is a measure for the variability in time of the ISKs. Certain nodes have a highly time-variable ISK.

network. The nodal balance is constant, but the zonal balance varies during the day. Moreover, the zonal balance is smaller than the nodal balance and fluctuates around zero (i.e., the zone is a net exporter during certain hours of the day and a net importer during others). The result is a strongly fluctuating ISK.

Clearly, using one fixed ISK per day is a rather strong approximation for nodes with a highly variable ISK. Therefore, another method is required which results in less time-variable ISKs. Such an improved method is proposed in the following section.

3.4.2 Improved injection shift keys

The accuracy of the ISKs can be improved by increasing the number of zones or by shortening the time frame for which the zonal network has to be valid. Both improvements are mostly not possible as the number of zones and the time frame are set fixed (e.g., flow-based market coupling framework in the Central Western European region (Amprion et al., 2014)).

The ISK matrix can also be improved by working with different ISK-matrices for different categories of generation and load units. Categories can refer to,

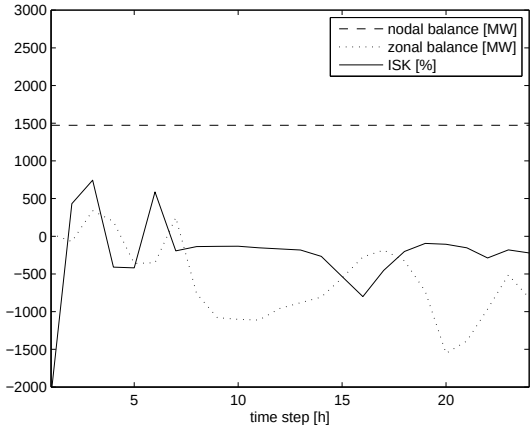

Figure 3.3: The ISK of a particular node can vary strongly during a day if the zonal balance fluctuates around zero and is small compared to the nodal balance. The daily average ISK of the considered node for the considered day is -230%, with a standard deviation of 520%.

for example, power injections from base load units, power injections from peak load units, load off-takes from industrial consumers and load off-takes from residential consumers.

The spatial distribution within one category varies less in time than the spatial distribution of the whole generation and load portfolio together. Consider for instance base load units. The aggregated generation from base load units is rather constant in time and the contribution of one base load unit to the aggregated base load generation is likely to be rather constant in time as well. Therefore, the ISKs for the category of base load generation vary little in time. As a result, less accuracy is lost with time averaging a ISK matrix which is specific for a certain category. When certain categories are predominant in some sub-regions, the category-specific ISK method is to a certain extent equivalent to dividing the system in smaller zones.

The ISK for category Y can be calculated as follows:

$$\begin{aligned} ISK^{Y}_{n,z,t} &= \frac{P^{Y,N}_{n,t}}{\sum_{n\in z} P^{Y,N}_{n,t}} \quad \forall\, z, \forall\, n \in z, \forall\, t \\ ISK^{Y}_{n,z,t} &= 0 \quad \forall\, z, \forall\, n \notin z, \forall\, t \end{aligned} \tag{3.17}$$

with $P_{n,t}^{Y,N}$ the nodal power injection of category Y. $P_{n,t}^{Y,N}$ is positive for injections in the network and negative for off-takes. Like in the basic ISK-method (see Eq. (3.11)), the nodal power injections are estimated a priori.

The zonal PTDF matrix is now different for the various categories:

$$\mathbf{PTDF^{Y,Z}} = \mathbf{PTDF^{N*}}\ \mathbf{ISK^{Y}} \tag{3.18}$$

The resulting DC power flow equation becomes:

$$\mathbf{F^{Z}} = \sum_{Y} \mathbf{PTDF^{Y,Z}}\ \mathbf{P^{Y,Z}} + \mathbf{F^{0,Z}} \tag{3.19}$$

or in scalar format:

$$F_{k,t}^{Z} = \sum_{z,y} PTDF_{k,z}^{Y,Z}\ P_{z,t}^{Y,Z} + F_{z}^{0,Z} \quad \forall\, k, \forall\, t \tag{3.20}$$

The zonal injection of category Y, $P_{z,t}^{Y,Z}$, is positive for generation-related categories and negative for load-related categories. The zonal injection per category is limited by the generation or load of that category:

$$\begin{aligned} 0 \leq P_{z,t}^{Y,Z} &\leq \sum_{n \in z} P_{n,t}^{Y,N} \quad \forall\, z, \forall\, y \in y_G, \forall\, t \\ 0 \geq P_{z,t}^{Y,Z} &\geq \sum_{n \in z} P_{n,t}^{Y,N} \quad \forall\, z, \forall\, y \in y_L, \forall\, t \end{aligned} \tag{3.21}$$

The net zonal injection is the sum of all zonal injection per category

$$P_{z,t}^{Z} = \sum_{y} P_{z,t}^{Y,Z} \quad \forall\, z, \forall\, t \tag{3.22}$$

The improved method is illustrated on the basis of the simple network in Fig. 3.1. Three different categories are considered: injections from base load generation (i.e., unit at node 1 and unit at node 4), injections from peak load generation (i.e., unit at node 2), and load off-takes (i.e., nodes 2 and 3). The ISKs per category for this example are:

$$\mathbf{ISK^{base}} = \begin{bmatrix} 1 & 0 \\ 0 & 0 \\ 0 & 0 \\ 0 & 1 \end{bmatrix} \tag{3.23}$$

$$\mathbf{ISK^{peak}} = \begin{bmatrix} 0 & 0 \\ 1 & 0 \\ 0 & 0 \\ 0 & 0 \end{bmatrix} \tag{3.24}$$

$$\mathbf{ISK^{load}} = \begin{bmatrix} 0 & 0 \\ 1 & 0 \\ 0 & 1 \\ 0 & 0 \end{bmatrix} \tag{3.25}$$

The zonal PTDF-matrices for the different categories then become:

$$\mathbf{PTDF^{base,Z}} = \begin{bmatrix} 0 & -0.50 \\ 0 & -0.50 \end{bmatrix} \tag{3.26}$$

$$\mathbf{PTDF^{peak,Z}} = \begin{bmatrix} -0.25 & 0 \\ -0.25 & 0 \end{bmatrix} \tag{3.27}$$

$$\mathbf{PTDF^{load,Z}} = \begin{bmatrix} -0.25 & -0.75 \\ -0.25 & 0.25 \end{bmatrix} \tag{3.28}$$

The DC power flow equation for the example in Fig. 3.1 becomes:

$$\begin{aligned} \mathbf{F^Z} = \mathbf{PTDF^{base,Z}}\ \mathbf{P^{base,Z}} + \mathbf{PTDF^{peak,Z}}\ \mathbf{P^{peak,Z}} \\ + \mathbf{PTDF^{load,Z}}\ \mathbf{P^{load,Z}} + \mathbf{F^{0,Z}} \end{aligned} \tag{3.29}$$

3.5 Evaluation of improved injection shift keys

The central European electricity system is studied to evaluate the improved ISK-method.

3.5.1 Case study - Central European electricity network

The case study considers the interconnected high-voltage electricity system of 10 Central European countries: Austria, Belgium, Switzerland, Czech Republic,

Germany, Denmark (West), France, Luxembourg, the Netherlands and Poland.[6]

The nodal network model contains 2,339 nodes, 3,367 line elements (transmission lines and transformers) (ENTSO-E, 2013). The generation portfolio consists of 511 generation units with a total installed capacity of 205 GW (82 GW nuclear units, 73 GW coal-fired units, 40 GW gas-fired units and 10 GW internal combustion engines). Residual load time series with an hourly time resolution are studied for two specific days: a high-load day with peak load of 200 GW (i.e., based on a working day in the winter of 2012) and a low-load day with peak load of 155 GW (i.e., based on a weekend day in the summer of 2012) (ENTSO-E, 2015a). The residual load is the original electricity load minus generation from non-dispatchable renewable and cogeneration units. It is assumed that the residual load is fully inelastic.

The optimal operational generation schedule for this electricity system is determined for three different network models:

(1) a nodal network model as reference case;

(2) a *simple* zonal network model with 40 zones;

(3) an *improved* zonal network model with the same 40 zones as in the simple zonal network, but different ISK-matrices for 2 categories: generation-related injections, represented by so-called generation shift keys (GSKs), and load-related injections, represented by so-called demand shift keys (DSKs).

The nodes are clustered in 40 zones by a k-means algorithm as implemented in Matlab. The k-means clustering algorithm assigns iteratively nodes to zones based on nodal PTDF-values (the PTDF-values for congested lines in the nodal simulation are considered). Each zone is characterized by a centroid, which is a vector of average PTDF-values of all nodes in a zone. Each node is assigned to the zone with the smallest squared Euclidean distance between the PTDF-values of the node and the centroid of the zone. Table 3.1 gives the distribution of zones over the considered countries. The resulting zonal network contains 315 inter-zonal lines.

The optimal generation schedule follows from a deterministic generation dispatch model formulated as a linear program in GAMS 24.2 and solved by Cplex 12.6. Note that this linear program is a relaxation of the mixed-integer program described in chapter 2. The objective function is to minimize the total

[6]The ENTSO-E Regional Group of Continental Europe consists of 24 countries, but only 10 countries are considered in this chapter in order to keep simulations computationally tractable.

Country	Zones	Country	Zones
Belgium	1	Germany, Austria, Luxembourg	10
Czech Republic	2	Netherlands	2
Denmark	1	Poland	2
France	19	Switzerland	3

Table 3.1: Number of zones per country for the 40-zones network.

operational system cost for the simulated days:

$$\min \quad \sum_{i,t} MC_i \, gen_{i,t} \tag{3.30}$$

The objective function is subject to the market clearing constraint (Eq. (3.31) for a nodal and Eq. (3.32) for a zonal network model), the power plant generation limits (Eq. (3.33)), the transmission line limits (Eq. (3.34) for a nodal and Eq. (3.35) for a zonal network model), and the DC power flow equations (Eqs. (3.4) and (3.36) for a nodal network, Eqs. (3.16) and (3.37) for a simple zonal network and Eqs. (3.20) and (3.37) for an improved zonal network). For the improved zonal network, Eqs. (3.21)-(3.22) are taken into account as well.

$$A^{plant,N}_{n,i} \, gen_{i,t} = D^N_{n,t} + P^N_{n,t} \quad \forall\, n, \forall\, t \tag{3.31}$$

$$A^{plant,Z}_{z,i} \, gen_{i,t} = D^Z_{z,t} + P^Z_{z,t} \quad \forall\, z, \forall\, t \tag{3.32}$$

$$0 \leq gen_{i,t} \leq \overline{P}_i \quad \forall\, i, \forall\, t \tag{3.33}$$

$$-\overline{F}^N_l \leq F^N_{l,t} \leq \overline{F}^N_l \quad \forall\, l, \forall\, t \tag{3.34}$$

$$-\overline{F}^Z_k \leq F^Z_{k,t} \leq \overline{F}^Z_k \quad \forall\, k, \forall\, t \tag{3.35}$$

$$\sum_n P^N_{n,t} = 0 \quad \forall\, t \tag{3.36}$$

$$\sum_z P^Z_{z,t} = 0 \quad \forall\, t \tag{3.37}$$

3.5.2 Time variability of the injection shift keys

The ISK-matrices for the case study are determined with Eqs. (3.11) and (3.17), respectively for the simple zonal network and the improved zonal network. The nodal power injections, needed in Eqs. (3.11) and (3.17), are taken from the

nodal simulation results. The zonal configuration is determined as described in section 3.5.1.

The zonal network model is determined on a daily basis. This implies that the ISKs are averaged over 24 hours, in order to derive a zonal network which is valid for a whole day. As mentioned before, this entails a loss in accuracy. The larger the variability in time of the ISKs, the larger the loss in accuracy due to time averaging.

Fig. 3.2 and Fig. 3.4 show the daily average ISK and the standard deviation in time for the simple zonal model and the improved zonal model, respectively. It is clear that the time-variability of the ISKs reduces drastically with the improved zonal method. The average ISK also becomes smaller in the improved method. In the simple method, ISKs are calculated as the nodal injections divided by the zonal balance. The zonal balance can become small for almost balanced zones, resulting in high (average) ISKs. By splitting the zonal balance in zonal load and zonal generation in the improved method, the (average) ISK becomes smaller as the zonal generation or load is always at least as large as the nodal generation or load. The standard deviation of the ISKs in the improved method is maximal for average ISKs around 50%. For average ISK close to 0 (i.e., the node does not contribute to the zonal balance) or close to 1 (i.e., the node is the only contribution to the zonal balance), the standard deviation becomes zero.

In short, the improved method thus results in less time-variable ISKs. This implies that less accuracy is lost by time averaging the ISK matrix.

3.5.3 Flows through the network

The power flows through the network follow from the generation dispatch model. Depending on the network model, different flows are obtained. Table 3.2 shows the mean absolute error between the inter-zonal flows from a zonal and a nodal simulation. Table 3.2 indicates that the improved zonal network approximates the inter-zonal flows better than the simple zonal network.

Working with ISKs for different categories (i.e., GSKs for generation-related injections and DSKs for load-related off-takes) results in a more accurate time averaging of ISKs, as seen in the previous subsection. However, introducing categories leads to additional freedom for the generation scheduling algorithm. With multiple categories, the algorithm has the freedom to choose which category exports to other regions (in case of generation-related injections) or imports from other regions (in case of load-related injections). For instance, consider a zone with a positive zonal generation balance of 100 MW, an aggregated zonal

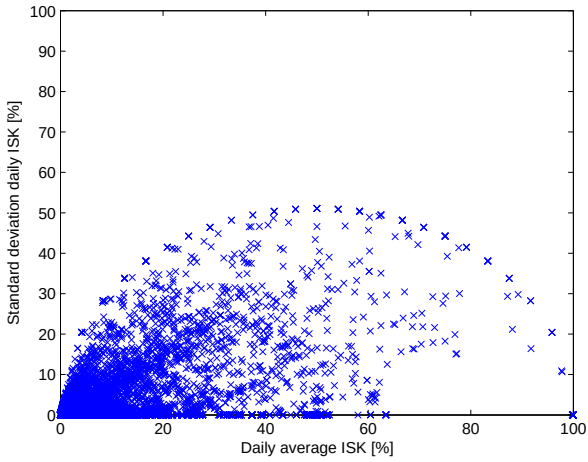

Figure 3.4: Daily average ISKs and standard deviation for the improved zonal network with 2 different categories. The standard deviation reduces drastically in the improved ISK-method, compared to Fig. 3.2 (note the different scale of the axes).

generation of 350 MW and a zonal load of 250 MW. In the simple zonal network, the zonal power injection $P^Z_{z,t}$ is 100 MW, whereas in an improved zonal network with generation-related and load-related injections, the zonal generation-related injection can vary from 0 to 350 MW and the zonal load-related off-take from 0 to 250 MW (as long as the net zonal balance remains 100 MW). Depending on the specific PTDF-matrices for both categories, the algorithm can choose to minimize zonal import/export and cover the zonal load with zonal generation, or to maximize zonal import/export and import all zonal load and export all zonal generation, or any situation in between. Both situations will result in different flows through the network.

Inter-zonal flows can deviate from the optimal flows (as given by the nodal network model) as long as the line capacities are respected. However, this is not always the case. Table 3.3 shows how often a line overloading occurs if the zonal generation schedules are imposed to the nodal network. Line overloadings occur more often during the high-load day as the network is more used at these moments. Line overloadings occur also more often on inter-zonal lines than on intra-zonal lines. This can be explained by the fact that the zones were clustered such that intra-zonal congestion occured as little as possible. The improved zonal network model results in fewer line overloadings than the simple zonal network.

MAE inter-zonal flow [MW]	low-load day	high-load day
Simple zonal network	1,058	470
Improved zonal network	266	316

Table 3.2: Mean absolute error (MAE) of inter-zonal flows, comparing the zonal with the nodal simulation results (total inter-zonal transmission capacity is 578,800 MW). A low-load and a high-load day are considered, each with an hourly time resolution.

Overloading penetration rate [%]	low-load day		high-load day	
	inter	intra	inter	intra
Simple zonal network	4.7	0.4	42.2	22.6
Improved zonal network	3.0	0.1	30.1	14.1

Table 3.3: The overloading penetration rate is defined as the sum of overloaded lines over all time steps divided by the number of lines and the number of time steps (inter: inter-zonal lines; intra: intra-zonal lines).

3.5.4 Zonal generation balances

Different zonal import/export balances are obtained if different network models are used in the generation scheduling model. Table 3.4 shows the mean absolute error between the hourly zonal generation balances from a zonal and a nodal network model. Again, the improved zonal network model outperforms the simple zonal network model.

The zonal balance error is larger in a low-load day than in a high-load day. In a high-load day, almost all generation units are used to fulfill load. Therefore, the generation scheduling algorithm has less options to optimize the generation schedule, leading to fewer deviations between the different network models.

3.5.5 Computational tractability

The previous subsections have focussed on the accuracy of the zonal network models. This subsection deals with the computational cost (see Table 3.5). Simulations were run on an Intel®Core™ i7-2620M CPU@2.7 GHz, 8 GB RAM.

The size of the problem, i.e., the number of equations and variables, is an order of magnitude larger with the nodal network than with the various zonal networks. The improved zonal network results in a slightly larger optimization problem compared to the simple zonal network model. The run time with a

MAE zonal balance [MW]	low-load day	high-load day
Simple zonal network	777	440
Improved zonal network	347	335

Table 3.4: Mean absolute error (MAE) of hourly zonal balance, comparing the zonal with the nodal simulation result. A low-load and a high-load day are considered, each with an hourly time resolution.

	Equations	Variables	Run time
Nodal network	$51.4 \cdot 10^5$	$28.7 \cdot 10^5$	206min
Simple zonal network	$5.1 \cdot 10^5$	$3.0 \cdot 10^5$	23s
Improved zonal network	$5.8 \cdot 10^5$	$3.3 \cdot 10^5$	38s

Table 3.5: Computational cost of the different network models (generation scheduling optimization, 24 time steps, 511 generation units, nodal network with 2,339 nodes, zonal network with 40 nodes).

nodal network is two orders of magnitudes larger than the run time with a zonal network model. The run times for the zonal network models increase by adding categories, but stay within the same order of magnitude.

In this chapter, an economic dispatch model, formulated as a linear program, is used. However, if one wants to include the dynamic constraints of the generation portfolio (e.g., minimum operation point, minimum down times), a mixed-integer program is needed, introducing binary variables in the optimization problem. This increases the computational cost of the optimization problem drastically, which makes it more important to limit the size and the computational cost of the network representation. Moreover, a rather short time frame is considered in this chapter, i.e., one day. The computational cost increases exponentially if longer time frames are considered, again underlining the importance of computational tractable network models.

3.6 Summary and conclusions

Network constraints become increasingly relevant in generation scheduling models, due to the coupling of electricity markets and the deployment of renewables in remote areas. The non-linear AC load flow is mostly computationally too demanding to use in unit commitment models, and therefore the linearized DC power flow is used. However, a full nodal DC power flow can also be computationally intractable for large-scale power systems. As such, reduced zonal network models are needed to take network constraints

into account in generation scheduling models without losing computational tractability. A full nodal network can be reduced to a zonal network model by clustering nodes into zones and replacing the nodes in the same zone by one equivalent node.

Injection shift keys (ISK) are needed to group nodes into zones and determine the zonal power transfer distribution factors (PTDF). ISKs give the nodal contribution to the zonal balance. They are estimated a priori and often averaged over multiple time steps in order to derive a zonal network model which is valid for multiple time steps.

This chapter presents an improved method to calculate ISKs. According to this improved method, the injections and off-takes from the network are split in different categories and the ISKs are determined separately for the different categories. A category can refer to, for example, power injections from base load generation or power off-takes from industrial consumers. The method is based on the insight that the ISKs from one category vary less in time than the ISK of the whole system. The improved method thus results in less time-variable injection shift keys and a lower loss in accuracy by time averaging the ISK matrix. Besides, the improved method allows taking account of, for instance, flexible load as a variable in the zonal network model.

The improved method is evaluated by means of a case study of the Central European electricity network. The study shows that an improved zonal network model, with generation-related injections (represented by generation shift keys) considered separately from load-related off-takes (represented by demand shift keys), is able to better approach the flows and zonal generation balances than a simple zonal network model with the same number of zones, and this with only a modest increase in computational cost.

Chapter 4

Cycling of conventional power plants

Chapter based on:

K. Van den Bergh and E. Delarue. Cycling of conventional power plants: technical limits and actual costs. Energy Conversion Management, 97:70-77, 2015.

Abstract: Cycling of conventional generation units is an important source of operational flexibility in the electricity generation system. Cycling is changing the power output of conventional units by means of ramping and switching (starting-up and shutting-down). In the literature, a wide range of technical and cost-related cycling parameters can be found. Different studies allocate different cycling parameters to similar generation units. This chapter assesses the impact of different cycling parameters allocated to a conventional generation portfolio. Both the technical limitations of power plants and all costs related to cycling are considered. The results presented in this chapter follow from a unit commitment model, used for a case study based on the German 2013 system. The conventional generation portfolio has to deliver different residual load time series, corresponding to different levels of renewables penetration. The study shows, under the assumptions made, that although the dynamic limits of some units are reached, the limits of the conventional generation portfolio as a whole are not reached, even if stringent dynamic parameters are assigned to the generation portfolio and a highly variable residual load is imposed to the system. The study shows also the importance of including full cycling costs in

the unit commitment scheduling. The cycling cost can be reduced by up to 40% when fully taken into account.

Keywords: Power plant cycling, cycling costs, power plant scheduling.[1]

4.1 Introduction

The way of operating conventional power plants is changing as a consequence of the increasing penetration of intermittent renewables in the electricity generation system (Perez-Arriaga and Batlle, 2012). Electricity generation from intermittent renewable sources, like wind energy and solar energy, is variable, partly unpredictable and not or limitedly dispatchable (Delarue et al., 2009). As a consequence, a flexible electricity system is required to deal with the variations in renewable generation and to cope with forecast errors (Luickx et al., 2008). Holttinen (2005) estimated that, for a 10% energy penetration level of wind in Scandinavia, reserve requirements increase with 1.5-4% of installed wind capacity. Albadi and El-Saadany (2010) foresee an increase in balancing costs with increasing wind penetration.

A well developed and flexible grid, responsive electricity demand, curtailment of renewable generation and storage of electric energy are often cited as operational flexibility options to accommodate intermittent renewables in the electricity generation system (Critz et al., 2013). However, these flexibility sources are only to a limited extent available in current systems. The main source of operational flexibility nowadays is cycling of conventional power plants. Cycling is defined as changing the output of a power plant by starting-up, shutting-down, ramping up or ramping down (Meibom et al., 2009). Conventional power plants refer to centralized and dispatchable units, like nuclear power plants, coal and lignite-fired steam power plants, and gas-fired plants.

The integration of intermittent renewables in the electricity generation system causes an increase in conventional power plant cycling. The link between renewables deployment and cycling behavior of conventional power plants is extensively discussed in the literature. Troy et al. (2010) show that, based on a case study of the 2020 Irish electricity system, cycling of base-load generation units increase with increasing wind penetration. Cochran et al. (2013) discuss the evolution of coal-fired units from base-load to peak-load generation. Tuohy et al. (2009) show that more robust and cost efficient generation schedules are produced by stochastic optimization which takes account of the intermittent character of renewables. Including cycling costs is likely to increase renewables

[1] All abbreviations and symbols used in this chapter are listed and explained at the outset of this dissertation.

curtailment and the occurrence of negative prices (Deng et al., 2015). Although cycling costs are increasing at higher renewables penetration, overall operational generation costs decrease due to fossil fuel savings as shown by Strbac et al. (2007) for a case study of the UK and by Ummels et al. (2007) for the Dutch system.

Different studies allocate different cycling parameters – costs and technical limits – to similar generation units. In the literature, a wide range of technical cycling parameters is reported. However the sensitivity of the allocated cycling parameters on the final cycling behavior is never investigated. This chapter complements the existing literature on conventional power plant cycling by focusing on the cycling parameters itself and their impact on cycling behavior, rather than on the cause of the increased cycling behavior. An important question is how flexible conventional generation units are – from a technical viewpoint – and what the additional costs are related to a flexible operation of these units (Rodilla et al., 2014; Benato et al., 2014). This chapter investigates the influence of the variability in technical parameters on the operation of power plants. The scheduling of the same set of power plants is optimized for a case with high-dynamic cycling parameters and a case with low-dynamic cycling parameters assigned to the power plants. In addition, the different costs of conventional cycling and their impact on the total generation costs are quantified in this study. The results presented in this chapter follow from a case study based on the 2013 German generation system. A dedicated operational partial equilibrium model of the electricity generation sector, i.e., the unit commitment model LUSYM (see chapter 2), is used for this study.

The added value of this chapter to the literature lies in its focus on the uncertainty related to cycling parameters–both technical and cost-related parameters. To address this issue, the impact of different cycling parameters on the power plant scheduling is studied. As such, this study contributes to the ongoing discussion on compatibility between variable generation of renewables and conventional electricity generation (Energiewende, 2013).

Section 4.2 discusses the technical and cost-related aspects concerning conventional power plant cycling. Section 4.3 presents the 2013 German electricity generation system as a case study and describes the unit commitment model used in this chapter. Section 4.4 presents the results and discussion, and section 4.5 concludes.

4.2 Cylcing of conventional units

Cycling of conventional units causes additional costs for generators and is limited by the technical characteristics of the unit. Both aspects are discussed in detail in this section.

4.2.1 Cycling cost

Cycling has a degenerating effect on units. When a generation unit varies its output, various components in the unit are subject to stresses and strains. During the shut-down of a unit, components undergo large temperature and pressure stresses. These stresses and strains lead to accelerated component failures and forced outages (Lefton et al., 1997). Starting-up a unit is even more demanding. Wear and tear on the components of the generation units is exacerbated by a phenomenon known as creep-fatigue interaction (Denny and O'Malley, 2009).

The cost associated with power plant cycling consists of several components. Kumar et al. (2012) mention 5 distinct groups of cycling costs:

1. the cost for fuel, CO_2 emissions and auxiliary services during start-up, further referred to as direct start costs;
2. the capital replacement costs and maintenance cost due to start-ups, further referred to as indirect start costs;
3. the cost of forced outages due to cycling, which is the opportunity cost of not generating during an outage, further referred to as forced outage costs;
4. the capital replacement costs and maintenance cost related to load following, further referred to as ramping costs;
5. the cost of a decrease in rated efficiency due to cycling, further referred to as efficiency costs.

The total cost of cycling is not always well understood. Operators might underestimate total cycling costs and only take the fuel and CO_2 emission cost of a start-up (i.e., direct start cost) into account when making unit commitment decisions, even though this cost might be quite small compared to the total cycling cost. Cycling costs depend on many factors like the type and age of the power plant. It is difficult to put one number on the cycling costs of conventional power plants. According to Lefton et al. (1997), it is estimated

that cycling costs of conventional fossil-fuel-fired power plants can range from US$ 2,500 to US$ 500,000 per single on/off cycle, depending on the type of the unit, age, usage pattern, etc. Similarly, Kumar et al. (2012) report cycling costs with a factor 100 difference between the lowest and highest cycling cost. A study of Schröder et al. (2013) on the costs of electricity generation also reports such a wide range of cycling costs. In an electricity generation system with increasing levels of renewables, cycling costs are a growing concern for power plant operators and system operators. Therefore, taking the correct cycling costs into account during the scheduling of the units is of great importance.

An important challenge is to allocate correctly the long-term cycling costs, such as indirect start costs and efficiency costs, into a short-term operational decision like power system scheduling. One possible approach is to model cycling cost dynamically, i.e., as a function of the number of start-ups (Troy et al., 2012). This approach is especially valuable when looking at one generation unit in detail. Another approach, more common for studies with a system perspective, is to work with one fixed start-up cost for each generation type. This start-up cost represents the short-term operational costs related to the start-up, but a markup is added to correct for long-term costs. The latter approach is applied in this chapter.

4.2.2 Technical cycling limits

Technical limits constrain the cycling of conventional power plants. A power plant operates between a minimum and maximum power output and its ramping is constrained by ramping limits. A third technical cycling constraint imposes minimum up and down times. Conventional power plant cycling is also closely related to partial load operation. Operating a power plant at less than its rated power output goes together with a decrease in operating efficiency.

In the literature a wide range of cycling parameters, used in generation scheduling models, can be found. Table 4.1 gives an overview of outer limits of cycling parameters and Fig. 4.1 shows typical part load efficiency curves (as used in this study). A cycling parameter can reflect a hard-technical constraint (e.g., a minimum down time is needed to synchronize a generator to the grid frequency) or a more cost-related constraint (e.g., an operator might impose minimum up times to reduce the cost of start-ups and shut-downs). The cycling parameters allocated to power plants might hence reflect just the technical limits of the power plant or could also include cost-related considerations.

In this chapter, simulations are run for a low-dynamic power plant portfolio and for a high-dynamic power plant portfolio. Both portfolios contain the same set of power plants, but with different cycling parameters. In the low-dynamic

	$\underline{P}$ [$\%\overline{P}$]	RU,RD [$\%\overline{P}$/min]	SU,SD [$\%\overline{P}$/switch]	MUT [h]	MDT [h]
NUC	40-50	0.25-5	50-100	0.25-24	24
SPP-C	25-40	0.66-4	40-100	0.25-10	3-10
SPP-L	40-60	0.66-4	60-100	0.25-10	3-10
SPP-G	40	0.83-6	40-100	0.25-6	1-6
CCGT	30-50	0.83-10	50-100	0.25-6	0.5-6
OCGT	20-50	0.83-25	50-100	0.25-1	0.25-1

Table 4.1: Overview of the range of technical cycling data (Schröder et al., 2013) (NUC: nuclear power plants; SPP-C: coal-fired steam power plants; SPP-L: lignite-fired steam power plants; SPP-G: gas-fired steam power plants; CCGT: combined-cycle gas turbines; OCGT: open-cycle gas turbines).

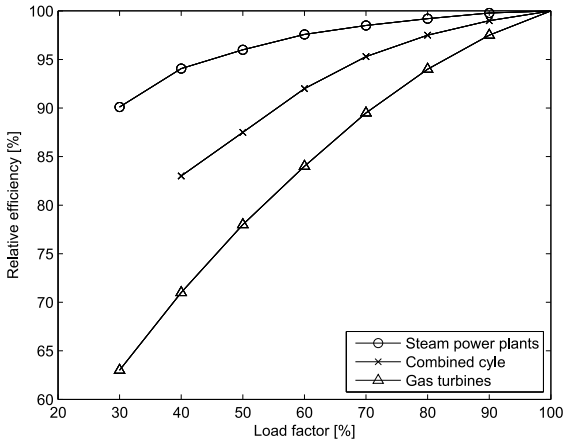

Figure 4.1: Power plant efficiencies decrease in partial load operation (Rolf et al., 1999; Linnenberg and Kather, 2009).

portfolio, the power plants have stringent cycling parameters (see Table 4.1, upper bound of minimum power output, lower bound of ramping gradients and upper bound of minimum up and down times). In the high-dynamic portfolio, less constraining cycling parameters are assigned to the same set of power plants (see Table 4.1, lower bound of minimum power output, upper bound of ramping gradients and lower bound of minimum up and down times). The difference between the low and high-dynamic portfolio can be interpreted as a difference in technical characteristics of the power portfolio or as a difference in the way the portfolio is operated (e.g., stringent limits reflect a more conservative mode

of operation). In both portfolios, the operators face the same cost parameters for generation and cycling.

4.3 System and model description

The studied electricity generation system is based on the 2013 German system. Cycling of conventional units within this system is simulated by means of a dedicated operational partial equilibrium model of the power sector, i.e, the unit commitment model LUSYM (see chapter 2). The studied system and the model are discussed in this section.

4.3.1 System description

The considered system is based on the 2013 German electricity generation system, consisting of a set of conventional generation units, a demand time series, renewable generation time series and an electricity grid. A unit commitment model is used to determine the optimal scheduling of the conventional units in order to meet the residual load. The residual load is calculated as the (inelastic) electricity demand minus generation from renewables.[2] The variability and the magnitude of the residual load both have an impact on the cycling behavior of the conventional portfolio. Four weeks are considered in detail, reflecting all different combinations of variability and magnitude of the residual load.[3]

The residual load time series is imposed to the conventional portfolio, which has to follow this variable residual load by means of cycling. The residual load time series is determined as the original demand time series minus the renewable time series. Different renewables time series are considered by scaling up or down the historical time series, reflecting different levels of renewables generation. Historical time series for the original demand and renewable generation with a quarter-hourly time resolution originate from the TSOs (50Hertz, 2015; Amprion, 2015; Transnet BW, 2015; Tennet, 2015a).

Table 4.2 gives an overview of the installed conventional generation capacity, together with the rated efficiency of the units (Umweltbundesamt, 2015). Different rated efficiencies are assigned to power plants depending on the

[2]The electricity demand time series is corrected for generation from cogeneration units, generation/consumption of pumped hydro units and import/export with neighboring countries.

[3]The following weeks are considered in detail; April 22-28 (week 17, low average load, high variable load), May 27-June 2 (week 22, low average load, low variable load), Sept 9-15 (week 37, high average load, high variable load), and Oct 28-Nov 3 (week 44, high average load, low variable load).

	# units	Capacity [GW]	Efficiency [%]
NUC	9	12.7	33
SPP-C	40	16.0	35/40/46
SPP-L	41	21.7	35/40/46
SPP-G	6	2.4	36/41
CCGT	48	15.4	40/48/58
OCGT	19	3.3	35/42

Table 4.2: Germany 2013 conventional generation portfolio (Umweltbundesamt, 2015) (NUC: nuclear power plants; SPP-C: coal-fired steam power plants; SPP-L: lignite-fired steam power plants; SPP-G: gas-fired steam power plants; CCGT: combined-cycle gas turbines; OCGT: open-cycle gas turbines).

commissioning year of the plant. The highest rated efficiency is allocated to units commissioned or retrofitted after 2000, the middlemost to units commissioned between 1980 and 2000, and the lowest to units commissioned before 1980.

The grid model used in this chapter comes from the ELMOD model and consists of 26 zones and 159 lines (Leuthold et al., 2008a). The electricity grid is represented by a DC power flow network.

Average 2013 fuel prices and CO_2 emission price are used (EEX, 2015a). All system data are scaled to match aggregated data from ENTSO-E (2015a) to overcome deviation between different data sources.

Load shedding and curtailment of renewable generation is possible at a very high cost (10,000 EUR/MWh). Loss of load and curtailment both indicate system infeasibilities.

Note that the aim is not to simulate the operation of the electricity market, but rather to focus on the techno-economic characteristics of the electricity generation system. Several differences between the electricity market design and this study exists. For instance, no electricity grid constraints within bidding zones are taken into account in the electricity market clearing, whereas this chapter considers a full DC power flow of the studied electricity generation system.

4.3.2 Model description

The optimal scheduling of the electricity generation system is determined with the dedicated deterministic unit commitment model LUSYM (see chapter 2). The model is formulated as a mixed-integer linear program (MILP) in GAMS

and solved using the Cplex 12.6 solver. The model simulates each considered week with a quarter-hourly time resolution.

For the sake of clarity, the relevant equations of the LUSYM model are repeated here. For definition of the symbols, the reader is referred to the list of symbols at the outset of the dissertation. The objective function of the unit commitment model is minimization of the total operational system cost, consisting of generation costs, start-up costs, ramping costs, load curtailment costs and renewables curtailment costs:

$$\min \sum_{i,t} \left(NC_i \, z_{i,t} + MC_i \, g_{i,t} + SUC_i \, v_{i,t} + cost_{i,t}^{ramp} \right) + \sum_{n,t} \left(LCC_n \, lc_{n,t} + RCC_n \, rc_{n,t} \right) \tag{4.1}$$

with the ramping costs defined as follows:

$$\begin{aligned} 0 \leq cost_{i,t}^{ramp} &\geq RC_i \left(g_{i,t} - g_{i,t-1} \right) \\ 0 \leq cost_{i,t}^{ramp} &\geq RC_i \left(g_{i,t-1} - g_{i,t} \right) \end{aligned} \tag{4.2}$$

The objective function is subject to the market clearing condition (Eq. (4.3)), power plant generation limits (Eq. (4.4)), power plant ramping limits (Eqs. (4.5)-(4.6)), minimum up and down times (Eqs. (4.7)-(4.8)), the binary relation (Eq. (4.9)), the DC power flow equations (Eqs. (4.10)-(4.11)), curtailment limits (Eqs. (4.12)-(4.13)) and binary constraints (Eq. (4.14)). No power plant outages occur, no spinning reserve requirements are imposed and no storage units are included.

$$\sum_i A_{n,i}^{plant} \left(z_{i,t} \, \underline{P}_i + g_{i,t} \right) + RES_{n,t} - rc_{n,t} = D_{n,t} - lc_{n,t} + p_{n,t} \;\; \forall n, \forall t \tag{4.3}$$

$$0 \leq g_{i,t} \leq \left(\overline{P}_i - \underline{P}_i \right) z_{i,t} \qquad \forall i, \forall t \tag{4.4}$$

$$g_{i,t} - g_{i,t-1} \leq RU_i \, z_{i,t} + \left(SU_i - \underline{P}_i - RU_i \right) v_{i,t} \qquad \forall i, \forall t \tag{4.5}$$

$$g_{i,t-1} - g_{i,t} \leq RD_i \, z_{i,t-1} + \left(SD_i - \underline{P}_i - RD_i \right) w_{i,t} \qquad \forall i, \forall t \tag{4.6}$$

$$z_{i,t} \geq \sum_{t'=t+1-MUT_i}^{t} v_{i,t'} \qquad \forall i, \forall t \tag{4.7}$$

$$1 - z_{i,t} \geq \sum_{t'=t+1-MDT_i}^{t} w_{i,t'} \qquad \forall i, \forall t \tag{4.8}$$

$$z_{i,t-1} - z_{i,t} + v_{i,t} - w_{i,t} = 0 \qquad \forall i, \forall t \tag{4.9}$$

$$\underline{F}_l \leq \sum_n PTDF_{l,n}\, p_{n,t} \leq \overline{F}_l \qquad \forall l, \forall t \tag{4.10}$$

$$\sum_n p_{n,t} = 0 \qquad \forall t \tag{4.11}$$

$$0 \leq rc_{n,t} \leq RES_{n,t} \qquad \forall n, \forall t \tag{4.12}$$

$$0 \leq lc_{n,t} \leq D_{n,t} \qquad \forall n, \forall t \tag{4.13}$$

$$z_{i,t}\,,\, v_{i,t}\,,\, w_{i,t} \in \{0,1\} \qquad \forall i, \forall t \tag{4.14}$$

The model is validated so that the generation in a simulation with historical input data matches the historical observed fuel mix. It takes about 3 hours to solve the unit commitment model for one week with the low-dynamic portfolio and 1 hour with the high-dynamic portfolio (163 power plants, 672 time steps, 1% relative optimality gap, solved on an Intel®Core$^{\text{TM}}$ i7-2620M CPU@2.7GHz, 8 GB RAM).

4.4 Results and discussion

The conventional generation portfolio is scheduled for different residual load time series, corresponding to different levels of wind and solar photovoltaics in the electricity generation system. Higher renewables shares lead to more variable and on average lower residual load time series. In this results section, the different residual load time series are referred to with their corresponding share of wind and solar photovoltaics.

4.4.1 Cycling in a high and low-dynamic portfolio

Fig. 4.2 shows the amount of cycling as function of the wind and solar share for a high-dynamic and a low-dynamic power plant portfolio (average of the considered weeks). The total amount of cycling is determined as the change in power output per quarter-hour, aggregated over all power plants (rescaled to MW per minute). The gross amount of cycling is based on the absolute value of every power output change of each individual power unit. The net amount of cycling is based on the absolute value of the aggregated power output change of the whole portfolio. Cycling clearly increases with the amount of renewable injections, which is consistent with results presented in the literature. However, this chapter distinguishes between net and gross cycling and between

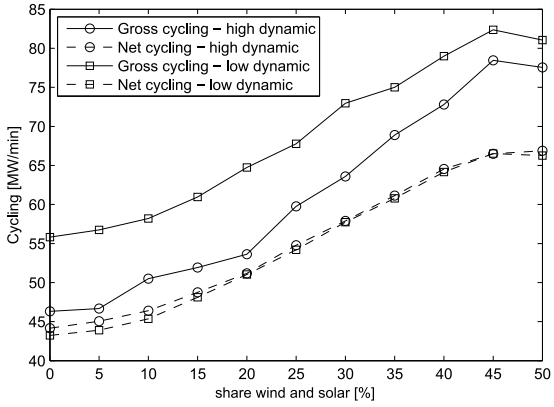

Figure 4.2: The amount of cycling increases with the amount of wind and solar generation (average cycling in the considered weeks). The gross cycling does not account for counteractive cycling whereas the net cycling does.

a low-dynamic and a high-dynamic portfolio. The net amount of cycling is lower as upward and downward cycling plants will cancel each other out to a certain extent. The net amount of cycling is about equal for both power plant portfolios as the required net amount of cycling is determined by the variability in residual load (identical for both portfolios). The minor differences between net cycling in a low-dynamic and a high-dynamic portfolio are caused by differences in loss of load and renewables curtailment. The difference between the gross amount of cycling and the net amount of cycling is caused by counteractive cycling, i.e., power plants cycling in the opposite direction at the same time. The power plant portfolio is forced to counteractive cycling by dynamic constraints. Without any dynamic constraint, no counteractive cycling would occur as every operating unit would produce at rated power output and only the last generating unit would operate in partial load. With dynamic constraints, counteractive cycling occurs. Hence, the difference between the gross amount of cycling and the net amount of cycling is a measure for the dynamic limits of the whole generation portfolio. In the low-dynamic portfolio, more counteractive cycling occurs, caused by the stringent dynamic limits of the system. In the high-dynamic portfolio, almost no counteractive cycling occurs at small amounts of wind and solar photovoltaics, but at high amounts of wind and solar photovoltaics, counteractive cycling takes place. At wind and solar photovoltaics levels of 45-50%, the net amount of cycling flattens out. At such high levels of renewables penetration, the residual load becomes almost zero during most hours of the day, reducing as such the need for cycling of conventional units. This also

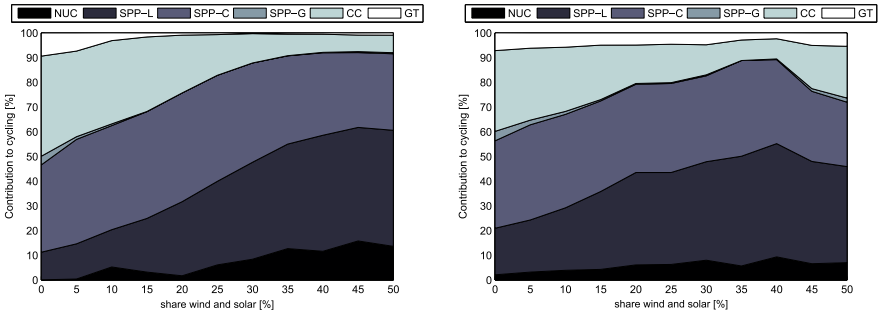

(a) High-dynamic portfolio.

(b) Low-dynamic portfolio.

Figure 4.3: Wind and solar generation causes a shift towards base load cycling– average cycling in the considered weeks (NUC: nuclear power plants; SPP-L: lignite-fired steam power plants; SPP-C: coal-fired steam power plants; SPP-G: gas-fired steam power plants; CC: combined-cycle gas turbines; GT: open-cycle gas turbines).

explains the reduction in gross cycling going from 45% to 50% wind and solar photovoltaics.

Besides the amount of cycling, the way of cycling changes as well. Fig. 4.3 shows the contribution to cycling of each power plant type, respectively in a high-dynamic portfolio (Fig. 4.3.a) and a low-dynamic portfolio (Fig. 4.3.b). As more wind and solar generation is introduced in the system, more cycling comes from lignite-fired plants and nuclear plants. The contribution of coal-fired plants is more or less constant whereas the contribution of combined-cycle plants and gas turbines diminishes with increasing wind and solar generation. In a high-dynamic portfolio, nuclear units and steam power plants contribute more to cycling at high levels of wind and solar photovoltaics, compared to a low-dynamic portfolio. In a high-dynamic portfolio, these units are flexible enough to cope with the variability in residual load whereas in a low-dynamic portfolio, combined-cycle units and gas turbines are needed.

This is further illustrated by the dispatch of the conventional power plants (see Fig. 4.4 for the power plant dispatch decision of one specific day). First, it is clear from Fig. 4.4 that the economic dispatch changes drastically with increasing levels of wind and solar penetration. At zero wind and solar share, power plants are dispatched almost solely based on to their marginal generation costs (since dynamic constraints are not binding). With increasing wind and solar generation, less conventional power plant generation is dispatched. Moreover,

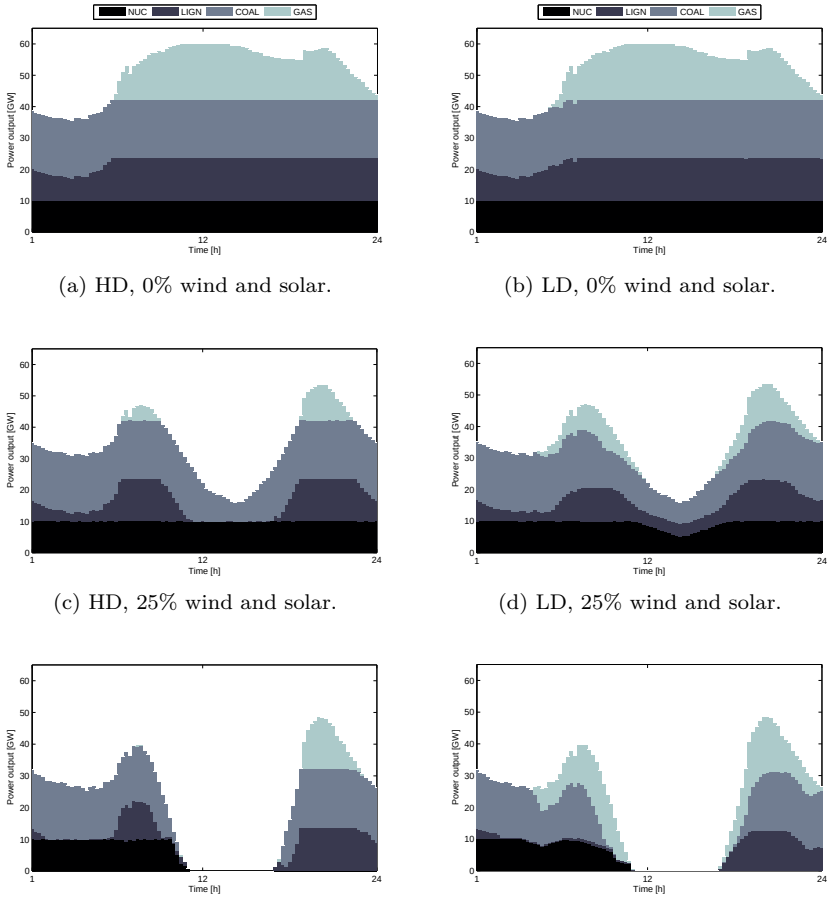

(a) HD, 0% wind and solar.

(b) LD, 0% wind and solar.

(c) HD, 25% wind and solar.

(d) LD, 25% wind and solar.

(e) HD, 50% wind and solar.

(f) LD, 50% wind and solar.

Figure 4.4: Dispatch of conventional power plants for one specific day (first day of week with high average load and high variable load), for a high- and low-dynamic portfolio and for different wind and solar shares (NUC: nuclear power plants; LIGN: lignite-fired power plants; COAL: coal-fired power plants; GAS: gas-fired power plants including open-cycle and combined-cycle turbines; HD: high-dynamic portfolio; LD: low-dynamic portfolio).

dynamic power plant limits become constraining, leading to dispatch decisions in which marginal power plants with higher generation costs are online while power plants with lower marginal generation costs are not operating at full

capacity (e.g., at 50% wind and solar share, gas-fired power plants are online when no nuclear power plants are generating). Second, comparing the dispatch in the high-dynamic and the low-dynamic portfolio, Fig. 4.4 shows that the dispatch decisions differ more with increasing wind and solar shares. At zero wind and solar generation, dispatch decisions in both portfolios are identical. At higher wind and solar shares, the high-dynamic portfolio tends to dispatch more low-marginal generation cost units (i.e., lignite-fired and coal-fired power plants) while the low-dynamic portfolio tends to dispatch more high-marginal generation cost units (i.e., gas-fired power plants). Compare, for instance, the dispatch decisions at 50% wind and solar share. In the high-dynamic portfolio, lignite-fired and coal-fired power plants are flexible enough to deal with the morning peak followed by the strong dip in residual load in the middle of the day. In the low-dynamic portfolio, however, gas-fired units are needed to deliver this flexibility, at the expense of lignite-fired and nuclear power plant generation.

4.4.2 Technical limits of cycling

Conventional cycling is constrained by the technical characteristics of the power plant portfolio. Wind and solar generation pushes the electricity generation system towards these limits and maybe beyond, leading to system infeasibilities. The unit commitment model in this study allows load shedding (i.e., reducing the electricity demand in order to lower the residual load) and renewables curtailment (i.e., reducing the generation from wind and solar photovoltaics in order to increase the residual load) to avoid system infeasibilities. The cost of load shedding and renewables curtailment is set very high (10,000 EUR/MWh) to make sure that these system flexibilities are used only when all conventional cycling flexibility is depleted. Renewables curtailment occurs when renewables generation exceeds demand or when the conventional portfolio is not able to follow the variability in residual load. Only the latter reflects the cycling limits of the conventional generation portfolio. Analogously, load shedding occurs when demand exceeds available generation capacity or when the conventional portfolio is not able to follow the variability in residual load. Again, only the latter reflects the cycling limits of the conventional generation portfolio.

Fig. 4.5 shows the "amount of infeasibilities", expressed as share of demand, caused by the limits of conventional cycling to cope with a variable residual load. Both types of infeasibilities–renewables curtailment and loss of load–occur rarely (less than 0.25% of demand) for renewables shares up to 50%. There is no difference between the low-dynamic portfolio and the high-dynamic portfolio (the minor differences between both portfolios are within the tolerance margin of the solution process). It turns out that the conventional power plant portfolio is able to deliver the flexibility up to a level corresponding to wind and solar

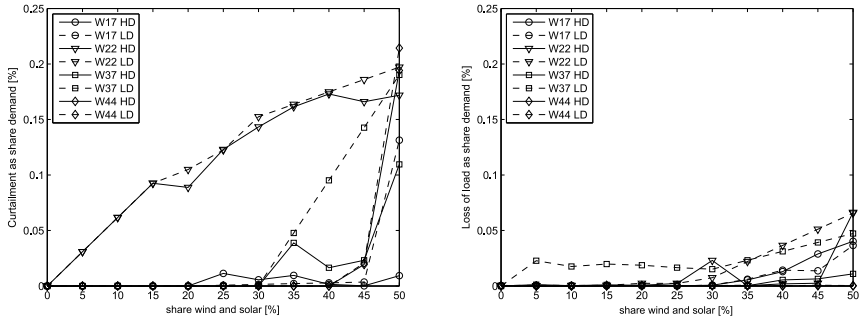

(a) Infeasibilities (renewables curtailment).

(b) Infeasibilities (loss of load).

Figure 4.5: Little system infeasibilities, which are caused by the limits of conventional cycling, occur (HD: high-dynamic portfolio, LD: low-dynamic portfolio, weekly aggregated).

shares of 50%, regardless of the technical cycling parameters allocated to the portfolio in the unit commitment model (high-dynamic versus low-dynamic). In other words, the dynamic limits of the conventional portfolio as a whole are not reached, even not if stringent cycling parameters are assigned to the generation portfolio. However, certain power plants might be bounded in operation.

4.4.3 The cost of cycling

Section 4.2 mentioned five types of cycling costs: direct start costs, indirect start costs, forced outage costs, ramping costs and efficiency costs. These different costs are often hard to quantify, except for the direct start cost (i.e., fuel and CO_2 emission cost during start-up), and vary in a wide range depending on the plant characteristics. Therefore, it is not straightforward to determine the cycling cost that has to be taken into account during the generation scheduling. Table 4.3 shows average cycling cost data for the different types of power plants.

In all simulations so far, only the direct start costs are taken into account in the unit commitment model, assuming that the operator has no information about the other cycling costs or that these other costs are zero. Fig. 4.6 shows the resulting operational system cost. The total operational system cost consists of generation costs and cycling costs.[4] The generation cost includes fuel costs,

[4]The cost of load shedding and renewables curtailment is, within the scope of this study, a system infeasibility cost, not a regular operational system cost, and therefore excluded from Fig. 4.6.

	Direct start [EUR/ΔMW]	Indirect start [EUR/ΔMW]	FO [h/cycle]	Ramping [EUR/ΔMW]	Eff. decr. [%-p/cycle]
NUC	35	-	-	-	-
SPP-C	25	55	0.63	1.8	0.44
SPP-L	28	55	0.63	1.8	0.44
SPP-G	33	40	0.39	1.4	0.20
CCGT	5	40	0.35	0.5	0.20
OCGT	2.4	40	0.69	0.8	0.10

Table 4.3: Cycling costs–average values (Kumar et al., 2012)(NUC: nuclear power plants; SPP-C: coal-fired steam power plants; SPP-L: lignite-fired steam power plants; SPP-G: gas-fired steam power plants; CCGT: combined-cycle gas turbines; OCGT: open-cycle gas turbines; Eff. decr.: decrease in rated efficiency).

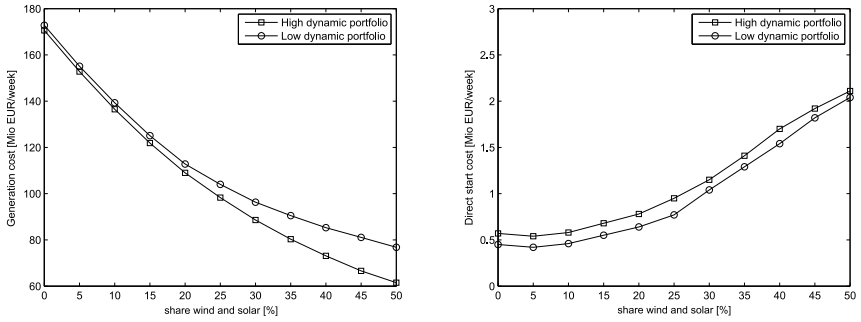

(a) Generation cost.

(b) Direct start cost.

Figure 4.6: The reduction in generation cost due to wind and solar generation outweighs the increase in direct start costs (average for considered weeks).

CO_2 emission costs and variable operations and maintenance (O&M) costs. The generation cost declines when wind and solar injections are introduced (Fig. 4.6.a). The low-dynamic portfolio has higher generation costs than the high-dynamic portfolio as more expensive power plants–in terms of marginal generation costs–have to be online to deliver flexibility (i.e., combined-cycle units and gas turbines), whereas in the high-dynamic portfolio, flexibility can be delivered by less expensive power plants (i.e., steam power plants). A high-dynamic portfolio entails generation cost savings with respect to a low-dynamic portfolio, which increases with increasing renewables generation. The direct start costs on the other hand rise with increasing wind and solar generation

(Fig. 4.6.b). The high-dynamic portfolio has slightly higher start costs as more start-ups occur in this portfolio. The decrease in generation costs due to renewable injections is in this case about two orders of magnitude larger than the increase in direct start costs. As a result, the total operational system cost decreases with increasing wind and solar share.

The generation cost, shown in Fig. 4.6.a, includes partial load operation. Increasing renewables generation tends to increase the partial load operation of conventional plants. In partial load, power plants generate at efficiencies below their rated efficiency (Fig. 4.1). This efficiency effect is included in the generation costs, which are calculated based on the actual operating efficiency of the power plants. Recalculating the generation costs at rated efficiency (same generation, but primary fuel emission costs determined with the rated efficiency instead of the actual operating efficiency) gives generation costs which are 0-3% lower. The cost of partial load operation is hence rather small compared to the renewables cost savings.

The potential total cycling costs can be calculated ex-post based on the data in Table 4.3 and turns out to be about a factor 5 to 10 higher than the direct start costs in this case (Fig. 4.7). The reduction in generation cost due to renewables however still outweighs the increase in total cycling costs. The indirect start cost, representing capital replacement and maintenance costs, is about 40% of total cycling costs. The ramping costs, i.e., capital and maintenance costs due to load following, are rather small. The costs of increased forced outages caused by cycling are about 5% of total cycling cost. Each start-up/shut-down cycle results in a small increase in the forced outage rate. The cost of forced outages is the value lost due to these extra outages. In this chapter, it is assumed that the lost generation is replaced by gas turbines. The cost of forced outages is given by the difference between the cost of replacing the lost generation with gas turbines and the cost of the original generation. Finally, cycling causes a decrease in rated efficiency. The cost of this decreasing rated efficiency can be expressed as the difference in generation cost between a case with all generation at the decreased efficiency and a case with all generation at the original efficiency. The costs of increasing forced outage rates and decreasing rated efficiencies are calculated per week. However, these costs might persist for the remaining life time of the power plant if no proper maintenance and replacement actions are taken.

Up to now, only the direct start cost was taken into account in the unit commitment model. By taking the full cycling cost into account during the generation scheduling, the total cycling cost decreases. Fig. 4.8.a shows the total cycling cost if only the direct start costs are taken into account (solid line) and if total cycling costs are taken into account in the unit commitment (dashed line). The solid line gives the total cycling costs as shown in Fig. 4.7.

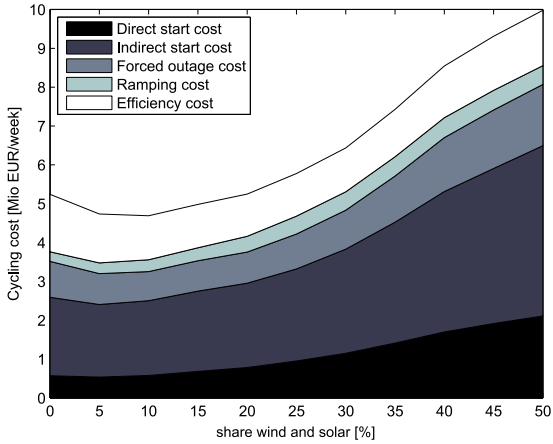

Figure 4.7: The total cycling cost is about a factor 5 to 10 higher than the direct start cost (average data for considered weeks, high-dynamic portfolio).

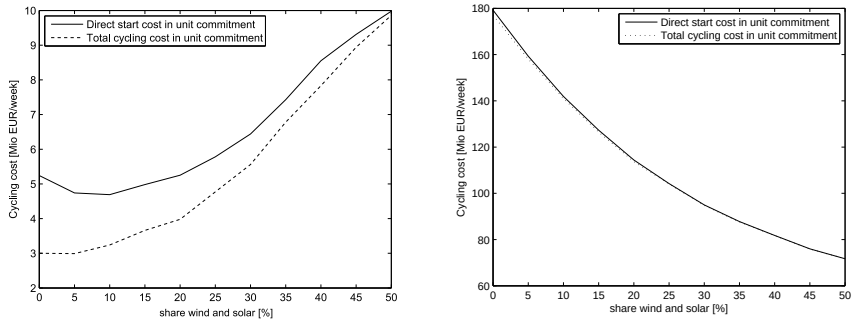

(a) Cycling costs.

(b) Total operational cost.

Figure 4.8: Cycling costs decrease if they are taken into account in the unit commitment decision, however, impact on the total operational cost is small (average data for all considered weeks, high-dynamic portfolio).

The difference between the solid and the dashed line indicates the possible cost savings by taking all cycling costs into account in the unit commitment decision. At low renewable generation, about 25-40% of the total cycling cost can be saved (equal to about 1% of the total operational system cost). At higher renewables share the cycling costs converge as cycling is needed to keep the system feasible,

regardless of its costs. The total operational costs are barely influenced by the cycling costs taken into account in the unit commitment model (see Fig. 4.8.b).

In conclusion of this subsection, the generation costs decrease with increasing renewable generation due to less fossil fuel consumption. The fossil fuel savings largely outweigh the decrease in operating efficiencies due to partial load operation. These results are consistent with the literature. This chapter additionally shows that all types of cycling costs increase with increasing renewables. Overall, the total operational system cost decreases with increasing renewable generation. This conclusion holds for the low and the high-dynamic portfolio.

4.5 Summary and conclusions

Conventional power plant cycling is an important source of operational flexibility in an electricity generation system with a large penetration level of intermittent renewables like wind and solar photovoltaics. Cycling is constrained by the dynamic limits of the generation portfolio and entails a range of costs. This chapter quantifies the limits and costs of conventional power plant cycling, based on a case study inspired by the German 2013 electricity generation system. The focus of this chapter lies on the wide range of cycling parameters reported in the literature and their impact on the cycling behavior of the conventional generation portfolio.

Two different sets of dynamic parameters are assigned to the same set of power plants. The first set represents a low-dynamic portfolio whereas the second set corresponds to a high-dynamic portfolio. It turns out that both portfolios are able to meet the residual load (i.e., the electricity demand minus generation from renewables), even up to a level where the residual load corresponds to a 50% wind and solar share. In other words, the dynamic limits of the generation portfolio as a whole are not reached.

All cycling costs rise with increasing variability in the residual demand. The direct start-up cost, which is often the only cycling cost included in unit commitment models, could be only 10-20% of the total cycling cost. Considering all cycling costs in the unit commitment scheduling can decrease the total cycling cost with up to 40%. This chapter solely focusses on the costs caused by cycling of a power plant in the day-ahead electricity market. However, other revenue streams for a power plant operator might exist besides the day-ahead market, e.g., remunerations for ancillary services or capacity payments, which should also be considered in assessing the economic viability of a power plant.

Cycling of conventional units could be reduced by increasing the availability of other short-term flexibility options, such as electric storage, demand response, curtailment of renewable generation and increased transmission flexibility. For instance, in terms of system inertia, a lot is expected from renewables contributions connected through power electronics. Future work should address these other flexibility options and investigate the reduction in cycling costs that can be achieved by deploying them.

Chapter 5

Redispatching with high renewables penetration

Chapter based on:

K. Van den Bergh, D. Couckuyt, E. Delarue, and W. D'haeseleer. Redispatching in an interconnected electricity system with high renewables penetration. Electric Power Systems Research, 127:64-72, 2015.[1]

Abstract: Grid congestion management is gaining importance in certain parts of the European electricity grid. The deployment of renewable electricity sources at locations with a weak grid connection and far from the load centers can lead to overloading of transmission lines. Redispatching, i.e., rearranging scheduled generation and consumption, might be needed to obtain a feasible and safe operational state of the electricity system. This chapter studies the impact of three parameters on the redispatching quantities and costs: (1) loop flows through the electricity system, (2) an increase in renewable generation in remote areas, and (3) a corrective and preventive N-1 security criterion. Towards this aim, a dedicated generation scheduling model is developed, consisting of a day-ahead market and a redispatch phase. The Belgian power system is considered as case study. Three general conclusions can be drawn from this chapter. First, it is important to consider loop flows when quantifying redispatching, especially in a highly interconnected electricity system as the European system. The case study shows that loop flows can more than double

[1]The publication on which this chapter is based benefited from discussions with, apart from the co-authors, C. Bastiaensen, S. Van Campenhout, G. Van Cauwenbergh, P. Van Roy and T. Wijsmans (all with Elia System Operator).

the need for redispatching. Second, transmission grid constraints might restrict the deployment of renewables in certain areas. Third, relaxing the N-1 security criterion in congested grid areas from preventive to corrective can drastically reduce the redispatch costs.

Keywords: Congestion management, redispatching, renewables integration, loop flows, N-1 security.[2]

5.1 Introduction

Transmission constraints restrict the amount of electric power that can be transported between two points in the grid. A grid congestion occurs whenever the physical or operational transmission limit of a line is reached or violated (Bompard et al., 2003). Congestion management can be defined as all actions taken to avoid or relieve congestion in the electricity grid (Kumar et al., 2005).

Congestion management is becoming increasingly important in a system with a high penetration of intermittant renewables. According to ENTSO-E (2012b), the association of European Transmission System Operators for Electricity, 80% of the bottlenecks identified in the European grid are directly related to renewables integration. Renewable generation units are often installed in areas with a high load factor, but not necessarily close to the load center or to the existing high voltage grid (e.g., offshore wind farms) (Burke and O'Malley, 2010). ENTSO-E distinguishes between direct connection issues (i.e., the connection between the renewable generation unit and the existing grid) and congestion issues (i.e., congestion in the existing grid between the renewable generation unit and the load center). The latter is dealt with in this chapter.

Often, transmission constraints are only taken into account to a limited extent in electricity markets. The European market clearing algorithm determines the accepted generation and consumption bids within a bidding zone, and the exchange with other zones.[3] The transmission limits between different bidding zones are considered in market clearing, but transmission constraints within a bidding zone are neglected. This can lead to grid congestion which needs to be solved by proper congestion management.

[2] All abbreviations and symbols used in this chapter are listed and explained at the outset of this dissertation.

[3] Allocation of the cross-border capacity to generators or consumers can happen explicitly or implicitly. In explicit cross-border allocation, a market player first has to obtain the right to use the cross-border capacity before electricity can be traded with a market player in another bidding zone. In implicit cross-border allocation, cross-border capacity is allocated together with the trade of electricity between different bidding zones.

Different forms of congestion management are discussed in the literature. One can distinguish between a centralized or a decentralized approach (Christie et al., 2000). According to the first approach, one centralized entity is responsible for managing grid congestion. This entity is typically the Transmission System Operator (TSO) or the Independent System Operator (ISO). In such centralized approach, generators and consumers trade electricity and schedule their generation and consumption units without taking account of the grid constraints within their bidding zone. The system operator then undertakes all required actions after the market clearing to avoid line overloading within the bidding zone. One of the possible remedial actions is redispatching. Redispatching is defined as rearranging the generation (and consumption) schedule in order to obtain a feasible schedule that respects all transmission constraints (Yamina and Shahidehpour, 2003; Dutta and Singh, 2008; Linnemann et al., 2011). Other short-term remedial actions are changing the set point of flexible transmission systems like phase shifting transformers (Yousefi et al., 2012). In the longer run, the system operator might invest in grid reinforcements to solve structural grid congestion (Acharya and Mithulananthan, 2007; Waniek et al., 2008; Afkousi-Paqaleh et al., 2010). According to the decentralized approach, the size of bidding zones is reduced and more transmission constraints are taken into account in the market clearing (i.e., the transmission constraints between the bidding zones). In the limit, every node in the electricity grid is a bidding zone. The result is locational price signals, i.e., electricity prices which can differ between different places in the grid when congestion occurs (Singh et al., 1998). In the short term, locational electricity prices give an incentive to generate and consume electricity at places in the grid which do not lead to congestion (Stoft, 1998; Hogan, 1999; Leuthold et al., 2008b). In the longer term, locational price signals would drive generators and consumers to install new generation or consumption units at places in the grid with little grid congestion.

Redispatching is an important congestion management measure in the European electricity sector, and this for two reasons. First, a centralized approach to congestion management is implemented, where the TSOs have the responsibility to reduce and avoid grid congestion within their bidding zone. Second, due to the rapid deployment of renewable electricity, grid congestion becomes more common. In the short term, redispatching is the main tool for the TSO to relieve grid congestion. Due to these two reasons, one sees an increase in redispatching in the European electricity grid (Linnemann et al., 2011). In Germany, for instance, redispatching is a pressing issue at the time of writing.

This chapter focusses on redispatching as congestion management tool. The aim of this study is to quantify the redispatch quantities and costs for a realistic case study, and investigate the impact of loop flows, increasing renewable generation

and the N-1 security criterion. Towards this aim, the Belgian electricity system is studied in detail. The Belgian system is an exemplary case to illustrate the congestion issues that can arise due to renewables deployment. Belgium aims to integrate a considerable amount of offshore wind generation, but the current grid connection between the shore and the main load centers is rather weak, causing grid congestion. Similar situations occur in other places in the European grid. Although the results presented in this chapter are case-specific, general trends and conclusions can be derived.

This chapter addresses congestion management with a market oriented approach. The focus lies on the market design in place to deal with congestion management and the redispatching that results from it. In this regard, a proper modeling of the generation portfolio is important in order to take account of dynamic power plant constraints which can impact redispatch costs (e.g., minimum up and down times). Another approach to congestion management is taken by a series of papers which focuses on the computational challenges related to models that determine a safe and secure grid operation, i.e., optimal power flow (OPF) models (Capitanescu et al., 2011). An OPF determines the optimal network operation. A security constrained optimal power flow (SCOPF) is a generalization of the OPF that additionally considers a set of postulated contingencies in the OPF (Capitanescu and Wehenkel, 2013). The (SC)OPF is a non-linear, non-convex, optimization problem which makes it hard to solve for large-scale electricity systems. However, large scale studies exist which present SCOPF case studies of, for instance, Great Britain (Macfie et al., 2010) and Poland (Jabr et al., 2012).

The added value of this chapter to the existing literature is twofold. First, the results presented in this chapter follow from a case study with very detailed grid data and time series, based on a real-life electricity system. This is unlike most market-oriented case studies on redispatching presented in the literature, which typically use a simplified or methodological test system (Yamina and Shahidehpour, 2003; Acharya and Mithulananthan, 2007; Yousefi et al., 2012). Second, this chapter studies quantitatively the impact of various parameters on redispatching (loop flows, increased renewable generation, and N-1 security criterion) whereas the existing literature takes these parameters as fixed. This chapter complements the existing literature and indicates the complexity of redispatching.

The chapter proceeds as follows. Section 5.2 gives an overview of the different redispatch options and costs for the TSO. Section 5.3 describes the model that is used to simulate the day-ahead generation scheduling and the redispatching phase. Section 5.4 presents the Belgian electricity system as case study. Section 5.5 presents and discusses the results. Finally, section 5.6 concludes.

5.2 Redispatch actions and costs

Electricity markets in Europe are zonal markets, meaning that every bidding zone is represented as one single node and connected to other nodes by cross-border links.[4] As a result, the market clearing does not take into account transmission limits within a bidding zone, and this may lead to technically infeasible generation schedules.[5] At this point, the TSO comes into play. The TSO performs an ex-post analysis to validate the feasibility of the generation schedule (i.e., after the day-ahead market has cleared but before the intra-day market starts). If grid congestion occurs within the bidding zone (or between bidding zones), the TSO issues redispatch orders to generators to reschedule their generation.

The TSO can issue different types of redispatch orders, each with a related cost (or revenue):

- A TSO can request an increase in power output of a conventional generation unit.[6] In return, the generator will expect a compensation for increasing its power output, equal to at least the additional generation cost. The additional generation cost consists of the cost for additional fuel, CO_2 emissions and possibly extra start-ups.
- A TSO can request a decrease in power output of a conventional generation unit. The generator will pay the TSO to decrease its power output, equal to at most the avoided generation cost.[7] The avoided generation cost consists of the cost for the non-used fuel, CO_2 emissions and possibly avoided start-ups.
- A TSO can request a decrease in renewable generation, if technically, practically and regulatory feasible.[8] The renewable generator will expect

[4]Most bidding zones in Europe coincide with countries, e.g., Belgium is one bidding zone, but exceptions exist. For instance, Germany and Austria are one bidding zone while Italy and the Scandinavian countries consist of multiple bidding zones per country.

[5]Since May 2015, flow-based market coupling is in place in Belgium, France, Germany and the Netherlands. In flow-based market coupling, transmission limits within zones can be taken into account (see chapter 7 for a description of flow-based market coupling).

[6]Conventional generation units refer to centralized and dispatchable units. In this chapter, conventional generation units refer to nuclear units and gas-fired units (no coal-fired units are operational in the considered electricity system).

[7]The running generation units have sold their electricity already in the day-ahead market at the day-ahead price. Conventional generators have the same pay-off when they run and incur generation costs than when they are off-line and pay the avoided generation costs to the TSO.

[8]A renewable generation unit can be used for redispatching purposes if curtailment of its power output is technically feasible, can be measured for billing purposes and is allowed by regulation.

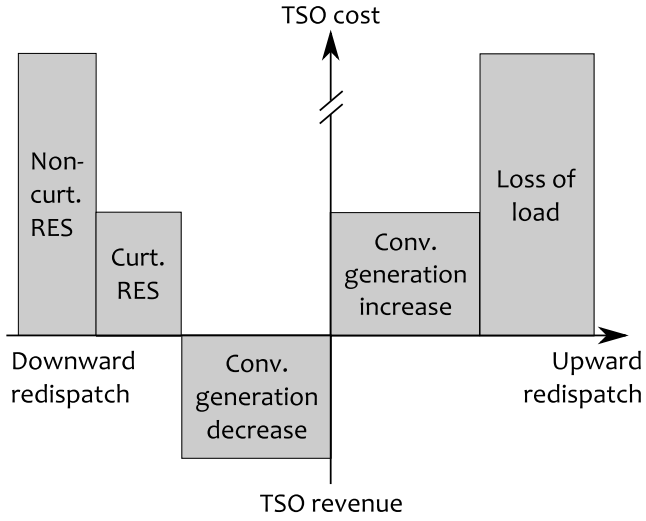

Figure 5.1: Schematic overview of possible redispatch actions for the Transmission System Operator (TSO) (RES: renewables, Curt.: curtailment, Conv.: conventional).

a compensation for curtailing its generation equal to at least the missed financial support for renewables (assuming a zero marginal generation cost).

Fig. 5.1 gives a schematic overview of the possible redispatch actions and costs for the TSO. The following numbers are used in this study and can give an idea of the costs and revenues related to redispatch orders (numbers are based on realistic costs for the Belgian system). The marginal generation costs of conventional units range from 18 EUR/MWh for nuclear units to 95 EUR/MWh for open-cycle gas turbines. The renewable support for curtailable renewables goes from 0 to 100 EUR/MWh. The cost used in this chapter for loss of load and curtailment of renewables with priority access is 10,000 EUR/MWh (i.e., indicating system infeasibilities). The net redispatch cost of the TSO will always be positive as the starting point of the redispatch phase, i.e., the day-ahead market outcome, is the result of a minimization of generation costs (without considering grid constraints). In the redispatch phase, expensive generation, which was not scheduled in the day-ahead market, needs to replace cheaper generation, which was scheduled in the day-ahead market.

Other redispatch actions than the ones mentioned in this section might be possible, such as topological actions and the use of phase shifters. However,

they are not dealt with in this chapter as they are not applicable to the considered case study. Topological actions are not used by the Belgian TSO to avoid redispatching of conventional generation units due to the short-term and time-variable character of redispatching, especially when caused by intermittent renewable generation. Moreover, by not using topological actions for short-term congestion management, a certain margin is still available to guarantee a safe grid operation, which can be used to deal with grid maintenance situations. No phase shifters are present within the studied electricity network (although there are phase shifters installed on the borders of the considered case study but they are used to control loop flows through the system and not for dealing with local congestion within the grid).

Note that this chapter only deals with day-ahead congestion caused by neglecting network constraints within bidding zones in the day-ahead market. Congestion that occurs intra-day or real-time due to contingencies or large variations in renewable generation is not discussed. However, a similar approach as presented in this chapter can be used to address the latter (although possibly without contingency constraints).

5.3 Model description

To study redispatching, the LUSYM model (see chapter 2) has been extended. The model consists of two sub-models which are solved sequentially, reflecting a two-step approach. In a first step, the optimal day-ahead generation schedule is determined with LUSYM, without taking into account the transmission limits within the bidding zone. In a second step, the day-ahead generation schedule is evaluated by means of a DC power flow and redispatch actions are taken to avoid transmission line overloading in the bidding zone. This two-step approach corresponds to the actual market design in which generators first schedule their generation units without considering intra-zonal transmission limits, followed by a feasibility evaluation of the generation schedule by the TSO. See also, for instance, van der Weijde and Hobbs (2011) who used a similar model set up to study closely related issues.

The optimal day-ahead generation schedule is determined by a unit commitment model. The output of the unit commitment model is the generation schedule that fulfills load at minimal operational generation cost. As already mentioned, transmission constraints within the considered bidding zone are not considered in this first step. Commercial exchange of electric power with neighboring bidding zones is limited by the Net Transfer Capacity (NTC) of the cross-border connections.

If the day-ahead generation schedule is infeasible due to grid constraints, generation needs to be rearranged. Any deviation from the day-ahead generation schedule will result in a net cost for the TSO as generation needs to be replaced by more expensive generation. The optimal redispatch schedule is determined by a redispatch model that minimizes the cost for the TSO. However, the possible redispatch actions are constrained by the unit commitment decision taken in the day-ahead market. The redispatch model determines a corrective N-1 secure system operation, meaning that the solution of the redispatch model is able to deal with line contingencies if corrective actions are allowed after the contingency occurred. Corrective actions refer to changing the economic dispatch of conventional generation units and changing the curtailment of renewables (Capitanescu et al., 2011).

The optimization model is meant to be used for market oriented studies of redispatching, and can be used towards this aim by researchers, policy makers, TSOs and regulators.

Both sub-models–unit commitment and redispatch–are formulated as mixed-integer linear programs in GAMS and solved with Cplex 12.6, using an optimality gap of 0.1%. The considered time period is one year with an hourly time step. The models solve blocks of two days, with one day overlap to ensure a correct coupling between the consecutive days.[9]

The applied methodology entails certain assumptions. First, the study is fully deterministic, meaning that no stochastic variables are considered (e.g., wind power forecast errors). The input parameters are the same in the day-ahead market and the redispatch model and are assumed to be perfectly known to all generators in advance. Second, the models use an hourly time step since the day-ahead markets in Europe are currently based on an hourly time resolution. Within this time resolution, not all variations in the time series for load and renewable generation are seen. Moreover, the (technical) ramping constraint of conventional units is not restricting on an hourly basis; no ramping constraints are considered in this study. Third, the modeling framework assumes a centrally cleared and perfectly competitive electricity market. In Belgium (and other European countries), electricity is traded day-ahead bilaterally and through power exchanges with (simplified) bidding. However, assuming a perfect competitive market, the market outcome of both market designs is very similar (Boucher and Smeers, 2001; Metzler et al., 2003). Fourth, it is assumed that all conventional units can be called upon by the TSO for redispatching at a

[9]The one-day overlap is based on the largest minimum up/down time in the generation portfolio (i.e., a 24 hour minimum up/down time for nuclear units, see Table 5.1). By working with a one-day overlap, the model considers the full length of the nuclear minimum up/down time when taking a decision to start-up/shut-down a nuclear unit at the end of the first considered day.

cost (revenue) equal to the additional (avoided) generation cost for increasing (decreasing) their power output. However, this might not be the case as the bidding strategies and generation costs are private and confidential information.

5.3.1 Day-ahead model (unit commitment)

The day-ahead unit commitment decision is determined by LUSYM (see chapter 2). For the sake of clarity, the relevant equations of the LUSYM model are repeated here. For clarification on the symbols, the reader is referred to the list of symbols at the outset of the dissertation. The superscript DA refers to the outcome of the day-ahead model. The objective function of the unit commitment model is the minimization of the operational costs, consisting of generation costs (fuel and CO_2 emissions) and start-up costs:

$$\min \sum_{i,t} NC_i \, z_{i,t}^{DA} + MC_i \, g_{i,t}^{DA} + SUC_i \, v_{i,t}^{DA} \tag{5.1}$$

The objective function is subject to the market clearing constraint (Eq. (5.2)), generation limits of conventional units (Eqs. (5.3)-(5.4)), minimum up and down time constraints (Eqs. (5.5)-(5.6)), the logic relation between different states of the power plants (Eq. (5.7)), upward and downward spinning reserves for conventional units (Eqs. (5.8)-(5.9)), binary constraints (Eq. (5.10)) and non-negative constraints (Eq. (5.11)). Renewables and load curtailment are not allowed in the day-ahead market, storage units are not included, no power plant outages occur and no ramping constraints and costs are imposed.

$$\sum_{i} z_{i,t}^{DA} \, \underline{P}_i + g_{i,t}^{DA} = \sum_{n} D_{n,t} - RES_{n,t} \qquad \forall t \tag{5.2}$$

$$0 \leq g_{i,t}^{DA} - r_{i,t}^{-,DA} \qquad \forall i, \forall t \tag{5.3}$$

$$g_{i,t}^{DA} + r_{i,t}^{+,DA} \leq (\overline{P}_i - \underline{P}_i) \, z_{i,t}^{DA} \qquad \forall i, \forall t \tag{5.4}$$

$$z_{i,t}^{DA} \geq \sum_{t'=t+1-MUT_i}^{t} v_{i,t'}^{DA} \qquad \forall i, \forall t \tag{5.5}$$

$$1 - z_{i,t}^{DA} \geq \sum_{t'=t+1-MDT_i}^{t} w_{i,t'}^{DA} \qquad \forall i, \forall t \tag{5.6}$$

$$z_{i,t-1}^{DA} - z_{i,t}^{DA} + v_{i,t}^{DA} - w_{i,t}^{DA} = 0 \qquad \forall i, \forall t \tag{5.7}$$

$$\sum_{i \notin I^{nuc}} r_{i,t}^{+,DA} \geq SR^{+} \qquad \forall t \tag{5.8}$$

$$\sum_{i \notin I^{nuc}} r_{i,t}^{-,DA} \geq SR^{-} \qquad \forall t \tag{5.9}$$

$$z_{i,t}^{DA},\, v_{i,t}^{DA},\, w_{i,t}^{DA} \in \{0,1\} \qquad \forall i, \forall t \tag{5.10}$$

$$g_{i,t}^{DA}, r_{i,t}^{-,DA}, r_{i,t}^{+,DA} \geq 0 \qquad \forall i, \forall t \tag{5.11}$$

5.3.2 Redispatch model

The redispatch model is very similar to the day-ahead model, with four differences: (1) the objective function changed to minimization of redispatch costs, (2) DC power flow constraints are imposed, (3) different line contingencies are considered in the constraints and (4) the day-ahead unit commitment decision of the nuclear units is set fixed. Again, the reader is referred to the list of symbols at the outset of the dissertation for clarification on the symbols. The superscript *RD* refers to the outcome of the redispatch model. The objective function of the redispatch model is:

$$\min \sum_{i,t} \Big(NC_i \,(z_{i,t}^{RD} - z_{i,t}^{DA}) + MC_i \,(g_{i,t,1}^{RD} - g_{i,t}^{DA}) + SUC_i \,(v_{i,t}^{RD} - v_{i,t}^{DA}) \Big) + \sum_{n,t} (RCC_n \, rc_{n,t,1}^{RD} + LCC_n \, lc_{n,t,1}^{RD}) \tag{5.12}$$

Only the N-situation is considered in the objective function (c equal to 1), but all N-1 situations are considered in the constraints. The objective function is subject to the market clearing constraint (Eq. (5.13)), the day-ahead on/off-decision for nuclear units (Eq. (5.14)), generation limits of conventional units (Eqs. (5.15)-(5.17)), minimum up and down time constraints (Eqs. (5.18)-(5.19)), the logic relation between different states of the power plants (Eq. (5.20)), upward and downward spinning reserves for conventional units (Eqs. (5.21)-5.22), renewables and load curtailment limits (Eqs. (5.23)-(5.24)), grid limitations (Eqs. (5.25)-(5.26)), binary constraints (Eq. (5.27)) and non-negative constraints (Eq. (5.28)). Storage units are not included, no power plant outages occur and no ramping constraints and costs are imposed.

$$\sum_{i} A_{n,i}^{plant} \,(z_{i,t}^{RD} \, \underline{P}_i + g_{i,t,c}^{RD}) + RES_{n,t} - rc_{n,t,c}^{RD} = D_{n,t} - lc_{n,t,c}^{RD} + p_{n,t,c}^{RD} \qquad \forall n, \forall t, \forall c \tag{5.13}$$

$$z_{i,t}^{RD} = z_{i,t}^{DA} \qquad \forall i \in I^{nuc}, \forall t \tag{5.14}$$

$$0 \leq g_{i,t,c}^{RD} \leq (\overline{P}_i - \underline{P}_i)\, z_{i,t}^{RD} \qquad \forall i, \forall t, \forall c \tag{5.15}$$

$$0 \leq g_{i,t,1}^{RD} - r_{i,t}^{-,RD} \qquad \forall i, \forall t \tag{5.16}$$

$$g_{i,t,1}^{RD} + r_{i,t}^{+,RD} \leq (\overline{P}_i - \underline{P}_i)\, z_{i,t}^{RD} \qquad \forall i, \forall t \tag{5.17}$$

$$z_{i,t}^{RD} \geq \sum_{t'=t+1-MUT_i}^{t} v_{i,t'}^{RD} \qquad \forall i \notin I^{nuc}, \forall t \tag{5.18}$$

$$1 - z_{i,t}^{RD} \geq \sum_{t'=t+1-MDT_i}^{t} w_{i,t'}^{RD} \qquad \forall i \notin I^{nuc}, \forall t \tag{5.19}$$

$$z_{i,t-1}^{RD} - z_{i,t}^{RD} + v_{i,t}^{RD} - w_{i,t}^{RD} = 0 \qquad \forall i, \forall t \tag{5.20}$$

$$\sum_{i \notin I^{nuc}} r_{i,t}^{+,RD} \geq SR^{+} \qquad \forall t \tag{5.21}$$

$$\sum_{i \notin I_{nuc}} r_{i,t}^{-,RD} \geq SR^{-} \qquad \forall t \tag{5.22}$$

$$0 \leq rc_{n,t,c}^{RD} \leq RES_{n,t} \qquad \forall n, \forall t, \forall c \tag{5.23}$$

$$0 \leq lc_{n,t,c}^{RD} \leq D_{n,t} \qquad \forall n, \forall t, \forall c \tag{5.24}$$

$$\underline{F}_{l,c} \leq \sum_{n} PTDF_{l,n,c}\, p_{n,t,c}^{RD} \leq \overline{F}_{l,c} \qquad \forall l, \forall t, \forall c \tag{5.25}$$

$$\sum_{n} p_{n,t,c}^{RD} = 0 \qquad \forall t, \forall c \tag{5.26}$$

$$z_{i,t}^{RD}\,,\, v_{i,t}^{RD}\,,\, w_{i,t}^{RD} \in \{0,1\} \qquad \forall i, \forall t \tag{5.27}$$

$$g_{i,t,c}^{RD}\,,\, r_{i,t}^{-,RD}\,,\, r_{i,t}^{+,RD} \geq 0 \qquad \forall i, \forall t, \forall c \tag{5.28}$$

The redispatch model is developed by the author and dedicated to this study. A DC power flow model of the electricity network is being used. The main advantage of a DC power flow model is its linearity compared to the non-linear AC power flow model. This allows solving large power systems for multiple time steps in a limited run time. The disadvantage of a DC power flow is its reduced accuracy. The literature mentions, for high voltage grids, an average 5% deviation between line flows in a DC power flow model and in an AC power flow model (Purchala et al., 2005b). However, the use of a DC power flow is justified in this chapter given its focus on yearly aggregated redispatch quantities and costs, rather than on particular line flows in specific hours.

5.4 The Belgian power system as case study

The case study presented in this chapter is the expected Belgian 2016 system (see Fig. 5.2). Belgium has a well developed and meshed high voltage grid, connecting the main load and generation centers. Therefore, grid congestion and congestion management were never a pressing issue for the Belgian TSO in the past. However, this has changed due to the deployment of offshore wind power in the Belgian North Sea. Over the last years, about 800 MW of offshore wind power has been commissioned. This raises congestion issues as the transmission grid connecting the shore with the 380 kV grid was not designed to accommodate large landward power flows from offshore wind. As a result, congestion in the existing 150 kV grid in the coastal area becomes more apparent. At the same time, injections of onshore renewable generation in this area are increasing as well, further worsening the situation. The Belgian case is exemplary for the difficulties associated with the deployment of renewable generation in areas where the grid was not built to accommodate these new injections.[10]

The model to simulate the electricity grid in this study (in the redispatch model) is a detailed DC power flow model with 161 nodes and 241 line elements (transmission lines, transformers and couplings). The whole Belgian 380 kV transmission grid is included, together with the 150 kV grid in the Western part of Belgium. The remaining part of the 150 kV grid and the 220 kV grid are represented by equivalent lines and nodes. The grid model allows to study grid congestion in the coastal region in detail. Not all line contingencies are considered in the N-1 analysis. Eight critical line outages are determined ex-ante by the TSO experts and taken into account in the redispatch optimization. In a N-1 situation, transmission flows can go to 120% of the rated line capacity.

Historical nodal load measurements are scaled up and used as demand time series. The annual electric energy demand is 90.2 TWh, with a peak demand of 13.9 GW in the winter and the lowest demand in the summer of about 6 GW. About 7% of the electricity consumption is located in the coastal region. The load time series are corrected for commercial exchange with neighboring countries. The commercial cross-border trade is imposed on the model as an exogenous parameter. In the case study, Belgium imports on an annual basis 10.8 TWh from France and 3.3 TWh from the Netherlands. Note that no direct connection with Germany exists at the present time.

The generation portfolio consists of 23 conventional generation units, with

[10]The Belgian TSO is, at the time of writing, strengthening the grid with a new 380 kV connection between the shore and the existing 380 kV grid. This new connection is not expected to be in place before the end of 2016.

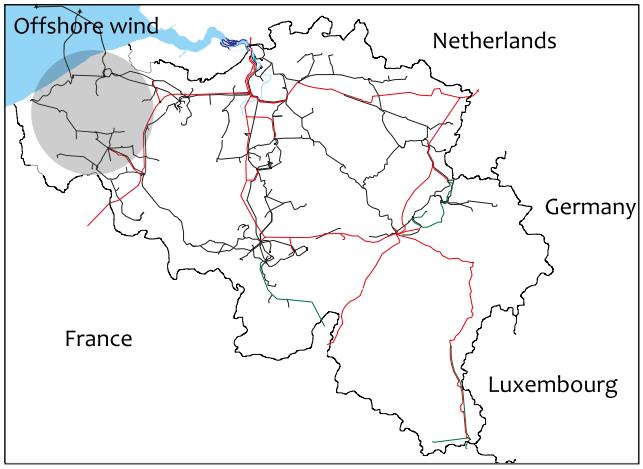

Figure 5.2: Overview of the Belgian high voltage grid (red: 380 kV lines, green: 220 kV lines, black: 150 kV lines) (Elia, 2014). Grid congestion occurs in the grey area between the offshore wind farms in the North Sea and the 380 kV grid.

	$\sum \overline{P}$ [GW]	$\underline{P}$ [%$\overline{P}$]	MUT,MDT [h]	NC [kEUR/h]	MC [EUR/MWh]	SUC [kEUR/start]
NUC	5.1	95	24	8-18	18	6
CCGT	2.9	35	3	1.2-16	65-95	83-555
OCGT	0.6	30	1	1-4	70-85	28

Table 5.1: Overview of technical characteristics per technology (NUC: nuclear, CCGT: combined-cycle gas turbines, OCGT: open-cycle gas turbines, $\overline{P}$: maximum power output, $\underline{P}$: minimum power output, MUT: minimum up time, MDT: minimum down time, NC: generation cost at $\underline{P}$, MC: marginal generation cost, SUC: start-up cost) (Schröder et al., 2013).

an aggregated capacity of 8.6 GW. Table 5.1 shows the technical parameters and generation costs allocated to the conventional generation units (Schröder et al., 2013). In this study, the author assumes that all online conventional units can ramp-up and ramp-down for redispatching purposes. Gas-fired units (combined-cycle gas turbines and open-cycle gas turbines) can also start-up and shut-down for redispatching purposes. Nuclear units cannot change their on/off-state for redispatching purposes due to too large minimum up and down times.

Historical time series for renewable generation and generation from cogeneration

units are scaled up and used. Renewable generation refers to generation from conventional hydro, wind energy (offshore and onshore), bio-energy and photovoltaic energy. Three types of renewables are considered, based on the curtailment cost for redispatching purposes. One distinguishes onshore renewable generation with a flexible contract, offshore wind generation and onshore renewable generation with priority grid access. The flexible onshore renewable generation is located in the coastal area and connected to the grid under the condition that the TSO can curtail them at zero cost for redispatching purposes. About 180 MW of renewable generation capacity is operated under such a flexible capacity, accounting for a generation of 0.4 TWh/a. Offshore wind can be curtailed in the redispatch phase at the cost of the financial support for offshore wind generation, i.e., 100 EUR/MWh. By 2016, 870 MW of offshore wind capacity is expected in the Belgian North Sea, accounting for a generation of 3.1 TWh/a (i.e., normal wind year with a load factor of 40 %). The onshore renewable generation capacity with priority access to the grid is about 6.2 GW, responsible for a yearly generation of 11.2 TWh. The redispatch model allows curtailment of these last renewable generation units only at a very high cost of 10,000 EUR/MWh. Moreover, 4.1 GW of cogeneration units (electric capacity) is installed, with a yearly electricity generation of 23.5 TWh/a. No curtailment of cogeneration units is allowed.

Recall that the studied power system is the expected 2016 Belgian power system, based on hypotheses regarding the development of generation capacity and demand. As such, the presented results should be interpreted with caution.

5.5 Results and discussion

This section presents the redispatch quantities and the redispatch costs due to grid congestion in the considered case study. First the reference case is presented, i.e., the anticipated Belgian 2016 power system. In the following subsections, the impact of loop flows, increasing offshore wind and the N-1 security criterion are discussed.

5.5.1 Reference scenario: Belgian 2016 power system

The day-ahead market outcome for the reference scenario is shown on Fig. 5.3. In terms of TWh/a, the system load is mainly covered by renewable generation and cogeneration units (42%), nuclear generation (38%) and import (16%). CCGTs generate 2.5 TWh/a (load factor of the operating CCGTs is only 18%; part of the CCGT units is never used) and OCGTs generate 1 TWh/a (load

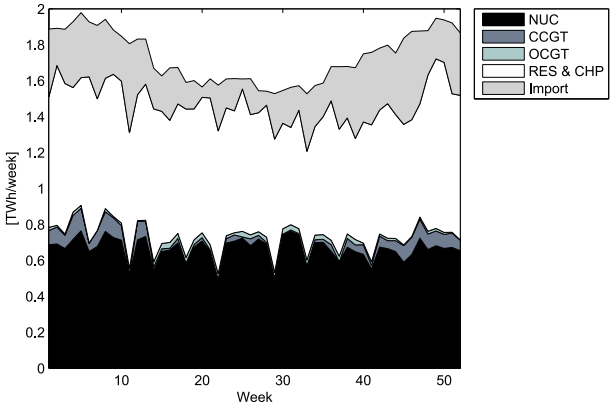

Figure 5.3: Weekly day-ahead generation schedule in the reference scenario (NUC: nuclear, CCGT: combined-cycle gas turbines, OCGT: open-cycle gas turbines, RES: renewables, CHP: cogeneration).

factor of 17%). These gas units are mainly brought online to fulfil the spinning reserve requirement. The total annual generation cost (fuel, CO_2 emissions and start-ups, excluding the cost of import) is 899 Mio EUR.

This day-ahead market solution then possibly needs to be adapted to get a feasible generation schedule that takes account of the grid constraints. The feasibility of the day-ahead generation schedule can be checked by calculating the grid flows through all transmission lines resulting from the day-ahead generation schedule, and this for the N-state and each considered N-1 state. If the capacity of at least one transmission line is exceeded, redispatching will be needed. It turns out that during 1,972 hours of the year (23% of the time), grid congestion occurs and redispatching will be needed.

The TSO has one option for upward redispatching–increasing conventional generation (Conv+)–and two for downward redispatching–decreasing conventional generation (Conv-) and curtailing flexible onshore renewable generation and offshore wind (RES-). From the redispatch simulation, it follows that 34.3 GWh/a of upward redispatching is required. The amount of upward and downward redispatching is by definition equal (the electricity demand still has to be met). The downward redispatching consists of 29.3 GWh/a of conventional generation that is ramped down and 5 GWh/a of curtailed renewable generation. Overall, the amount of redispatching is very limited as only 0.08% of the annual load is redispatched, or put differently, the hourly average redispatching is 4

MWh/h (compared to the average system load of 10 GW).[11] Loss of load and curtailment of renewable generation with priority access is only possible at the very high cost of 10,000 EUR/MWh, indicating system infeasibilities. However, neither loss of load nor curtailment of renewable generation with priority access occurs in the reference case. The annual redispatch cost is 2.9 Mio EUR.

The total amount of downward redispatching, i.e., 34.3 GWh/a, can be split in 15 GWh/a of downward redispatching in the coastal area and 19.3 GWh/a of downward redispatching in the rest of Belgium. The downward redispatching in the coastal area is a direct consequence of grid congestion (i.e., there is not enough transmission capacity to transport all planned generation from the coastal area landward). Downward redispatching in the rest of Belgium is caused by the minimum operating point of the units delivering upward redispatching. If a unit starts up for redispatch purposes, that unit has to operate above its minimum operating point. Therefore, additional downward redispatching might be needed elsewhere.

5.5.2 Impact of loop flows

In the reference case, only the commercial exchange of electricity with the neighboring countries was considered. However, the actual power flows on the cross-border lines can largely deviate from the commercial cross-border exchange, due to loop flows. Loop flows are power flows through the Belgian grid caused by a combination of injections and/or withdrawals in other parts of the European grid. As these loop flows enter and leave the control area (by the same amount), they do not impact the net exchange position of the Belgian system, but they do impact the flows through the transmission lines in the Belgian system and hence also the need for redispatching. This is clarified in an example below.

Loop flows are particularly important in a highly interconnected electricity grid like the European grid. The Belgian electricity grid is connected to the Netherlands in the north and to France in the south. The northern border has a Net Transfer Capacity (NTC) of 1,000 to 1,500 MW and the southern border has a NTC-value of 2,000 to 2,500 MW, both for the importing direction (Elia,

[11] The redispatch simulations indicate redispatch due to two reasons; grid congestion and renewables curtailment. In the day-ahead market, no renewables curtailment is allowed, while in the redispatch phase curtailment of flexible onshore renewables and offshore wind is possible. If renewables curtailment is a cost-efficient measure, the model will perform curtailment in the redispatch phase and reduce overall system costs (i.e., a net income for the TSO). However, this study only deals with redispatching due to grid congestion. Therefore the numbers shown in this chapter refer only to redispatching due to grid congestion.

2015).[12] The NTC-values are given to the electricity market as import/export constraint and used for commercial exchange between different market zones.

To check the effect of loop flows, an annually fixed loop flow is added to the commercial cross-border flow in the redispatch phase. The positive direction of the loop flow is defined from north to south (i.e., from the Netherlands to France). Consider, for instance, a certain time step where Belgium imports commercially net 1,000 MW from France in the south and 500 MW from the Netherlands in the north (net exchange position of Belgium is -1,500 MW). If a loop flow of 100 MW is imposed, the resulting physical flow on the southern border is 900 MW (net import) and 600 MW on the northern border (net import). The net exchange position of the Belgium area stays the same (-1,500 MW), but the power flows within the Belgium system are impacted by the loop flow.

Fig. 5.4 and Fig. 5.5 show the impact of loop flows on the amount of redispatching and the redispatch costs, respectively. Loop flows are varied from -2,000 MW to 2,000 MW in steps of 500 MW. The zero loop flow scenario corresponds to the reference case discussed in the previous subsection. Fig. 5.4 shows, for each loop flow scenario, the amount of upward redispatching (left bar, consisting of increasing conventional generation and loss of load) and the amount of downward redispatching (right bar, consisting of decreasing conventional generation and renewables curtailment). As explained before, the amount of upward and downward redispatching are equal. Redispatching occurs only in a limited amount of hours (i.e., in about 7-10% of the hours). At very negative loop flows, redispatch costs are mainly driven by offshore wind curtailment (i.e., 100 EUR/MWh curtailed offshore wind energy). Note that the redispatching costs shown on Fig. 5.5 excludes loss of load cost, while 2 GWh annual loss of load occurs at loop flows of -2,000 MW (see Fig. 5.4).

The impact of loop flows on redispatching is considerable. The redispatched energy and the redispatch costs more than double for large negative loop flows, i.e., northward loop flows. At a loop flow of -2,000 MW, loss of load is needed in the simulations, indicating system infeasibilities (all nodal load can no longer be met). Curtailment of renewables with priority access, i.e., another system infeasibility, never occurs. It turns out that loop flows from the south to the north strongly increase the need for redispatching, whereas loop flows in the other direction have a more modest impact on redispatching. This can be understood as follows; grid congestion is mainly caused by west-east flows in the coastal region (offshore wind generation needs to be transported from the Sea in the west to the main load centers landinward). A loop flow from France to

[12] The NTC-value of a cross-border link depends on the direction (import or export) and the considered moment in time.

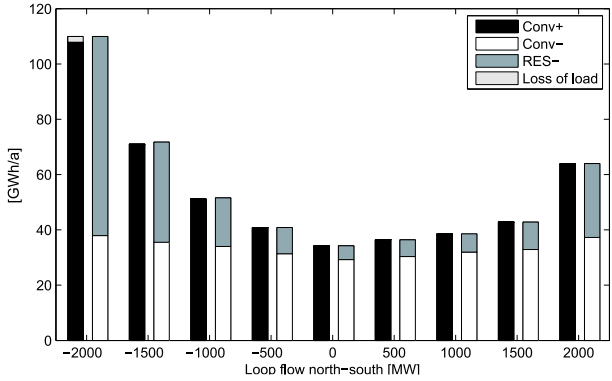

Figure 5.4: Impact of loop flows on redispatching for 9 loop flow scenarios. The left bar of each loop flow scenario shows the amount of upward redispatching (Conv+: increased conventional generation, and loss of load) and the right bar the amount of downward redispatching (Conv-: decreased conventional generation, and RES-: decreased flexible onshore renewable generation and offshore wind generation). Large negative loop flows can more than double the amount of redispatching.

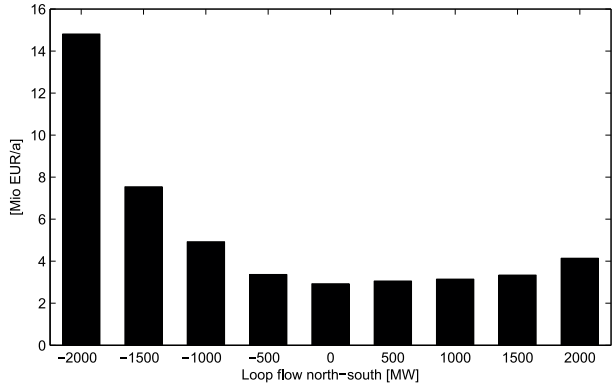

Figure 5.5: Impact of loop flows on redispatch costs for 9 loop flow scenarios (excluding loss of load cost). Redispatch costs increase drastically for large negative loop flows.

the Netherlands increases this west-east flow as part of the loop flow will enter Belgium in the south-west and leave Belgium in the north-east. A loop flow from the Netherlands to France counteracts the west-east flow, relieving congestion

in this direction. However, a north-south loop flow causes new congestion on the north-south lines in the coastal area. Both effects cancel each other out, resulting in more or less stable redispatch costs for increasing north-south loop flows.

Recall that in this section, it was assumed that a constant loop flow occurs during the whole year. In reality, different loop flows occur every hour, changing in magnitude and direction. Moreover, loop flows are equally distributed over the cross-border lines, whereas in reality–depending on the location of injections and withdrawals in the neighboring countries and/or the setting points of the phase shifting transformers–loop flows are mostly not equally distributed over the cross-border lines[13].

Loop flows can–to a certain extent–be mitigated by phase shifting transformers. The redispatch cost savings that can be obtained by mitigating loop flows can be read from Fig. 5.5 by comparing the costs in a loop flow scenario with the cost in a zero loop flow scenario. Installing a phase shifter to mitigate redispatch costs can be interesting if the avoided redispatch costs surpass the investment and maintenance costs over the life time of the phase shifter (although various other aspects should be considered, such as the controllability of the phase shifter).

5.5.3 Impact of increasing offshore wind

Offshore wind energy is–by definition–deployed in remote areas and has as such often a considerable impact on the transmission network. To investigate the effect of increasing offshore wind capacity, a sensitivity analysis is performed. The installed offshore wind capacity is varied from 800 MW to 2,300 MW in steps of 500 MW (offshore wind capacity in the reference case is 870 MW, expected offshore wind capacity by 2020 is about 2,300 MW). The offshore wind generation profile is scaled up in proportion to the installed capacity. This increased offshore generation impacts both the day-ahead generation schedule and the need for redispatching. The redispatching model considers only a case with zero loop flows.

The increase in offshore wind generation in the day-ahead market is compensated by a decrease in generation from nuclear power plants and gas-fired power plants. Offshore wind generation increases from 2.8 TWh/a to 8.1 TWh/a for 800 MW and 2,300 MW of installed capacity, respectively. Additional offshore wind generation pushes out first the most expensive conventional units, i.e., gas-fired

[13]There are phase shifting transformers installed on the Belgian border with the Netherlands and with France, with the aim to mitigate loop flows.

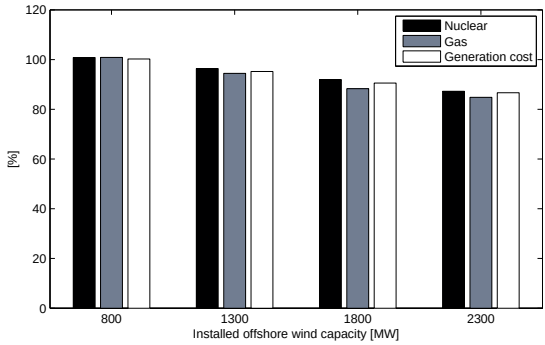

Figure 5.6: Impact of additional offshore wind capacity on conventional generation and operational generation costs in the day-ahead market. The figure shows the annual nuclear generation, the annual gas-fired generation and the annual generation system costs, all expressed relatively to the reference case with 870 MW offshore wind capacity.

power plants. However, additional offshore wind generation increases the need for flexibility which is preferably delivered by gas-fired generation. These two effects cancel out each other, resulting in both a decrease in gas-fired generation and nuclear generation for an increasing amount of offshore wind capacity (see Fig. 5.6). The operational generation cost decreases with increasing offshore wind generation, from 901 Mio EUR for 800 MW offshore wind capacity to 779 Mio EUR for 2,300 MW offshore wind capacity.

Fig. 5.7 and Fig. 5.8 show the amount of redispatching and the redispatch costs for increasing offshore wind capacity. The amount of redispatching and the redispatch costs increase drastically with increasing offshore wind generation. For 2,300 MW of offshore wind capacity, about 3% of the annual electricity demand needs to be redispatched. As of 1,800 MW of offshore wind, loss of load occurs in the redispatch simulations, indicating system infeasibilities (i.e., 56 GWh/a at 1800 MW offshore wind and 100 GWh/a at 2300 MW offshore wind). It might seem counter-intuitive that more installed offshore wind capacity leads to more loss of load, but more offshore wind generation reduces the upward redispatch options. Due to more offshore wind generation, some nuclear units are shut down during certain days in the day-ahead generation schedule. These nuclear units cannot be started up again in the model for redispatching purposes when it turns out that not all scheduled offshore generation can be transported to the load centers. This might lead to loss of load in the redispatch phase. The redispatch costs rise drastically for increasing offshore wind capacity (see Fig. 5.8, loss of load costs not included). This increase is to a large extent

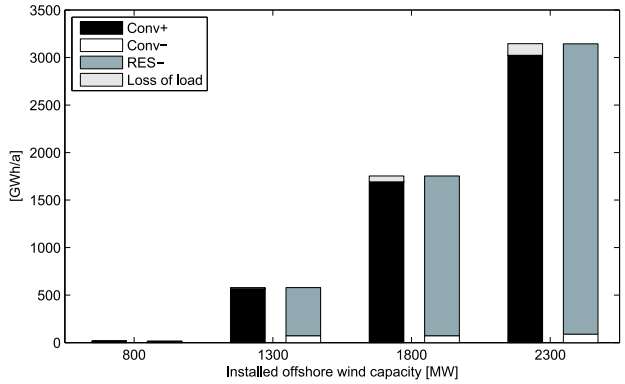

Figure 5.7: Impact of additional offshore wind on redispatching. The left bar of each offshore wind scenario shows the amount of upward redispatching (Conv+: increased conventional generation, and loss of load) and the right bar the amount of downward redispatching (Conv-: decreased conventional generation, and RES-: decreased flexible onshore renewable generation and offshore wind generation). The amount of redispatching increases drastically above 1,000 MW offshore wind capacity.

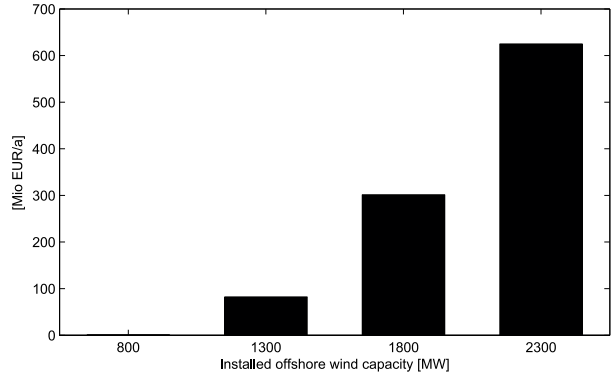

Figure 5.8: Impact of additional offshore wind on redispatch costs (excluding loss of load cost). Redispatch costs explodes with increasing offshore wind.

caused by the curtailment of offshore wind at a cost of 100 EUR/MWh. At high installed offshore wind capacities, most of the generation of every additional MW offshore wind has to be curtailed to avoid line overloading.[14]

[14]The Belgian TSO is, at the time of writing, strengthening the grid connection between the shore and the main load centers inland in order to accommodate an increase in offshore

5.5.4 Impact of preventive N-1 security criterion

A corrective N-1 security criterion has so far been implemented in the redispatch phase. In a corrective N-1 secure system, the economic dispatch of conventional units and the curtailment of renewables can be changed after the line contingency occurred. In a preventive N-1 secure system, a line contingency has to be passed without changing the economic dispatch or curtailment. A preventive N-1 secure system is hence more stringent than a corrective system. This subsection discusses the impact on redispatching of the more stringent preventive N-1 security criterion, compared to a corrective N-1 security criterion.

The redispatch model is extended with the following three equations to impose a preventive N-1 security criterion, instead of a corrective one:

$$g^{RD}_{i,t,c} = g^{RD}_{i,t,1} \qquad \forall i, \forall t, \forall c \tag{5.29}$$

$$rc^{RD}_{n,t,c} = rc^{RD}_{n,t,1} \qquad \forall n, \forall t, \forall c \tag{5.30}$$

$$lc^{RD}_{n,t,c} = lc^{RD}_{n,t,1} \qquad \forall n, \forall t, \forall c \tag{5.31}$$

Eqs. (5.29)-(5.31) impose on the model that the economic dispatch, renewables curtailment and loss of load have to be the same for every N-1 situation. Recall that eight critical line outages, which are determined ex-ante by TSO experts, are considered in the N-1 analysis, and that transmission flows can go to 120% of the rated line capacity in a N-1 situation,.

Fig. 5.9 shows the impact of the N-1 security criterion on the redispatch quantities for the reference case (i.e., 870 MW offshore wind, no loop flows). Without a N-1 security criterion, almost no redispatching is required. With a corrective N-1 security criterion, 34.3 GWh/a of redispatching is needed (i.e., the reference case). This increases to 220 GWh/a in case of preventive N-1 security (of which 3 GWh/a loss of load). With preventive N-1, loss of load occurs, indicating system infeasibilities.

The redispatch cost increases from 0.2 Mio EUR without a N-1 security criterion to 2.9 Mio EUR with corrective N-1 and 25.9 Mio EUR with preventive N-1 (excluding loss of load costs). This allows to determine the cost of N-1 security as the difference between the cost with and without N-1 security. For the considered power system, the annual cost of a corrective N-1 criterion is 2.7 Mio EUR and 25.7 Mio EUR for a preventive N-1 criterion.

wind. With this additional grid connection in place, the Belgian electricity grid will be able to facilitate the envisaged amount of offshore wind generation and redispatching due to offshore wind generation will no longer be an issue.

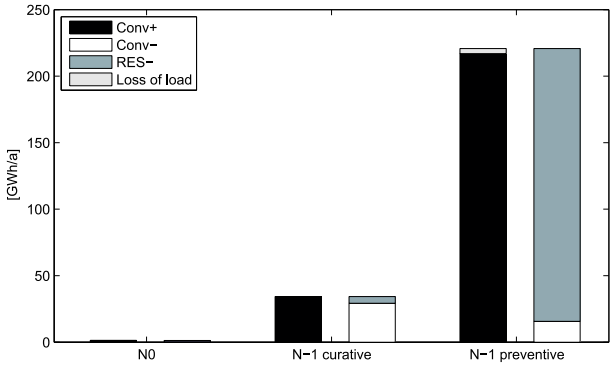

Figure 5.9: Impact of the N-1 security criterion on redispatching. The left bar of each security criterion shows the amount of upward redispatching (Conv+: increased conventional generation, and loss of load) and the right bar the amount of downward redispatching (Conv-: decreased conventional generation, and RES-: decreased flexible onshore renewable generation and offshore wind generation). The amount of redispatching depends heavily on the N-1 security criterion.

5.6 Summary and conclusions

This chapter discusses redispatching as tool for congestion management in interconnected electricity systems with a high penetration of renewables. The Belgian electricity system is studied as a case study. The Belgian system is embedded in the European electricity system and faces grid congestion issues due to the deployment of offshore wind without a strong grid connection between the shore and the main load centers inland. Based on the results presented in this chapter, three conclusions can be drawn.

First, it is shown that loop flows can have a considerable impact on redispatching. Loop flows are unintended power flows through a bidding zone, caused by injections and withdrawals outside the bidding zone. In the case study, redispatch quantities and costs increase with more than a factor 2 at high loop flows. Loop flows are relevant in a highly interconnected electricity system such as the European system. One can conclude that the impact of loop flows is too large to neglect and should therefore be considered, in particular in a highly interconnected power system.

Second, redispatch amounts and costs can increase drastically when additional (renewable) generation is added to congested areas. In the case study, the

increase in redispatching amounts and costs with increasing offshore wind capacity is very steep. One can conclude that transmission grid constraints restrict the deployment of renewables in certain areas, once grid congestion starts to occur. The amount of offshore wind capacity is, for the considered case study, the most important investigated parameter with respect to impact on redispatching.

Third, it is shown that the stringency of the N-1 security criterion imposed to the system has a large impact. In the case study, redispatch costs are a factor 8 higher if a preventive N-1 security criterion is imposed, compared to a corrective N-1 security criterion. One can conclude that relaxing the stringency of the N-1 security criterion, i.e., going from preventive to corrective N-1 security, can reduce redispatch costs drastically.

Chapter 6

Benefits of coordinating reserves among market zones

Chapter based on:

K. Van den Bergh, R. Broder Hytowitz, K. Bruninx, E. Delarue, W. D'haeseleer, and B. Hobbs. Benefits of coordinating sizing, allocation and activation of reserves among market zones. Submitted for publication, 2016.

Abstract: Due to the increased penetration of intermittent renewables, operating reserves are becoming increasingly important in electricity markets. Coordinating the sizing, allocation and activation of reserves among market zones can decrease operational costs and enhance system reliability. However, network limitations constrain reserve coordination among zones. This chapter investigates the value of interzonal coordination of reserve sizing, allocation and activation. A series of three models that simulate unit commitment and dispatch decisions within network-constrained markets simulate the impact of intermarket coordination of each of these sets of decisions. A case study for the Central Western European electricity system indicates that such coordination can lower operational costs and increase system reliability. However, the best performing strategy for the considered case study turns out to be a strategy with coordinated activation but uncoordinated sizing and allocation of reserves due to suboptimal coordination of sizing and allocation with activation. In particular, because transmission constraints are simplified when sizing and allocating reserves, reserves might not actually be deliverable to where renewable output is different from forecast.

Keywords: Power system analysis, unit commitment, reserves, cross-border coordination, Central Western European electricity system.[1]

6.1 Introduction

Short-term reserves are needed in electricity systems to balance demand and supply at all times. Short-term reserves or operational flexibility is defined as the ability of a system to deploy its resources to respond to changes in load or generation within the time frame of minutes to hours (Lannoye et al., 2012). Electricity systems have always embedded a certain level of flexibility in order to deal with variable load, load forecast errors and unexpected power plant or transmission outages. However, short-term reserves are gaining importance in today's electricity markets due to the rapid growth of intermittent renewable sources (Perez-Arriaga and Batlle, 2012). Intermittent renewables, such as wind and solar photovoltaics, are characterized by variable output that is only partially predictable and dispatchable. As a result, the need for short-term reserves has increased in systems with large amounts of intermittent generation from wind and solar photovoltaics (Holttinen et al., 2011; Van den Bergh and Delarue, 2015).

An important source of reserves in today's electricity systems is the flexible operation of conventional generation units (Cochran et al., 2014). Conventional generation units can deliver reserves by ramping-up or down (i.e., spinning reserves), and starting-up or shutting-down (i.e., non-spinning reserves). It is, however, uncertain whether today's fleet of conventional generators is able to deliver enough reserves at an acceptable cost to deal with an increasing penetration of intermittent renewables (Troy et al., 2010). Therefore, other operational flexibility options such as storage, demand response and curtailment of renewable oversupply, are extensively discussed in the academic literature and policy documents (Cochran et al., 2014). More flexible operation of the power system can also be obtained by coordinating reserve procurement and deployment among different market zones. As a result, system imbalances can be netted and the least costly generation unit, although possibly located in another market zone, can be scheduled and activated to deliver reserves.

This chapter focuses on reserves delivered by conventional power plants under various degrees of coordination between market zones. The following general procedure for operational reserve planning is simulated: (1) sizing of the need for reserves (i.e., how many MW of reserves should be scheduled day-ahead),

[1] All abbreviations and symbols used in this chapter are listed and explained at the outset of this dissertation.

(2) day-ahead allocation of reserves (i.e., which flexible units are scheduled to provide those reserves in real-time) and (3) real-time activation of reserves (i.e., which reserve capacity actually provides regulation services in real-time if needed).

Note that the term reserve is used in this chapter and not the more general term operational flexibility. Here, reserves refer to the short-term flexibility that can be delivered between day-ahead scheduling and real-time by conventional generation units in order to deal with renewables forecast errors. This definition of reserves is different from the definition typically used in the context of Transmission System Operators (TSOs). TSOs contract reserves and activate them in real-time to maintain the real-time system balance. This chapter, however, not only considers TSO reserves but also intra-day schedule adjustments by generators and consumers. Furthermore, this chapter focusses only on reserves needed to deal with renewables forecast errors, not with other sources of uncertainty such as load forecast errors or contingencies.

The benefits of coordinating activation of reserves are widely accepted in the literature. Meeus et al. (2005) and Vandezande et al. (2010) emphasize the importance of cross-border balancing in a cost-effective and efficient electricity market. van der Weijde and Hobbs (2011) quantify the cost savings that arise from coordination of real-time markets for a simple 4-node system. Cost savings turn out to be always positive, but the exact magnitude of the savings depends on various system parameters such as cross-border transmission capacity. A similar analysis is performed by Oggioni and Smeers (2013). They show, based on an illustrative network, that coordination between different system operators can reduce the cost of real-time counter-trading. Vandezande et al. (2009) estimated that the balancing costs in Belgium and the Netherlands could have been 40% lower in 2008 if cross-border balancing were in place. But despite these apparent benefits, coordination of real-time and balancing markets is still limited in Europe (Doorman and van der Veen, 2013).

While some papers explore reserves and balancing, they do not explicitly consider cross-border coordination of reserve sizing and allocation. The coordination of the sizing and allocation phases is more complex since the future system state is uncertain, whereas reserve activation happens in real-time when the system state is known. As such, deliverability of procured and scheduled reserves cannot be guaranteed since transmission constraints can hinder real-time reserve activation. One possible approach to including transmission constraints in coordinated sizing and allocation is to consider post-contingency states in the reserve allocation model (Chen et al., 2014). Another approach is to make reserve zones dynamic and adjust them to changing system states (Lyon et al., 2015; Wang and Hedman, 2015). However, both approaches are not applicable to the current deterministic and zonal European market design.

This chapter builds upon and generalizes the existing literature. This work makes two contributions:

1) It is investigated whether it is beneficial for market zones to coordinate sizing, allocation, and activation of reserves. Towards this aim, models are developed that determine the optimal sizing, allocation and activation of reserves, with and without coordination between market zones.

2) Coordinating reserve sizing and allocation can lead to cost reductions due to spatial smoothing of forecast errors and spatial arbitrage. However, coordination can also lead to suboptimal market outcomes as network constraints are typically neglected in the sizing and allocation phase. This trade-off is discussed in detail and quantified for a case study of the 2013 Central Western European electricity system (i.e., Belgium, France, Germany and the Netherlands).

Section 6.2 discusses the methodology and mathematical formulations. Section 6.3 presents and discusses the results for each of the three stages. Section 6.4 concludes the chapter.

6.2 Methodology

This chapter aims to analyze the benefits of coordinating the sizing, allocation and activation of reserves among different market zones. This section discusses the framework used to quantify those benefits, describes the simulation model and summarizes the case study of Central Western Europe.

6.2.1 Framework

Three sequential steps can be distinguished in the procedure of deploying reserves. First, the amount of reserves required to guarantee a safe and secure system operation is determined in the sizing phase. In this chapter, dynamic probabilistic sizing is applied, with two sources of uncertainty: solar power forecast errors (SPFE) and wind power forecast errors (WPFE). Second, the required reserves are allocated to conventional generation units in the allocation phase. Allocation happens simultaneously with the day-ahead energy market clearing. Finally, in the real-time activation phase, the scheduled reserves can generate power if needed to deal with SPFE and WPFE. In that phase, the unit commitment of slow units (i.e., nuclear units, coal-fired and lignite-fired units) is set fixed to the day-ahead market outcome, although the economic dispatch of all spinning units can still be changed.

	Scenario A	Scenario B	Scenario C	Scenario D
Sizing	-	-	-	+
Allocation	-	-	+	+
Activation	-	+	+	+

Table 6.1: Overview of the considered scenarios (+: coordination among market zones, -: no coordination among market zones).

In each of the three phases, the separate market zones can coordinate their activities. If activation is coordinated, scheduled reserves in one market zone can be used to cover forecast errors in another market zone. In a coordinated allocation phase, conventional generation units can be scheduled in one market zone in order to meet reserve requirements in another zone. In coordinated reserve sizing, multiple market zones determine their aggregate need for reserves together. However, not all combinations of coordination are meaningful. It makes no sense to coordinate reserve sizing but not allocation and activation. Analogously, it makes no sense to coordinate allocation but not activation. The possible combinations of coordination are shown in Table 6.1. In scenario A there is no coordination; every market zone is responsible for the sizing, allocation and activation of reserves in its market zone. This scenario corresponds, roughly speaking, to the current situation in European electricity markets. In scenario B, the activation of reserves is coordinated, but not sizing and allocation decisions. In scenario C, also the allocation of reserve is coordinated. Scenario D represents a fully coordinated situation.

Network constraints are considered in the scheduling of energy, i.e., in the day-ahead energy market clearing and in the real-time activation of reserves, but not in the sizing and allocation of reserves. This approach to network constraints reflects what is currently done in today's European markets (ENTSO-E, 2015b).

The deployed framework is based on certain assumptions. First, the modeling framework corresponds to a power pool model with joint energy and reserve scheduling, which does not fully correspond to the actual market design in Europe. European electricity markets consist of a mix of bilateral trading and power exchanges with (simplified) bidding for electric energy and long-term contracts for reserves. However, assuming a perfectly competitive energy market, the power pool model and the European market design should give similar outcomes in terms of generation quantities. Besides, the chapter assumes a perfect market for reserves, meaning that reserves are delivered by the units with the lowest allocation costs and this on a quarter-hourly basis, whereas reserves are contracted in Europe by means of long-term contracts (although reserve markets are moving towards more short-term contracts, i.e., daily or weekly instead of monthly or yearly). This is however a justifiable assumption,

as all simulations are based on the same simplification. Second, the chapter considers two snap shots: day-ahead and real-time. In reality, an intra-day market is organized between day-ahead and real-time in which generators can adapt their day-ahead position in response to continuously updated wind and solar forecasts. However, the model allows fast generation units (i.e., gas-fired units and oil-fired units) to start-up and shut-down in the real-time phase, hereby giving more flexibility to the real-time phase than strictly available in real-time. Moreover, the actual wind and solar power generation stays rather uncertain until only a couple of hours before the actual moment of delivery (Doherty and O'Malley, 2005). Therefore, neglecting the intra-day market has a limited impact on the presented results. Third, no uncertainty occurs in the real-time activation phase. The activation phase is implemented as a one-shot optimization with perfect information on wind and solar generation during the considered day. Finally, this chapter only deals with wind and solar forecast errors. In reality, other contingencies must also be taken into account, such as load forecast errors and power plant or line outages. However, focus is on the impacts of coordination and insights from this chapter will be useful to study other types of contingencies.

The analysis presented in this chapter focusses on the techno-economic aspects of sizing, allocating and activating reserves in a coordinated and uncoordinated manner. The author does not aim to duplicate, discuss or evaluate market designs. Therefore, no conclusions should be drawn from this analysis regarding market design or market rules. However, this analysis aims to provide additional insight in the costs and technical constraints faced by electricity generators and/or system operators when sizing, allocating and activating reserves (regardless of the market design and market rules in place).

6.2.2 Model description

The model contains three modules: a reserve sizing module, a day-ahead module which determines the optimal energy scheduling and reserve allocation, and a real-time reserve activation module.

Dynamic probabilistic reserve sizing

Probabilistic reserve sizing is based on the knowledge of the probability density functions (PDFs) of the probabilistic parameters in the power system, i.e., WPFE and SPFE in this chapter. The reserve need is determined in such a way that the forecast errors can be covered with a predefined probability. Dynamic reserve sizing refers to a time-varying reserve requirement. Conditional PDFs

are used, which allow calculating the probability for a forecast error given a day-ahead wind or solar forecast, resulting in different reserve requirements for different hours.

The conditional PDFs for WPFE and SPFE are derived from historical data on wind and solar day-ahead forecasts and actual realizations published by the Belgian and German TSOs (Elia, 2015; EEX, 2015b).[2] Forecast-dependent PDFs for WPFE are derived for Belgium and the Netherlands (based on Belgian data) and for France and Germany (based on German data). Analogously, forecast-dependent PDFs for SPFE are derived for Belgium and the Netherlands (based on Belgian data) and for France and Germany (based on German data). The same conditional PDFs are assumed for Belgium-Netherlands and Germany-France, given the similar size of the countries. The empirical observed conditional PDFs are approximated by a beta-distribution, which outperforms the Gaussian distribution for the description of WPFE and SPFE (Bludszuweit et al., 2008).

The PDF for combined WPFE and SPFE, given a certain day-ahead wind and solar forecast, follows from the convolution of their PDFs. The resulting PDF is only valid if WPFE and SPFE are uncorrelated. Historical WPFE and SPFE in Belgium and Germany show a correlation of 0.2 or less, which justifies this assumption.

Once the PDF for combined WPFE and SPFE is known, the upward and downward reserve requirement can be derived in order to cover the forecast errors with a certain probability, i.e., the reliability level (see Fig. 6.1) (Bruninx and Delarue, 2014). Positive forecast errors are dealt with by downward reserves, and negative forecast errors by upward reserves. This analysis can be repeated for every time step (given a different wind and solar forecast), resulting in a time series for upward and downward reserve requirements. The reserve requirement is split between spinning reserves and non-spinning reserves. A minimum requirement of 50% spinning reserves is assumed (CAISO, 2006).

Both uncoordinated and coordinated reserve sizing are considered in this chapter, resulting in different reserve requirements. In uncoordinated sizing (i.e., in scenarios A-B-C), each market zone determines the required reserves for its own zone. In other words, a convolution of the PDFs of WPFE and SPFE is

[2]The conditional PDF for WPFE follows from 5 years of quarter-hourly observations (about 175,000 observations): 2012/2014 for Belgium and 2010-2012 for Germany. The conditional PDF for SPFE follows from 3 years of quarter-hourly observations (about 105,000 observations): 2014 for Belgium and 2011-2012 for Germany. 2013 data is not used for deriving the conditional PDFs as we consider 2013 in the case study. No historical data on WPFE and SPFE in France and the Netherlands is publicly available. Historical forecasts and forecast errors are converted to per-unit values and discretized in power intervals of 0.025 p.u.

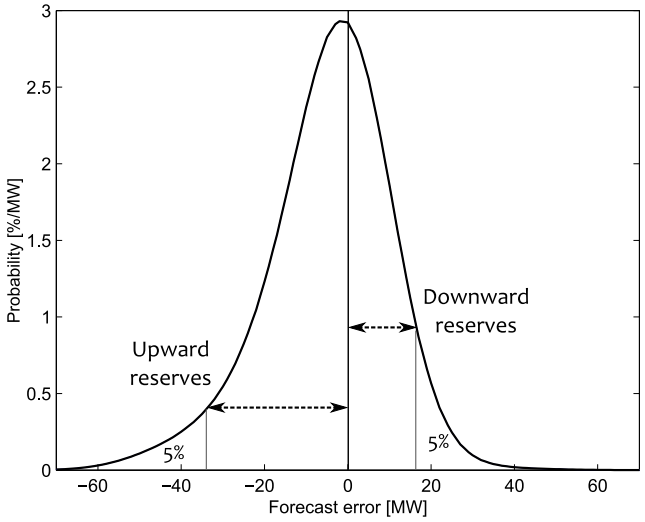

Figure 6.1: An illustrative conditional probability density function of day-ahead wind and solar power forecast errors. The required upward and downward reserves follow from the conditional probability density function and the required reliability level, i.e., 90% on this figure.

performed for each market zone separately. The total reserve requirement is then the sum of the requirements in each zone. In coordinated sizing (i.e., scenario D), the market zones determine together the required reserves. In other words, one convolution of the WPFE and SPFE for all zones is performed, meaning that we disregard how transmission constraints may affect the deliverability of those reserves.

Day-ahead energy scheduling and reserve allocation

The day-ahead market is represented by the deterministic unit commitment model LUSYM that jointly optimizes the scheduling of electric energy and reserves (see chapter 2). The model is formulated as a mixed-integer linear program in GAMS and solved using the Cplex 12.6 solver. The optimality gap is 0.05%.

For the sake of clarity, the relevant equations of the LUSYM model are repeated here. The reader is referred to the list of symbols at the outset of the dissertation for clarification on the symbols. The objective function of the unit commitment model is minimization of the total operational system

cost, consisting of generation costs, start-up costs and curtailment costs for load and renewables curtailment:

$$\min \sum_{i,t} NC_i\, z_{i,t} + MC_i\, g_{i,t} + SUC_i\, v_{i,t} + \sum_{n,t} LCC\, lc_{n,t} + RCC\, rc_{n,t} \quad (6.1)$$

The objective function is subject to the market clearing condition (Eq. (6.2)), power plant generation limits (Eqs. (6.3)-(6.4)), minimum down and up times (Eqs. (6.5)-(6.6)), the binary relation (Eq. (6.7)), the trade-based network equations (Eqs. (6.8)-(6.9)), curtailment constraints (Eqs. (6.10)-(6.11)) and non-negative and binary constraints (Eqs. (6.12)-(6.13)). Load curtailment and renewables curtailment are assumed to be only possible at a very high cost (i.e., $LCC = RCC = 3{,}000$ EUR/MWh).

$$\sum_i A_{n,i}^{plant}(z_{i,t}\,\underline{P}_i + g_{i,t}) + RES_{n,t} - rc_{n,t} = D_{n,t} - lc_{n,t} + p_{n,t} \qquad \forall n, \forall t \quad (6.2)$$

$$0 \leq g_{i,t} - r_{i,t}^{-} \qquad \forall i, \forall t \quad (6.3)$$

$$g_{i,t} + r_{i,t}^{+} \leq (\overline{P}_i - \underline{P}_i)\, z_{i,t} \qquad \forall i, \forall t \quad (6.4)$$

$$1 - z_{i,t} \geq \sum_{t'=t+1-MDT_i}^{t} w_{i,t'} \qquad \forall i, \forall t \quad (6.5)$$

$$z_{i,t} \geq \sum_{t'=t+1-MUT_i}^{t} v_{i,t'} \qquad \forall i, \forall t \quad (6.6)$$

$$z_{i,t-1} - z_{i,t} + v_{i,t} - w_{i,t} = 0 \qquad \forall i, \forall t \quad (6.7)$$

$$p_{n,t} = \sum_l A_{l,n}\, f_{l,t} \qquad \forall n, \forall t \quad (6.8)$$

$$\underline{F}_l \leq f_{l,t} \leq \overline{F}_l \qquad \forall l, \forall t \quad (6.9)$$

$$0 \leq rc_{n,t} \leq RES_{n,t} \qquad \forall n, \forall t \quad (6.10)$$

$$0 \leq lc_{n,t} \leq D_{n,t} \qquad \forall n, \forall t \quad (6.11)$$

$$p_{i,t}\,,\, r_{i,t}^{+}\,,\, r_{i,t}^{-} \geq 0 \qquad \forall i, \forall t \quad (6.12)$$

$$z_{i,t}\,,\, v_{i,t}\,,\, w_{i,t} \in \{0,1\} \qquad \forall i, \forall t \quad (6.13)$$

Finally, a reserve requirement for spinning reserves is imposed (Eqs. (6.14)-(6.15)). Spinning reserve scheduling is constrained by the power output limits

(Eqs. (6.3)-(6.4)). Non-spinning reserve requirements are not imposed to the unit commitment model but checked ex-post. Notice that only power flows resulting from energy scheduling are included in the network equations, and not reserve scheduling (i.e., the feasibility of the deployment of scheduled reserves w.r.t. grid constraints is not enforced).

$$\sum_i A_{s,i}^{rsr}\, r_{i,t}^{+} \geq SR_{s,t}^{+} \qquad \forall s, \forall t \tag{6.14}$$

$$\sum_i A_{s,i}^{rsr}\, r_{i,t}^{-} \geq SR_{s,t}^{-} \qquad \forall s, \forall t \tag{6.15}$$

The model simulates each day with a quarter-hourly time resolution (i.e., generators and consumers submit their output/consumption schedules to the TSO with a 15 minute resolution). Consecutive days are linked to each other via sequential boundary conditions.[3] A simplified trade-based network representation is implemented with one fixed transmission capacity between market zones and no transmission constraints within market zones (consistent with the European Available Transfer Capacity system of market coupling). In a trade-based network representation, Kirchhoff's current law is taken into account and Kirchhoff's voltage law is neglected. The import/export position of each node is linked to the flows in the network by means of the network incidence matrix A which indicates for every line the starting node ($A_{l,n} = 1$) and ending node ($A_{l,n} = -1$) (see, e.g., Hobbs and Rijkers (2004)).

If reserve allocation is coordinated (scenarios C and D), only one reserve zone exists covering all market zones (the number of reserve zones S = 1). In scenario C (with uncoordinated sizing but coordinated allocation), the reserve requirement for the single reserve zone is the sum of the reserve requirements in each zone. In scenario D (with coordinated sizing and allocation), one reserve requirement is obtained for all zones together. In scenarios A and B, each country is a separate reserve zone with a separate reserve requirement (with now the number of reserve zones S equal to the number of zones N).

Real-time reserve activation

The model formulation of the real-time market is very similar to the day-ahead market model. The differences are (1) that updated time series of wind and

[3] An overlap of 12 hours between two days is implemented, based on the largest minimum up/down time in the generation portfolio (i.e., a 12 hour minimum up/down time for nuclear units, see Table 6.3). As such, the model considers the full length of the nuclear minimum up/down time when taking a decision to start-up/shut-down a nuclear unit at the end of the considered day.

solar generation are imposed (i.e., the actual generation instead of the forecasted generation), (2) reserve requirements are no longer necessary (i.e., Eqs. (6.14)-(6.15)) are purposely disregarded), and (3) commitment decisions for generation units that cannot deliver non-spinning reserves (i.e., nuclear units, coal-fired units and lignite-fired units) are fixed to the day-ahead market outcome:

$$z_{i,t}^{RT} = z_{i,t}^{DA} \qquad \forall i \notin I^{nsr}, \forall t \tag{6.16}$$

$$v_{i,t}^{RT} = v_{i,t}^{DA} \qquad \forall i \notin I^{nsr}, \forall t \tag{6.17}$$

$$w_{i,t}^{RT} = w_{i,t}^{DA} \qquad \forall i \notin I^{nsr}, \forall t \tag{6.18}$$

The superscript RT refers to the real-time market outcome and the superscript DA refers to the day-ahead market outcome.

In case of uncoordinated activation (scenario A), the zonal generation balance in the real-time market must be the same as in the day-ahead market. This means that the system operator in each zone deals with its own wind and solar forecast errors. In other words, the cross-border flows in the real-time market are set fixed to the day-ahead cross-border flows:

$$f_{l,t}^{RT} = f_{l,t}^{DA} \qquad \forall l, \forall t \tag{6.19}$$

In the case of coordinated activation (scenarios B, C and D), Eq. (6.19) is not imposed, allowing zones to change the amounts they export and import.

6.2.3 Case study

The 2013 Central Western European (CWE) electricity sector is considered as a case study. The CWE area covers Belgium, Luxembourg, France, Germany and the Netherlands. Luxembourg is considered as a part of the Belgian system. Each country is one market zone.[4] A time series for a full year is considered with a quarter-hourly time resolution.

The aggregated annual electricity consumption is 1,214 TWh, with a peak of 193 GW (ENTSO-E, 2015a). The actual electricity consumption (1,161 TWh/a) is corrected for net export to neighboring countries outside the CWE region (48 TWh/a) and net consumption of pumped storage units (5 TWh/a). Annual consumption is higher in France (42%) and Germany (40%) than in Belgium (8%) and the Netherlands (10%).

[4] Germany forms a single market zone together with Austria, but is in this study considered as a separate market zone.

The conventional generation portfolio consists of 625 units with an aggregated generation capacity of 177 GW (Platts, 2014).[5] Table 6.2 gives an overview of the installed conventional generation capacity per country and per generation type. Power plant characteristics are taken from ENTSO-E (2012a) and shown in Table 6.3. Different rated efficiencies are allocated to power plants based on their commissioning year. Average fuel and CO_2 emission prices for 2013 are used.[6] It is assumed that all conventional generation units can deliver spinning reserves. Combined-cycle gas turbines, open-cycle gas turbines and internal combustion units can also deliver non-spinning reserves.

Historical generation time series from small cogeneration units and renewables are imposed as an exogenous input to the model, since these generation units are (mainly) non-dispatchable from an electricity market perspective. Generation data from conventional hydro (i.e., run-of-river units and water dams), bio-energy units (including cogeneration) and fossil-fuel cogeneration units are taken from ENTSO-E (2015a). Wind and solar profiles for Belgium and Germany, both day-ahead forecasts and actual realizations, originate from the Belgian TSO (Elia, 2015) and the German TSOs (EEX, 2015b), respectively. France's actual wind and solar generation is taken from the French TSO (RTE, 2015). The actual wind and solar generation profile for the Netherlands is obtained by rescaling the historical Belgian profile. Day-ahead forecasted time series are generated for France and the Netherlands as described in Bruninx et al. (2014, 2016). The share of renewable generation in annual CWE electrical energy consumption is 19%, varying from 11% in Belgium and the Netherlands to 28% in Germany.

The net transfer capacity (NTC) for February 2015 is used as transmission capacity between the different countries in the trade-based network model (ENTSO-E, 2015c).

To validate the model, the outcome for scenario A (no interregional cooperation) is compared with historical observed generation (ENTSO-E, 2015a). The capacity of nuclear units is derated in order to match simulated nuclear generation and historical nuclear generation.

[5]Large cogeneration units (i.e., with an electric power output larger than 400 MW) are considered as dispatchable in the electricity market and hence included in the conventional generation portfolio.

[6]The following fuel prices are used: 10 EUR/MWh_{th} for coal, 27 EUR/MWh_{th} for natural gas, 55 EUR/MWh_{th} for light fuel oil, 50 EUR/MWh_{th} for heavy fuel oil. A fuel price of 2.3 EUR/MWh_{th} for uranium and 5 EUR/MWh_{th} for lignite is assumed. A CO_2 emission cost of 5 EUR/tCO_2 is used.

[GW]	BE	FR	DE	NL
Nuclear units	4.5	57.9	10.7	0.3
Steam-cycle units	0.9	10.5	47.8	4.7
Combined-cycle gas turbines	4.4	5.5	12.3	10.9
Open-cycle gas turbines	0.8	1.9	3.2	0.6
Internal combustion units	-	0.3	-	-

Table 6.2: Overview of installed conventional generation capacity per market zone and generation type (BE: Belgium, FR: France, DE: Germany, NL: the Netherlands)

	Efficiency [%]	$\underline{P}$ [%$\overline{P}$]	MUT,MDT [h]
Nuclear units	33	50	12
Steam-cycle units	35/40/45	43	6/12
Combined-cycle gas turbines	40/48/58	35	3
Open-cycle gas turbines	35/42	30	1
Internal combustion units	35/40	30	1

Table 6.3: Overview of technical characteristics per generation type (different efficiencies are used depending on the commissioning year of a power plant, lignite steam-cycle units have a larger MUT and MDT than coal steam-cycle units.)

6.3 Results and discussion

This section presents results for the sizing, allocation and activation of reserves in the considered case study, i.e., the CWE 2013 system, under the different scenarios (see Table 6.1) for coordination among market zones.

6.3.1 Reserve sizing

Fig. 6.2 shows boxplots of the upward and downward reserve requirements for the cases of uncoordinated and coordinated sizing, as a function of the reliability level. Fig. 6.2 is constructed as follows; for every quarter-hour, the appropriate PDF is taken for WPFE and SPFE in every country, depending on the wind and solar forecasts for that quarter-hour in that country. The combined WPFE and SPFE PDF follows then from the convolution of the separate PDFs (separately for every market zone in uncoordinated sizing and joined in coordinated sizing; see section 6.2.2). The upward and downward

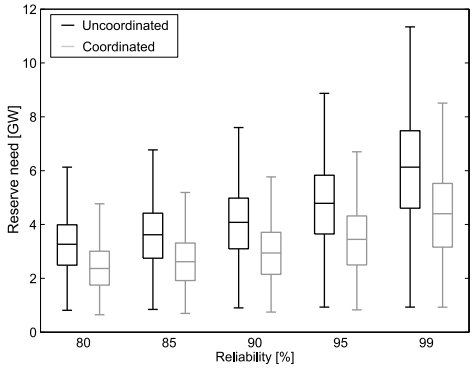

(a) Upward reserves.

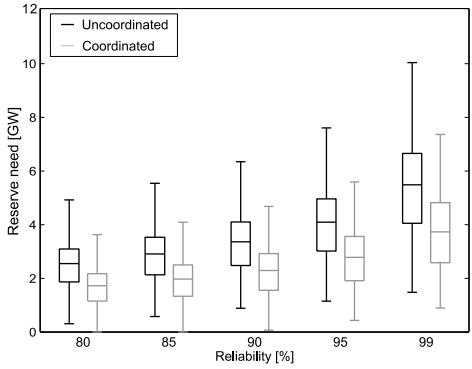

(b) Downward reserves.

Figure 6.2: Boxplots of the need for upward and downward reserves in an uncoordinated and coordinated sizing scenario, as a function of the required reliability level (the central mark is the median, the edges of the boxes are the 25^{th} and 75^{th} percentile, and the whiskers extend to the most extreme observations without excluding any outliers). The reliability level corresponds to the highest cumulative probability that the reserves cover wind and solar forecast errors. Coordinated sizing results in an on average 28% and 33% lower need for upward and downward reserves, respectively.

reserve requirement can be derived from the combined conditional PDF as shown in Fig. 6.1. This procedure results in a time series of reserve requirements which can be represented by a boxplot.

The general trends are clear. First, reserve requirements increase with increasing reliability level; in later sections of this chapter, we use values based upon the

95% reliability level. Second, more upward reserves are needed than downward reserves. Third, coordinated sizing results in lower reserve requirements than uncoordinated sizing. For upward and downward reserves, respectively, the median reserve requirement is on average 28% and 33% lower with coordinated sizing. In an uncoordinated sizing scenario, each market zone calculates the reserves needed in its zone. In an extreme case, a market zone might be forced to activate all of its scheduled reserves to deal with an extreme forecast error. However, the probability that an extreme forecast error occurs simultaneously in each market zone is very small. Therefore fewer reserves in total are required if the different market zones determine the need for reserves together (for the same reliability level with respect to short-term adequacy). This effect is referred to as spatial smoothing.

Germany's renewable capacity dominates the sizing decision. The installed capacity of wind and solar photovoltaics in Germany is at least a factor of five higher than in the other countries.[7] As a result, the reserve requirement for Germany is also at least five times as much.

6.3.2 Reserve allocation

Table 6.4 summarizes the main simulation results from the allocation phase. Scenarios A and B (no coordination in sizing and allocation, coordination only in activation) lead to the same allocation results since both scenarios differ only in the subsequent activation phase. In scenario C, allocation is coordinated but sizing is uncoordinated, leading to a reduction in aggregated day-ahead annual operational costs of 0.23% compared to scenarios A and B. In scenario D, with coordinated allocation and coordinated sizing, the total operations cost is 0.28% lower than in scenarios A and B. The cost reductions are small since reserve allocation is, in terms of system-wide fuel and carbon costs, of minor importance compared to energy scheduling. However, the cost reductions become more pronounced if expressed as a reduction in payment for reserves. The annual payment for reserves follows from the multiplication of the shadow prices of the spinning reserve constraints with the reserve requirements, aggregated over all time steps. This shadow price is 1.5 EUR/MW/h for upward spinning reserves in A and B, averaged over the year. Downward spinning reserve constraints are almost never binding, resulting in zero shadow costs. Coordination in the allocation phase (C) leads to a reduction in payments for reserves by 83%. If also the sizing is coordinated (D), payment for reserves decrease by 92% compared to scenarios A and B. No load curtailment or renewables curtailment occurs in the allocation phase. The availability of non-spinning reserves is controlled after

[7] Installed wind and solar photovoltaic capacities are 4.0 GW in Belgium, 12.3 GW in France, 62.8 GW in Germany and 3.2 GW in the Netherlands.

	Scen. A & B	Scen. C	Scen. D
Operational costs [Mio EUR]	17,450	17,409	17,401
relative to scenarios A & B		-0.23%	-0.28%
Payment for reserves [Mio EUR]	31.9	5.4	2.5
relative to scenarios A & B		-83%	-92%

Table 6.4: Overview of the allocation phase results (yearly aggregated).

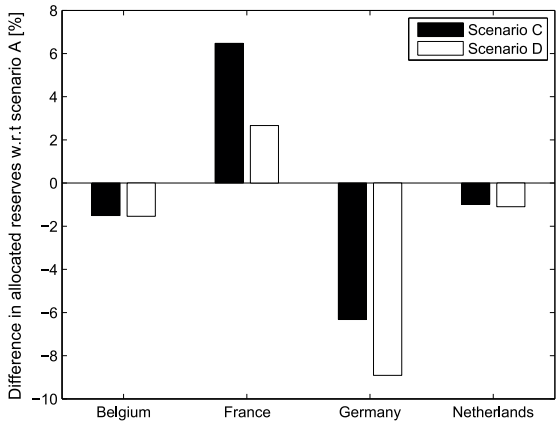

Figure 6.3: Difference in allocated upward spinning reserves per country between a coordinated allocation phase (respectively, scenario C and D) and an uncoordinated allocation phase (scenario A), expressed as % of the total scheduled reserves in scenario A. The allocation of spinning reserves shifts towards France in a coordinated allocation case.

the day-ahead market clearing. It turns out that there is enough non-spinning reserve in the system.

Most of the reserves are needed in Germany, since it has by far the largest wind and solar photovoltaic generation capacity. France, on the other hand, possesses cheap reserves in the form of nuclear generation units which operate sometimes at the margin of the merit order and can hence be scheduled as upward spinning reserves (it is assumed that nuclear generation units can deliver spin). As a result, the allocation of reserves shifts from Germany (and to a lesser extent from Belgium and the Netherlands) towards France if the allocation is coordinated (see Fig. 6.3). In scenario D (with coordinated sizing) fewer reserves have to be allocated, resulting in less reserves procured in Germany,

relative to scenario A. Note that Fig. 6.3 only shows the change in geographical distribution for upward spinning reserves. Downward spin constraints almost never bind in any market zone, and so the geographical distribution of scheduled downward reserves is not improved by coordinated allocation.

6.3.3 Reserve activation

Table 6.5 summarizes the activation phase simulation results. The annual fuel and carbon costs in the activation phase are higher than in the allocation phase since renewable output is overforecasted on average (i.e., the net forecast error is negative for the considered period, totaling -2.6 TWh or 2.3% of annual wind and solar generation). In a fully uncoordinated scenario, i.e., scenario A, the operational generation costs are 17,546 Mio EUR per year (excluding the cost of load and renewables curtailment).

Both load and renewable curtailment occur. Loss of load results from the combination of large negative forecast errors and too little available upward reserves. Renewables curtailment occurs when positive forecast errors coincide with too little available downward reserves. Note that the load and renewables curtailment shown in Table 6.5 can be interpreted as regulation services delivered by curtailable load and renewables, respectively, rather than "true" curtailment. When the activation is coordinated (i.e., scenario B), operating costs decrease by 0.15%, no renewables are curtailed, and load curtailment decreases considerably.

However, when allocation is also coordinated (i.e., scenarios C and D), generation costs and load and renewables curtailment decrease compared to scenario A, but increase relative to scenario B. Table 6.5 clearly shows that coordination in the sizing and allocation phase is not always beneficial in terms of cost reductions and system reliability. The reason is that transmission constraints are neglected in the coordinated sizing and allocation phases, which might lead to an overly optimistic sizing and allocation of reserves. As a result, the activation phase–where transmission constraints do play a role–may not be able to adjust or deliver generation in the places needed to compensate for forecast errors.

Cost differences among the scenarios are small, since the activation of reserves is only a minor part of the total operations costs. However, cost differences become more visible when expressed as the difference between the costs in the activation phase and the costs in the allocation phase (excluding load and renewables curtailment costs). This cost difference can be viewed as the cost of activating reserves, and is positive for negative forecast errors (i.e., the expense of activating upward reserves) and negative in the case of positive forecast errors

	Scen. A	Scen. B	Scen. C	Scen. D
Operational costs [Mio EUR]	17,546	17,519	17,532	17,534
relative to scenario A		-0.15%	-0.08%	-0.07%
Load curtailment [MWh]	2,968	210	409	427
Renewables curtailment [MWh]	11,677	0	0	0
Activation cost (up) [Mio EUR]	188.3	169.9	211.1	220.7
relative to scenario A		-9.8%	12.1%	17.2%
Activation cost (down) [Mio EUR]	-91.5	-99.5	-87.5	-87.1
relative to scenario A		-8.8%	4.4%	4.8%

Table 6.5: Overview of the activation phase results (yearly aggregated).

(i.e., cost saving from activating downward reserves).[8] Compared to scenario A (no coordination), the cost of upward reserve activation decreases by 9.8% in scenario B but increases by 12.1% and 17.2% in C and D, respectively. Note that this is only the activation cost and, since the allocation cost was lower in scenarios C and D, overall operating costs are still lower than in scenario A. Meanwhile, the activation cost of downward reserves is negative (i.e., cost savings). The cost savings are 8.8% higher in scenario B, and 4.4% and 4.8% lower in scenarios C and D, respectively, relative to scenario A.

The activation phase is based on the full historical time series for 2013, based on daily simulation results. Treating the 365 observations as an independent sample, the statistical significance of the differences among the solutions' total operating costs in the activation phase is examined (including curtailment costs). In particular, using a paired Wilcoxon signed rank test, the null hypothesis that the observed differences among the scenarios, in terms of total daily costs, come from a distribution with zero median, is tested. This is done six times, once for each pair of scenarios (A-B, A-C, A-D, B-C, B-D, C-D). For all except pair C-D, the differences are significant at a 1% level, and the null hypothesis is rejected; however, the difference between scenarios C-D turns out to be statistically insignificant at the 10% level. Thus, it does not appear that coordinating sizing matters as much as coordination in allocation and activation, at least in this particular case study.

[8]The activation cost is calculated as the cost difference between the generation costs of the four zones together in the activation phase and the generation costs of the four zones together in the allocation phase, and this for every time step. The activation cost consists of (avoided) generation costs and (avoided) start-up costs.

6.3.4 Discussion

The results presented in the previous subsections indicate that there is a potential for cost reduction and reliability increase when the sizing, allocation and activation of reserves are coordinated among market zones. However, costs and infeasibilities (i.e., load and renewables curtailment) do not necessarily always decrease with increasing level of coordination because of simplified treatment of transmission constraints when sizing and allocating reserves.

Coordinating activation of reserves never leads to higher cost (and most likely leads to lower costs) than in an uncoordinated activation scenario. In the activation phase, network constraints are taken into account and hence there is no risk of a suboptimal market outcome. Whether it is beneficial to coordinate the sizing and allocation of reserves depends on the trade-off between reducing allocation costs and increasing activation costs. Coordinated reserve sizing results in lower reserve requirements due to the spatial smoothing of forecast errors, and hence lower allocation costs. Coordinated reserve allocation results in lower allocation costs due to spatial arbitrage. However, since network constraints are neglected in the sizing and allocation phases, coordinated sizing and allocation may result in suboptimal market outcomes with higher activation costs.

This trade-off between allocation cost savings and activation cost savings is shown in Fig. 6.4 for the considered case study. The black bars in Fig. 6.4 show the reduction in allocation costs for each scenario, relative to scenario A (calculated as the difference in operational costs in the allocation phase; see Table 6.4). The grey bars in Fig. 6.4 show the reduction in activation costs for each scenario relative to scenario A (calculated as the difference in activation costs; see Table 6.5). The white bars in Fig. 6.4 show the net cost savings relative to scenario A. Scenarios C and D lead to allocation cost savings, but part of these savings are lost due to higher activation costs. For the considered case study (with 95% reliability level), scenario B gives the optimal level of coordination with the largest net cost savings. This is, however, not a general conclusion, but depends on the power system at hand as well as the assumed reliability level. Simulations run at a 99% reliability level (instead of 95%) indicate that scenario D (and no longer scenario B) is the most optimal one for this specific system.

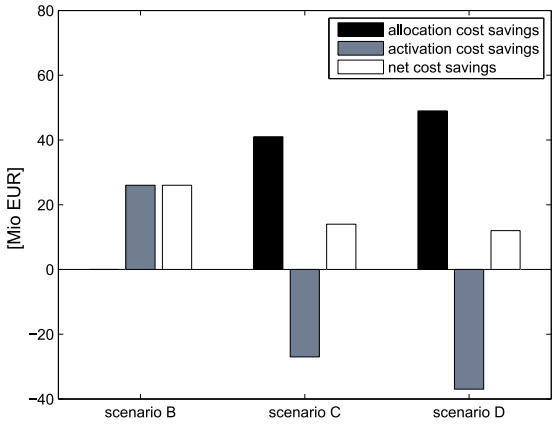

Figure 6.4: Annual allocation cost savings, activation cost savings and net cost savings of scenarios B, C and D, relative to scenario A (positive means that A has higher cost). Scenario B turns out to be optimal in this case.

6.4 Summary and conclusions

In today's European electricity markets, sizing, allocation and activation of reserves happens mainly uncoordinated, meaning that every market zone is responsible for the reserves in its own zone. This chapter has examined whether it is beneficial for different market zones to coordinate in not only the activation of reserves, but also in their sizing and allocation. Decreased generation costs and increased system reliability would be expected when market zones coordinate reserve decisions, due to spatial smoothing of forecast errors and spatial arbitrage. However, as network constraints are generally not taken into account when coordinating sizing and allocation, suboptimal market outcomes might be obtained and coordination might actually worsen system performance. This chapter shows that the value of coordination is determined by a trade-off between reducing sizing and allocation costs (due to spatial smoothing and arbitrage) and increasing activation costs (due to suboptimal sizing and allocation). In short, coordination of reserve activation always reduces cost but coordination in the allocation and sizing phase might not due to neglect of transmission constraints in the sizing and allocation phase. In the worst case, total costs can even increase as a result of coordinating the sizing and allocation of reserves.

The Central European electricity system is considered as a case study, with a reserves level corresponding to 95% system reliability. Coordinated

sizing results in 28% and 33% lower requirements for upward and downward reserves, respectively, using dynamic probabilistic reserve sizing. Coordinated allocation reduces market payments for reserves by 83% and 92% compared to uncoordinated allocation. However, not all of these cost savings can be realized due to transmission constraints in the real-time activation phase. The case study shows the lowest overall cost occurs in a scenario with coordinated activation of reserves, but uncoordinated allocation and sizing.

Chapter 7

Flow-based market coupling in Central Western Europe

Chapter based on:

K. Van den Bergh, J. Boury, and E. Delarue. The flow-based market coupling in Central Western Europe: concepts and definitions. The Electricity Journal, 29:24-29, 2016.[1]

Abstract: As of May 20$^{\text{th}}$ 2015, Flow-based market coupling is used for cross-border capacity allocation in Central Western European day-ahead markets (i.e., Belgium, the Netherlands, France and Germany/Luxembourg/Austria), replacing the available transfer capacity method. This chapter describes concepts and definitions of the flow-based market coupling. As such, this chapter can serve as a starting point for further research on the methodology and market impact of flow-based market coupling.

Keywords: Cross-border capacity allocation; flow-based market coupling; Central Western European electricity market.[2]

[1]The publication on which this chapter is based benefited from discussions with, apart from the co-authors, R. Belmans (KU Leuven), A. Marien and P. Luickx (CREG), P. Reniers (Fluxys), O. Bronckart and J. Van Roost (Elia System Operator), Y. Langer (Belpex) and A. Papavasiliou (UCL).

[2]All abbreviations and symbols used in this chapter are listed and explained at the outset of this dissertation.

7.1 Introduction

The European Union is striving for the completion of a liberalized single market for electric energy (Meeus et al., 2005; Batlle et al., 2014). The envisaged market design is referred to as the European target model for electricity. The target model is an extensive and complicated set of proposals and network codes, see ENTSO-E (2015b) for an overview, based on two broad principles: (1) energy-only regional markets and (2) market coupling between the different regional markets (Keay, 2013). Flow-based market coupling (FBMC) is a mechanism to couple different electricity markets and is as such related to the second principle of the target model.

Coupling electricity markets increases economic efficiency (Weber et al., 2010). However, the available transmission capacity between different market zones has to be taken into account properly. This is not straightforward since electricity does not flow directly from generator to consumer, but spreads out over all parallel paths in the network according to Kirchhoff's laws. There is hence a fundamental difference between commercial flows (i.e., the shortest path in the network between generator and consumer) and physical flows through the grid. As a consequence, the transmission capacity between two market zones cannot be fully allocated to commercial trade between these market zones since some of the capacity will be used by parallel flows resulting from trade between or within other market zones. The issue of allocating transmission capacity to the electricity market is referred to as cross-border capacity allocation.

Electricity markets in Europe are gradually integrating. A first major step was taken in November 2006 with the market coupling of the Belgian, Dutch and French day-ahead market (PowerNext, 2006). This trilateral market coupling was stepwise extended until the now-coupled area called multi-regional coupling, covering 19 countries (EpexSpot, 2015), resulting in efficiency benefits (Newbery et al., 2015).[3] Initially, the day-ahead market coupling was based on the available transfer capacity (ATC) method for cross-border allocation, and it still is for most of the market zones in the market coupling. However, since May 20$^{\text{th}}$ 2015, flow-based market coupling (FBMC) is being used for cross-border capacity allocation in Central Western European (CWE) day-ahead markets (i.e., Belgium, the Netherlands, France and Germany/Luxembourg/Austria) (Tennet, 2015b).

Flow-based market coupling is a mathematical methodology, used by transmission system operators (TSOs) to calculate the transmission capacity between

[3]The market coupling covers Belgium, Denmark, Estonia, Finland, France, Germany/Luxembourg/Austria, Great Britain, Italy, Latvia, Lithuania, the Netherlands, Norway, Poland (via the SwePol Link), Portugal, Slovenia, Spain and Sweden.

market zones that can be made available to the market for commercial transactions. The flow-based market coupling is based on a zonal approach (i.e., every market zone is represented by one node in the market clearing algorithm, resulting in a uniform price per market zone) and a DC power flow. The output of the flow-based methodology consists of a zonal network description and cross-border transmission capacities.

The CWE FBMC was initiated in June 2007 with a memorandum of understanding between energy ministers, transmission system operators (TSOs), power exchanges (PXs), national regulatory authorities (NRAs) and market parties platforms, stating the intention to implement FBMC in the CWE region (Amprion, 2007). The FBMC methodology has been developed, evaluated and improved over an eight-year period. This process is communicated in three important reports: the CWE FBMC feasibility report in 2011 (Amprion et al., 2011), the CWE FBMC intuitiveness report in 2013 (Amprion et al., 2013) and the CWE FBMC approval package in 2014 (Amprion et al., 2014). The FBMC methodology has been tested during 2 years with off-line parallel runs (2013-2014). These parallel runs have demonstrated a welfare increase in the day-ahead market compared to the ATC method, better price convergence between the different market zones and a good and sufficient level of reliability, stability and robustness of the FBMC system (Joint Allocation Office, 2015). Therefore, the national regulatory authorities approved the launch of the CWE FBMC in March 2015 (ACM et al., 2015).

The FBMC methodology is an important cornerstone of the European target model. If the FBMC methodology turns out to be successful in the CWE day-ahead market, an extension to other market zones and markets (e.g., intra-day market) is likely. Despite its importance, the FBMC methodology is complex and poorly understood by market participants. A public consultation of the national regulatory authorities mentions that respondents assess their knowledge of the FBMC methodology as intermediate (ACM et al., 2014). Moreover, little literature on FBMC is publicly available. The FBMC methodology reports are the main source of information. Aguado et al. (2012) applied FBMC on historical order books and conclude that the transmission capacity provided by the FBMC methodology is larger than by the ATC methodology. As a result, social welfare and price convergence increase under FBMC. Waniek et al. (2010) came to similar conclusions, based on a model of the CWE region. Marien et al. (2013) show based on a simple model that the impact of various FBMC parameters on the market outcome is considerable. Based on this observation, they advocate for a transparent and adequate monitoring of the FBMC calculation process. Although insightful, none of the above mentioned literature presents a clear description of the FBMC methodology itself (partly because the FBMC methodology was still under construction at the time of

writing).

This chapter aims to present a clear and full description of the flow-based market coupling as implemented in the Central Western European day-ahead market. This chapter can serve as a starting point for further research on the FBMC methodology, possible improvements and its impact on the market outcome.

The chapter continues as follows. Section 7.2 discusses different methodologies for cross-border capacity allocation. Section 7.3 explains in detail the flow-based market coupling methodology as implemented in Central Western European day-ahead markets. Section 7.4 concludes and formulates policy recommendations.

7.2 Cross-border capacity allocation

Electricity generators trade electricity with electricity retailers and large industrial consumers on power exchanges (PXs).[4] The focus of this chapter is on the day-ahead market, since FBMC is at the time of writing only implemented in the CWE day-ahead markets (market coupling in forward markets and intra-day markets is still ATC-based). The power exchange collects generation and consumption bids and determines the optimal market outcome, i.e., the market outcome with maximum social welfare (consumer surplus, producer surplus and congestion rent). The objective function of the market clearing algorithm can be written in a simplified form as:

$$\max \sum_{b,z} Q^{Q}_{b,z}\, Q^{P}_{b,z}\, x_{b,z} \tag{7.1}$$

with $Q^{Q}_{b,z}$ the quantity of bid b in market zone z in [MW] (generator bids are negative, consumption bids positive), $Q^{P}_{b,z}$ the price of bid b in market zone z in [EUR/MWh], and $x_{b,z}$ the accepted share of bid b in market zone z ($0 \leq x_{b,z} \leq 1$). Note that the actual market clearing algorithm used in European day-ahead markets, i.e., the Euphemia model, is much more complex than described here (Price Coupling of Regions, 2013).

The market outcome is subject to the market clearing condition, i.e., zonal generation equals zonal consumption plus net export:

$$\sum_{b} Q^{Q}_{b,z}\, x_{b,z} + NEX_z = 0 \qquad \forall z \tag{7.2}$$

[4] Electricity can also be traded bilaterally, meaning that a generator and retailer/large consumer interact directly with each other and agree upon a trade contract.

with NEX_z the net exchange position of market zone z in [MW]. A positive net exchange position indicates net export, a negative net import.

The market outcome is constrained by the available transmission capacity:

$$\underline{F}_l \leq F_l \leq \overline{F}_l \qquad \forall l \tag{7.3}$$

$$F_l = f(NEX_z) \qquad \forall l \tag{7.4}$$

with $\overline{F}_l$ the maximum transmission capacity of line l available for the market in [MW], with $\underline{F}_l$ the minimum transmission capacity of line l available for the market in [MW], F_l the flow through transmission line l in [MW], and f a function linking the net exchange positions with flows through the network. The market clearing algorithm (Eqs.(7.1)-(7.4)) is solved for every time step of the electricity market (e.g., for every hour in the European day-ahead electricity market).[5] A detailed description of the market clearing algorithm used in the European day-ahead market can be found in Price Coupling of Regions (2013).

The cross-border capacity allocation consists of two sub-problems:

1. What is the transmission capacity available to the market, see $\underline{F}_l$ and $\overline{F}_l$ in Eq. (7.3)?
2. What is the relationship between the net exchange positions and flows through the grid, see f in Eq. (7.4)?

The fundamental difficulty with cross-border capacity allocation is that commercial flows (i.e., shortest path between generator and consumer) differ from physical flows (i.e., flows through all parallel paths according to Kirchhoff's laws). This is illustrated on Fig. 7.1 where a commercial transaction between two nodes causes physical flows through the whole grid. Physical transmission constraints need to be translated into commercial transaction constraints or commercial transactions need to be translated into physical flows (Hobbs and Rijkers, 2004).

Different capacity allocation methods exist and are being used in electricity markets. The remainder of this section discusses three different methods: nodal market clearing, the available transfer capacity (ATC) method, and flow-based market coupling (FBMC).

[5] Different time steps can be linked to each other in the market clearing algorithm by complex bids such as block bids.

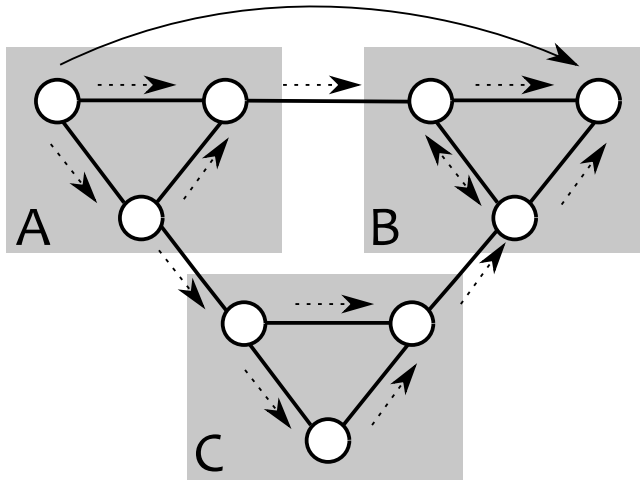

Figure 7.1: A commercial transaction between a node in market zone A and a node in market zone B (see solid arrow) results in physical flows in the whole grid (see dashed arrows).

7.2.1 Nodal market clearing

In an electricity market with nodal market clearing, all (relevant) physical transmission constraints are taken into account in the market clearing algorithm (Fig. 7.2 shows the grid model of the running example in a nodal market clearing). As such, commercial transactions are correctly translated into physical flows and physical constraints are correctly accounted for in commercial transactions. In other words, capacity allocation happens simultaneously with the market clearing in a nodal market.

In a nodal market clearing, every node in the electricity grid is considered as one market zone. This implies that the number of constraints and variables in the market clearing algorithm increases (the set Z equals now the number of nodes in the electricity grid, i.e., every node can be considered as a separate market zone, and the set L contains all (critical) transmission lines) and that the net exchange position equals the nodal grid injection ($NEX_z = P_n$). The transmission constraints in the market clearing algorithm become:

$$-\overline{F}_l \leq F_l \leq \overline{F}_l \qquad \forall l \tag{7.5}$$

$$F_l = \sum_n PTDF^N_{l,n} P_n \qquad \forall l \tag{7.6}$$

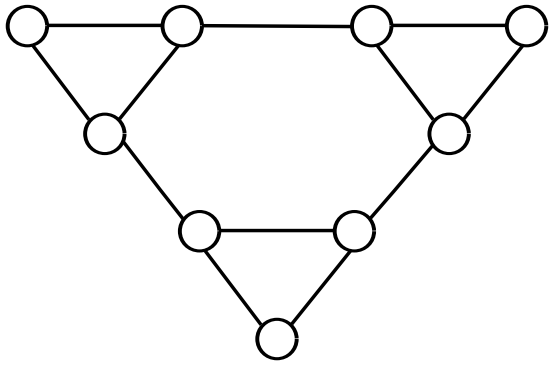

Figure 7.2: In a nodal market clearing, all (relevant) nodes and (critical) lines are taken into account in the market clearing algorithm. In this simple example, the nodal network consists of 9 nodes and 12 lines.

with $\overline{F}_l$ the maximum allowable power flow on transmission line l in [MW] which is the same in both line directions, $PTDF^N_{l,n}$ the nodal power transfer distribution factors and P_n the nodal power injections. The maximum line capacity follows from the physical line capacity, reduced with a security margin to guarantee an N-1 secure market outcome. The nodal PTDF gives the linear relationship between injections in the grid and flows through lines. The nodal PTDF results from a DC power flow analysis of the electricity grid.

A nodal market clearing is implemented in several US electricity markets such as the PJM market (Hogan, 1999). Although nodal market clearing is based on a physically more correct representation of the electricity grid, it is not part of the European target model for electricity. The European target model proposes a zonal market clearing with one uniform electricity price per zone.

7.2.2 Available transfer capacity

In the available transfer capacity (ATC) method, the link between commercial transactions and the physical characteristics of the electricity grid is strongly simplified. The nodes within a zone are grouped and replaced by an equivalent node, and only cross-border links are considered (see Fig. 7.3.a). In the ATC method, TSOs calculate the available capacity for the market $\underline{F}_l$ and $\overline{F}_l$ based on assumptions of the eventual market outcome and concomitant physical flows. In other words, capacity allocation takes place before the market clearing in the ATC-method.

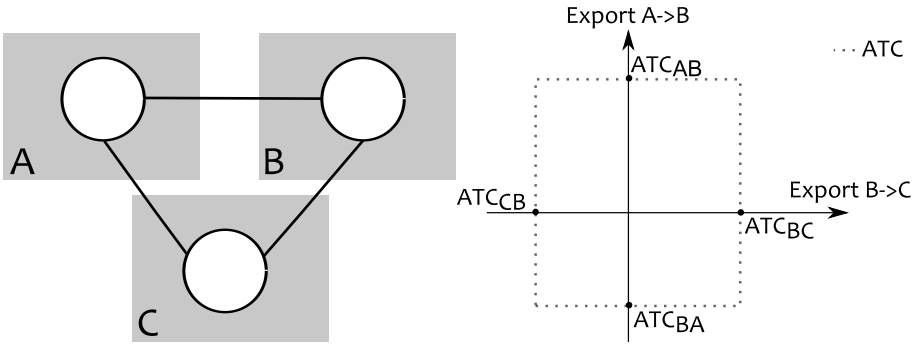

(a) Zonal market model. (b) Flow domain.

Figure 7.3: In the ATC method, only one equivalent node per zone is considered, with one cross-border link connecting the market zones. In this simple grid, the zonal network consists of 3 nodes and 3 cross-border links. The ATC flow domain is a rectangle, characterized by the ATC-values.

The available transfer capacity (ATC) is calculated as the maximum commercial exchange between two market areas, compatible with the physical transmission constraint and operational security standards (ETSO, 2001). The ATC of a cross-border link is independent of the flow on other cross-border links (see Fig. 7.3.b). In order to calculate the ATC, TSOs estimate the parallel flows that will result from the market outcome. The ATC calculation method is based on heuristic rules and day-2 estimations of the market outcome (i.e., the so-called base case). The ATC value is determined for each cross-border link (the set L equals the number of cross-border links now, no longer all transmission lines). The transmission constraints in the market clearing algorithm become:

$$\underline{ATC}_l \leq F_l \leq \overline{ATC}_l \qquad \forall l \tag{7.7}$$

$$NEX_z = \sum_l A_{l,z}\, F_l \qquad \forall z \tag{7.8}$$

with $\underline{ATC}_l$ and $\overline{ATC}_l$ the ATC-value in the negative and positive direction, respectively, and $A_{l,z}$ the network incidence matrix. ATC-values can depend on the flow direction of the line due to the assumptions made in the ATC parameter calculation. The incidence matrix indicates whether a cross-border link is starting at a market zone ($A_{l,z} = 1$), ending at a market zone ($A_{l,z} = -1$) or not connected to a market zone ($A_{l,z} = 0$).

The ATC-market coupling is currently used in European electricity markets, except for the day-ahead market in Central Western Europe (which is using

flow-based market coupling). Although the market clearing algorithm is rather simple with ATC market coupling, the calculation of the ATC-value itself is rather opaque and non-transparent for regulators. Moreover, the transmission capacity which is made available to the market is likely to be a conservative estimate of the available capacity (TSOs want to ensure a safe grid operation and therefore tyeh tend to consider the worst case distribution of load and generation when calculating the ATC-value). Given the strong assumptions inherent to the ATC method, the ATC value needs to be conservative to avoid physical line overloadings. Therefore, a new market coupling methodology has been put in place in the CWE day-ahead market; the flow-based market coupling.

7.2.3 Flow-based market coupling

Flow-based market coupling (FBMC) can be seen as a combination of the zonal approach from the ATC-method with the physical transmission constraints from the nodal market clearing. In FBMC, the physical transmission constraints are taken into account in the market clearing. However, since the zonal approach is retained, the grid constraints need to be simplified (see Fig. 7.4). In other words, the capacity allocation in FBMC happens partly before the market clearing, and partly simultaneously with the market clearing.

In FBMC, all critical lines in the electricity grid are taken into account in the market clearing (the set L hence equals the number of critical lines, see section 7.3 for more information on critical lines).[6] The transmission constraints in the market clearing algorithm become:

$$RAM_l^- \leq F_l \leq RAM_l^+ \qquad \forall l \tag{7.9}$$

$$F_l = \sum_z PTDF_{l,z}^Z \, NEX_z \qquad \forall l \tag{7.10}$$

with RAM_l^+ and RAM_l^- the remaining available margin of critical line l in the positive and negative direction, respectively, in [MW] and $PTDF_{l,z}^Z$ the zonal power transfer distribution factors. The zonal PTDF gives the linear relationship between net exchange positions and flows through critical lines.

The RAM and the zonal PTDF are determined by the TSOs before the market clearing. These parameters are further referred to as the FBMC parameters

[6] Critical lines are considered in the N-state and in critical N-1 states. Each index l refers to a combination of a critical line under a critical state, referred to as critical branch critical outage (CBCO). The size of the set L is hence the multiplication of the number of critical lines and the number of critical N-1 states (plus one for the N-state).

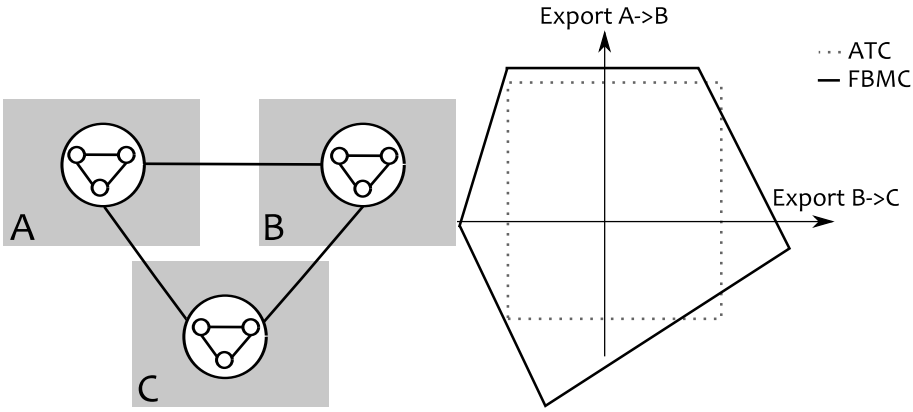

(a) Zonal market model. (b) Flow domain.

Figure 7.4: In the FBMC method, only one equivalent node per zone is considered, but all (critical) lines are taken into account. In this simple grid, the zonal network consists of 3 nodes and 12 lines. The FBMC flow domain is larger than the ATC flow domain as the physical characteristics of the grid are better represented in the FBMC method.

and extensively discussed in section 7.3. The FBMC parameters define the flow domain (see Fig. 7.4). Each boundary of the FBMC flow domain refers to the limit of a critical line. The allowable commercial export/import between two market zones is no longer independent from the allowable commercial export/import between other market zones (unlike the ATC method). As the physical characteristics of the grid are better represented in the FBMC than in the ATC method, the FBMC parameters can be determined in a less conservative way. As a result, the FBMC flow domain is likely larger than the ATC flow domain.

7.3 Flow-based market coupling parameters

As mentioned in the previous section, two FBMC parameters are needed: the zonal power transfer distribution factors (zonal PTDF) and the remaining available margin (RAM). The FBMC parameter calculation is started two days before the delivery day (i.e., D-2) and finished the morning day-ahead, so that they can be used in the day-ahead market clearing.

However, the day-ahead market outcome has to be known already to calculate

the zonal PTDF and the RAM. This is a circular problem, in which the FBMC parameters are needed to clear the day-ahead market, and the day-ahead market outcome is needed to determine the FBMC parameters. This circular problem is tackled as follows: the zonal PTDF and the RAM are determined based on a forecast of the state of the electricity system at the moment of delivery (i.e., the D-2 congestion forecast). These FBMC parameters are then communicated to the day-ahead market clearing algorithm.

7.3.1 Zonal power transfer distribution factors

The zonal PTDF matrix can be derived from the nodal PTDF matrix by means of generation shift keys (GSKs). GSKs give the nodal contribution to a change in zonal balance. For instance, $GSK_{n,z} = 0.3$ indicates that the generation at node n increases with 0.3 MW if the zonal balance of zone z increases with 1 MW. The zonal PTDF matrix can then be calculated as follows:

$$PTDF^{Z}_{l,z} = \sum_{n} PTDF^{N}_{l,n}\, GSK_{n,z} \qquad \forall l, \forall z \tag{7.11}$$

$$GSK_{n,z} = \frac{d\,P_n}{d\,NEX_z} \qquad \forall n, \forall z \tag{7.12}$$

Eq. (7.11) shows that the columns of the zonal PTDF matrix are a weighted sum of the columns of the nodal PTDF matrix, with the GSKs as weights.

The zonal PTDF is an approximation of the real physical characteristics of the grid. First, there is an inherent loss in accuracy by grouping nodes into zones. Information on the exact nodal injections in the grid is lost. Second, the GSKs are based on predictions of the market outcome, since the actual market outcome is not known yet. This implies that GSKs are subject to forecast errors. These two simplifications result in deviations between flows that are seen in the FBMC market clearing (i.e., flows based on the zonal PTDF) and the actual flows in the grid. Therefore, the transmission capacity available to the market is reduced with a safety margin to compensate for the approximations made by the zonal PTDF (see section 7.3.2).

In general, the GSKs include only power plants that are market-driven and flexible in changing the electric power output: coal fired plants, gas fired plants, oil fired plants, pumped storage units and conventional hydro units.[7] Each TSO in the CWE region calculates (or estimates) the GSKs for its own control area. Different GSK methods are used by different TSOs. The Austrian TSO and each German TSO determines two GSK-matrices per day (peak and off-peak),

[7] Nuclear units are also taken into account in GSKs in France.

based on reference days, after which the different GSK- matrices are combined into one GSK matrix for the whole German/Luxembourg/Austrian market zone. Elia (Belgium) and Tennet NL (the Netherlands) determine one GSK matrix per day, pro rata with predefined maximum and minimum production levels of power plants. RTE (France) determines a GSK matrix for every hour, pro rata with generation in the base case.

7.3.2 Remaining available margin

The second FBMC parameter is the remaining available margin (RAM). The RAM is the line capacity that can be used by the day-ahead market. The RAM procedure consists of two main steps. First, the critical branches and critical outages are determined (the set of lines l equals the number of critical branches under the critical outages). Second, the RAM is calculated for these critical branches under critical outages (in both flow directions).

A critical branch is a transmission element (cross-border line, internal transmission line or transformer) which is significantly impacted by cross-border trade given an operational situation (normal N-state or contingency cases such as an N-1 state). A transmission line is considered to be significantly impacted if a zonal PTDF for that line is larger than 5%. The critical branches are determined by each TSO for its own network.[8] For each critical branch, the maximum allowable power flow $\overline{F}_l$ is determined as the physical (thermal) limit of the transmission element.

For each critical branch and both flow directions, the RAM is calculated as follows (the set L refers now to the number of critical branches):

$$RAM_l = \overline{F}_l - F_l^{ref} - FAV_l - FRM_l \qquad \forall l \tag{7.13}$$

with

- $\overline{F}_l$ the maximum allowable power flow on critical branch l in [MW];
- F_l^{ref} the reference flow on critical branch l in [MW] caused by commercial transactions outside the day-ahead power exchange (bilateral trades, forward markets, intra-day markets and real-time balancing). These commercial transactions can be internal (within a market zone) or external (between market zones);[9]

[8] TSOs have already significant experience with the determination of critical branches since it is also part of the ATC capacity allocation method.

[9] The reference flow follows from $F_l^{ref} = F_l^{bc} - \sum_z PTDF_{l,z}^{Z} NEX_z$, with F_l^{bc} the transmission flows in the Base Case in [MW].

- FAV_l the final adjustment value on critical branch l in [MW]. The FAV allows TSOs to take account of knowledge and experience that cannot be introduced in the formal FBMC method, such as an additional margin due to complex remedial actions or active topology control, and can be positive or negative;
- FRM_l the flow reliability margin on critical branch l in [MW]. The FRM is a safety margin that needs to compensate for approximations and simplifications made in the FBMC methodology such as the assumptions inherent to a zonal PTDF (see 7.3.1), unintentional flow deviations due to load-frequency control, and the use of a linear grid model with a simplified topology.

The exact definition of the different flows in Eq. (7.13) is confusingly and inconsistently formulated in the existing FBMC reports. Especially the definitions of F_l^{ref} and FRM_l are ambiguous, since some documents allocate part of the reference flows to the flow reliability margin (Amprion et al., 2014). More information on the calculation of the remaining available margin can be found in Boury (2015).

7.3.3 Base case (day-2 congestion forecast)

The base case is a forecast of the state of the electricity system at moment of delivery, made two days before the delivery day. The base case is also referred to as the day-2 congestion forecast (D-2CF).[10] The base case is needed for (certain) GSK methods and to determine the reference flows in the RAM calculation.

The base case is determined in two main steps. First, every TSO estimates the local base case for its own control area. In a second step, the different local base cases are merged to one common base case.

Each TSO estimates its local base case based on a reference day. A reference day is a day for which the market outcome is known (i.e., a day in the past) with similar system conditions (e.g., weekday/weekend, winter/summer). The market outcome of the reference day is then updated with day-2 renewable generation forecasts, load forecasts and outage schedules for generation units and grid elements. In this first step, the TSOs coordinate the net exchange positions of the reference day (in order to have a balanced CWE system), but

[10] Besides a D-2CF, also a day-ahead congestion forecast (DACF) exists. The DACF is composed day-ahead in the evening (after the day-ahead market clearing) and is hence more precise than the D-2CF. The term "base case" is sometimes used to refer to the D-2CF and sometimes to the DACF. In this chapter, the term "base case" always refers to the D-2CF.

each TSO applies a slightly different methodology to update the reference day. Note that the base case is also needed in the ATC capacity allocation method.

7.3.4 Summary

Two parameters need to be determined before the day-ahead market clearing: the zonal power transfer distribution factors (zonal PTDF) and the remaining available margin (RAM). In order to calculate the zonal PTDF, generation shift keys (GSK) are needed, which can follow from the base case. In order to calculate the RAM, the reference flows are needed, which can be derived from the base case.

The focus of this chapter is on the FBMC methodology. However, the FBMC methodology is adjusted to account for several operational considerations. A backup procedure and fallback procedure are foreseen, in case of missing input data or the impossibility to calculate the FBMC parameters, respectively. After the FBMC parameters are calculated, a qualification and verification process takes place to check, amongst others, whether the flow-based domain does not jeopardize grid security. Besides, TSOs can impose specific limitations to the allowable export/import in their network, so-called external constraints, in order to avoid market outcomes which lead to stability problems. A full description of these operational considerations can be found in Amprion et al. (2014). Finally, the FBMC methodology was adapted to avoid counter-intuitive flows (i.e., flows from a market zone with a high price to a market zone with a low price). This adapted version is referred to as the intuitive flow based market coupling (Amprion et al., 2013).

7.4 Summary and conclusions

Flow-based market coupling (FBMC) is in operation in the Central Western European day-ahead markets since May 20$^{\text{th}}$ 2015 (i.e., Belgium, the Netherlands, France and Germany/Austria). The FBMC replaced the available transfer capacity (ATC) methodology. In FBMC, the allocation of transmission capacity is partly done simultaneously with the market clearing, unlike ATC where the allocation of transmission capacity is done before the market clearing. As such, more transmission capacity is made available to the market in FBMC. This is confirmed by off-line test runs of the FBMC, which indicate an increase in social welfare due to more transmission capacity, compared to ATC.

This chapter presents FBMC in detail. It is clear that the methodology to calculate the FBMC parameters is complex. The complexity roots in the aim to combine a zonal approach with an improved physical representation of the grid. Due to this conflicting aims, several assumptions and approximations have to be made in the FBMC parameter calculation, making the methodology difficult to understand.

An often discussed issue regarding FBMC is transparency. Whether or not FBMC is a transparent cross-border capacity allocation mechanism is open for debate. On the one hand, the FBMC methodology is defined more accurately and strictly than the ATC methodology, and as such regulating authorities can better supervise the FBMC parameter calculations, although the FBMC methodology still leaves room for TSOs to steer the calculation process (Marien et al., 2013). From a regulatory perspective, FBMC can thus be considered as more transparent than ATC. On the other hand, once the capacity allocation parameters are determined, an ATC-value indicates more clearly the transmission capacity available to the market, compared to the FBMC parameters (zonal PTDF and RAM). Hence, from a market player's perspective, the transparency of FBMC can be questioned.

To end, three policy recommendations are formulated. First, the expected benefits of FBMC should be empirically evaluated based on historical market data (available as of May 20$^{\text{th}}$, 2015). Second, coordination between TSOs should be improved further. With the introduction of the FBMC, bilateral coordination between TSOs (border-by-border, to determine the ATC-value) was replaced by regional coordination among all CWE TSOs. However, different TSOs still apply different methodologies in the FBMC process (e.g., base case determination, GSK calculation). Third, the performance of the FBMC depends on the market zone configuration. Smaller market zones allow a better representation of the physical characteristics of the grid, resulting in a better performance of the FBMC. In this respect, it might be useful to reconsider the market zone configuration in Europe.

Chapter 8

CO_2 abatement in the electricity sector

Chapter based on:

K. Van den Bergh and E. Delarue. Quantifying CO_2 abatement costs in the power sector. Energy Policy, 80:88-97, 2015.

E. Delarue and K. Van den Bergh. Carbon mitigation in the electric power sector under cap-and-trade and renewables policies. Energy Policy, 92:34-44, 2016.

Abstract: In Europe, CO_2 emissions from the electricity generation sector and energy intensive industries are capped under a cap-and-trade system, i.e., the European emission trading system (EU ETS), resulting in a CO_2 emission price. To assess the impact of a CO_2 emission price, marginal abatement cost curves (MACCs) are a commonly used tool by policy makers, providing a direct graphical link between a CO_2 price and the expected CO_2 emission abatement. First, this chapter presents a new methodology that improves the understanding of the relation between a CO_2 emission price and CO_2 abatement in the electricity generation sector. The methodology is based on the insight that CO_2 emissions in the electricity sector are driven by the composition of the conventional generation portfolio, the residual load and the generation costs of conventional units. The methodology addresses both the robustness issue and the granularity issue related to MACCs, and offers policy makers a new tool to assess CO_2 abatement options. Second, the methodology also illustrates interaction effects between direct CO_2 emission policies, such as a cap-and-trade system, and indirect policies, such as a push for renewables in the

electricity generation sector. These interaction effects have implications on the overall CO_2 price and on CO_2 emissions both from the electricity sector and the other sectors under the cap. The second part of this chapter aims to quantify these interactions by means of impact curves. Impact curves give the set of possible combinations of CO_2 price changes and CO_2 emission displacements. The methodology presented in this chapter is mainly based on a bottom-up approach, using the LUSYM unit commitment model, and is applied to a case study of the 2012 Central Western European power. The focus is on short-run CO_2 abatement (i.e., not based on investment).

Keywords: CO_2 emission policy, marginal abatement cost curves, electricity generation sector, cap-and-trade, European emission trading system, policy interactions.[1]

8.1 Introduction

Policy measures aiming at reducing CO_2 emissions are becoming increasingly widespread. In this respect the electricity generation sector plays an important role due to its notable share in total emissions–about 30% of European CO_2 emissions originate from the electricity generation sector (Eurostat, 2014)–and its considerable abatement potential (Rootzén and Johnsson, 2013).

Two main types of (direct) emission policies exist; a price instrument imposing a fixed payment per emitted unit (e.g., a CO_2 emission tax) and a quantity instrument imposing an aggregated emission cap, possibly combined with a trade mechanism in emission allowances (e.g., a cap-and-trade mechanism).[2] Both types of policy result in a cost of emitting CO_2. A widely used tool to think about the impact of emission policy is the concept of marginal abatement cost curves (MACCs). A MACC plots the shadow price corresponding to an emission constraint of increasing severity against the quantity abated. A point on the MACC represents the marginal cost of abating an additional unit of emissions (Ellerman and Decaux, 1998). As such, a MACC links emission abatement to an emission cost (being a CO_2 tax or a CO_2 price).

Roughly speaking, two main methods are used to develop MACCs. The first method consists of a top-down approach based on macroeconomic models,

[1] All abbreviations and symbols used in this chapter are listed and explained at the outset of this dissertation.

[2] Besides pure price-instruments and pure quantity-instruments, several other emission policies exist, such as hybrid systems (i.e., a quantity-instrument with price floors, see Regional Greenhouse Gas Initiative in the North-East of the United States) or direct emission regulations (i.e., performance standards for emitters, see for instance the Large Combustion Plant Directive in Europe) (Murray and Maniloff, 2015; European Commission, 2016c).

often in a general equilibrium framework. The second method uses a bottom-up approach, based on detailed optimization models or expert knowledge of a system, mostly in a partial equilibrium framework (Jacoby, 1998). The advantage of the top-down approach is that it aims to capture all effects of a CO_2 price, including feedback loops like changes in fossil fuel prices and changes in income and purchases. However, these top-down models are limited to less detailed representations of each sector and each country. The engineering bottom-up approach allows a very detailed description of a certain sector, but this comes at the expense that not all effects and feedback loops in the system can be captured (Jacoby, 1998). The trade-off between bottom-up and top-down models is a reoccurring discussion in energy systems modeling and often aspects from both approaches are combined (Labandeira et al., 2009). Note that also microeconomic models (partial equilibrium models) of electricity and fuel markets can account for fuel price effects. This is a microeconomic approach, which closes income and other loops in the economy and attempts to represent all sectors. Models often referred to in the literature on MACCs are, among others, the EPPA model of MIT (Paltsev et al., 2005), the POLES model developed by IEPE (Criqui et al., 1999; European Commission, 2010) and the DART model developed at the Kiel Institute for World Economics (Klepper et al., 2003).

Although MACCs are a commonly used tool to analyze the impact of a CO_2 price on CO_2 abatement–or vice versa, some general issues can be raised with regard to these curves. For the construction of MACCs, models are often based on a centralized optimization, with perfect information. In reality, specific technical constraints, and elements of imperfect information and risk perception result in abatement measures getting implemented over a range of CO_2 prices, rather than on distinct CO_2 prices. MACCs are also rather static snap-shots (Vogt-Schilb and Hallegatte, 2014). As CO_2 prices rise, measures will get implemented and learning effects will be triggered. In this regard, as different abatement measures relate to different time horizons (e.g., pure operational measures versus long term investments) it might not be straightforward putting them on a single axis.

When derived from modeling (either top-down or bottom-up), some further reflections are to be made regarding MACCs. Kesicki and Ekins (2012) give an overview of the shortcomings of MACCs, with robustness being one of the most critical ones. Each model used to derive MACCs is based on external parameters (Kesicki, 2013). A MACC is robust if it is insensitive to changes in these parameters. In the literature, consensus seems to be that MACCs are not very robust (Klepper and Peterson, 2006; Fischer and Morgenstern, 2006; Delarue et al., 2010; Morris et al., 2012). Another issue with regard to MACCs is the level of granularity. A MACC with high granularity might give a detailed

cost-emission relation of a single abatement technology, without taking account of overlapping and mutually influencing abatement technologies. On the other hand, a MACC with low granularity might give an aggregated cost-emission relation but without revealing the driving technology of the abatement at a certain CO_2 emission cost.

Despite its shortcomings, MACCs are often used to study emission trading systems, including the European emission trading system (EU ETS). CO_2 emissions, however, are not only affected by the CO_2 price resulting from the cap-and-trade system. Other determinants can relate to energy market effects (such as fossil fuel prices), but can also often (directly) result from policies other than directly setting a CO_2 cap, such as renewable energy policies (Johnson and Novacheck, 2015). Hence, under a cap-and-trade system, such other policies on their turn can have an impact on the CO_2 price and can create shifts of emissions between different sectors under the cap. In other words, policy interaction occurs between direct emission policies, such as the EU ETS, and indirect emission policies, such as renewables deployment.

This chapter consists of two main parts. The first part deals with MACCs of the electricity generation sector. The second part deals with interaction between the EU ETS and renewables deployment in the electricity generation sector. In the first part of the chapter, a new methodology is developed, based on knowledge of the drivers of CO_2 emissions in the electricity generation sector. A key concept of the presented methodology is the so-called absolute emission plane, which represents the relation between CO_2 emissions in the electricity generation sector and its drivers. MACCs can be derived from the absolute emission plane by combining it with the relation between a CO_2 emission cost and the respective emission drivers. The methodology provides insight in the way that a MACC is composed combining several abatement technologies (i.e., the granularity issue). The methodology further illustrates how changes in external parameters influence the MACC (i.e., the robustness issue). Moreover, the methodology can be used to study abatement in the short run and in the long run. The focus of this chapter is on short-term CO_2 abatement. The main objective of the presented methodology is to deepen the understanding of the relation between a CO_2 emission price and CO_2 emission abatement in the electricity generation sector.

The second part of the chapter studies the interaction between a cap-and-trade system for CO_2 emissions, such as the European emission trading system, and other indirect CO_2 emission measures. Specific focus is on how measures in one sector under the cap have an impact on overall CO_2 emission price and how these can create shifts in emissions between different sectors under the cap. Focus is mainly on the push for renewables as indirect measure. However, as will also be briefly illustrated in Appendix C, the methodology is generally

applicable to other measures, such as support for electric vehicles. This second part gives an comprehensive literature overview of the interaction effects between cap-and-trade mechanisms and indirect emission policies, and introduces impact curves, which can be derived from the absolute emission plane and quantify the range of these interaction effects.

The methodologies presented in this chapter are based on a bottom-up approach. To this end, the LUSYM model is used, describing the electricity generation sector with a high level of detail (see chapter 2). The methodology is illustrated with a case study of the Central Western European (CWE) electricity generation sector (i.e., Germany, France, Belgium, The Netherlands, and Luxembourg).

This chapter proceeds as follows. First, section 8.2 introduces the case study of the CWE region and briefly discusses the LUSYM model. The same case study will be used throughout the whole chapter. The first part of this chapter, i.e., the part dealing with marginal abatement cost curves, consists of section 8.3 and section 8.4. Section 8.3 describes a framework to think about CO_2 emissions and CO_2 abatement in the electricity generation sector, resulting in the so-called absolute emission plane. Section 8.4 derives marginal abatement cost curves from the absolute emission plane. The second part of this chapter, i.e., the part dealing with policy interaction, consists of section 8.5 and section 8.6. Section 8.5 gives a detailed description of the European emission trading systems and its interaction effects with other policy measures such as the deployment of renewables. In section 8.6, these interaction effects are quantified by means of impact curves. Finally, section 8.7 concludes.

8.2 System and model description

This section presents the studied electricity system, i.e., the 2012 Central Western European system, and briefly describes the unit commitment model which is used in this study, i.e., the LUSYM model.

8.2.1 System description

Central Western European (CWE) electricity sector is studies in this chapter, based on 2012 data. The CWE region covers France, Germany, Belgium, The Netherlands and Luxembourg. Each country is represented by one node and the market coupling is established according to the net transfer capacity (NTC) method. The conventional generation portfolio in this region consists of 342 units with a total generation capacity of 175 GW. The composition of the

	Capacity [GW]	Efficiency [%]	$\underline{P}$ [%$\overline{P}$]	MDT,MUT [h]
NUC	82	33	50	168
SPP-C	26	35/40/46	43	6
SPP-L	22	35/40/46	43	24
SPP-G	4	35/40/46	32	5
CCGT	31	40/48/58	35	3
OCGT	5	35/42	30	1
IC	5	35/40/48	35	3

Table 8.1: Overview of installed capacity in the 2012 Central Western European region. Different rated efficiencies are allocated depending on the year of commissioning. The highest rated efficiency is allocated to units commissioned or retrofitted after 2000, the middlemost to units commissioned between 1980 and 2000, and the lowest to units commissioned before 1980 (NUC: nuclear units; SPP-C: coal-fired steam power plant; SPP-L: lignite-fired steam power plant; SPP-G: gas-fired steam power plant; CCGT: combined-cycle gas turbine; OCGT: open-cycle gas turbine; IC: internal combustion engine).

conventional portfolio is considered to be fixed in the remainder of the study (only the impact on CO_2 emissions of the residual load and marginal generation costs are investigated). Table 8.1 gives an overview of the installed capacity together with the parameters assigned to the respective units. Different rated efficiencies are allocated to power plants depending on the year of commissioning. Average 2012 fuel prices have been used (EEX, 2015a).

A whole year is considered in order to take the seasonality of the electricity demand and renewables generation into account. The 2012 annual demand in the CWE region was 1220 TWh (demand corrected for neglected import and export with countries not included in the model). 16% of this demand was fulfilled by renewable generation (wind, photovoltaic, bio, and hydro) and 13% by electricity from cogeneration units. The remaining residual load, to be fulfilled by the conventional portfolio, was 866 TWh. Historical hourly demand time series and renewable generation time series are used. Demand data, renewables data, NTC values and power plant portfolio data originates from ENTSO-E (2015a,c), Elia (2015), Tennet (2015a) and Umweltbundesamt (2015).

8.2.2 Model description

The LUSYM model is used to simulate the CWE power system (see chapter 2 for a detailed description of the LUSYM model). LUSYM is a partial equilibrium model of the electricity sector that determines the optimal scheduling of a given set of power plants to meet the electricity demand, taking account of operational constraints (i.e., a unit commitment model). The LUSYM model is purely operational (i.e., no investments in generation or transmission capacity are considered), deterministic and assumes an inelastic electricity demand. The objective function of the model is minimization of the total operational system cost, consisting of generation costs and start-up costs, subject to the market clearing condition, load and renewables curtailment limits, power plant generation limits, minimum down and up times and trade-based network constraints. Storage units, power plant outages, ramping constraints and reserve constraints are not considered in this case study. The problem is formulated as a mixed-integer linear program (MILP) in GAMS 24.2 and solved by Cplex 12.6 with a relative optimality gap of 1%. The model solves a whole year with an hourly time resolution in weekly blocks. Different weekly optimizations overlap with one day and are coupled by means of sequential boundary conditions, in order to ensure a feasible and optimal coupling between the different optimizations. The model is calibrated so that the simulated generation in a simulation with historical input data matches the historical observed generation in the 2012 CWE power system. It takes about 3 hours to solve the unit commitment model for one year for the CWE region on an Intel®Core^{TM} i7-2620M CPU@2.7 GHz with 8 GB RAM.

8.3 CO_2 emissions in the electricity generation sector

First, a framework is presented to structure the drivers of CO_2 emissions in the electricity generation sector. Second, so-called absolute emission planes follow from this framework, giving a graphical representation of the link between the drivers and the CO_2 emissions in the electricity sector.

8.3.1 CO_2 emission drivers

Different parameters that influence the CO_2 emissions from the electricity generation sector can be identified and classified in 3 main categories of CO_2 emission drivers:

1) the composition of the conventional power plant portfolio;
2) the residual load to be met by the conventional power plant portfolio;
3) the marginal generation costs of the conventional power plant portfolio.

Each of these drivers is discussed more in detail in this section.

Conventional generation portfolio

The conventional generation portfolio consists of power plants that can be actively controlled by generation companies. The most common conventional units are nuclear power plants and fossil fuel-fired power plants (coal, gas, lignite, and fuel oil). Renewables generation (wind and solar energy) can only be actively controlled to a limited extent and are therefore not considered as part of the conventional portfolio (but accounted for in the residual load).

The composition of the conventional generation portfolio is a first important driver of the CO_2 emissions in the electricity generation sector. Depending on the fuel mix and the average power plant age (impacting, among others, the operating efficiency), portfolios can have very different CO_2 intensities. To illustrate this, Fig. 8.1 shows the CO_2 intensity of electricity generation for some European member states. The French generation portfolio consists mainly of nuclear power plants and hydro power plants, resulting in a very low CO_2 intensity. Electricity generation in Poland, on the other hand, is to a large extent based on coal and lignite-fired plants, resulting in a high CO_2 intensity. The other shown member states have CO_2 intensities between these two relative extreme values.

CO_2 abatement can be achieved by changing the installed conventional generation capacity or its technical parameters. Possible abatement actions are (non-exhaustive list):

- investments in nuclear power plants (CO_2 free electricity generation);
- investments in new gas-fired plants (relatively low CO_2 emissions);
- closing down lignite or coal-fired plants (relatively high CO_2 emissions);
- retrofitting existing fossil fuel-fired plants (resulting in a higher efficiencies);
- changing the power plant fuel (e.g., burning biomass instead of coal);
- implementing carbon capture and storage.

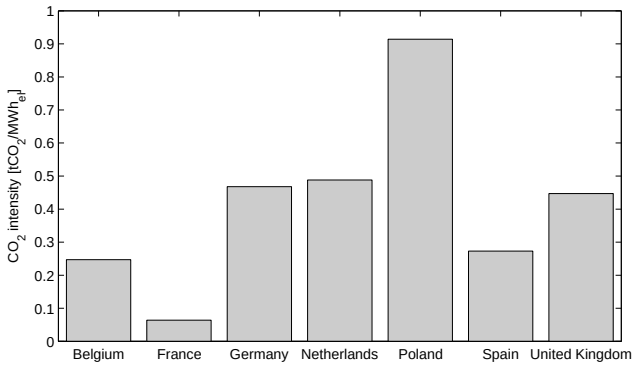

Figure 8.1: The CO_2 intensity of electricity generation varies strongly from country to country, depending to a large extent on the installed generation portfolio - 2009 data (Eurelectric, 2011).

A CO_2 price might trigger CO_2 abatement by changing the conventional power plant portfolio through one of the listed abatement options. Conventional power plant portfolios are relatively inert, implying that a CO_2 price causes CO_2 abatement by changing the composition of the conventional portfolio only in the long term. For example, typical lead times for new conventional plants range from 2 years for combined-cycle units up to 7 years for nuclear units (IEA, 2010).

Residual load

The residual load that has to be met by the conventional power plant portfolio is the original electricity demand minus generation from renewables and cogeneration units. Logically, the higher the residual load, the higher the CO_2 emissions from the power system. CO_2 abatement can be achieved by reducing the residual load. Possible abatement actions are (non-exhaustive list):

- investments in renewable generation capacity (wind and solar energy);
- increasing the energy efficiency of electrical appliances;
- price-elasticity of demand (Chen et al., 2008).

A CO_2 price might trigger CO_2 abatement by decreasing the residual load through one of the listed abatement options. Decreasing the residual load plays

a role in the medium term. For example, lead times of new wind and solar capacity are about 1 year (IEA, 2010). In the short term (days to weeks), electricity demand is rather inelastic. In the medium term, however, the electricity demand can be expected to be partially elastic, representing, among others, investments in more efficient appliances.

Note that renewable generation is included in the residual load since it is a CO_2-free source of electricity generation and as such reduces the generation from CO_2 emitting power plants. This does not imply that renewables are considered to be of minor importance (today's renewable shares in the electricity sector are far from negligible) or that renewables can not take part in the electricity market operation (e.g., curtailment of renewables generation at a certain price). However, for the sake of clarity and in line with the framework presented in this section, the term residual load will be used throughout this chapter.

Marginal generation costs

The marginal generation costs of the available conventional plants determine the merit order. The merit order is a ranking of all available conventional power plants in ascending order of marginal generation cost. The intersection of the merit order with the residual electricity load divides the power plant portfolio in operating power plants, i.e., the ones at the left of the intersection, and non-operating power plants, i.e., the ones at the right of the intersection (see Fig. 8.2).[3] Power plants with low marginal generation costs are thus more likely to be online than power plants with higher marginal generation costs. At 2014 fuel and CO_2 prices in Europe, the ranking of conventional units in the merit order is roughly speaking the following: nuclear units, lignite-fired units, coal-fired units, gas-fired units and fuel oil-fired units. At the time of writing, coal-fired plants are hence more likely to produce in Europe than gas-fired power plants.

CO_2 abatement can be achieved by changing the marginal generation costs of conventional power plants, resulting in so-called fuel switching. Fuel switching occurs when the marginal generation cost of high-emitting plants (e.g., coal-fired plants) becomes higher than the marginal generation cost of low-emitting plants (e.g., gas-fired plants), leading to a switch of these plants in the merit order. The result is that more generation is coming from low-emitting plants and overall CO_2 emissions decrease. Appendix C gives a detailed description of fuel switching.

[3] This is only true by approximation. Dynamic power plant constraints might cause power plants with higher marginal generation costs to be online while plants with lower marginal costs are offline.

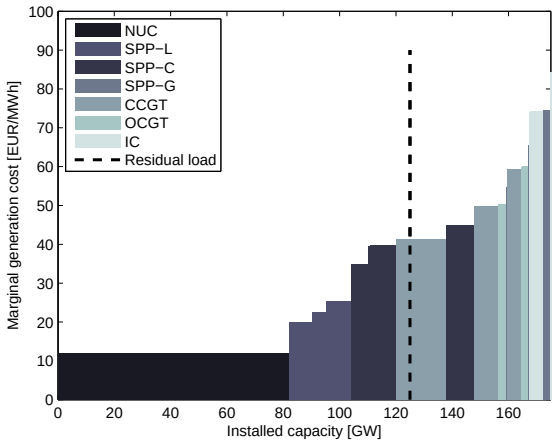

Figure 8.2: Merit order of the CWE region (based on 2012 data) and the inelastic average residual load. NUC: nuclear units, SPP-L: lignite-fired steam power plants, SPP-C: coal-fired steam power plants, SPP-G: gas-fired steam power plants, CCGT: combined-cycle gas turbines, OCGT: open-cycle gas turbines, IC: internal combustion engines.

Note that fuel switching, as used in this chapter, refers to a change in the dispatch of (at least) two power plants. This effect is also sometimes referred to as emissions dispatch (see for instance Heslin and Hobbs (1989)). One can also reduce CO_2 emissions by switching the fuel of one power plant, e.g., burning biomass instead of coal (see for instance Hobbs et al. (1994)). However, the latter might be a long-term abatement option, depending on how flexibly fuels can be switched. In this chapter, the focus is on fuel switching, defined here as reducing CO_2 emissions by changing the dispatch of power plants. Changes in the fuel burned in power plants are not considered.

A CO_2 price might trigger fuel switching by increasing the marginal generation costs of emitting units. Fuel switching is a pure operational abatement technology, responding rapidly to a CO_2 price (power plant operators schedule their plants on an hourly to daily basis).

Summary

This section discusses the three main drivers of CO_2 emissions in the electricity generation sector. All possible abatement options can be assigned to one of these

CO_2 abatement options	Time frame
Conventional portfolio	long term
- investments in nuclear power plants	(several years)
- investments in gas-fired plants	
- closing down lignite or coal-fired plants	
- retrofitting fossil fuel-fired plants	
- changing the power plant fuel	
- carbon capture and storage	
Residual load	medium term
- investments in renewable generation capacity	(months-years)
- increasing the efficiency of appliances	
- demand reduction (higher electricity prices)	
Marginal generation costs	short-term
- fuel switching	(days-months)

Table 8.2: Overview of various CO_2 abatement options in the electricity sector, ordered according to their emission driver.

drivers. Each driver is linked to a certain time frame. Table 8.2 summarizes this section. An abatement option can be triggered by a CO_2 price, but also by other energy and climate policies (e.g., renewables support schemes can trigger investments in renewables) or by macroeconomic evolutions (e.g., changing fuel prices might trigger fuel switching) (Van den Bergh et al., 2013). The interaction between a cap-and-trade system and other energy and climate policies is discussed in detail in sections 8.5 and 8.6.

8.3.2 Absolute emission plane

The absolute emission plane of the electricity generation sector is, in its complete form, a 4-dimensional surface, containing the relation between the three CO_2 emission drivers and the CO_2 emissions in the electricity generation sector. Each point on the absolute emission plane represents a possible operational state of the electricity generation sector, given a certain power plant portfolio composition, certain marginal generation costs and a residual load. Each point on the absolute emission plane follows from a detailed simulation for a whole year (8760 hours) with the LUSYM unit commitment model as described in section 8.2.

In this chapter, the composition of the conventional generation portfolio is assumed fixed. As such, the absolute emission plane reduces to a 3-dimensional surface. Fig. 8.3 shows the absolute emission plane of the 2012 CWE

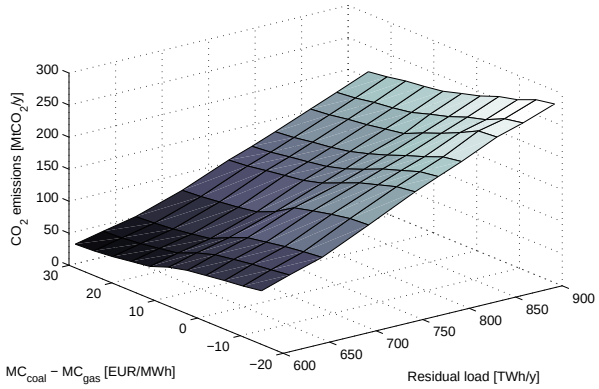

Figure 8.3: The absolute emission plane of the Central Western European electricity generation sector, based on 2012 data.

electricity generation sector. The figure indicates that absolute CO_2 emissions decrease with decreasing residual load and with increasing difference in marginal generation costs between coal-fired and gas-fired plants. Note that the absolute emission plane of Fig. 8.3 is based on specific 2012 data (e.g., 2012 time series for demand and renewables generation). Other time series would result in a slightly different absolute emission plane, however, the main trends and order of magnitudes would remain.

In this chapter, the residual load is varied by scaling up or down renewables time series. This is a justifiable approximation when studying the impact of a CO_2 price on residual load through renewables investments. However, when the residual load is affected by a CO_2 price through other abatement options, e.g., energy-efficient appliances, the residual load should be varied in another way, in line with the characteristics of the studied abatement option (e.g., scaling up or down the residual load time series when studying energy-efficient appliances).

A metric is required containing information about all generation costs in the generation portfolio. The proposed metric is the difference between the average marginal generation cost of a coal-fired power plant and the average marginal generation cost of a gas-fired power plant. The rationale is that coal-fired and gas-fired units are the main source of fuel switching as they are operating close to the margin (i.e., close to the intersection of the merit order with the demand curve). The metric contains average marginal generation costs, averaged in time and averaged over different units (with different efficiencies).

8.4 Marginal abatement cost curves

8.4.1 Methodology

Based on the insights in the CO_2 emissions drivers, a detailed marginal abatement cost curve of the electricity generation sector can be composed in three steps:

1) Quantify the relation between a CO_2 price and each of the 3 drivers of CO_2 emissions in the electricity generation sector (conventional generation portfolio, residual load and marginal generation costs). This relation can be based on a modeling exercise or expert knowledge.

2) Quantify the relation between the aggregated CO_2 emissions in the electricity generation sector and its 3 drivers, resulting in a 4-dimensional surface (three CO_2 drivers plus the aggregated CO_2 emissions), referred to as the absolute emission plane. This step has already been taken in this chapter (see section 8.3). A 3-dimensional version of the emission plane is considered.

3) Merge the information of the two previous steps to find the relation between a CO_2 price and CO_2 emissions in the electricity generation sector. This relation leads to the marginal abatement cost curve of the electricity generation sector.

The different effects of a CO_2 price on each CO_2 driver may not just be summed up, as the relation between a CO_2 emission driver and the aggregated CO_2 emissions depends on the other CO_2 emission drivers as well. For instance, a change in marginal generation costs–caused by a CO_2 price–has a different effect on the CO_2 emissions, depending on the change in residual load–caused by the same CO_2 price. This indicates interaction between the different CO_2 emission drivers, which is captured by the partial equilibrium model and represented by the absolute emission plane.

If a parameter which is external to the analysis changes (e.g., fossil fuel prices or capital costs of renewables), the first and the third step of the analysis plan have to be repeated. This illustrates the robustness issue. Changes in external parameters affect the MACC.

In the third step of the analysis plan, several abatement technologies are combined into one single CO_2 price-emission relation. The bottom-up nature of this methodology allows decomposing the total CO_2 abatement in its driving abatement technologies. This relates to the granularity issue.

The methodology, which is described in rather abstract terms up until now, will be illustrated in the next subsection for a real-life case study of the Central Western European electricity generation sector, considering two abatement technologies: fuel switching and investments in wind energy. Fuel switching is a significant abatement option in the electricity generation sector. Wind energy can be an important source of CO_2 free electricity generation, with a levelized cost of electricity (LCOE) which is several times lower than the LCOE of photovoltaic energy (IEA, 2010).[4] The case study considers a medium term time frame. Within this time frame, both fuel switching and investments in wind energy might take place. The composition of the conventional generation portfolio, which can change only in the long term, is assumed to be fixed.

The presented methodology implicitly assumes that the three CO_2 emission drivers are only linked through a CO_2 price. The interdependencies between marginal generation costs (fossil fuel prices), conventional power plant portfolios (fossil fuel-fired capacities) and residual load (electricity demand and renewable investments), caused by factors other than a CO_2 price, are not captured by the methodology. This originates from the bottom-up nature of the presented methodology.

8.4.2 Results

The analysis plan discussed in the previous subsection is illustrated in this section based on a case study of the CWE electricity generation sector. First, the relation between a CO_2 price and two CO_2 drivers (the marginal generation costs and the residual load) is derived. Only two different abatement options are investigated in detail in this study (i.e., fuel switching and wind energy), but the methodology can be easily extended to other abatement options. Afterwards, the marginal abatement cost curve can be derived based on merging the first step with the absolute emission plane.

CO_2 price versus marginal generation costs: fuel switching

The relation between a CO_2 price and a marginal generation cost is different for each power plant, depending on the generation type and its efficiency. The marginal generation cost MC_i of a power plant is the derivative of the total

[4]Note that the LCOE of renewable energy sources can change drastically from region to region and typically decreases over time, especially for solar photovoltaics. As such, it is important to work with the correct and latest LCOE-values if this analysis is repeated for other case studies.

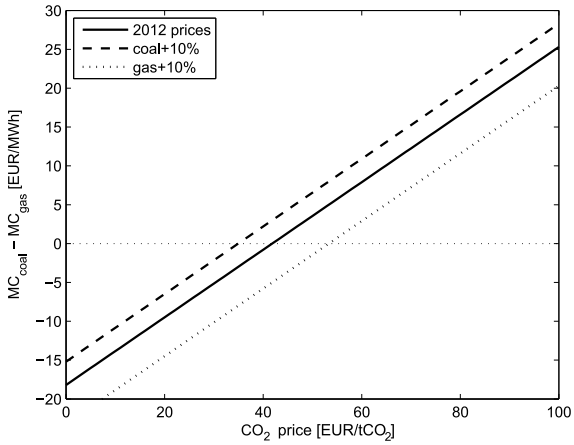

Figure 8.4: Relation between a CO_2 price and the difference in average marginal generation cost between coal and gas-fired power plants, used as a metric for the marginal generation costs of the conventional generation portfolio.

generation cost function TC_i with respect to the power output gen_i.

$$TC_i = \frac{FC_i + EF_i\, CC}{\eta_i}\, gen_i \tag{8.1}$$

$$MC_i = \frac{FC_i + EF_i\, CC}{\eta_i} \tag{8.2}$$

with FC_i the fuel cost in [EUR/MWh$_{\text{th}}$], EF_i the emission factor in [tCO$_2$/MWh$_{\text{th}}$], CC the CO_2 price in [EUR/tCO$_2$] and η_i the rated efficiency. The operating efficiency of the power plant is function of the power output of the unit (the operating efficiency decreases in part load operation). However, for the sake of simplicity, the dependence of the efficiency on the power output is neglected in this section.[5] Note that the marginal generation cost (Eq. (8.2)) is used in the objective function of the LUSYM model (Eq. (2.2) in chapter 2).

Fig. 8.4 shows the relation between a CO_2 price and the difference in average marginal generation costs between coal-fired and gas-fired plants. Fig. 8.4 is based on 2012 average fuel price data (12 EUR/MWh$_{\text{th}}$ for coal and 25

[5]The dependence of the efficiency on the power output is taken into account in the unit commitment model. The non-linear production cost curve is approximated by a linear approximation (see Eq. (2.2) in chapter 2).

EUR/MWh_{th} for gas) and average power plant characteristics (EEX, 2015a).[6] To investigate the impact of changes in external parameters, the relation between a CO_2 price and marginal generation costs is also considered for a case with a 10% higher coal price and the 2012 gas price, and for a case with a 10% higher gas price and the 2012 coal price. Fig. 8.4 indicates that coal-fired power plants become more expensive than gas-fired power plants, in terms of marginal generation costs and at 2012 fuel prices, as of a CO_2 price of 40 EUR/tCO_2.

CO_2 price versus residual demand: wind energy investments

A CO_2 price might promote investments in wind generation capacity, resulting in a lower residual demand to be fulfilled by the conventional power plant portfolio. In this study, a dedicated model is used and set up to determine the relation between a CO_2 price and wind energy investments (i.e., a different model than the unit commitment model discussed in section 8.2). The model gives the amount of installed wind capacity, assuming the conventional portfolio to be fixed and solely based on 2012 power system data (fuel prices, demand data, etc.). The investments in wind energy are solely triggered by a CO_2 emission price, as no subsidies for wind energy are considered in the investment model.

The model considers one period with the annually average residual demand and a merit order of the conventional generation portfolio (based on annually average fuel prices). The model estimates the wholesale electricity price as the marginal generation cost of the last generating unit in the merit order needed to meet the average residual demand. If the electricity price is higher than the levelized cost of electricity (LCOE) of wind, an extra MW of wind energy is installed resulting in a decrease in the average residual demand with 0.2 MW for onshore wind (20% capacity factor) and 0.3 MW for offshore wind (30% capacity factor). Then the new electricity price is calculated as the marginal generation cost of the last generation unit in the merit order needed to meet the reduced average residual demand. This electricity price will be lower than the previous calculated price. This iterative process continues until the estimated electricity price equals the LCOE of wind or the wind capacity potential is reached (Kagiannas et al., 2004). The simulations are repeated for different CO_2 emission prices. The model gives a rough estimation of the investments in wind triggered by a CO_2 price. The amount of installed wind is translated into a decrease in residual demand by subtracting the wind generation (estimated based on a 20% capacity factor for onshore wind and 30% capacity factor for

[6] A coal price of 12 EUR/MWh_{th} corresponds to a price of 120 $/ton and a gas price of 25 EUR/MWh_{th} corresponds to a price of 10 $/MMBtu (2012 dollar-euro exchange rate).

	LCOE [EUR/MWh]		Tech. potential [GW]	
	onshore	offshore	onshore	offshore
Belgium	68	128	250	11
The Netherlands	58	88	350	110
Germany	71	94	2000	80
France	61	98	2700	90

Table 8.3: Overview of the levelized cost of electricity (LCOE) and the technical potential of wind energy in the Central Western Europe region (EEA, 2009; IEA, 2010).

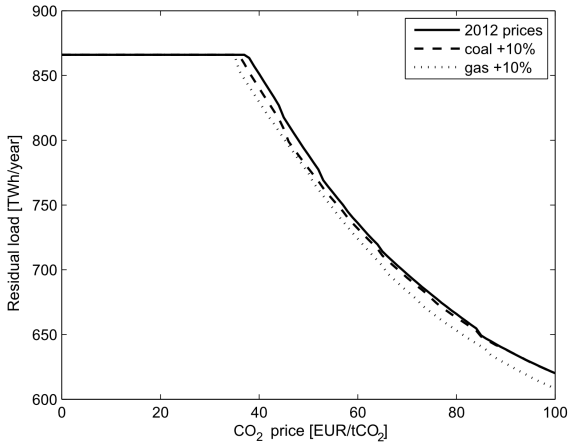

Figure 8.5: Relation between a CO_2 price and the residual load, caused by investments in new wind capacity (assuming a yearly distribution of load and wind).

offshore wind) from the original residual demand. Table 8.3 shows the data used in this investment model.

Fig. 8.5 shows the residual demand including the additional wind generation as a function of the CO_2 price. Again, the relation between a CO_2 price and the residual demand is considered for a case with a 10% higher coal price and the 2012 gas price, and for a case with a 10% higher gas price and the 2012 coal price. This change in fuel prices impacts the decision of the wind investors as it changes the electricity price, but only to a limited extent. At higher fuel prices, wind investments start taking place at slightly lower CO_2 emission prices. The technical potential limit is not reached within the considered CO_2 price range.

Deriving a marginal abatement cost curve

A marginal abatement cost curve of the electricity generation sector can be derived, based on the relation between a CO_2 price and the CO_2 emission drivers on the one hand, and the relation between the CO_2 emission drivers and aggregated CO_2 emissions on the other hand. The following steps need to be taken:

1. Indicate the appropriate reference point on the absolute emission plane (see point R at Fig. 8.6.a). The reference point gives the CO_2 emissions in the electricity generation sector in case of a zero CO_2 emission price, and is indicated by the residual load and marginal cost difference that would occur in absence of a CO_2 emission price. The reference point R at Fig. 8.6.a corresponds to the residual load and marginal cost difference in the CWE 2012 power system at zero CO_2 price.

2. Project the relation between a CO_2 price and each of the relevant CO_2 emission drivers on the absolute emission plane (see dashed lines at Fig. 8.6.a). Each dashed line corresponds to a CO_2 emission driver for a CO_2 price ranging from 0 to 100 EUR/tCO_2, assuming the other CO_2 emission drivers fixed. The curve representing the relation between a CO_2 price and marginal generation costs starts in the reference point and is parallel to the marginal cost axis (i.e., perpendicular to the residual load axis). This curve is the projection of Fig. 8.4 on the absolute emission plane. The curve representing the relation between a CO_2 price and residual load starts also in the reference point but is parallel to the residual load axis (i.e., perpendicular to the marginal cost axis). This curve is the projection of Fig. 8.5 on the absolute emission plane.

3. Compose the different CO_2 price-CO_2 driver relations into one relation between a CO_2 price and CO_2 emissions. This latter relation is represented by a trajectory on the emission plane (see solid line at Fig. 8.6.a). The solid line is a collection of points on the absolute emission plane corresponding to the CO_2 emission drivers for a CO_2 price ranging from 0 to 100 EUR/tCO_2. For CO_2 prices up to 35 EUR/tCO_2, no investments in wind energy occur and the residual load remains unchanged. As a result, the first part of the solid line follows the dashed line corresponding to the relation CO_2 price vs. marginal generation costs. At higher CO_2 prices, both dashed lines are influencing the trajectory of the solid line.

4. In a final step, the CO_2 price-emission relation can be expressed relative to the CO_2 emissions in the reference point, which leads to the marginal abatement cost curve (see Fig. 8.6.b).

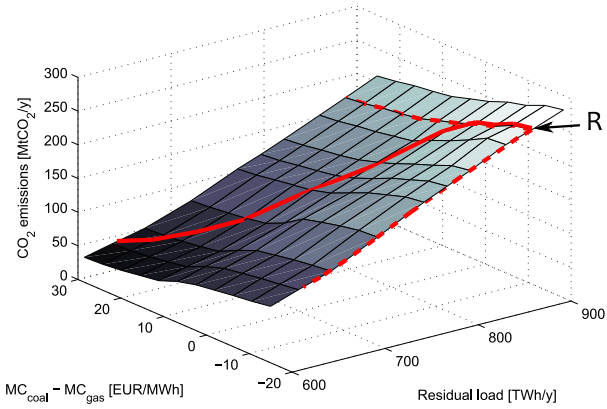

(a) Absolute emission plane.

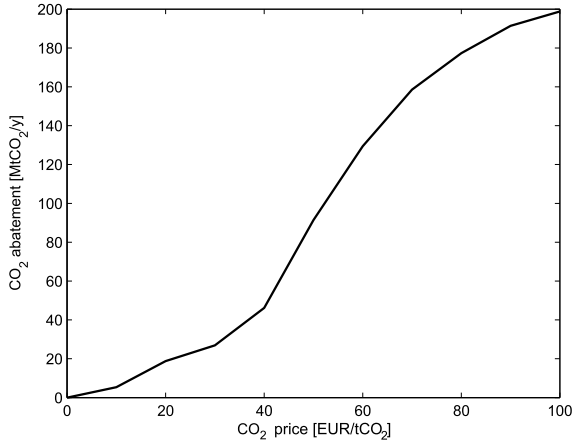

(b) Marginal abatement cost curve.

Figure 8.6: The marginal abatement cost curve can be derived by projecting the CO_2 price-driver relations on the absolute emission plane. Figs. 8.4-8.5 link the top panel with the bottom panel.

8.4.3 Discussion

The methodology presented in this chapter gives insight in the impact of changing external parameters. Consider again a case with a 10% higher coal

price and the 2012 gas price, and a case with a 10% higher gas price and the 2012 coal price. These changes in fossil fuel prices impact the relation between a CO_2 price and each of the CO_2 emission drivers (see Figs. 8.4-8.5). As a result, the MACC of the electricity generation sector will change as well. Fig. 8.7 shows the marginal abatement cost curve and the corresponding trajectories on the absolute emission plane for different fossil fuel prices. This example relates to the robustness issue of MACCs and shows how the proposed methodology can bring insight in the mechanisms behind a changing external parameter–although the robustness issue is not very strong in this particular example. Note that a change in an external parameter changes both the reference point on the absolute emission plane, as well as the trajectory of the CO_2 price-emission relation. Both aspects impact the shape of the marginal abatement cost curve.

The robustness of the CO_2 abatement caused by a CO_2 price should be considered when designing CO_2 emission policies. As has been demonstrated, a CO_2 price affects emissions in the electricity generation sector via different ways. Careful assessment is required to capture the non-linear effects occurring in the electricity generation sector. On top, other policies might target the drivers of emissions as well in parallel, and as such create interaction. An example is a policy that affect the residual load such as the support for renewables, or a policy targeting the power system composition, such as decisions on a nuclear phase out, or specific requirements on fossil-fired generation such as the European large combustion plant (LCP) directive (European Commission, 2001). Clearly, it is crucial to take into account these effects when designing policies. Finally, the shape of a derived MACC might impact the choice for either a price or a quantity based instrument.

The methodology also allows breaking up the MACC in its driving abatement technologies. Figs. 8.4-8.5 indicate that up to a CO_2 emission price of 35 EUR/tCO_2, all CO_2 abatement is caused by fuel switching. At higher CO_2 emission prices, both fuel switching and wind energy investments cause CO_2 emission abatement. The relative contribution of the different abatement technologies can be approximated based on the absolute emission plane. However, the relative contribution of the different abatement technologies can only be approximated as different abatement technologies interact with each other, meaning that the presence of one abatement technology can change the impact of the other abatement technology. Therefore, it is not possible to fully allocate abatement to one specific abatement technology. Fig. 8.8 shows the contribution of fuel switching and wind energy investments in the marginal abatement cost curve of the electricity generation sector based on 2012 prices in case of no interaction between both abatement technologies (based on the imaginary case where only one abatement technology is present), and the total abatement if both abatement technologies are in place. The abatement caused

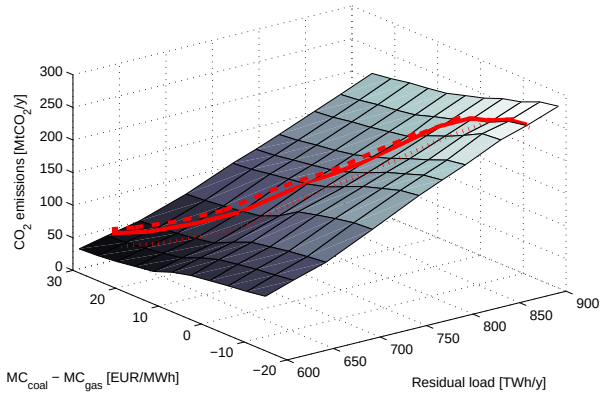

(a) Absolute emission plane.

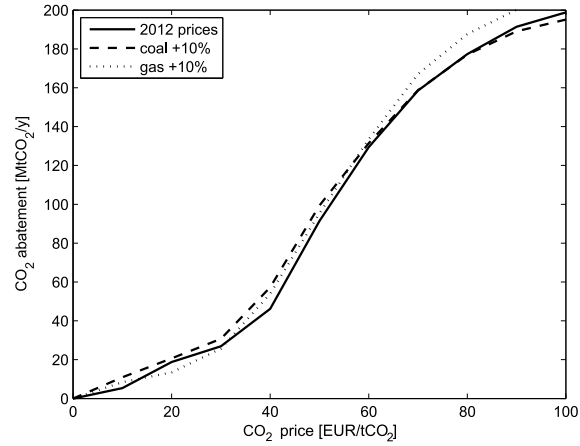

(b) Marginal abatement cost curve.

Figure 8.7: The marginal abatement cost curve depends on the fossil fuel prices imposed to the power system.

by fuel switching as the only abatement technology follows from projecting Fig. 8.4 on the absolute emission plane (see dotted line parallel to the marginal generation cost axis on Fig. 8.6.a). Analogously, the abatement caused by wind energy investments as the only abatement option follows from projecting Fig. 8.5 on the absolute emission plane (see dotted line parallel to residual load axis on Fig. 8.6.a). It turns out that at higher CO_2 prices, negative interaction

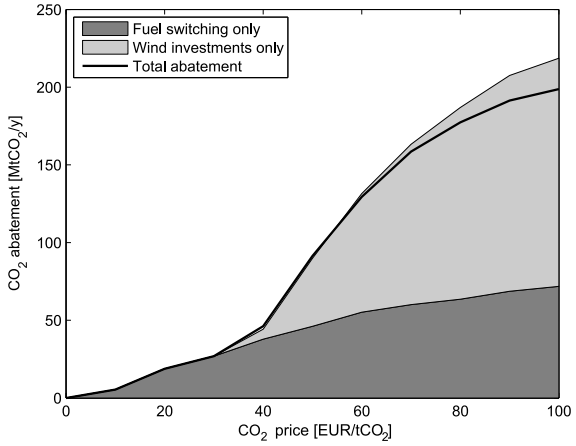

Figure 8.8: Relative contribution of fuel switching and wind energy investments to CO_2 abatement.

occurs, meaning that the total abatement caused by fuel switching and wind together is lower than the sum of the abatement if the abatement technologies are separately in place. Put differently, the presence of fuel switching reduces the impact of wind energy investment on CO_2 emission, and vice versa. This is however not a general conclusion, but determined by the values for the CO_2 emission drivers as used in this study (generation costs, residual load, power plant portfolio). Another setting of the CO_2 emissions drivers might lead to positive interaction (Weigt et al., 2013). With positive policy interaction, the impact of one policy instrument is enlarged by the presence of another policy instrument.

Several abatement options cause CO_2 abatement in a different but partially overlapping range of CO_2 prices, and interact with each other. Although it is difficult to precisely quantify ex-ante the CO_2 price range in which a particular CO_2 abatement option will be active and what the interaction will be with other abatement options, policy makers should be aware of interaction effects between different CO_2 abatement options.

The remainder of this chapter deals with interaction between emission policies. Note that the interaction between direct and indirect emission policies (e.g., cap-and-trade systems and renewables deployment) is not the same as the interaction between different abatement options (e.g., fuel switching and decrease in residual load). The interaction between abatement options, as discussed in this section, is of secondary importance compared to interactions between emission policies.

8.5 Interaction between the EU ETS and other policies

This section starts off with a description of the European emission trading system and continues with a literature overview on policy interaction.

8.5.1 The European emission trading system

Initiated in 2005, the European emission trading system (EU ETS) puts a cap on the CO_2 emissions of the European electricity generation sector, other heavy industry (e.g., steel, aluminum, cement, pulp and paper), and more recently aviation (flights within Europe). Within the EU ETS, the electricity generation sector is responsible for about half of the CO_2 emissions, while the other industries take up the other half (Ellerman et al., 2014). The EU ETS covers about 45% of total European greenhouse gas emissions. For every ton of CO_2 emitted, an allowance has to be handed in. These allowances can be traded freely on the market, between companies, active in the different sectors under the cap. This way, CO_2 emissions are abated where it is cheapest and CO_2 emissions are displaced from sectors with cheap abatement possibilities towards sectors with more expensive abatement options. After a trial period running from 2005 to 2007, the second ETS trading period spanned the Kyoto commitment period (2008-2012). The third period currently runs from 2013 till 2020. Allocation of allowances was initially largely for free (till 2012). As from 2013, the major share of allowances is auctioned (at least in the electricity generation sector). For more background on the functioning of the EU ETS, the reader is referred to Ellerman et al. (2010) and Richstein et al. (2015).

The ETS sectors face an absolute cap on CO_2 emissions, declining each year, to reach a 21% reduction in 2020 compared to 2005. The tightness of the cap determines the level of abatement required compared to business as usual (no cap), and hence sets the price of the allowances (marginal abatement cost). With an absolute cap, the demand for allowances is, however, also heavily influenced by external factors. A first example is the economic/financial crisis reigning in Europe from 2008 onwards, clearly having an impact on industrial activity and hence CO_2 emissions (Declercq et al., 2011; Koch et al., 2014). Second, also certain policy measures can affect the demand for allowances, e.g., imposing targets for renewable energy, this way pushing carbon free electricity into the system, again reducing the tightness of the cap. These two effects, together with a relatively high inflow of international credits (which can cover part of the emissions under the cap), have led to a surplus of allowances, gradually built

up since the second trading period.[7] Allowances are furthermore bankable to subsequent trading periods. The surplus being built up in the second period was as such transferred to the third trading period, leading to a surplus of allowances of over 2000 $MtCO_2$ in 2014 (European Commission, 2014a). Correspondingly, for several years the EUA price has been consistently low, between 4 and 8 EUR/tCO_2.

While CO_2 emissions are below the cap and hence meet the target set, a current concern in the policy debate is the resulting CO_2 price, which is too low to serve as a solid signal for low carbon investments deemed crucial for the transition to a low-carbon energy system in the longer term. In this regard, the European Commission (EC) has implemented a backloading measure in the third phase and a more structural reform through a market stability reserve as from 2019 (with the back-loaded allowances being put directly in this reserve). Despite these current issues, the EU ETS is still considered as Europe's main instrument to reduce carbon emissions.

Next to the EU ETS, especially renewables have played an important role in Europe's recent climate and energy policy. By 2020, 20% of Europe's final energy consumption is to come from renewables (European Commission, 2009). The 20% target is translated to binding individual member state targets. Member states are free to adopt appropriate support measures (such as feed-in tariffs or green certificates) to achieve their renewables target.

8.5.2 Policy interaction: literature overview

Different policy instruments can be deployed to mitigate CO_2 emissions. These can range from a direct CO_2 emission price or emission performance standard to measures related to fossil fuel taxation, energy efficiency measures, renewables deployment policies or R&D funding. From a wider economic perspective, arguments could be raised to call for multiple instrument deployment. Fischer and Preonas (2010) review in this sense the conditions that would make different policies necessary. Fischer and Newell (2008) present an analysis to come to an optimal overall policy to reduce emissions, which involves a portfolio of different instruments due to knowledge spillover. Beato and Delgado (2015) claim that the use of various instruments is justified under circumstances that undermine the effectiveness of carbon markets, such as market design flaws or innovation externalities. However, it is shown by Tuladhar et al. (2014) that under a mixed

[7] Ellerman et al. (2015) point out that the term "surplus" should be used carefully. Part of the allowances being banked (i.e., saved up for being used later) can be banked intentionally, to minimize overall abatement costs over a longer time period, given the continuously decreasing cap. This explains at least part of the difference between the cap and actual emissions.

policy regime, a CO_2 price is an unsuitable indicator of economic costs of carbon mitigation.

Focusing on the electricity generation sector, the interaction between a direct CO_2 policy being implemented as tradable permit system with a fixed cap, and renewable energy polices, has been discussed in various contributions in the literature (see del Río González (2007) for a literature overview). An electricity generation investment model is typically set up and deployed to address these interactions. We refer in this instance to Abrell and Weigt (2008); De Jonghe et al. (2009); Böhringer and Rosendahl (2010); Tsao et al. (2011); Rocha et al. (2015). In general, these publications find that the more stringent the CO_2 cap, the less binding the RES target becomes, to eventually become superfluous. Alternatively, if RES targets increase under a given CO_2 cap, at first space is provided to increase CO_2 intensive electricity generation (such as coal or lignite), to eventually make the CO_2 cap superfluous. In an early publication on this topic, Morthorst (2001) discusses the interaction implications dependent on how policy schemes are implemented (e.g., country basis versus European wide). As a case study illustration, Hindsberger et al. (2003) discuss the implications for electricity generation and investment patterns in the Baltic Sea Region, when multiple instruments are in place. Finally, regarding these policy instrument interactions, Jensen and Skytte (2003) and Linares et al. (2008) have focused on the impact of instrument choice on consumer prices.

When focusing on short-term, operational aspects of the electricity generation sector, a readily available abatement option without requiring investment is fuel switching, i.e., scheduling low carbon electricity generation such as natural gas-fired power plants instead of a carbon intensive electricity generation such as coal-fired generation (see Appendix C for a detailed description of fuel switching). Delarue et al. (2010) have investigated the impact of fuel prices and hourly electricity demand on CO_2 abatement by fuel switching, under different CO_2 prices. Considering fuel switching as alternative abatement option to RES deployment, Weigt et al. (2013) start from a system where both a RES policy and CO_2 price are in place. The impact of these instruments is addressed when combined, and when applied in an isolated manner (i.e., only CO_2 price or only RES deployment). They find that the impact of one instrument can be reinforced by the presence of the other (i.e., the combination of a CO_2 price and RES might have a larger impact on CO_2 emissions than taking the sum of the individual impact of these instruments). They however find that this interaction is very sensitive to the actual hourly electricity demand and instantaneous RES infeed, and might fluctuate over time, reaching negative values as well. They present a case study for the German electricity system for the years 2006-2010. Van den Bergh et al. (2013) have presented an ex-post quantitative assessment of the impact of RES deployment on the CO_2 price and emissions for a large

part of Europe, for the years 2007-2010.

The remainder of this chapter complements the above mentioned literature by developing a new methodology to derive the so-called impact curve. This impact curve presents the impact of RES deployment on the CO_2 price and on shifts of CO_2 emissions between sectors, and as such allows to assess interaction effects in a quantitative way, from a bottom-up perspective. The impact curve is derived from an emission plane, obtained from a set of detailed electric power system simulations, for different levels of CO_2 price and residual demand. The presented framework allows estimating the impact of renewables deployment on CO_2 emission shifts and on CO_2 price in the whole ETS, while only looking in detail at the electricity generation sector. Under the ETS emission cap, any change in CO_2 emissions from the electricity generation sector due to a change in one of the CO_2 determinants will result in a change in the CO_2 price and/or a displacement of CO_2 emissions between the electricity generation sector and the other ETS sectors, in order to keep aggregated emissions equal to the cap. A decrease in CO_2 emissions from the electricity generation sector will lower the CO_2 price and/or shift CO_2 emissions from the electricity generation sector towards other ETS sectors. An increase in CO_2 emissions from the electricity generation sector will have the reverse effect.

Focus is on short-term abatement from fuel switching triggered by a CO_2 price, interacting with the level of residual demand (e.g., affected through the deployment of RES).

8.6 Impact curves

This section presents a framework to analyze the interaction between a cap-and-trade emission instrument and indirect policies, such as renewables support. Renewables support schemes push CO_2 free generation into the electricity generation system, resulting in a decreasing CO_2 price (since the aggregated demand for emission allowances decreases) and a displacement of CO_2 emissions between the different sectors under the emission cap (see Fig. 8.9).

First, the boundaries for both the impact on CO_2 emission price and the impact on shifts of emissions between sectors are derived and described. Second, the results are presented for a case study of the 2012 CWE electricity system.

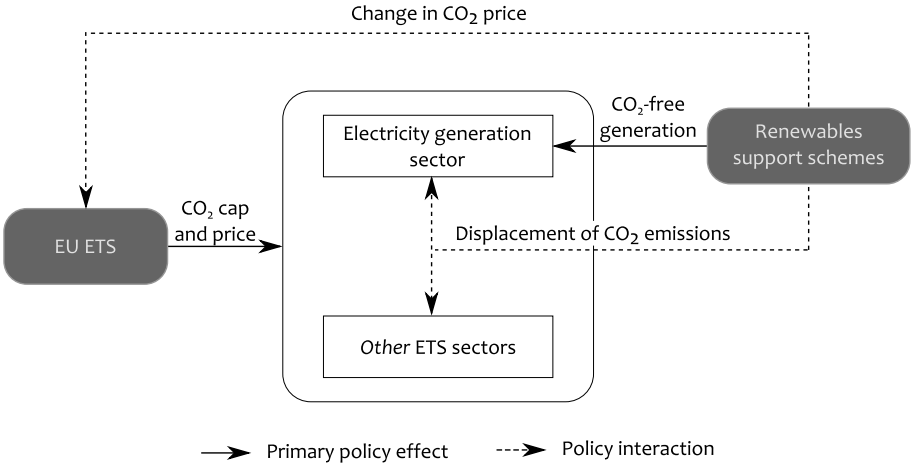

Figure 8.9: Schematic overview of the policy interaction effects between renewables support schemes and the EU ETS.

8.6.1 Methodology

Consider the whole EU ETS, consisting of the electricity generation sector and other ETS sectors. Introducing extra renewables in the electricity generation sector shifts CO_2 emissions from the electricity generation sector to the other ETS sector and causes a reduction in the CO_2 price. Theoretically, there are two extremes possible:

(1) Assume the marginal abatement cost curve of the other ETS sectors is a horizontal line at the current CO_2 price (see panel (a) of Fig. 8.10), meaning that the other ETS sectors can decrease (or increase) CO_2 abatement without a change in CO_2 price. In this case, the introduction of (additional) renewables causes CO_2 displacement from the electricity generation sector to other ETS sectors, but without any change in the CO_2 price. The electricity generation sector can thus be considered as being subject to a CO_2 emission tax. This situation is referred to as the *ETS-price assumption* and gives the outer limit of CO_2 displacement from the electricity generation sector to the other ETS sectors due to extra renewables.

(2) Assume the marginal abatement cost curve of the other ETS sectors is a vertical line at the current CO_2 abatement in the other ETS sectors (see panel (b) of Fig. 8.10), meaning that no change in CO_2 emissions from the other ETS sectors will be triggered at any relevant CO_2 price. In this case,

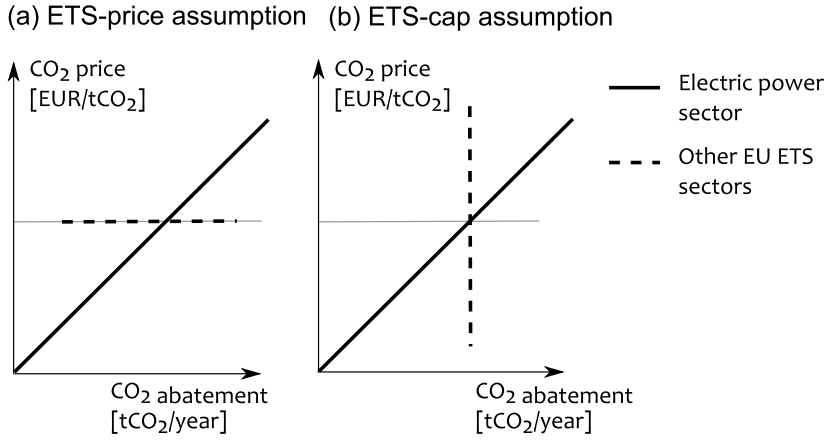

Figure 8.10: Conceptual marginal abatement cost curves for two extreme situations of the CO_2 abatement potential in the other ETS sectors. Panel (a) represents the ETS-price assumption (i.e., the electricity generation sector perceives the cap-and-trade system as a fixed CO_2 emission price) and panel (b) represents the ETS-cap assumption (i.e., the electricity generation sector perceives the cap-and-trade system as a sector-specific emission cap).

> the introduction of (additional) renewables causes no CO_2 displacement from the electricity generation sector to the other ETS sectors, but the CO_2 price decreases up to a level where the electricity generation sector itself compensates for the emission-free renewable injections. The electricity generation sector can thus be considered as operating under its own emission cap. This situation is referred to as the *ETS-cap assumption* and gives the outer limit of the CO_2 price decrease due to extra renewables.

In reality, the introduction of extra renewables causes a situation somewhere between these two extremes, with a CO_2 price decline between zero and the CO_2 price decline following from the ETS-cap assumption, and a CO_2 emission displacement from the electricity generation sector to the other ETS sectors between zero and the CO_2 emission displacement following from the ETS-price assumption. All possible combinations of a CO_2 price change and CO_2 displacement result in the so-called impact curve.

8.6.2 Results

The previous section introduces the boundary conditions for impacts of RES on CO_2 price or emission shifts under the cap. This section shows how the impact curve (range between these two extremes) can be derived, and how this can be applied to analyze the interaction between a cap-and-trade policy and renewables targets.

The impact curve for renewables in the electricity sector

The impact curve presents the impact of RES on both CO_2 emission displacement and the CO_2 price. This curve is now derived from the absolute emission plane (see Fig. 8.3, section 8.3). Note that in this section, the marginal generation cost metric (i.e., the difference in marginal generation costs between coal-fired and gas-fired power plants) is replaced by the CO_2 price as we only consider fuel switching as abatement option (and not a change in residual load), see Fig. 8.3 versus left panel of Fig. 8.11.

First a reference point needs to be set. Consider, e.g., a reference situation (with RES) with a CO_2 price of 10 EUR/tCO_2, a residual demand of 800 TWh/year and 222 MtCO_2 emissions a year (see point R on Fig. 8.11). In this reference situation, a certain level of abatement is achieved through fuel switching, triggered by a present CO_2 price. Starting from this initial situation, an amount of renewable injections is removed from the power system: 100 TWh/year in this example, increasing the annual residual demand to 900 TWh/year. This will cause an increase in CO_2 price and will create a displacement of CO_2 emissions from the other ETS sectors to the electricity generation sector.

First, consider the ETS-price assumption, i.e., the CO_2 price stays fixed at 10 EUR/tCO_2 (see point P on Fig. 8.11). The impact of increasing the residual demand under this fixed price assumption can be visualized on the emission plane by making an intersection of the emission plane perpendicular to the CO_2 price axis at 10 EUR/tCO_2 (see solid green line at Fig. 8.11). The resulting curve shows the CO_2 emissions in the electricity generation sector at different residual demand levels, given a fixed CO_2 price–10 EUR/tCO_2 in this case (see right top panel of Fig. 8.11). According to this ETS-price assumption, about 50 MtCO_2 is displaced towards the electricity generation sector when residual demand increases from 800 TWh/year to 900 TWh/year.

Second, consider the ETS-cap assumption, i.e., the CO_2 cap stays fixed at 222 MtCO_2 for the electricity generation sector (see point C on Fig. 8.11). This assumption corresponds to a section of the emission plane perpendicular to the emission axis at 222 MtCO_2 (see dash-dotted blue line at Fig. 8.11). The

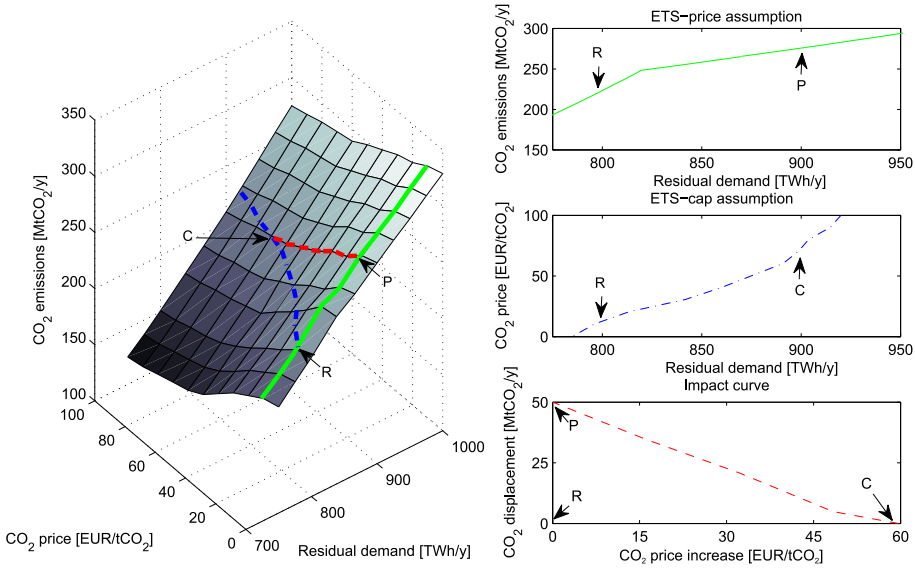

Figure 8.11: The impact of removing renewable injections on the CO_2 price and the CO_2 emissions in the CWE electricity generation sector. The emission plane on the left panel is identical to Fig. 8.3. Point R refers to the reference point, P to the ETS-price assumption and C to the ETS-cap assumption.

resulting curve shows the CO_2 price needed to keep the emissions constant at different demand levels (see right middle panel of Fig. 8.11), i.e., the level of fuel switching can be increased to still respect the CO_2 cap. According to this ETS-cap assumption, a residual demand increase from 800 TWh/year to 900 TWh/year results in a 60 EUR/tCO_2 upsurge in the CO_2 price.

Finally, the impact curve can be drawn as the trajectory on the emission plane between the ETS-price assumption and the ETS-cap assumption. When assuming that the CO_2 price has no impact on triggering RES deployment (i.e., only considering fuel switching as a consequence of the CO_2 price), the intersection is made with a plane perpendicular to the residual demand axis (see dashed red dotted line at Fig. 8.11). The resulting curve is the impact curve, showing all possible combinations of CO_2 price declines and CO_2 displacements (see right bottom panel of Fig. 8.11). In Appendix C, the methodology is demonstrated when investments in RES triggered by a CO_2 price are accounted for.

Every point on the impact curve presents a possible equilibrium point (combination of a CO_2 price change and shift of emissions). The combination of

the impact curve with the marginal abatement cost curve (MACC) of the other ETS sectors results in the actual CO_2 price increase and CO_2 displacement due to removing renewable injections (in this case). These other ETS sectors in this case refer to all sectors subject to the overall ETS cap, outside of the modeled electricity generation sector.[8] The top left panel of Fig. 8.12 shows illustrative marginal abatement cost curves of the other ETS sectors. The point R corresponds to the reference situation (with RES, CO_2 emission price of 10 EUR/tCO_2). When removing RES, the CO_2 price will increase and CO_2 emissions in the other ETS sectors will decrease (abatement will increase). Accordingly, the relevant part of the marginal abatement cost curve is the part right of the reference point R. If this part of the marginal abatement cost curve is drawn together with the renewables impact curve (see top right panel of Fig. 8.12), the actual CO_2 price increase and CO_2 displacement due to removing renewables can be derived by the intersection with the impact curve (see point R'): removing renewable injections results in a CO_2 price increase with A EUR/tCO_2 and displaces B MtCO_2/year emissions from the other ETS sectors to the electricity generation sector. The point R' represents the new equilibrium situation in the EU ETS after removing renewable injections. This implies that for a CO_2 price increase of A, the other ETS sectors have to abate B million ton CO_2 more on a yearly basis.

If additional abatement in the other ETS sectors is elastic in the relevant range of abatement, the MACC of the other ETS sectors is steeper and the intersection with the renewables impact curve moves towards the ETS-price extreme, i.e., the intersection will be closer to the vertical axis (see MACC (2) at bottom left panel of Fig. 8.12)). If additional abatement in the other ETS sectors is inelastic in the relevant range of abatement, the MACC of the other ETS sectors is flatter and the intersection with the renewables impact curve moves towards the ETS-cap extreme, i.e., the intersection will be closer to the horizontal axis (see MACC (3) at bottom left panel of Fig. 8.12)).

Historical impact curve for CWE: electricity generation sector

In the CWE 2012 power system, the annual electricity demand was 1,236 TWh. This demand was partially met with generation from cogeneration units[9] (180

[8]The electricity generation sector in this section refers to the part of the overall electricity generation sector covered in the model (CWE region). In the EU ETS, both the rest of the European electricity generation sector and the other ETS sectors (energy intensive industries, aviation) are covered. When combining the impact curve of the CWE electricity generation sector, with a marginal abatement cost curve of the "other" sectors, this "other" covers both the non-CWE part of the European electricity generation sector (i.e., the part not modeled) and the other ETS sectors.

[9]Excluding bio-fuel-fired cogeneration units.

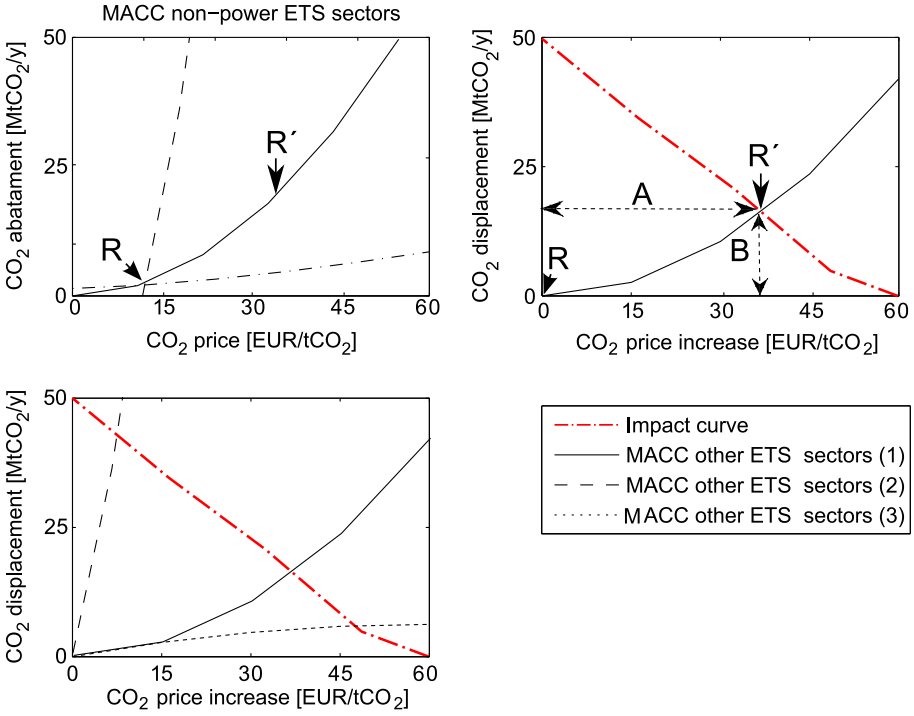

Figure 8.12: The intersection of the MACC of the other ETS sectors (sectors next to modeled CWE electricity generation sector under ETS cap) and the impact curve indicates the new equilibrium due to removing renewable injections.

TWh), conventional hydro units (45 TWh), bio-energy units (43 TWh), wind energy (69 TWh) and solar energy (33 TWh). The resulting 2012 residual demand was thus 866 TWh. About 145 TWh of the renewables generation (i.e., wind, solar and bio) are mainly driven by support schemes. The 2012 CO_2 emission price varied between 5 EUR/tCO_2 and 10 EUR/tCO_2. At these levels of residual demand and CO_2 price, annual aggregated emissions in the modeled electricity generation were about 260 MtCO_2.

Looking back and making the assumption that all generation from wind, solar and bio-energy can be assigned to RES support policies, an ex-post estimation can be made on what the CO_2 price would have been in absence of RES support policies. Without generation from wind, solar and bio, the residual demand would have been about 1,000 TWh. Analogously to the analysis in the previous subsection, the ETS-cap assumption gives a maximum CO_2 price change of more than 100 EUR/tCO_2 and the ETS-price assumption gives a maximum

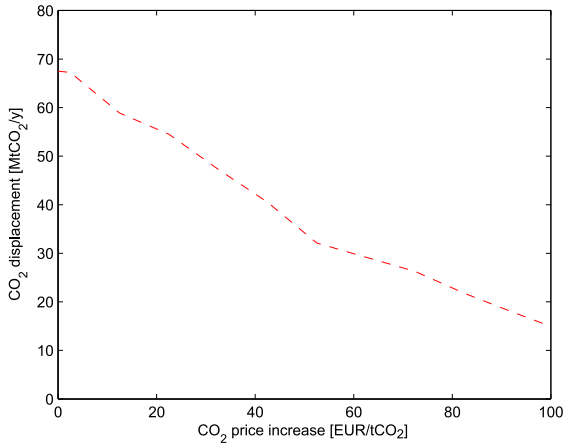

Figure 8.13: Ex-post impact curve of the 2012 CWE electric power system for renewable generation from wind, solar and bio.

emission displacement away from the electricity generation sector of 68 $MtCO_2$ (26% of 2012 historical CWE emissions). The resulting impact curve is given by Fig. 8.13.

Quantitative results, however, should be interpreted with care, taking into account the limitations of the analysis. The model used for this study is a pure operational model of the electricity generation sector, considering fuel switching as the only abatement option (triggered by a CO_2 price) in the electricity generation sector. This implies that the conventional power plant portfolio is assumed to be fixed, regardless of the amount of renewables in the system. Besides, one might expect that at high CO_2 prices (i.e., in absence of renewables), investments in low-carbon technologies (such as renewables or carbon capture and storage) would mature, limiting the CO_2 price increase (see Appendix C for an example with RES investments triggered by a high CO_2 price). Hence, parts of the impact curve that are far from today's equilibrium merely serve as trend indications, rather than as exact numbers.

Another limitation of the approach refers to banking of allowances. According to the ETS-cap assumption, it is assumed that the historical amount of emissions equals the emission cap set by the EU. However, as emission allowances can be banked, the real emission cap might be higher than the emission cap imposed in the model, which is set equal to historical emissions. Hence, accounting for this banking effect would limit the CO_2 price effect due to renewables. Another issue worth mentioning concerning banking is the "link-in-time". The analysis

presented in this chapter is static, based on one snap shot and neglecting system dynamics over the course of various years. However, banking links different years. Therefore, the expectations of CO_2 emitters on future developments of for instance renewable deployment, is already accounted for in today's CO_2 prices (e.g., if emitters expect more renewables in the system in the future, leading to lower CO_2 prices in the future, less allowances will be banked today).

These limitations need to be considered, when applying the methodology to real-life cases. To some extent this explains the differences with existing work indicating a rather limited impact of RES on ETS prices. For example, Rickels et al. (2015) do not find strong evidence for the impact of renewables on EUA prices (except for Norwegian hydro). Koch et al. (2014) identify the growth of wind and solar electricity generation as an important determinant of the ETS price (ex-ante, simulation based), though find a moderate impact when empirically determined ex-post. Alternatively, these studies (that find moderate/low impact of RES on ETS price) might also point to the ETS-price assumption in our work being closer to reality, i.e., RES having an impact on emissions shifts between sectors, rather than on the CO_2 price.

8.7 Summary and conclusions

This chapter presents a methodology that deepens the insight in the relation between a CO_2 price and CO_2 emission reductions in the electricity generation sector. The methodology is based on the insight that CO_2 emissions in the electricity generation sector are driven by the composition of the conventional power portfolio, the residual load (i.e., electricity demand minus renewables generation) and the generation costs of the conventional units. According to the presented methodology, a marginal abatement cost curve (MACC) of the electricity generation sector can be composed in three steps. First, the relation between a CO_2 price and each of the CO_2 emission drivers has to be determined. Second, the relation between the CO_2 emission drivers and the CO_2 emissions in the electricity generation sector has to be determined, resulting in a so-called emission plane. Third, the previous steps can be combined to determine the relationship between a CO_2 price and CO_2 emissions in the electricity generation sector.

The main goal of the methodology is to give additional insight in the CO_2 price-emission relationship, rather than deriving marginal abatement cost curves (MACCs). MACCs are facing the issue of robustness (i.e., sensitive to changes in external parameters) and granularity (i.e., not revealing the driving abatement technology at a certain CO_2 price). The presented methodology addresses both

issues by showing the effect of changing external parameters and identifying the driving abatement technologies behind the aggregated MACC. The methodology also quantifies the interaction between different CO_2 abatement options. All this makes the methodology appropriate for policy makers, who can use the methodology to gain understanding of the impact of a CO_2 price on the electricity generation sector and evaluate the robustness of this impact.

The absolute emission plane is then used to reflect upon interaction effects between a direct CO_2 policy, such as a cap-and-trade system, and other policies, such as RES support. Under a cap-and-trade system that covers multiple sectors, as for example the European emission trading system, CO_2 price changes and CO_2 emission shifts might be caused by other policies. The impact curve is derived from the absolute emission plane, quantifying the change in CO_2 price and CO_2 emissions due to RES deployment. The interaction between RES support policies and the ETS is quantified for the 2012 Central Western European power system (i.e., Belgium, France, Germany, Luxembourg and the Netherlands), according to the approach presented in this chapter. The analysis shows that if no RES support would have been in place, the CO_2 price and/or CO_2 emissions in the electricity generation sector would have been likely significantly higher.

Based on the methodology and the case study discussed in this chapter, three important policy implications can be formulated. First, policy makers should design their CO_2 emission policy in accordance with the robustness of the CO_2 abatement caused by an emission price. The developed methodology provides insight (both qualitative and quantitative) in the CO_2 emission drivers in the electricity generation sector, and in how these can be influenced by a CO_2 price. Clearly, these drivers are also influenced by external factors or other policies. As such, a MACC (abatement potential at certain cost) is dependent on boundary conditions and should always be positioned as such. This can also impact the choice or preference between either a price or a quantity based instrument directly targeting CO_2.

Second, CO_2 abatement options are gradually deployed in a range of CO_2 prices. The case study shows that in the CWE electricity generation sector, investments in wind energy are only triggered as of a CO_2 price of about 35 EUR/tCO_2 (at 2012 prices and cost parameters). At lower CO_2 prices, only fuel switching occurs. However, fuel switching is still occurring at CO_2 prices above 35 EUR/tCO_2.

Third, the analysis shows the very large influence of the residual electricity demand on CO_2 emissions from the electricity generation sector (and hence, on CO_2 emission shifts and/or CO_2 price). The residual demand can be affected directly by other policies (e.g., RES support or push for electric transport), but

can clearly also be affected by external factors (such as the economic recession). As future changes or even shocks in residual demand might obviously occur (in both directions), this conflicts with having a stable (and sufficiently high) CO_2 price. The market stability reserve aims to address this issue, by aiming for a target range of surplus of allowances in the market (as a proxy of tightness of the cap).

Chapter 9

Summary, conclusions and suggestions for further research

This final chapter summarizes the main contributions and findings of this dissertation, and gives suggestions for further research.

9.1 Summary and conclusions

Unit commitment modeling with network constraints

A state-of-the art unit commitment model has been developed and is presented in chapter 2. This model, i.e., LUSYM (Leuven University System Model), is a large-scale, deterministic, security-constrained unit commitment model, formulated as a mixed-integer linear program (MIP). The model includes power plant constraints, renewables curtailment, load curtailment, storage units, transmission grid constraints and spinning reserve constraints. The LUSYM model is able to solve real-life electricity systems (e.g., several hundreds of power plants and several thousands of time steps) in the time frame of several hours. The run time of the LUSYM model is limited by a tight and compact formulation of the problem, an efficient implementation in GAMS and Matlab, and the use of best-in-class MIP solvers like Cplex or Gurobi.

Conclusion. Benchmarking simulations presented in chapter 2 show that the LUSYM model is competitive or outperforms commercial unit commitment packages in terms of optimality of simulation results and/or run times. A comparison of the LUSYM simulation results for the 2013 European electricity system show that LUSYM is able to reproduce historically observed generation data with acceptable accuracy.

Different network models are implemented in LUSYM; a trade-based grid model and a DC power flow model. Often simplified zonal DC power flow models are used in unit commitment modeling. In a zonal network model, different nodes are grouped into one equivalent node, as such reducing the size of the network model. In order to simplify nodal network models to zonal network models, an estimation has to be made on the contribution of each node to the zonal generation balance. This contribution is expressed in injection shift keys.
Conclusion. Chapter 3 proposes an improved method to determine zonal network models, based on different injection shift keys per category of injections (e.g., injections from generation and injections/off-takes from load). Test simulations for a case study of the Central European electricity network indicate that the improved zonal network model is able to better approach the flows and zonal generation balances, with only a modest increase in computational cost.

Deployment of intermittent renewables

Chapter 4 studies the impact of the variable character of renewables generation on cycling of conventional power plants. Cycling of conventional power plants, i.e., changing the power output and/or the on/off-state, is constrained by technical limits and entails costs. A broad range of technical and cost-related cycling parameters can be found in the literature.
Conclusion. This dissertation shows that, for a case study of the German electricity system, the conventional generation portfolio is flexible enough to deal with the variable character of wind and solar photovoltaics, even when stringent cycling parameters and large renewables shares are imposed to the generation portfolio. The analysis also shows the importance of correctly taking cycling costs into account in the unit commitment decision. Considering all cycling costs, including long-term cycling costs such as increased operations and maintenance costs, in the short-term unit commitment decision can reduce system costs considerably.

Chapter 5 studies the impact of remotely deployed renewables, such as offshore wind, on redispatching due to grid congestion.
Conclusion. The analysis shows that, for the considered case study of the Belgian electricity system, redispatching costs can increase rapidly with

increasing renewable capacity when the grid is not capable of facilitating the renewable grid injections. However, redispatch costs can be limited by relaxing the preventive N-1 security criterion to a corrective N-1 security criterion. Moreover, it is shown that loop flows, i.e., power flows through a market zone caused by injections and off-takes outside of that market zone, can either improve or worsen redispatch costs, depending on the direction of the loop flows. This is in particular important for a relative small market zone, such as Belgium, which can be subject to relatively large loop flows.

Integration of electricity markets

Chapter 6 studies the coordination of reserves among market zones. The procedure for operational reserve planning can be split in three steps: the sizing of the reserve need, the day-ahead allocation of reserves and the real-time activation of reserves. Each of these three steps can be coordinated among different market zones.
Conclusion. Coordination can lead to cost reductions due to the spatial smoothing of imbalances caused by, for instance, renewables forecast errors and by spatial arbitrage during the allocation and activation of reserves. However, coordination is constrained by the available cross-border transmission capacity. A case study of Central Western Europe indicates cost reductions when the reserve procedure is coordinated among different market zones, but transmission constraints should be taken into account when sizing and allocating reserves. Otherwise, suboptimal market outcomes might be obtained.

Chapter 7 discusses flow-based market coupling. Flow-based market coupling is since May 2015 the methodology used in Central Western Europe to calculate the cross-border transmission capacity that can be made available to the day-ahead electricity market.
Conclusion. Flow-based market coupling is expected to increase day-ahead market welfare, as more transmission capacity can be made available to the day-ahead market. The flow-based methodology, which is based on a zonal DC power flow representation of the transmission grid, is rather complex and opaque. Chapter 7 presents a clear description of the concepts and definitions of the flow-based market coupling, serving as a starting point for further research.

Reducing greenhouse gas emissions

Since 2005, electricity generators in Europe operate under the European emission trading system (EU ETS). This implies that fossil-fuel-power plant operators face a cost of emitting CO_2. Chapter 8 studies the impact of a CO_2 price on

the CO_2 emissions in the electricity sector.
Conclusion. Based on the insight that CO_2 emissions in the electricity sector are driven by the composition of the conventional generation portfolio, the residual load and the marginal generation costs of conventional plants, a so-called absolute emission plane can be constructed. The absolute emission plane gives a graphical representation of the relationship between the CO_2 emission drivers and the CO_2 emissions in the electricity sector. Based on this absolute emission plane, marginal abatement cost curves of the electricity sector can be derived.

The European emission trading system, which sets a cap to the CO_2 emissions of electricity generators and heavy industry in Europe (and domestic aviation), interacts with other indirect emission policies such as the deployment of renewables in the electricity system. CO_2-free generation from renewables decreases the CO_2 emission price, as they lower the demand for emission allowances, and shifts CO_2 emissions from the electricity sector to other sectors under the EU ETS cap (the aggregated emissions within the EU ETS are set fixed by the cap).
Conclusion. Chapter 8 quantifies this interaction between the EU ETS and renewables deployment by means of impact curves. Impact curves give the range of possible CO_2 price changes and CO_2 emission displacement between ETS sectors, caused by renewables deployment. A case study of the 2012 Central Western European electricity system shows that the impact of renewables deployment on the CO_2 price and/or CO_2 emissions in the electricity sector is considerable.

9.2 Suggestions for further research

Unit commitment modeling with network constraints

The computational tractability is still limiting the size and level of detail of electricity systems that can be considered with unit commitment models. As such, improving this computational tractability remains a first important field of future work. In short, computational tractability can be improved in three different ways: (1) improving the tightness and compactness of the unit commitment formulation, (2) improving the implementation of the unit commitment formulation in, for instance, GAMS and (3) improving the performance of MIP solvers.

Second, correctly representing the intermittent character of renewables in unit commitment models becomes increasingly important. In the LUSYM

model, the variability of renewables is represented by historical time series, the limited dispatchability is represented by the possibility to curtail renewable generation and the partially unpredictability can be represented by deterministic reserve constraints. Stochastic unit commitment models better represent the unpredictable character of intermittent renewables, as they consider the full probability distribution of renewables' unpredictability. However, stochastic unit commitment models are computationally more demanding to solve. Incorporating the unpredictable character of renewables in large-scale unit commitment models is therefore a challenging but important field of future work. So-called hybrid unit commitment models which combine deterministic and stochastic elements are promising in this regard (Bruninx et al., 2016).

Third, short-term flexibility options in the electricity system–such as flexible load, flexible transmission elements and storage units–are gaining importance in electricity systems with high share of intermittent renewables. Implementing these flexibility options in unit commitment models, while taking account of their technical limits and corresponding costs, is an interesting field of future work.

Deployment of intermittent renewables

Chapter 4 and chapter 5 discuss the impact of intermittent renewables on cycling of conventional power plants and on redispatching to avoid line congestion, respectively. In these chapters, focus is mainly on quantifying these effects of intermittent renewables on the electricity generation system. Future work should focus on options to limit these effects, and as such prepare the electricity generation system to accommodate larger shares of intermittent renewables. Flexible load, storage units and flexible grid elements are three possible flexibility options, which are currently only to a limited extent available in electricity systems, to facilitate intermittent renewables and reduce the effects discussed in chapter 4 and chapter 5. Future work should deal with the technical characteristics of the various flexibility options in the electricity system, but also focus on their costs and benefits.

Integration of electricity markets

Chapter 6 illustrates the benefits of coordinating reserves among market zones, but also shows that cross-border transmission constraints should be correctly account for in cross-border reserve markets. Future work should focus on heuristically-based rules to take into account network constraints in the sizing and allocation of reserves. Examples of heuristically-based rules could be to

reserve ex-ante part of the transmission capacity for use in the real-time market or to coordinate only part of the allocation and/or sizing decisions.

Chapter 7 presents the flow-based market coupling, which is being used since May 2015. Future work should focus on the empirical evaluation of flow-based market coupling, based on actual market outcomes since May 2015. Flow-based market coupling is expected to increase day-ahead market welfare, but this should be empirically verified. Furthermore, flow-based market coupling in the day-ahead market impacts the remaining cross-border capacity for intra-day and real-time markets. A comprehensive evaluation of the flow-based market coupling should hence consider all aspects of the electricity market.

Reducing greenhouse gas emissions

This dissertation has focused on CO_2 emissions as the main greenhouse gas emitted in the electricity sector. The methodology presented in chapter 8 can be used to evaluate changes in the EU ETS design and their impact on the electricity generation sector, such as the back-loading measure and the market stability reserve (European Commission, 2016b). Moreover, the modeling approach can be applied to other emission trading systems, such as the Chinese pilot projects (Chang and Wang, 2010).

In today's EU ETS, with a large surplus of emission allowances and a low but non-zero CO_2 emission price, banking of emission allowances plays an important role in the price setting. Linking a banking model with the modeling approach presented in chapter 8 would allow to study the impact of banking on CO_2 abatement in the electricity sector.

Appendix A

Benchmarking case studies

A.1 Benchmarking with existing unit commitment models

A 2030 scenario of the Central Western European electricity system is considered for the benchmarking of LUSYM with other unit commitment models (ENTSO-E, 2014). The geographical scope covers Belgium (BE), France (FR), Germany (GE), Luxembourg (LU) and the Netherlands (NL). A full year is considered with an hourly time step. This appendix gives an overview of the system input data.

	BE	FR	DE	LU	NL
Nuclear plants	-	34.9	-	-	-
Lignite-fired plants	-	-	11.8	-	-
Coal-fired plants	-	1.5	21.1	-	-
CCGT	10.1	7.7	29.3	0.3	12.6
OCGT	0.6	3.1	1.6	-	0.4
TJ	-	3.2	1.1	-	-

Table A.1: Aggregated installed conventional generation capacity per country and per generation technology (in GW) (ENTSO-E, 2014).

	efficiency [%]	MUT/MDT [h]	MC [EUR/MWh]
Nuclear plants	33	168	11
Lignite-fired plants	40	24	115
Coal-fired plants	35-46	6	112-139
CCGT	40-58	3	95-132
OCGT	35-42	1	126-149
TJ	35-40	1	115-129

Table A.2: Power plant characteristics per generation technology. Efficiencies are allocated based on the commissioning or retrofitting year of the power plant (more recently committed units have higher efficiencies). The following fuel prices are assumed: 1.4 EUR/MWh_{th} for nuclear, 1.6 EUR/MWh_{th} for lignite, 8.0 EUR/MWh_{th} for coal, 28.5 EUR/MWh_{th} for natural gas, 47.5 EUR/MWh_{th} for oil, and a CO_2 emission price of 93 EUR/tCO_2. Start-up costs are plant-specific and range from 2 to 90 kEUR/start-up (ENTSO-E, 2012a, 2014).

	BE	FR	DE	LU	NL
Installed capacity [GW]	1.3	6.3	10.9	1.3	-
Energy capacity [GWh]	5.6	1000	86.8	5.0	-
Efficiency [%]	75	75	75	75	-

Table A.3: Overview of pump storage units per country (ENTSO-E, 2014).

	BE	FR	DE	LU	NL
Peak load [GW]	11.3	60.1	88.7	0.9	15.6
Annual consumption [TWh]	81.2	422.5	489.7	6.2	105.1

Table A.4: Overview of load per country (ENTSO-E, 2014).

	BE	FR	DE	LU	NL
Wind	21.5	92.4	181.4	0.2	31.0
Solar PV	6.4	37.7	79.8	0.1	8.7
Conv. hydro	0.4	41.9	19.2	0.2	0.8
Biofuels	10.5	40.2	64.5	0.3	3.6
Non-RES CHP	17.6	7.4	14.8	0.8	27.7

Table A.5: Overview of annual generation from renewables and cogeneration per country and per generation source (in TWh). Conventional hydro refers to run-of-river units and water dams (ENTSO-E, 2014).

from/to	BE	FR	DE	LU	NL
BE	-	3.8	2.4	1.4	2.4
FR	5.3	-	5.1	-	-
DE	2.4	5.1	-	2.3	6.4
LU	1.4	-	2.3	-	-
NL	2.4	-	6.4	-	-

Table A.6: Overview transmission capacity between countries (in GW) (ENTSO-E, 2014).

A.2 Benchmarking with historical generation data

The 2013 European electricity system is considered for the benchmarking of LUSYM with historical generation data. The geographical scope covers the full ENTSO-E area, consisting of 32 countries: Austria (AT), Belgium (BE), Bosnia-Herzegovina (BA), Bulgaria (BG), Croatia (HR), Czech Republic (CZ), Denmark (DK), Estonia (EE), Finland (FI), France (FR), Germany (DE), Greece (GR), Hungary (HU), Ireland (IE), Italy (IT), Latvia (LV), Lithuania (LT), Luxembourg (LU), Macedonia (MK), Montenegro (ME), Netherlands (NL), Norway (NO), Poland (PL), Portugal (PT), Romania (RO), Serbia (RS), Slovakia (SK), Slovenia (SI), Spain (ES), Sweden (SW), Switzerland (CH) and the United Kingdom (UK). A full year is considered with an hourly time step. This appendix gives an overview of the system input data.

A trade-based representation of the electricity grid is used in the model. The grid model consists of 32 nodes (i.e., each country is one node) and 56 lines. The NTC-values for the summer of 2010 are taken from ENTSO-E (ENTSO-E, 2015a). It is assumed that Denmark East and Denmark West are perfectly connected.

	Capacity
Nuclear plants	129.4
Lignite-fired plants	64.4
Coal-fired plants	110.4
CCGT	165.1
OCGT	27.2
TJ	56

Table A.7: Aggregated installed generation capacity per generation technology (in GW) (Platts, 2014).

	efficiency [%]	MUT/MDT [h]	SU [MWh_{th}/MW]	VOM [EUR/MWh]
Nuclear plants	33	24	3.9	9.0
Lignite-fired plants	35-46	24	13.9	3.3
Coal-fired plants	35-46	6	13.9	3.3
CCGT	48-58	3	7.8	1.6
OCGT	35-42	1	1.9	1.6
TJ	35-40	1	7.8	3.3

Table A.8: Power plant characteristics per generation technology. Rated efficiencies are allocated based on the commissioning or retrofitting year of the power plant (the more recently committed, the higher the efficiency). Historical fuel prices and CO_2 emission price are used. SU: start-up energy consumption; VOM: variable operations and maintenance costs (ENTSO-E, 2012a). Daily changing and location-dependent fuel prices are used, the average fuel prices are 1.7 EUR/MWh_{th} for nuclear, 4.0 EUR/MWh_{th} for lignite, 7.5 EUR/MWh_{th} for coal, 26.8-30.2 EUR/MWh_{th} for natural gas, 50.4 EUR/MWh_{th} for heavy fuel oil, 63.0 EUR/MWh_{th} for light fuel oil and a CO_2 emission price of 4.5 EUR/tCO_2 (KU Leuven, 2015).

	Capacity [GW]	Energy [GWh]		Capacity [GW]	Energy [GWh]
AT	2.7	622.5	LT	0.9	10.8
BE	1.4	5.8	LU	1.3	4.9
BA	0.4	2.6	MK	-	-
BG	1.4	11.1	ME	-	-
HR	0.3	2.3	NL	-	-
CZ	. 1.1	5.7	NO	1.0	6.1
DK	-	-	PL	1.7	7.4
EE	-	-	PT	1.2	24.4
FI	-	-	RO	-	-
FR	5.6	83.5	RS	0.6	3.7
DE	6.5	38.0	SK	1.0	5.3
GR	0.7	5.1	SI	0.2	0.5
HU	-	-	ES	5.1	95.5
IE	0.3	1.8	SE	0.4	74.5
IT	6.7	52.9	CH	1.6	288.3
LV	-	-	UK	3.0	17.9

Table A.9: Overview of pump storage units per country. A round-trip efficiency of 75% is assumed for all pump storage units (Platts, 2014; Geth et al., 2015).

	Consumption [TWh]	Peak load [GW]		Consumption [TWh]	Peak load [GW]
AT	69.5	11.4	LT	10.6	1.8
BE	85.6	13.3	LU	5.9	1.0
BA	12.4	2.1	MK	8.1	1.5
BG	36.0	6.7	ME	4.6	0.8
HR	17.1	2.8	NL	114.0	18.4
CZ	62.8	10.1	NO	128.1	24.2
DK	33.6	6.1	PL	152.2	25.8
EE	7.9	1.4	PT	49.1	8.3
FI	81.4	14.0	RO	50.6	8.3
FR	492.4	92.1	RS	39.7	6.9
DE	526.8	96.0	SK	27.8	4.1
GR	53.2	9.2	SI	12.8	2.0
HU	39.0	5.8	ES	246.4	39.6
IE	25.8	4.5	SE	137.5	26.6
IT	316.0	54.0	CH	64.8	11.0
LV	7.3	1.4	UK	336.1	60.8

Table A.10: Overview of load per country. Aggregated annual consumption is 3,243 TWh, with a peak load of 520 GW. The load time series give the total consumption of electric energy, i.e., including consumption of electric energy generated by distributed sources. Load time series are corrected for import/export with countries outside of the model (ENTSO-E, 2015a).

	Wind	Solar PV	Conv. hydro	Biofuels	Non-RES CHP
AT	2,843	510	37,464	1,553	8,019
BE	3,057	2,437	358	3,142	17,493
BA	-	-	6,972	-	601
BG	1,260	1,220	3,834	-	3,901
HR	494	-	7,934	121	1,469
CZ	474	1,966	2,815	-	12,440
DK	11,128	456	14	1,832	10,503
EE	500	-	25	545	812
FI	774	-	12,672	11,347	8,924
FR	15,883	4,544	70,171	6,210	22,026
DE	47,186	29,694	18,833	37,405	90,630
GR	3,392	3,355	6,631	210	11,825
HU	694	-	207	737	9,645
IE	4,642	-	552	113	8,179
IT	14,852	22,014	51,050	5,287	80,181
LV	120	-	2,893	479	1,215
LT	600	-	513	338	3,006
LU	80	68	61	122	607
MK	-	-	1,553	-	333
ME	-	-	2,741	-	-
NL	5,574	543	-	6,741	21,207
NO	1,888	-	127,989	-	1,274
PL	5,689	-	2,327	6,471	18,620
PT	11,685	441	13,484	2,700	9,067
RO	4,597	410	14,752	316	8,715
RS	-	-	10,293	-	-
SK	-	587	4,672	732	4,976
SI	-	176	4,479	-	1,002
ES	54,467	12,765	36,087	6,320	65,561
SE	9,891	33	60,817	10,335	9,526
CH	108	613	37,973	915	2,885
UK	18,625	2,757	2,821	-	86,680

Table A.11: Overview of annual generation from renewables and cogeneration per country and per generation source (in GWh). Conventional hydro refers to run-of-river units and water dams, non-RES CHP includes to fossil-fuel fired cogeneration with an electric output smaller than 100 MW (larger units are included in the conventional generation portfolio) (KU Leuven, 2015; ENTSO-E, 2015a; EWEA, 2015; EPIA, 2015).

Appendix B

Network models

The following notation rules are used in this appendix: parameters in bold and uppercase are matrices, parameters in bold and lowercase are vectors, and underlined parameters are complex numbers.

B.1 AC power flow

The purpose of an AC power flow is to calculate all line flows and nodal voltages, given a certain set of parameters which are known upfront (Elgerd, 1971). The unknown parameters are referred to as state variables, the known parameters as system variables.

The system variables are:

- Admittance matrix $\mathbf{Y}$ of the electricity grid, calculated as:

$$\mathbf{Y} = \mathbf{A}^T \cdot \mathbf{Y}_d \cdot \mathbf{A} \tag{B.1}$$

  with $\mathbf{A}$ the incidence matrix, describing the topology of the network[1], and $\mathbf{Y}_d$ the primitive admittance matrix, i.e., a diagonal matrix with line admittances. The line admittance $\underline{Y}_l$, in [S], can be written as:

$$\underline{Y}_l = G_l + jB_l = \frac{1}{\underline{Z}_l} = \frac{R_l}{{R_l}^2 + {X_l}^2} - j\frac{X_l}{{R_l}^2 + {X_l}^2} \tag{B.2}$$

[1]The incidence matrix is a L×N-matrix with $a_{l,n} = 1$ if line l starts at node n, $a_{l,n} = -1$ if line l ends at node n and $a_{l,n} = 0$ otherwise.

with G_l the line conductance in [S], B_l the line susceptance in [S], $\underline{Z}_l$ the line impedance in [Ω], R_l the line resistance in [Ω] and X_l the line reactance in [Ω].[2] If more than one transmission line between the same two nodes exists, the admittance of these transmission lines can be simply added to an equivalent admittance. Grid elements like transformers can be incorporated by their equivalent impedance.

- Active power injection P_n in [W] and reactive power injection Q_n in [VAr] at PQ-nodes, i.e., load nodes with known power off-takes.
- Nodal voltage magnitude $|V_n|$ in [V] and active power injection P_n in [W] at PV-nodes, i.e., generation nodes with known voltage and active power injection.
- Nodal voltage magnitude $|V_n|$ in [V] and voltage angle δ_n in [rad] at the reference node. The voltage angle at the reference node is set to zero, the active power injection is free, representing power losses in the grid, and the voltage magnitude is set to 1 p.u. There is only one reference node in the network.

Each node is characterized by four parameters: active power injection P_n, reactive power injection Q_n, voltage magnitude $|V_n|$ and voltage angle δ_n. Once these parameters are known, the flows through each line can be calculated. The state variables are:

- Voltage magnitude $|V_n|$ and voltage angle δ_n for each PQ-node.
- Reactive power injection Q_n and voltage angle δ_n for each PV-node.
- Active power injection P_n and reactive power injection Q_n at the reference node.

Often, the system and state variables are describes in per-unit values, relative to a base value. As such, electricity grids with different voltage levels can be analyzed. Note that the sign convention can be chosen by the user. In this dissertation, positive nodal power values refer to power injections in the grid, negative nodal power values refer to power off-takes from the grid.

The static power flow equations are derived as follows. Total power injection $\underline{S}_n$, in [VA], at node n is given by:

$$\underline{S}_n = P_n + j\,Q_n \tag{B.3}$$

[2] A line shorter than 500 km can be represented with acceptable accuracy by lumped parameters, instead of distributed parameters. For a line shorter than 100 km, the line representation can be further simplified to a series RL-branch by neglecting shunt capacitances and shunt susceptances.

The total power injection at node n can also be written as:

$$\underline{S}_n = \underline{V}_n \cdot \underline{I}_n^* \quad \text{with} \quad \underline{I}_n^* = \sum_q \underline{Y}_{nq}^* \cdot \underline{V}_q^* \tag{B.4}$$

with $\underline{Y}_{nq}$ the admittance of the line between nodes n and q, $\underline{I}_n$ the injected current at node n in [A] and $\underline{V}_n$ the voltage at node n in [V]. Eq. (B.4) results in

$$\underline{S}_n = |V_n|(\cos\delta_n + j\sin\delta_n)\sum_q (G_{nq} - jB_{nq})|V_q|(\cos\delta_q - j\sin\delta_q) \tag{B.5}$$

Combining Eqs. (B.3) and (B.5) results in

$$P_n = |V_n|\sum_q \left(G_{nq}\cos(\delta_n - \delta_q) + B_{nq}\sin(\delta_n - \delta_q)\right)|V_q| \tag{B.6}$$

$$Q_n = |V_n|\sum_q \left(G_{nq}\sin(\delta_n - \delta_q) - B_{nq}\cos(\delta_n - \delta_q)\right)|V_q| \tag{B.7}$$

These non-linear equations (Eqs. (B.6)-(B.7)) are referred to as the static power flow equations (SLFE) for an AC power flow.

In an electricity system with N nodes, 4N variables exist (P_n, Q_n, δ_n and $|V_n|$ for each node) and 2N power flow equations can be written down (see Eqs. (B.6)-(B.7)). Consequently, 2N variables have to be known upfront to solve the AC power flow.

The system of 2N non-linear static power flow equations for an electricity network with N nodes is solved iteratively. In a first step, the initial voltage at each node is often set to 1 p.u. with zero voltage angle (or a solution of a previously solved case is used). In a second step, the active and reactive power injection at each node is calculated with the estimated node voltages by Eqs. (B.6)-(B.7). Following from the difference in active and reactive power between two consecutive iteration steps, a new estimation of the voltage magnitudes and voltage angles can be made with the Gauss-Siedel method or the Newton-Raphson method. This iterative process continues until the difference in active and reactive power between two consecutive iterations steps is smaller than the optimality criterion.

The AC power flow as described in this section simulates the grid operation. If the purpose is to optimize the grid operation (e.g., minimize grid losses), one speaks of an optimal power flow analysis.

B.2 DC power flow

The DC power flow is a linearization of the AC power flow. As such, the DC power flow is computationally less complex than the AC power flow, at the expense of decreased accuracy (Purchala, 2005). The DC power flow is based on three assumptions:

1. Line resistances are negligible compared to line reactances ($R_l \ll X_l$). This implies that grid losses can be neglected and line parameters simplify to, see Eq. (B.2):

$$G_l = \frac{R_l}{{R_l}^2 + {X_l}^2} \approx 0 \qquad \forall l \tag{B.8}$$

$$B_l = \frac{-X_l}{{R_l}^2 + {X_l}^2} \approx -\frac{1}{X_l} \qquad \forall l \tag{B.9}$$

$$\underline{Y}_l = \frac{1}{\underline{Z}_l} \approx j\, B_l \approx \frac{1}{j\, X_l} \qquad \forall l \tag{B.10}$$

2. The voltage profile is flat, meaning that the voltage amplitude in per unit values is the same for all nodes:

$$|V_n| \approx 1\,\text{p.u.} \qquad \forall n \tag{B.11}$$

3. Voltage angle differences between neighboring nodes are small. This assumption results in a linearization of the sine and cosine terms in the AC power flow equations, see Eqs. (B.6)-(B.7):

$$\sin(\delta_n - \delta_q) \approx \delta_n - \delta_q \qquad \forall n \tag{B.12}$$

$$\cos(\delta_n - \delta_q) \approx 1 \qquad \forall n \tag{B.13}$$

The static AC power flow equation for active power injections (Eq. (B.6)) simplifies to the DC power flow equation for nodal active power balances (in scalar and matrix format, respectively):

$$P_n = \sum_q B_l\,(\delta_n - \delta_q) \tag{B.14}$$

$$\mathbf{p}_n = \left(\mathbf{A}^T\,\mathbf{B}_d\,\mathbf{A}\right)\,\boldsymbol{\delta}_n \tag{B.15}$$

with B_l the susceptance of the line between nodes n and q, $\mathbf{B}_d$ the primitive susceptance matrix, i.e., a diagonal matrix with line susceptances, and $\mathbf{A}$ the incidence matrix.

The active power flow through a lossless transmission line is given by:

$$F_l = -\frac{|V_n||V_q|}{X_l} \sin(\delta_n - \delta_q) \approx B_l \left(\delta_n - \delta_q\right) \tag{B.16}$$

$$\mathbf{f}_l = \left(\mathbf{B}_d \, \mathbf{A}\right) \, \boldsymbol{\delta}_n \tag{B.17}$$

Substituting the nodal voltage angles $\boldsymbol{\delta}_n$ from equations (B.15) and (B.17) gives the DC power flow equations.

$$\mathbf{f}_l = \left(\left(\mathbf{B}_d \, \mathbf{A}\right) \left(\mathbf{A}^T \, \mathbf{B}_d \, \mathbf{A}\right)^{-1} \right) \, \mathbf{p}_n \tag{B.18}$$

with

$$\mathbf{ISF}^{\mathrm{L}\times\mathrm{N}} = \left(\mathbf{B}_d \, \mathbf{A}\right) \left(\mathbf{A}^T \, \mathbf{B}_d \, \mathbf{A}\right)^{-1} \tag{B.19}$$

The DC power flow equations for nodal power balances (Eq. (B.15)) are linearly dependent. As a result, $(\mathbf{A}^T \, \mathbf{B}_d \, \mathbf{A})$ is a singular matrix and cannot be inverted. To overcome this issue, (at least) one node has to be designated as reference node and removed from the DC power flow equations. In $(\mathbf{B}_d \, \mathbf{A})$ the column corresponding to the reference node has to be removed while in $(\mathbf{A}^T \, \mathbf{B}_d \, \mathbf{A})$ both the column and row corresponding to the reference node have to be removed. The original dimensions of the matrices can be restored by inserting a zero column or row corresponding to the reference node. With respect to voltage angles, only the difference in voltage angles between two neighboring nodes matters. Therefore the voltage angle of the reference node is set to zero. Finally, one additional relationship has to be added to the DC power flow to make sure that one unique solution is found. This relationship expresses that the sum of all nodal power injections equals zero:

$$\sum_n P_n = 0 \tag{B.20}$$

The injection shift factors (ISF) describe the linear relationship between power injections in the grid and active power flows through the transmission lines. An element $ISF_{l,n}$ gives the power flow through transmission line l caused by the injection of a unit active power at node n and withdrawal of this active power at the reference node. The line flow at line l caused by an injection at node n with withdrawal at node q can then be written as a linear combination of the ISFs:

$$PTDF_{l,nq} = ISF_{l,n} - ISF_{l,q} \tag{B.21}$$

The power transfer distribution factor (PTDF) gives the sensitivity of the active power flow through line l with respect to an additional power injection at node

n with withdrawal at node q.

During the ISF calculation, at least one node has to be removed from the DC power flow equations to make the set of equations linearly independent (i.e., the reference node). Mathematically, the number of reference nodes can be determined as the difference between the number of nodes in the grid and the number of linearly independent columns in the incidence matrix of the grid. In a connected grid with only AC lines, one reference node is required to calculate the ISF matrix. In a connected grid with both AC and DC lines, it might happen that a sub-grid of AC lines exists which is only connected to the rest of the grid via a DC line. In this case, one reference node for each sub-grid is required. If the DC line is part of a meshed grid (instead of connecting two AC grids), one reference node for the whole grid is sufficient to calculate the ISF matrix. In a disconnected grid, at least two completely separated sub-grids exist and a reference node for each sub-grid is required to calculate the ISF matrix. Moreover, in this latter case, Eq. (B.20) has to be imposed to each sub-grid separately.

The DC power flow is a linearization of the non-linear AC power flow. It is both empirically and theoretically shown in the literature that the DC power flow equations are insensitive to the operating point (Baldick, 2003; Baldick et al., 2005). So in practice, one can use the same DC power flow equations for all possible operating points of the grid, as long as the grid topology remains the same.

The calculation of the DC power flow equations will be illustrated for a simple example (the same simple electricity network is used in chapter 3, see Fig. B.1).

For this simple network, the nodal power balances are, see Eq. (B.15):

$$\begin{bmatrix} P_1 \\ P_2 \\ P_3 \\ P_4 \end{bmatrix} = \begin{bmatrix} B_A + B_D & -B_D & -B_A & 0 \\ -B_D & B_C + B_D & 0 & -B_C \\ -B_A & 0 & B_A + B_B & -B_C \\ 0 & -B_C & -B_B & B_B + B_C \end{bmatrix} \begin{bmatrix} \delta_1 \\ \delta_2 \\ \delta_3 \\ \delta_4 \end{bmatrix} \tag{B.22}$$

The line flows are, see Eq. (B.17):

$$\begin{bmatrix} F_A \\ F_B \\ F_C \\ F_D \end{bmatrix} = \begin{bmatrix} B_A & 0 & -B_A & 0 \\ 0 & 0 & B_B & -B_B \\ 0 & -B_C & 0 & B_C \\ -B_D & B_D & 0 & 0 \end{bmatrix} \cdot \begin{bmatrix} \delta_1 \\ \delta_2 \\ \delta_3 \\ \delta_4 \end{bmatrix} \tag{B.23}$$

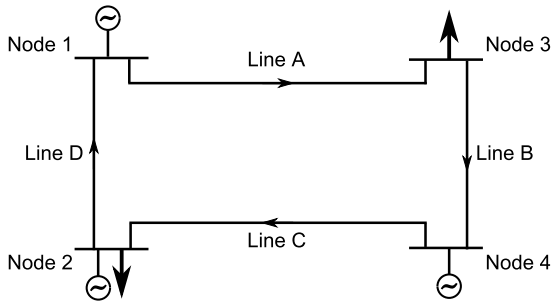

Figure B.1: Simple electricity network to illustrate the DC power flow.

Taking node 1 as reference node, Eqs. (B.22)-(B.23) reduce to respectively:

$$\begin{bmatrix} P_2 \\ P_3 \\ P_4 \end{bmatrix} = \begin{bmatrix} B_C + B_D & 0 & -B_C \\ 0 & B_A + B_B & -B_C \\ -B_C & -B_B & B_B + B_C \end{bmatrix} \begin{bmatrix} \delta_2 \\ \delta_3 \\ \delta_4 \end{bmatrix} \tag{B.24}$$

$$\begin{bmatrix} F_A \\ F_B \\ F_C \\ F_D \end{bmatrix} = \begin{bmatrix} 0 & -B_A & 0 \\ 0 & B_B & -B_B \\ -B_C & 0 & B_C \\ B_D & 0 & 0 \end{bmatrix} \cdot \begin{bmatrix} \delta_2 \\ \delta_3 \\ \delta_4 \end{bmatrix} \tag{B.25}$$

The ISF matrix follows then from:

$$\mathbf{ISF} = \begin{bmatrix} 0 & -B_A & 0 \\ 0 & B_B & -B_B \\ -B_C & 0 & B_C \\ B_D & 0 & 0 \end{bmatrix} \begin{bmatrix} B_C + B_D & 0 & -B_C \\ 0 & B_A + B_B & -B_C \\ -B_C & -B_B & B_B + B_C \end{bmatrix}^{-1} \tag{B.26}$$

Assuming the same susceptance for all lines, the ISF matrix becomes:

$$\mathbf{ISF} = \begin{bmatrix} 0 & -0.25 & -0.75 & -0.5 \\ 0 & -0.25 & 0.25 & -0.5 \\ 0 & -0.25 & 0.25 & 0.5 \\ 0 & 0.75 & 0.25 & 0.5 \end{bmatrix} \tag{B.27}$$

A zero column is added to the ISF matrix corresponding to the reference node. The ISF matrix shows, for example, that for an injection of 1 p.u. active power at node 2 (and off-take of this power at the reference node), -0.25 p.u. is flowing through lines A, B and C, and 0.75 p.u. is flowing through line D.

B.3 DC power flow with power flow controlling devices

Power flow controlling devices allow to control the active power flow through transmission lines. Two categories of power flow controlling devices can be distinguished: flexible AC transmission systems (FACTS such as phase shifting transformers) and high voltage DC lines (HVDC). This appendix gives an overview of power flow controlling devices and their representation in the DC power flow, based on Van Hertem (2009) and Verboomen (2008).

Recall that the power flow through a lossless transmission line l (between nodes n and q) is given by

$$F_l = -\frac{|V_n||V_q|}{X_l} \sin(\delta_n - \delta_n) \tag{B.28}$$

From equation B.28, it becomes clear that the power flow through a line can be controlled by changing the line impedance X_l or the voltage angle difference $(\delta_n - \delta_q)$. The voltage magnitudes $|V_n|$ and $|V_q|$ can not be used to control active power flows as they need to stay close to their predefined value to ensure safe grid operation. Altering the line impedance can be achieved by means of a mechanically switched series capacitor, a thyristor controlled series compensator, a static synchronous series compensator or fixed series compensation. These devices can be modeled as a variable line impedance. Altering the voltage angle difference between two nodes can be achieved by means of a phase shifting transformer (PST). A PST creates a voltage angle shift by inserting a voltage in quadrature to the phase voltage. All devices mentioned in this paragraph are examples of FACTS.

As part of a meshed grid, high voltage direct current (HVDC) lines can also be considered as power flow devices. The power flow through a HVDC line can be fully controlled by the AC-DC/DC-AC converters at its ends. If a HVDC is used for a point-to-point connection (e.g., connecting offshore wind turbines with the onshore grid or interconnection between two asynchronous power systems), then the HVDC link is not a true power flow controlling device. Only if embedded in a meshed grid, a HVDC link can be used as power flow controlling device.

In the remainder of this section, phase shifting transformers and HVDC lines are discussed in detail. The focus is on how these grid elements can be modeled in a DC power flow.

B.3.1 Phase shifting transformers

Resume the DC power flow equations for nodal power balances (Eq. (B.15)) and line flows (Eq. (B.17)). A phase shifting transformer (PST) at line l changes the voltage angle between the two adjacent nodes n and q with α_l. The DC power flow equation for nodal active power balances, for one node and in matrix form for all nodes respectively, become:

$$P_n = \sum_q B_l \left(\delta_n - \delta_q + \alpha_l\right) \tag{B.29}$$

$$\mathbf{p}_n = \left(\mathbf{A}^T \mathbf{B}_d \mathbf{A}\right) \boldsymbol{\delta}_n + \left(\mathbf{B}_d \mathbf{A}\right)^T \boldsymbol{\alpha}_l \tag{B.30}$$

The DC power flow equations for line flows, for one line and in matrix form for all lines respectively, become:

$$F_l = B_l \left(\delta_n - \delta_q + \alpha_l\right) \tag{B.31}$$

$$\mathbf{f}_l = \left(\mathbf{B}_d \mathbf{A}\right) \boldsymbol{\delta}_n + \mathbf{B}_d \boldsymbol{\alpha}_l \tag{B.32}$$

Substituting the nodal voltage angles δ_n from Eqs. (B.30) and (B.32) gives:

$$\mathbf{f}_l = \left(\left(\mathbf{B}_d \mathbf{A}\right)\left(\mathbf{A}^T \mathbf{B}_d \mathbf{A}\right)^{-1}\right) \mathbf{p}_n + \left(\mathbf{B}_d - \left(\mathbf{B}_d \mathbf{A}\right)\left(\mathbf{A}^T \mathbf{B}_d \mathbf{A}\right)^{-1}\left(\mathbf{B}_d \mathbf{A}\right)^T\right) \boldsymbol{\alpha}_l \tag{B.33}$$

with the ISF matrix the same as in the basic DC power flow:

$$\mathbf{ISF}^{\mathrm{L}\times\mathrm{N}} = \left(\mathbf{B}_d \mathbf{A}\right)\left(\mathbf{A}^T \mathbf{B}_d \mathbf{A}\right)^{-1} \tag{B.34}$$

and with phase shifter distribution factors (PSDF) given by:

$$\mathbf{PSDF}^{\mathrm{L}\times\mathrm{L}'} = \mathbf{B}_d - \left(\mathbf{B}_d \mathbf{A}\right)\left(\mathbf{A}^T \mathbf{B}_d \mathbf{A}\right)^{-1}\left(\mathbf{B}_d \mathbf{A}\right)^T \tag{B.35}$$

An element $PSDF_{l,l'}$ gives the impact of a change of one radian in the PST angle at line l' on the flow through transmission line l. Note that in the equations above, it is assumed that a positive PST angle increases the power flow in the positive direction through the line where the PST is located. The reverse assumption is possible as well, depending on the sign convention. Eqs. (B.30) and (B.32) assume a PST on each line. In reality, only a few lines in a grid are equipped with a PST. In that case, only the columns in the PSDF matrix corresponding to lines with a PST are useful and the other columns can be removed. In order to calculate the PSDF matrix, a reference node has to be chosen. However, unlike the ISF matrix, the PSDF matrix looks exactly the

same for every possible reference node.

The range of possible phase shifter angles is limited. Phase shifting transformers are typically operated in the range ±30° (±25° in Belgium).

$$\boldsymbol{\alpha}_l^{min} \leq \boldsymbol{\alpha}_l \leq \boldsymbol{\alpha}_l^{max} \tag{B.36}$$

To illustrate the implementation of PSTs in DC power flow, the PSDF matrix is derived for the simple example of Fig. B.1. The DC power flow equations for nodal power balances are, see Eq. (B.30):

$$\begin{bmatrix} P_1 \\ P_2 \\ P_3 \\ P_4 \end{bmatrix} = \begin{bmatrix} B_A + B_D & -B_D & -B_A & 0 \\ -B_D & B_C + B_D & 0 & -B_C \\ -B_A & 0 & B_A + B_B & -B_C \\ 0 & -B_C & -B_B & B_B + B_C \end{bmatrix} \begin{bmatrix} \delta_1 \\ \delta_2 \\ \delta_3 \\ \delta_4 \end{bmatrix} + \begin{bmatrix} B_A & 0 & 0 & -B_D \\ 0 & 0 & -B_C & B_D \\ -B_A & B_B & 0 & 0 \\ 0 & -B_B & B_C & 0 \end{bmatrix} \cdot \begin{bmatrix} \alpha_A \\ \alpha_B \\ \alpha_C \\ \alpha_D \end{bmatrix} \tag{B.37}$$

The DC power flow equations for line flows are, see Eq. (B.32): :

$$\begin{bmatrix} F_A \\ F_B \\ F_C \\ F_D \end{bmatrix} = \begin{bmatrix} B_A & 0 & -B_A & 0 \\ 0 & 0 & B_B & -B_B \\ 0 & -B_C & 0 & B_C \\ -B_D & B_D & 0 & 0 \end{bmatrix} \cdot \begin{bmatrix} \delta_1 \\ \delta_2 \\ \delta_3 \\ \delta_4 \end{bmatrix} + \begin{bmatrix} B_A & 0 & 0 & 0 \\ 0 & B_B & 0 & 0 \\ 0 & 0 & B_C & 0 \\ 0 & 0 & 0 & B_D \end{bmatrix} \begin{bmatrix} \alpha_A \\ \alpha_B \\ \alpha_C \\ \alpha_D \end{bmatrix} \tag{B.38}$$

Take node 1 as reference node again, which implies that P_1 and δ_1 are removed from Eqs. (B.37)-(B.38). The ISF matrix is the same as in the example without PSTs, see Eq. (B.27). The PSDF matrix is given by Eq. (B.35). Assuming the same line susceptance for all lines (i.e., -0.5 p.u.), the PSDF matrix becomes:

$$\mathbf{PSDF} = \begin{bmatrix} 0.5 & 0.5 & 0.5 & 0.5 \\ 0.5 & 0.5 & 0.5 & 0.5 \\ 0.5 & 0.5 & 0.5 & 0.5 \\ 0.5 & 0.5 & 0.5 & 0.5 \end{bmatrix} \tag{B.39}$$

The PSDF matrix shows that an increase of one radian in phase shifter angle at any line increases the power flow through all lines with 0.5 p.u. The PSDF is the same for every line given the symmetry in the considered network. PSDFs can be converted to [MW/°] by multiplying the original PSDFs, in [p.u./rad], with the power base (in MW) divided by 57.3.[3]

The DC power flow representation of PSTs causes an extra inaccuracy. Overall, the error introduced by a the DC power flow of a PST model is small. This error increases with higher phase shift angles, up to about 5% at maximum phase shift angles. This accuracy adds up to the 5% accuracy of the basic DC power flow, ending up with a 5-10% accuracy of DC power flow with PSTs (Van Hertem et al., 2006).

B.3.2 High voltage direct current lines

The power flow through a high voltage direct current (HVDC) line is fully controllable. Hence, a HVDC link can be modeled as a combination of a controllable positive and negative power injection at the receiving and sending end of the link. The flow through the HVDC link affects the flows in the AC lines and therefore an additional term has to be added to the DC power flow equations of the AC lines.

Retake the DC power flow equations for the AC grid, see Eqs. (B.18)-(B.19). The subscript AC is added to emphasize that we are dealing with AC lines.

$$\mathbf{f}_l^{\mathrm{AC}} = \mathbf{ISF}\, \mathbf{p}_n^{\mathrm{AC}} \tag{B.40}$$

So far, all nodal injections were injected in the AC grid. With HVDC lines in the grid, some of the injected power will flow through the HVDC grid and some through the AC grid.

$$\mathbf{p}_n^{\mathrm{AC}} = \mathbf{p}_n - \mathbf{p}_n^{\mathrm{DC}} \tag{B.41}$$

The flow through each HVDC line can be fully controlled. The relationship between the active power flow through the HVDC lines F_l^{DC} and the nodal injections P_n^{DC} is given by:

$$\mathbf{p}_n^{\mathrm{DC}} = \left(\mathbf{A}^{\mathrm{DC}}\right)^T \mathbf{f}_l^{\mathrm{DC}} \tag{B.42}$$

[3]One radian equals 57.3°.

with $\mathbf{A}^{\mathrm{DC}}$ the incidence matrix of the HVDC network. Combining Eqs. (B.40)-(B.42) gives the DC power flow equations for a network AC and HVDC lines.

$$\mathbf{f}_l^{\mathrm{AC}} = \mathbf{ISF}\,\mathbf{p}_n + \mathbf{DCDF}\,\mathbf{f}_l^{\mathrm{DC}} \tag{B.43}$$

with the direct current distribution factors (DCDF):

$$\mathbf{DCDF} = -\mathbf{ISF}\left(\mathbf{A}^{\mathrm{DC}}\right)^T \tag{B.44}$$

An element $DCDF_{l^{AC},l^{DC}}$ gives the impact of the controllable power flow in the HVDC line l^{DC} on the power flow in the AC line l^{AC}.

To illustrate the implementation of HVDC lines in DC power flow, the DCDF matrix is derived for the simple example of Fig. B.1. Assume that line B is a HVDC link (lines A, C and D are AC lines). The incidence matrices for the AC network and DC network become:

$$\mathbf{A}^{\mathrm{AC}} = \begin{bmatrix} 1 & 0 & -1 & 0 \\ 0 & -1 & 0 & 1 \\ -1 & 1 & 0 & 0 \end{bmatrix} \text{ and } \mathbf{A}^{\mathrm{DC}} = \begin{bmatrix} 0 & 0 & 1 & -1 \end{bmatrix} \tag{B.45}$$

The ISF matrix of the AC network follows from Eq. (B.19), with node 1 as reference node:

$$\mathbf{ISF} = \begin{bmatrix} 0 & 0 & -1 & 0 \\ 0 & 0 & 0 & 1 \\ 0 & 1 & 0 & 1 \end{bmatrix} \tag{B.46}$$

The DCDF matrix for the considered example follows from Eq. (B.44):

$$\mathbf{DCDF} = \begin{bmatrix} 1 \\ 1 \\ 1 \end{bmatrix} \tag{B.47}$$

The resulting DC power flow equations, in a network without PSTs, are:

$$\begin{bmatrix} F_A \\ F_C \\ F_D \end{bmatrix} = \begin{bmatrix} 0 & 0 & -1 & 0 \\ 0 & 0 & 0 & 1 \\ 0 & 1 & 0 & 1 \end{bmatrix} \begin{bmatrix} P_1 \\ P_2 \\ P_3 \\ P_4 \end{bmatrix} + \begin{bmatrix} 1 \\ 1 \\ 1 \end{bmatrix} F_B \tag{B.48}$$

F_B is the flow through the HVDC line and thus controllable.

B.4 DC power flow with N-1 security

The N-1 security criterion is defined by the CEER (2004) as the rule that the electric power networks shall withstand the unplanned outage of an element in the system and stay in operation without jeopardizing the operational integrity of the system. The unplanned outage of one element may refer to the failure of a transmission line, transformer, generating unit or a busbar. Often the term *contingency* is used to denote the unplanned outage of one element in the system. The system status before this contingency is referred to as the pre-contingency state (i.e., N-state), whereas the post-contingency refers to the system state after the contingency (i.e., N-1-state).

Grid models that determine a N-1 secure operation of the grid are referred to as security-constrained optimal power flow models (SCOPF). A SCOPF is an optimal power flow (OPF) problem which takes into account constraints arising from the operation of the system under a set of postulated contingencies (Capitanescu et al., 2011). Note the difference between security-constrained unit commitment (SCUC) and security-constrained optimal power flow (SCOPF). SCUC models determine the optimal generation scheduling taking account of the grid constraints in the N-state (mostly without considering contingencies). Generally speaking, the focus of SCUC models is on the generation units in the electricity system. SCOPF models determine the optimal system scheduling taking account of contingencies, with particular focus on the grid elements in the electricity system.

The N-1 security criterion has a preventive approach and a corrective approach. The preventive approach does not allow corrective actions after a contingency occurred, other than those that take place automatically (e.g., active power frequency control). The corrective approach does consider the possibility of corrective actions after a contingency occurred. Possible corrective actions are changing the power plant dispatch or setting point of power flow controlling devices. Note that N-1 security does only make sense in a nodal grid model in which each relevant transmission line and transformer is represented.

The N-1 security criterion can be compactly formulated as follows (Monticelli et al., 1987):

$$\min f(\mathbf{x}, \mathbf{u}_0) \tag{B.49}$$

$$g_0(\mathbf{x}, \mathbf{u}_0) = 0 \tag{B.50}$$

$$h_0(\mathbf{x}, \mathbf{u}_0) \leq 0 \tag{B.51}$$

$$g_k(\mathbf{x}, \mathbf{u}_c) = 0 \qquad \forall c \tag{B.52}$$

$$h_k(\mathbf{x}, \mathbf{u}_c) \leq 0 \qquad \forall c \tag{B.53}$$

with f a cost function, $\mathbf{x}$ the system variables that are the same in pre- and post-contingency state (i.e., the control variables) and u_c the system variables that can be changed following contingency c (i.e., the state variables). The index 0 refers to the pre-contingency state, index c refers to the state after contingency c occurred. Eq. (B.49) gives the objective function, i.e., minimization of the operational system cost in the pre-contingency state. Eqs. (B.50)-(B.51) represent the constraints in the pre-contingency state (e.g., technical power plant limits in case of a unit commitment model). Eqs. (B.52)-(B.53) represent the same set of constraints in the different post-contingency states.

Determining the optimal N-1 secure operation of a power system can be computationally challenging. Two important parameters that influence the solution time of the optimization model are the number of post-contingency actions and the number of considered contingencies. The number of possible post-contingency actions depends on the approach taken. The preventive approach does not allow post-contingency actions, whereas the corrective approach allows a change in the economic dispatch and the setting of flexible grid elements. The number of possible contingencies increases with the size of the electricity grid. In a grid with L lines, L+1 system states should be considered (i.e., one pre-contingency state and L post-contingency states). For a grid of realistic size, the number of possible contingencies might become large. Different ways exist to deal with the large number of possible contingencies;

- Full optimization. The optimal N-1 secure operation of the power system is determined if all possible contingencies are taken into account in the optimization. However, this approach can not always be used for a large-scale electricity grid as the optimization model will become computational intractable (especially when using AC power flows).

- Iterative approach. The optimal N-1 secure operation can be determined by adding iteratively contingencies to the optimization model. In a first iteration, the model determines the optimal system operation in the N state. The line outages for which this solution is not N-1 secure are added to the optimization model, after which a new optimization takes place. This iterative process continues until a N-1 secure solution is found. The disadvantage of this approach is that the optimality of the found solution is not guaranteed.

- Umbrella approach. In the umbrella approach, the critical contingencies are determined ex-ante and taken into account in the optimization. The set of critical line outages is defined as the set of minimum size that is required to describe the feasible solutions of the optimization Ardakani and Bouffard (2013).

- TSO expertise. The transmission system operator (TSO) might be able to define the critical contingencies ex-ante based on its knowledge of the power system. Taking these critical contingencies into account in the optimization should lead to a N-1 secure operation of the power system.

Appendix C

CO_2 emissions in the electricity sector

C.1 Fuel switching

In this appendix, some fundamental principles related to fuel switching are addressed. Fuel switching is a short-term CO_2 abatement option in the electricity generation sector.

It is instructive to think about CO_2 emissions and CO_2 abatement in the electricity generation sector from the perspective of the merit order. The merit order is a ranking of all available power plants in ascending order of marginal generation cost (see Fig. C.1). The intersection of the merit order with the electricity demand divides the power plant portfolio in operating power plants, i.e., the ones at the left of the intersection, and non-operating power plants, i.e., the ones at the right of the intersection.[1]

In this regard, three drivers for CO_2 emissions in the electricity generation sector can be identified, being the composition of the power plant portfolio, the ranking of the power plants in the merit order, and the (residual) demand. A short-term perspective is considered here, so the portfolio of conventional power plants and the level of electricity demand are assumed being fixed. The CO_2 price is assumed to have an impact through fuel switching only.

[1] This is only correct by approximation. Dynamic power plant constraints, such as minimum power output limitations, can force dynamic but more expensive power plants online while less expensive power plants are not operating at full capacity.

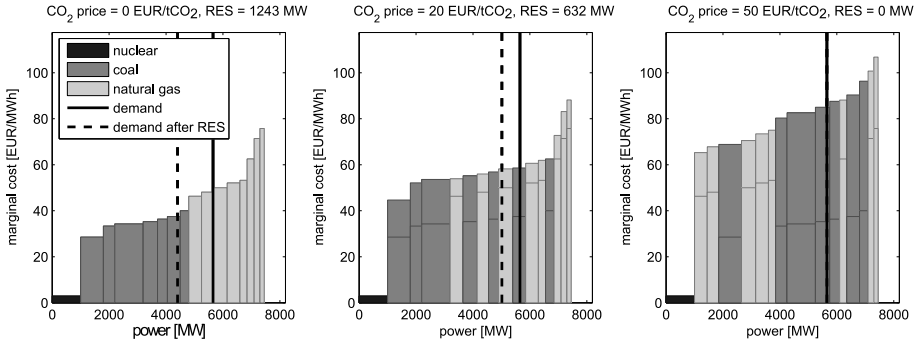

Figure C.1: Illustrative merit order, with original and residual demand intersection, for different combinations of CO_2 price and RES injection. The CO_2 emissions in each of the combinations are the same, i.e., 3.22 $ktCO_2/h$.

Three conditions must be fulfilled to cause abatement from fuel switching: (1) the original power plant portfolio must consist of CO_2 emitting plants, with high emitting plants ranked before lower emitting plants; (2) the CO_2 price must increase the marginal generation cost of the high-emitting plants above the marginal generation cost of the low-emitting plants and (3) the change in generation costs must result in a change in the optimal dispatch, switching off high-emitting power plants and switching on low emitting power plants.

In the merit order, power plants are ranked according to marginal cost MC_i expressed in [EUR/MWh]:

$$MC_i = \frac{FC_i}{\eta_i} + \frac{EF_i\, CC}{\eta_i} \tag{C.1}$$

which is a function of the fuel cost FC_i in [EUR/MWh_{th}], the efficiency η_i in [MWh/MWh_{th}], the emission factor of the power plant fuel EF_i in [tCO_2 /MWh_{th}] and the CO_2 price CC in [EUR/tCO_2]. The CO_2 emission EM_i in [tCO_2/h] of a certain power plant is determined as:

$$EM_i = \frac{EC_i}{\eta_i}\, gen_i \tag{C.2}$$

with gen_i the (instantaneous) electricity generation in [MW] of power plant i.

When introducing a certain amount of renewable generation (RES in [MWh/h]) into a system, this comes in at zero marginal cost. Hence, it can be included as negative demand. In a system consisting of coal and gas-fired power plants, the emission reduction triggered by RES (AB^{RES} in [tCO_2/h]) can be written as

the sum of the emissions of the coal and gas-fired power plants pushed out of the merit order by RES:

$$AB^{RES} = \sum_{i \in I^{c1}} \frac{EC_i}{\eta_i} gen_i + \sum_{i \in I^{g1}} \frac{EC_i}{\eta_i} gen_i \tag{C.3}$$

$$\sum_{i \in I^{c1}} gen_i + \sum_{i \in I^{g1}} gen_i = RES \tag{C.4}$$

with I^{c1} the set of coal-fired power plants pushed out of operation because of renewable generation RES, and I^{g1} the set of gas-fired power plants pushed out of operation because of renewable generation RES.

When a CO_2 price CC is in place, the CO_2 reduction triggered by fuel switching (AB^{FSW} in [tCO_2/h]) is equal to the emissions of the coal-fired power plants pushed out of operation, minus the emissions of the gas-fired power plants now brought online (compared to a reference stacking order without CO_2 price):

$$AB^{FSW} = \sum_{i \in I^{c2}} \frac{EC_i}{\eta_i} gen_i - \sum_{i \in I^{g2}} \frac{EC_i}{\eta_i} gen_i \tag{C.5}$$

$$\sum_{i \in I^{c2}} gen_i = \sum_{i \in I^{g2}} gen_i \tag{C.6}$$

with I^{c2} the set of coal-fired power plants pushed out of operation because of the CO_2 price CC (compared to reference case without CC), and I^{g2} the set of gas-fired power plants brought online because of the CO_2 price CC (compared to reference case without AC).

With these equations, it is possible to perform a first analysis, qualitatively illustrating how the residual demand can affect CO_2 emissions and/or CO_2 price.

First, the case is considered where the overall amount of CO_2 emissions in the electricity generation sector is held constant, under different combinations of residual demand (through RES) and CO_2 price. This can basically be obtained by keeping the sum of AB^{RES} and AB^{FSW} constant, from Eqs. (C.3)-(C.5) respectively. Fig. C.1 presents an example for a methodological power system, consisting mainly of coal and gas-fired power plants. The original (inelastic) demand is represented by a solid line, while the residual demand (i.e., demand minus RES) is depicted by the dashed line. Several merit orders are presented, for increasing levels of CO_2 price and decreasing levels of RES, such that the CO_2 emissions in all cases is the same, and equal to 3.22 ktCO_2/h. For this methodological example, the relation between the amount of RES and the

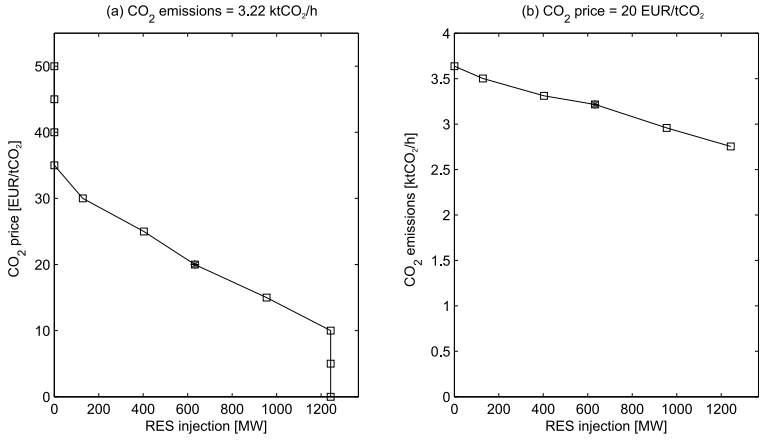

Figure C.2: (a) CO_2 price and RES injection couples, resulting in a same level of CO_2 emissions for the methodological power system as presented in Figure 1; (b) CO_2 emission level and RES injection couples, resulting in a same level of CO_2 price. The point common to both panel (a) and (b) is presented with a filled square (RES = 632 MW, CO_2 price = 20 EUR/tCO_2, CO_2 emissions = 3.22 ktCO_2/h).

required CO_2 price to obtain a same level of CO_2 emissions is presented in the LHS panel of Fig. C.2. One clearly sees that at some stages of RES injection (in this example notably a zero injection or an injection of 1,243 MW) several levels of CO_2 price exist. This illustrates that an increase in CO_2 price not necessarily triggers abatement by fuel switching (i.e., if the merit order is not affected, or if it is only changed in one or both sides from the residual demand independently, not making changes in which power plants are activated). The relatively high CO_2 prices required to trigger abatement levels similar to RES injection clearly can be observed.

Second, the case is considered where the CO_2 price is kept constant, and the impact of residual demand (RES) on CO_2 emissions is analyzed (determining AB^{RES}). The merit order in this case remains fixed (consider, e.g., the middle panel of Fig. C.1). When the amount of RES is now increased, an increasing amount of coal and gas-fired plants is pushed offline. As such, it has a direct impact on emissions. The relation between RES and CO_2 emissions under a fixed CO_2 price (in this case 20 EUR/tCO_2) is presented in the RHS panel of Fig. C.2. One can also read this figure as the CO_2 cap required under different levels of RES, to reach a constant CO_2 price.

C.2 Electric vehicles in the electricity sector

To demonstrate the general applicability of the methodology as developed and demonstrated in chapter 8 (section 8.6), the interaction between the EU ETS and the deployment of electric vehicles, i.e., another indirect CO_2 emission policy, is discussed in this appendix. This example is fully analogous to a reduction in renewable injections (see section 8.6).

Starting from the initial situation with a CO_2 price of 10 EUR/tCO_2, 800 TWh/year residual demand and 222 MtCO_2/year of emissions (see point R on Fig. C.3), 100 TWh/year of additional residual demand is introduced in the system due to electric vehicles (i.e., the residual demand increases from 800 to 900 TWh). This will lead to an increase in CO_2 price and a displacement of CO_2 emissions from the other ETS sectors towards the electricity generation sector.

First, the maximal CO_2 displacement towards the electricity generation sector is determined based on the ETS-price assumption (see point P on Fig. C.3).

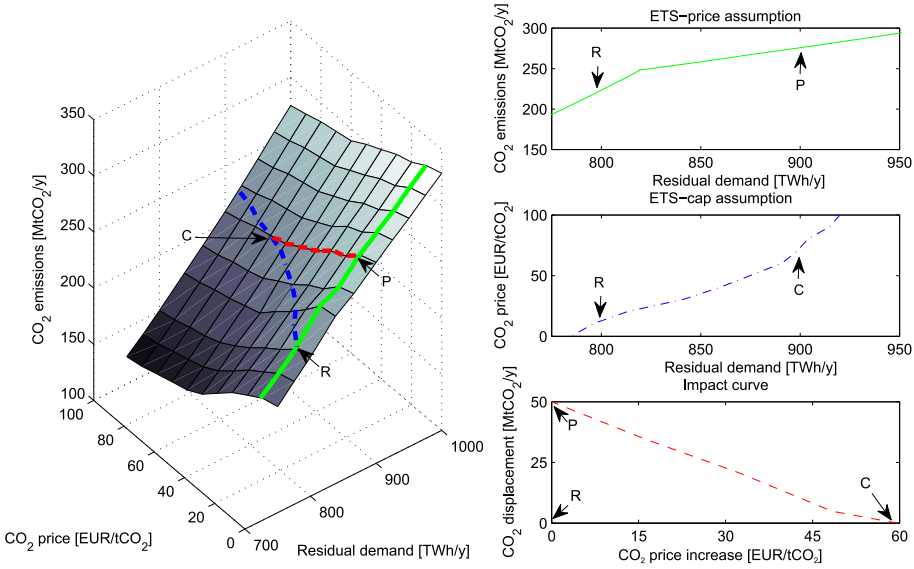

Figure C.3: The impact of deploying electric vehicles on the CO_2 price and the CO_2 emissions in the CWE electricity generation sector. Point R refers to the reference point, P to the ETS-price assumption and C to the ETS-cap assumption.

Consider the intersection of the emission plane perpendicular to the CO_2 price axis at 10 EUR/tCO_2 and its resulting curve (see solid green line at Fig. C.3). It becomes clear that an increase of residual demand from 800 to 900 TWh/year at constant CO_2 price results in an increase in CO_2 emissions in the electricity generation sector by about 50 MtCO_2/year.

Second, the maximal CO_2 price increase follows from the ETS-cap assumption (see point C on Fig. C.3). Consider the intersection of the emission plane perpendicular to the emission axis at 222 MtCO_2/year (see dash-dotted blue line at Fig. C.3). The resulting curve indicates that, with constant CO_2 emissions in the electricity generation sector, an increase in residual demand from 800 to 900 TWh/year leads to a CO_2 price increase of 60 EUR/tCO_2.

Finally, the impact curve is again the trajectory on the emission plane between the ETS-price assumption and the ETS-cap assumption, at the new residual demand level of 900 TWh/year, assuming no impact of the CO_2 price on the residual load (see dashed red line at Fig. C.3). The actual CO_2 price increase and displacement of CO_2 emissions from the other ETS sectors towards the electricity generation sector can be derived from the impact curve and the marginal abatement cost curve of the other ETS sectors, analogously to Fig. 8.12.

C.3 Renewables investments triggered by a CO_2 price

The methodology presented in chapter 8 (see section 8.6) is expanded in this appendix, now accounting for investments in RES triggered by a sufficiently high CO_2 price. It is possible to apply the developed methodology to derive the impact curve, when the relation between the deployment of RES (affecting the residual demand) and the CO_2 price is known. The relationship between a CO_2 price and investments in wind and solar PV is obtained by a separate model, considering one period with annual average residual load and the merit order of the conventional generation capacity, that gradually installs wind and solar PV capacity up to a level where the annual average electricity price (determined by the intersection of the residual load and the merit order) equals the levelized cost of electricity (LCOE) of wind and solar PV. A 25% capacity factor for wind is assumed, and a 12% for solar PV. Given the different lead times of renewable capacity investments (months to year) and fossil-fuel capacity investments (several years), the fossil-fuel generation capacity is assumed to remain the same for different levels of renewable investments.

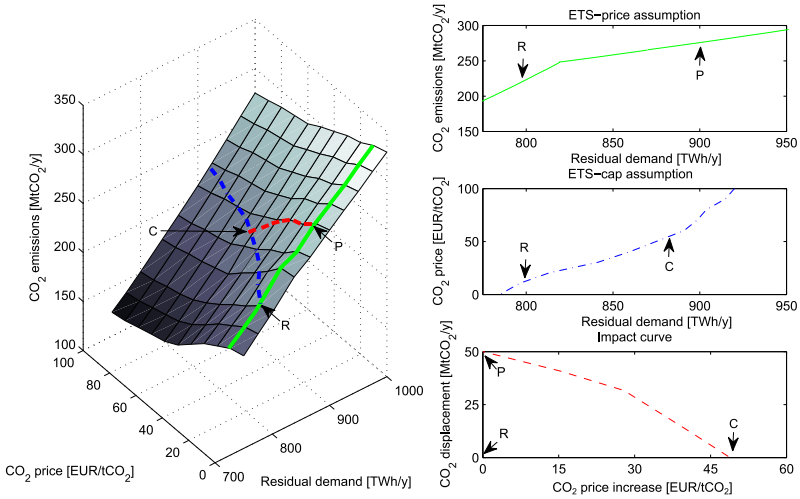

Figure C.4: The impact of removing renewable injections on the CO_2 price and the CO_2 emissions in the CWE electricity generation sector, with renewable investments triggered by a high CO_2 price. Point R refers to the reference point, P to the ETS-price assumption and C to the ETS-cap assumption.

Consider the initial situation with a CO_2 price of 10 EUR/tCO_2, 800 TWh/year residual demand and 222 MtCO_2/year of emissions (see point R on Fig. C.4). Starting from this initial situation, 100 TWh/year of support-driven renewable generation is removed from the system. The ETS-price assumption leads to the same equilibrium point as before (see point P on Fig. C.4, CO_2 price of 10 EUR/tCO_2, 900 TWh/year residual load and 270 MtCO_2/year CO_2 emissions). However, the ETS-cap assumption results in another equilibrium point compared to a case without impact of a CO_2 price on RES deployment (see point C on Fig. C.4, CO_2 price of 50 EUR/tCO_2, 880 TWh/year residual load and 222 MtCO_2/year CO_2 emissions). In the ETS-cap assumption, the CO_2 price increases to keep emissions the same when support-driven renewable generation is removed from the system. A higher CO_2 price can trigger investments in renewables that don't require financial support, lowering the residual demand. The impact curve trajectory now no longer lies on a single plane perpendicular to the residual demand axis, but rather on the intersection by a shape reflecting the CO_2 price-residual demand relationship which was derived exogenously.

This appendix considers the long-term implications of a CO_2 price on the residual load. However, a similar approach is applicable to study the long-

term implications of a CO_2 price on the conventional generation capacity. For instance, a CO_2 price can trigger investments in carbon capture and storage, drive mothballing of coal-intensive fossil-fuel-fired units, etc. The long-term implications on the conventional generation capacity can be investigated by imposing exogenously the relationship between a CO_2 price and a conventional capacity and recalculating the absolute emission plane for the changed generation portfolio.

References

50Hertz. Grid data. Available at `www.50hertz.com/en/grid-data`, 2015.

Abrell J. and Weigt H. The interaction of emissions trading and renewable energy promotion. Technical report, Dresden University of Technology, Working Paper no. WP-EGW-05, 2008.

Acharya N. and Mithulananthan N. Locating series facts devices for congestion management in deregulated electricity markets. *Electric Power Systems Research*, 77(3):352–360, 2007.

ACM, Bundesnetzagentur, CRE, CREG, E-control, and ILR. NRA public consultation on flow based market coupling: synthesis of respondent answers, 2014.

ACM, Bundesnetzagentur, CRE, CREG, E-control, and ILR. Position paper of CWE NRAs on flow-based market coupling, 2015.

Afkousi-Paqaleh M., Abbaspour-Tehrani Fard A., and Rashidinejad M. Distributed generation placement for congestion management considering economic and financial issues. *Electrical Engineering*, 92(6):193–201, 2010.

Aguado M., Bourgeois R., Bourmaud J., Van Casteren J., Ceratto M., Jakel M., Malfiet B., Mestdag C., Noury P., Pool M., et al. Flow-based market coupling in the Central Western European region: on the eve of implementation. *CIGRE, C5-204*, 2012.

Albadi M. and El-Saadany E. Overview of wind power intermittency impacts on power systems. *Electric Power Systems Research*, 80(6):627–632, 2010.

Amprion. Memoranding of understanding of the pentalateral energy forum on market coupling and security of supply in Central Western Europe. Available at `amprion.net/sites/default/files/pdf/Pentalateral%20MoU.pdf`, 2007.

Amprion. Grid data. Available at `www.amprion.net/en/grid-data`, 2015.

Amprion, APX-Endex, Belpex, Creos, Elia, EnBW, EpexSpot, RTE, and Tennet. CWE enhanced flow-based MC feasibility report, 2011.

Amprion, APX, Belpex, Creos, Elia, EpexSpot, RTE, Tennet, and Transnet BW. CWE enhanced flow-based MC intuitiveness report, 2013.

Amprion, APX, Belpex, Creos, Elia, EpexSpot, RTE, Tennet, and Transnet BW. Documentation of the CWE FB MC solution: as basis for the formal approval-request, 2014.

Ardakani A. and Bouffard F. Identification of umbrella constraints in DC-based security-constrained optimal power flow. *IEEE Transactions on Power Systems*, 28(4):3924–3934, 2013.

Arroyo J. and Conejo A. Optimal response of a thermal unit to an electricity spot market. *IEEE Transactions on Power Systems*, 15(3):1098–1104, 2000.

Baldick R. Variation of distribution factors with loading. *IEEE Transactions on Power Systems*, 18(4):1316–1323, 2003.

Baldick R., Dixit K., and Oberbye T. Empirical analysis of the variation of distribution factors with loading. In *IEEE Power Engineering Society General Meeting*, pages 221–229. IEEE, 2005.

Bart J. and Andreewsky M. Network modelling for congestion management: zonal representation versus nodal representation. In *15^{th} Power Systems Computation Conference*, pages 1–6, 2005.

Batlle C., Mastropietro P., and Gómez-Elvira R. Toward a fuller integration of the EU electricity market: physical or financial transmission rights? *The Electricity Journal*, 27(1):8–17, 2014.

Beato P. and Delgado J. Interactions between climate policies in the power sector. In *Green Energy and Efficiency*, pages 269–289. Springer, 2015.

Benato A., Stoppato A., and Bracco S. Combined cycle power plants: A comparison between two different dynamic models to evaluate transient behaviour and residual life. *Energy Conversion and Management*, 87:1269–1280, 2014.

Biskas P., Tsakoumis A., Bakirtzis A., Koronides A., and Kabouris J. Transmission loss allocation through zonal aggregation. *Electric Power Systems Research*, 81(10):1973–1985, 2011.

Bludszuweit H., Domínguez-Navarro J. A., and Llombart A. Statistical analysis of wind power forecast error. *IEEE Transactions on Power Systems*, 23(3): 983–991, 2008.

Böhringer C. and Rosendahl K. Green promotes the dirtiest: on the interaction between black and green quotas in energy markets. *Journal of Regulatory Economics*, 37(3):316–325, 2010.

Bompard E., Correia P., Gross G., and Amelin M. Congestion-management schemes: a comparative analysis under a unified framework. *IEEE Transactions on Power Systems*, 18(1):346–352, 2003.

Boucher J. and Smeers Y. Alternative models of restructured electricity systems-part 1: No market power. *Operations Research*, 49(6):821–838, 2001.

Boury J. Methods for the determination of flow-based capacity parameters: description, evaluation and improvements. KU Leuven Master Thesis, 2015.

Bruninx K. and Delarue E. A statistical description of the error on wind power forecasts for probabilistic reserve sizing. *IEEE Transactions on Sustainable Energy*, 5(3):995–1002, 2014.

Bruninx K., Delarue E., and D'haeseleer W. A practical approach on scenario generation and reduction algorithms for wind power forecast error scenarios. KU Leuven working paper, 2014.

Bruninx K., Van den Bergh K., Delarue E., and D'haeseleer W. Optimization and allocation of spinning reserves in a low-carbon framework. *IEEE Transactions on Power Systems*, 31(2):871–882, 2016.

Burke D. and O'Malley M. Maximizing firm wind connection to security constrained transmission networks. *IEEE Transactions on Power Systems*, 25(2):749–759, 2010.

CAISO. Spinning reserve and non-spinning reserve. Technical report, Available at `www.caiso.com/Documents/SpinningReserveandNonSpinningReserve.pdf`, 2006.

Capitanescu F. and Wehenkel L. Experiments with the interior-point method for solving large scale optimal power flow problems. *Electric Power Systems Research*, 95:276–283, 2013.

Capitanescu F., Martinez Ramos J., Panciatici P., Kirschen D., Marano Marcolini A., Platbrood L., and Wehenkel L. State-of-the-art, challenges, and future trends in security constrained optimal power flow. *Electric Power Systems Research*, 81(8):1731–1741, 2011.

Carrión M. and Arroyo J. A computationally efficient mixed-integer linear formulation for the thermal unit commitment problem. *IEEE Transactions on Power Systems*, 21(3):1371–1378, 2006.

CEER. Security of electricity supply report. Available at `www.ceer.eu/portal/page/portal/eer_home/eer_publications/ceer_papers/Electricity`, 2004.

Chang Y. and Wang N. Environmental regulations and emissions trading in China. *Energy Policy*, 38(7):3356–3364, 2010.

Chen Y., Sijm J., Hobbs B., and Lise W. Implications of CO_2 emissions trading for short-run electricity market outcomes in northwest Europe. *Journal of Regulatory Economics*, 34(3):251–281, 2008.

Chen Y., Gribik P., and Gardner J. Incorporating post zonal reserve deployment transmission constraints into energy and ancillary service co-optimization. *IEEE Transactions on Power Systems*, 29(2):537–549, 2014.

Cheng X. and Overbye T. PTDF-based power system equivalents. *IEEE Transactions on Power Systems*, 20(4):1868–1876, 2005.

Christie R. D., Wollenberg B. F., and Wangensteen I. Transmission management in the deregulated environment. *Proceedings of the IEEE*, 88(2):170–195, 2000.

Cochran J., Lew D., and Kumarb N. Flexible coal: evolution from baseload to peaking plant. National Renewable Energy Laboratory (NREL), 2013.

Cochran J., Miller M., Zinaman O., Milligan M., Arent D., Palmintier B., O'Malley M., Mueller S., Lannoye E., Tuohy A., Kujala M., Sommer H., Holttinen J., Kiviluoma J., and Soonee S. Flexibility in 21st century power systems. Technical report, National Renewable Energy Laboratory (NREL), 2014.

Criqui P., Mima S., and Viguier L. Marginal abatement costs of CO_2 emission reductions, geographical flexibility and concrete ceilings: an assessment using the poles model. *Energy policy*, 27(10):585–601, 1999.

Critz D., Busche S., and Connors S. Power systems balancing with high penetration renewables: The potential of demand response in hawaii. *Energy Conversion and Management*, 76:609–619, 2013.

Damcı-Kurt P., Küçükyavuz S., Rajan D., and Atamtürk A. A polyhedral study of ramping in unit commitment. BCOL resarch report 13.02, University of California,Berkeley, 2013.

De Jonghe C., Delarue E., Belmans R., and D'haeseleer W. Interactions between measures for the support of electricity from renewable energy sources and CO_2 mitigation. *Energy Policy*, 37(11):4743–4752, 2009.

De Jonghe C., Hobbs B., and Belmans R. Value of price responsive load for wind integration in unit commitment. *IEEE Transactions on Power Systems*, 29(2):675–685, 2014.

Deckmann S., Pizzolante A., Monticelli A., Stott B., and Alsac O. Numerical testing of power system load flow equivalents. *IEEE Transactions on Power Apparatus and Systems*, 6:2292–2300, 1980a.

Deckmann S., Pizzolante A., Monticelli A., Stott B., and Alsac O. Studies on power system load flow equivalencing. *IEEE Transactions on Power Apparatus and Systems*, 6:2301–2310, 1980b.

Declercq B., Delarue E., and D'haeseleer W. Impact of the economic recession on the European power sector's CO_2 emissions. *Energy Policy*, 39(3):1677–1686, 2011.

del Río González P. The interaction between emissions trading and renewable electricity support schemes. An overview of the literature. *Mitigation and adaptation strategies for global change*, 12(8):1363–1390, 2007.

Delarue E. *Modeling electricity generation systems - development and application of electricity generation optimization and simulation models with particular focus on CO_2 emissions*. PhD thesis, KU Leuven, 2009.

Delarue E., Luickx P., and D'haeseleer W. The actual effect of wind power on overall electricity generation costs and CO_2 emissions. *Energy Conversion and Management*, 50(6):1450–1456, 2009.

Delarue E., Ellerman D., and D'haeseleer W. Robust MACCs? the topography of abatement by fuel switching in the European power sector. *Energy*, 35(3): 1465–1475, 2010.

Deng L., Hobbs B., and Renson P. What is the cost of negative bidding by wind? A unit commitment analysis of cost and emissions. *IEEE Transactions on Power Systems*, 30(4):1805–1814, 2015.

Denny E. and O'Malley M. The impact of carbon prices on generation-cycling costs. *Energy Policy*, 37(4):1204–1212, 2009.

Doherty R. and O'Malley M. A new approach to quantify reserve demand in systems with significant installed wind capacity. *IEEE Transactions on Power Systems*, 20(2):587–595, 2005.

Doorman G. and van der Veen R. An analysis of design options for markets for cross-border balancing of electricity. *Utilities Policy*, 27:39–48, 2013.

Doquet M. Zonal reduction of large power systems: Assessment of an optimal grid model accounting for loop flows. *IEEE Transactions on Power Systems*, 30(1):503–512, 2015.

Doquet M., Gonzalez R., Lepy S., Momot E., and Verrier F. A new tool for adequacy reporting of electric systems: Antares. *CIGRE Session*, 2008.

Duthaler C., Emery M., Andersson G., and Kurzidem M. Analysis of the use of power transfer distribution factors (PTDF) in the UCTE transmission grid. In *16th Power Systems Computation Conference*, pages 1–6, 2008.

Dutta S. and Singh S. Optimal rescheduling of generators for congestion management based on particle swarm optimization. *IEEE Transactions on Power Systems*, 23(4):1560–1569, 2008.

EEA. Europe's onshore and offshore wind energy potential. Technical report, Technical report No 6/2009, 2009.

EEX. Market data. Available at `www.eex.com/en/market-data`, 2015a.

EEX. Transparency platform. Available at `www.eex-transparency.com`, 2015b.

Ehrenmann A. and Smeers Y. Inefficiencies in European congestion management proposals. *Utilities Policy*, 13(2):135–152, 2005.

Elgerd O. Electric energy systems theory: an introduction. McGraw-Hill, New York, 1971.

Elia. Map of the high voltage grid. Available at `www.elia.be/en/about-elia/publications/maps`, 2014.

Elia. Grid data. Available at `www.elia.be/en/grid-data/data-download`, 2015.

Ellerman D. and Decaux A. Analysis of post-kyoto CO_2 emissions trading using marginal abatement curves. MIT Joint Program on the Science and Policy of Global Change, Report No 40, 1998.

Ellerman D., Convery F., and De Perthuis C. *Pricing carbon: the European Union emissions trading scheme*. Cambridge University Press, 2010.

Ellerman D., Marcantonini C., and Zaklan A. The EU ETS: eight years and counting. Robert Schuman Centre for Advanced Studies Research Paper, 2014/04, 2014.

Ellerman D., Valero V., and Zaklan A. An analysis of allowance banking in the EU ETS. Robert Schuman Centre for Advanced Studies Research Paper, 2015/29, 2015.

Energiewende A. 12 insights on Germany's Energiewende. Available at www.agora-energiewende.de/fileadmin/downloads/publikationen/Impulse/12_Thesen/Agora_12_Insights_on_Germanys_Energiewende_web.pdf, 2013.

Energy Exemplar. Plexos Integrated Energy Model. Available at www.energyexemplar.com/software, 2015.

Enns M. and Quada J. Sparsity-enhanced network reduction for fault studies. *IEEE Transactions on Power Systems*, 6(2):613–621, 1991.

ENTSO-E. Pan-European market modelling database, 2012a.

ENTSO-E. Ten year network development plan 2012. Technical report, European Network of Transmission System Operators for Electricity, 2012b.

ENTSO-E. Study model 2020 - Continental Europe. Available at request via www.entsoe.eu, 2013.

ENTSO-E. Ten year network development plan 2014: maps and data. Available at www.entsoe.eu/major-projects/ten-year-network-development-plan/maps-and-data, 2014.

ENTSO-E. Data portal - statistical database. Available at www.entsoe.eu/data/data-portal, 2015a.

ENTSO-E. Network code overview. Available at www.entsoe.eu/major-projects/network-code-development, 2015b.

ENTSO-E. NTC values. Available at www.entsoe.eu/publications/market-reports/ntc-values/ntc-matrix, 2015c.

EpexSpot. Market Coupling – a major step towards market integration. Available at http://www.epexspot.com/en/market-coupling, 2015.

EPIA. Global market outlook for photovoltaics 2014-2018. Technical report, European photovoltaic industry association, 2015.

ETSO. Definitions of transfer capacities in libelarised electricity markets, 2001.

Eurelectric. Power statistics and trends 2011 – full report, 2011.

European Commission. Directive 2001/80/EC of the European Parliament and of the Council of 23 October 2001 on the limitation of emissions of certain pollutants into the air from large combustion plant, 2001.

European Commission. Directive 2009/28/EC of the European Parliament and of the Council of 23 April 2009 on the promotion of the use of energy from renewable sources, 2009.

European Commission. Prospective outlook on long term energy systems - POLES manual. Joint Research Centre, 2010.

European Commission. Proposal for a decision of the European parliament and of the council concerning the establishment and operation of a market stability reserve for the Union greenhouse gas emission trading scheme and amending Directive 2003/87/EC. 2014/0011 (COD), 2014a.

European Commission. A policy framework for climate and energy in the period from 2020 to 2030. Available at `eur-lex.europa.eu/legal-content/EN/TXT/PDF/?uri=CELEX:52014DC0015&from=EN`, 2014b.

European Commission. Energy Union factsheet. Available at `europa.eu/rapid/press-release_MEMO-15-4485_en.htm`, 2015.

European Commission. EU energy policy framework. Available at `ec.europa.eu/research/energy/eu/index_en.cfm?pg=policy`, 2016a.

European Commission. Structural reform of the European carbon market. Available at `ec.europa.eu/clima/policies/ets/reform`, 2016b.

European Commission. Large combustion plants directive. Available at `ec.europa.eu/environment/archives/industry/stationary/lcp/implementation.htm`, 2016c.

European Commission. 2020 climate and energy package. Available at `ec.europa.eu/clima/policies/strategies/2020`, 2016d.

Eurostat. Greenhouse gas emissions by sector. Available at `epp.eurostat.ec.europa.eu`, 2014.

EWEA. Wind in power – 2014 European statistics. Technical report, European wind energy association, 2015.

Farhat I. and El-Hawary M. Optimization methods applied for solving the short-term hydrothermal coordination problem. *Electric Power Systems Research*, 79(9):1308–1320, 2009.

Ferris M., Jain R., and Dirkse S. GDXMRW: Interfacing GAMS and Matlab, 2011.

Fischer C. and Morgenstern R. Carbon abatement costs: why the wide range of estimates? *The Energy Journal*, pages 73–86, 2006.

Fischer C. and Newell R. Environmental and technology policies for climate mitigation. *Journal of environmental economics and management*, 55(2): 142–162, 2008.

Fischer C. and Preonas L. Combining policies for renewable energy: Is the whole less than the sum of its parts? Resource for the Future Discussion Paper, No. 10-19, 2010.

Frangioni A., Gentile C., and Lacalandra F. Tighter approximated MILP formulations for unit commitment problems. *IEEE Transactions on Power Systems*, 24(1):105–113, 2009.

GAMS. The General Algebraic Modeling System. Available at `www.gams.com/download`, 2016.

Geth F., Brijs T., Kathan J., Driesen J., and Belmans R. An overview of large-scale stationary electricity storage plants in Europe: current status and new developments. *Renewable and Sustainable Energy Reviews*, 52:1212–1227, 2015.

Guler T., Gross G., and Liu M. Generalized line outage distribution factors. *IEEE Transactions on Power Systems*, 22(2):879–881, 2007.

Gurobi Optimization. Gurobi optimizer. Available at `www.gurobi.com`, 2016.

Heslin J. and Hobbs B. A multiobjective production costing model for analyzing emissions dispatching and fuel switching. *IEEE Transactions on Power Systems*, 4(3):836–842, 1989.

Hidalgo González I., Quoilin S., and Zucker A. Dispa-set 2.0: unit commitment and power dispatch model. European Commission, No. EUR 27015 EN, 2014.

Hindsberger M., Nybroe M., Ravn H., and Schmidt R. Co-existence of electricity, TEP, and TGC markets in the Baltic Sea Region. *Energy policy*, 31(1):85–96, 2003.

Hobbs B. and Rijkers F. Strategic generation with conjectured transmission price responses in a mixed transmission pricing system-Part I: formulation. *IEEE Transactions on Power Systems*, 19(2):707–717, 2004.

Hobbs B., Honious J., and Bluestein J. Estimating the flexibility of utility resource plans: an application to natural gas cofiring for SO_2 control. *IEEE Transactions on Power Systems*, 9(1):167–173, 1994.

Hobbs B., Rothkopf M., O'Neill R., and Chao H. The next generation of electric power unit commitment models. *Springer*, 36, 2001.

Hogan W. Transmission congestion: the nodal-zonal debate revisited. Harvard University, John F. Kennedy School of Government, Center for Business and Government, 1999.

Holttinen H. Impact of hourly wind power variations on the system operation in the nordic countries. *Wind Energy-Bognor Regis*, 8(2):197–218, 2005.

Holttinen H., Meibom P., Orths A., Lange B., O'Malley M., Tande J. O., Estanqueiro A., Gomez E., Söder L., Strbac G., Smith J., and van Hulle F. Impacts of large amounts of wind power on design and operation of power systems, results of IEA collaboration. *Wind Energy*, 14(2):179–192, 2011.

Housos E., Irisarri G., Porter R., and Sasson A. Steady state network equivalents for power system planning applications. *IEEE Transactions on Power Apparatus and Systems*, 6:2113–2120, 1980.

IBM. IBM ILOG Cplex Optimizer. Available at `www-01.ibm.com/software/commerce/optimization/cplex-optimizer`, 2016.

IEA. Projected costs of generating electricity. Technical report, OECD Publishing, Paris, 2010.

Jabr R., Martins N., Pal B., and Karaki S. Contingency constrained VAr planning using penalty successive conic programming. *IEEE Transactions on Power Systems*, 27(1):545–553, 2012.

Jacoby H. The uses and misuses of technology development as a component of climate policy. MIT Joint Program on the Science and Policy of Global Change, Report No 43, 1998.

Jensen S. and Skytte K. Simultaneous attainment of energy goals by means of green certificates and emission permits. *Energy policy*, 31(1):63–71, 2003.

Johnson J. and Novacheck J. Emissions reductions from expanding state-level renewable portfolio standards. *Environmental science & technology*, 49(9): 5318–5325, 2015.

Joint Allocation Office. CWE MC external parallel run. Available at `www.jao.eu`, 2015.

Kagiannas A., Askounis D., and Psarras J. Power generation planning: a survey from monopoly to competition. *International Journal of Electrical Power & Energy Systems*, 26(6):413–421, 2004.

Kang C., Chen Q., Lin W., Hong Y., Xia Q., Chen Z., Wu Y., and Xin J. Zonal marginal pricing approach based on sequential network partition and congestion contribution identification. *International Journal of Electrical Power and Energy Systems*, 51:321–328, 2013.

Kardakos E., Simoglou C., and Bakirtzis A. Optimal bidding strategy in transmission-constrained electricity markets. *Electric Power Systems Research*, 109:141–149, 2014.

Keay M. The EU target model for electricity markets: fit for purpose. Oxford Energy Comment, The Oxford Institute for Energy Studies, 2013.

Kesicki F. What are the key drivers of MAC curves? A partial-equilibrium modelling approach for the UK. *Energy Policy*, 58:142–151, 2013.

Kesicki F. and Ekins P. Marginal abatement cost curves: a call for caution. *Climate Policy*, 12(2):219–236, 2012.

Klepper G. and Peterson S. Marginal abatement cost curves in general equilibrium: The influence of world energy prices. *Resource and Energy Economics*, 28(1):1–23, 2006.

Klepper G., Peterson S., and Springer K. Dart97: A description of the multi-regional, multi-sectoral trade model for the analysis of climate policies. Technical report, Kiel Institute of World Economics, Working Paper 1149, 2003.

Klos M., Wawrzyniak K., Jakubek M., and Orynczak G. The scheme of a novel methodology for zonal division based on power transfer distribution factors. In *IEEE Industrial Electronics Society*, pages 1–7, 2014.

Koch N., Fuss S., Grosjean G., and Edenhofer O. Causes of the EU ETS price drop: recession, CDM, renewable policies or a bit of everything?—new evidence. *Energy Policy*, 73:676–685, 2014.

KU Leuven. TME database - Group Energy and Evironment. Internal database of electricity system data, 2015.

Kumar A., Srivastava S., and Singh S. A zonal congestion management approach using AC transmission congestion distribution factors. *Electric Power Systems Research*, 72(1):85–93, 2004.

Kumar A., Srivastava S., and Singh S. Congestion management in competitive power market: a bibliographical survey. *Electric Power Systems Research*, 76 (1):153–164, 2005.

Kumar N., Besuner P., Lefton S., Agan D., and Hilleman D. Power plant cycling costs. Technical report, Intertek APTECH, NREL, 2012.

Labandeira X., Linares P., and Rodríguez M. An integrated approach to simulate the impacts of carbon emissions trading schemes. *The Energy Journal*, 30(2): 217–239, 2009.

Lannoye E., Flynn D., and O'Malley M. Evaluation of power system flexibility. *IEEE Transactions on Power Systems*, 27(2):922–931, 2012.

Lefton S., Besuner P., and Grimsrud G. Understand what it really costs to cycle fossil-fired units. *Power*, 141(2):41–46, 1997.

Leuthold F., Weigt H., and Von Hirschhausen C. ELMOD: a model of the European electricity market, 2008a.

Leuthold F., Weigt H., and Von Hirschhausen C. Efficient pricing for European electricity networks: the theory of nodal pricing applied to feeding-in wind in Germany. *Utilities Policy*, 16(4):284–291, 2008b.

Leuthold F., Weigt H., and Von Hirschhausen C. A large-scale spatial optimization model of the European electricity market. *Networks and spatial economics*, 12(1):75–107, 2012.

Linares P., Santos F., and Ventosa M. Coordination of carbon reduction and renewable energy support policies. *Climate Policy*, 8(4):377–394, 2008.

Linnemann C., Echternacht D., Breuer C., and Moser A. Modeling optimal redispatch for the European transmission grid. In *PowerTech Trondheim*, pages 1–8. IEEE, 2011.

Linnenberg S. and Kather A. Evaluation of an integrated post-combustion CO_2 capture process for varying loads in a coal-fired power plant using monoethanolamine. In *4^{th} International Conference on Clean Coal Technologies*, pages 18–21, 2009.

Luickx P., Delarue E., and D'haeseleer W. Considerations on the backup of wind power: operational backup. *Applied Energy*, 85(9):787–799, 2008.

Lyon J., Wang F., Hedman K., and Zhang M. Market implications and pricing of dynamic reserve policies for systems with renewables. *IEEE Transactions on Power Systems*, 30(3):1593–1602, 2015.

Macfie P., Taylor G., Irving M., Hurlock P., and Wan H.-B. Proposed shunt rounding technique for large-scale security constrained loss minimization. *IEEE Transactions on Power Systems*, 25(3):1478–1485, 2010.

Marien A., Luickx P., Tirez A., and Woitrin D. Importance of design parameters on flow-based market coupling implementation. In *10^{th} International Conference on the European Energy Market*, pages 1–8, 2013.

MathWorks. Matlab. Available at `www.mathworks.com`, 2016.

Meeus L., Purchala K., and Belmans R. Development of the internal electricity market in europe. *The Electricity Journal*, 18(6):25–35, 2005.

Meibom P., Morthors P., Nielsen L. H., Weber C., Snader K., Swider D., and Ravn H. Power system models: a description of power markets and outline of market modelling in WILMAR. Technical report, Risoe National Laboratory, 2003.

Meibom P., Weber C., Barth R., and Brand H. Operational costs induced by fluctuating wind power production in Germany and Scandinavia. *Renewable Power Generation*, 3(1):75–83, 2009.

Metzler C., Hobbs B., and Pang J.-S. Nash-Cournot equilibria in power markets on a linearized DC network with arbitrage: formulations and properties. *Networks and Spatial Economics*, 3(2):123–150, 2003.

Mittelmann H. Mixed integer linear programming benchmark. Available at `plato.asu.edu/bench.html`, 2016.

Monticelli A., Pereira M., and Granville S. Security-constrained optimal power flow with post-contingency corrective rescheduling. *IEEE Transactions on Power Systems*, 2(1):175–180, 1987.

Morales-España G. *Unit commitment - computational performance, system representation and wind uncertainty management.* PhD thesis, Universidad Pontificia Comillas, 2014.

Morales-España G., Latorre J., and Ramos A. Tight and compact MILP formulation for the thermal unit commitment problem. *IEEE Transactions on Power Systems*, 28(4):4897–4908, 2013a.

Morales-España G., Latorre J., and Ramos A. Tight and compact MILP formulation of start-up and shut-down ramping in unit commitment. *IEEE Transactions on Power Systems*, 28(2):1288–1296, 2013b.

Morris J., Paltsev S., and Reilly J. Marginal abatement costs and marginal welfare costs for greenhouse gas emissions reductions: results from the EPPA model. *Environmental Modeling & Assessment*, 17(4):325–336, 2012.

Morthorst P. Interactions of a tradable green certificate market with a tradable permits market. *Energy policy*, 29(5):345–353, 2001.

Murray B. and Maniloff P. Why have greenhouse emissions in RGGI states declined? An econometric attribution to economic, energy market, and policy factors. *Energy Economics*, 51:581–589, 2015.

Newbery D., Strbac G., and Viehoff I. The benefits of integrating European electricity markets. *University of Cambridge-Energy Policy Working Group Working Paper*, 1504, 2015.

Oggioni G. and Smeers Y. Market failures of market coupling and counter-trading in Europe: an illustrative model based discussion. *Energy Economics*, 35:74–87, 2013.

Oh H. A new network reduction methodology for power system planning studies. *IEEE Transactions on Power Systems*, 25(2):677–684, 2010.

Oh H. Aggregation of buses for a network reduction. *IEEE Transactions on Power Systems*, 27(2):705–712, 2012.

Ostrowski J., Anjos M., and Vannelli A. Tight mixed integer linear programming formulations for the unit commitment problem. *IEEE Transactions on Power Systems*, 27(1):39–46, 2012.

Padhy N. Unit commitment: a bibliographical survey. *IEEE Transactions on Power Systems*, 19(2):1196–1205, 2004.

Paltsev S., Reilly J., Jacoby H., Eckaus R., McFarland J., Sarofim M., Asadoorian M., and Babiker M. The MIT emissions prediction and policy analysis EPPA model: version 4. MIT Joint Program on the Science and Policy of Global Change, Report No 125, 2005.

Papaemmanouil A. and Andersson G. On the reduction of large power system models for power market simulations. In *17th Power Systems Computation Conference*, pages 1–7, 2011.

Papavasiliou A. and Oren S. Large-scale integration of deferrable demand and renewable energy sources. *IEEE Transactions on Power Systems*, 29(1): 489–499, 2014.

Patteeuw D., Bruninx K., Arteconi A., Delarue E., D'haeseleer W., and Helsen L. Integrated modeling of active demand response with electric heating systems. *Applied Energy*, 151(1):306–3019, 2015.

Perez-Arriaga I. and Batlle C. Impacts of intermittent renewables on electricity generation system operation. *Economics of Energy & Environmental Policy*, 1(2), 2012.

Platts. World electric power plants database – Europe. `www.platts.com/products/world-electric-power-plants-database`, 2014.

PowerNext. Everything you need to know about TLC. Available at `static.epexspot.com/document/3830`, 2006.

Pöyry. BID3. Available at `www.poyry.com/BID3`, 2015.

Price Coupling of Regions. Euphemia public description: PCR market coupling algorithm. Available at `www.apxgroup.com/wp-content/uploads/Euphemia-Public-Documentation.pdf`, 2013.

Purchala K. *Modeling and analysis of techno-economic interactions in meshed high voltage grids exhibiting congestion*. PhD thesis, KU Leuven, 2005.

Purchala K., Haesen E., Meeus L., and Belmans R. Zonal network model of European interconnected electricity network. In *CIGRE/IEEE PES International Symposium*, pages 362–369, 2005a.

Purchala K., Meeus L., Van Dommelen D., and Belmans R. Usefulness of DC power flow for active power flow analysis. In *Power Engineering Society General Meeting*, pages 454–459. IEEE, 2005b.

Rajan D. and Takriti S. Minimum up/down polytopes of the unit commitment problem with start-up costs. *IBM Research Report*, 2005.

Richstein J., Chappin É., and de Vries L. The market (in-)stability reserve for EU carbon emission trading: Why it might fail and how to improve it. *Utilities Policy*, 35:1–18, 2015.

Rickels W., Görlich D., and Peterson S. Explaining European emission allowance price dynamics: evidence from phase ii. *German Economic Review*, 16(2): 181–202, 2015.

Rocha P., Das T., Nanduri V., and Botterud A. Impact of CO_2 cap-and-trade programs on restructured power markets with generation capacity investments. *International Journal of Electrical Power & Energy Systems*, 71:195–208, 2015.

Rodilla P., Cerisola S., and Batlle C. Modeling the major overhaul cost of gas-fired plants in the unit commitment problem. *IEEE Transactions on Power Systems*, 29(3):1001–1011, 2014.

Rolf B., Henrik N., and Judy W. *Combined-Cycle Gas and Steam Turbine Power Plants*. Pennwell Corp, 1999.

Rootzén J. and Johnsson F. Exploring the limits for CO_2 emission abatement in the EU power and industry sectors-awaiting a breakthrough. *Energy Policy*, 59:443–458, 2013.

RTE. Sustainable development – data. Available at `www.rte-france.com`, 2015.

Saravanan B., Das S., Sikri S., and Kothari D. A solution to the unit commitment problem: a review. *Frontiers in Energy*, 7(2):223–236, 2013.

Schröder A., Kunz F., Meiss J., Mendelevitch R., and Von Hirschhausen C. Current and prospective costs of electricity generation until 2050. Technical report, DIW Berlin - Data Documentation 68, 2013.

Sen S. and Kothari D. Optimal thermal generating unit commitment: a review. *International Journal of Electrical Power and Energy Systems*, 20(7):443–451, 1998.

Shayesteh E., Hobbs B., Soder L., and Amelin M. ATC-based system reduction for planning power systems with correlated wind and loads. *IEEE Transactions on Power Systems*, 30(1):429–438, 2015.

Sheble G. and Fahd G. Unit commitment literature synopsis. *IEEE Transactions on Power Systems*, 9(1):128–135, 1994.

Singh H., Hao S., and Papalexopoulos A. Transmission congestion management in competitive electricity markets. *IEEE Transactions on Power Systems*, 13 (2):672–680, 1998.

Stoft S. Congestion pricing with fewer prices than zones. *The Electricity Journal*, 11(4):23–31, 1998.

Stott B., Jardim J., and Alsac O. DC power flow revisited. *IEEE Transactions on Power Systems*, 24(3):1290–1300, 2009.

Strbac G., Shakoor A., Black M., Pudjianto D., and Bopp T. Impact of wind generation on the operation and development of the UK electricity systems. *Electric Power Systems Research*, 77(9):1214–1227, 2007.

Tahanan M., van Ackooij W., Frangioni A., and Lacalandra F. Large-scale unit commitment under uncertainty. *4OR*, 13(2):115–171, 2015.

Tennet. Network figures. Available at `www.tennet.org/english/operational_management`, 2015a.

Tennet. Flow-based methodology for CWE market coupling successfully launched. Available at `www.tennet.eu/nl/news/article/flow-based-methodology-for-cwe-market-coupling-succesfully-launched.html`, 2015b.

Tinney W. and Bright J. Adaptive reductions for power flow equivalents. *IEEE Transactions on Power Systems*, 2(2):351–359, 1987.

Transnet BW. Key figures. Available at `www.transnetbw.de/en/key-figures`, 2015.

Troy N., Denny E., and O'Malley M. Base-load cycling on a system with significant wind penetration. *IEEE Transactions on Power Systems*, 25(2): 1088–1097, 2010.

Troy N., Flynn D., Milligan M., and O'Malley M. Unit commitment with dynamic cycling costs. *IEEE Transactions on Power Systems*, 27(4):2196–2205, 2012.

Tsao C., Campbell J., and Chen Y. When renewable portfolio standards meet cap-and-trade regulations in the electricity sector: Market interactions, profits implications, and policy redundancy. *Energy Policy*, 39(7):3966–3974, 2011.

Tuladhar S., Mankowski S., and Bernstein P. Interaction effects of market-based and command-and-control policies. *Energy Journal*, 35:61–88, 2014.

Tuohy A., Meibom P., Denny E., and O'Malley M. Unit commitment for systems with significant wind penetration. *IEEE Transactions on Power Systems*, 24(2):592–601, 2009.

Ummels B., Gibescu M., Pelgrum E., Kling W., and Brand A. Impacts of wind power on thermal generation unit commitment and dispatch. *Energy Conversion, IEEE Transactions on*, 22(1):44–51, 2007.

Umweltbundesamt. Datenbank Kraftwerke in Deutschland. Available at `www.umweltbundesamt.de/dokument/datenbank-kraftwerke-in-deutschland`, 2015.

Van den Bergh K. and Delarue E. Cycling of conventional power plants: technical limits and actual costs. *Energy Conversion and Management*, 97:70–77, 2015.

Van den Bergh K., Delarue E., and D'haeseleer W. Impact of renewables deployment on the CO_2 price and the CO_2 emissions in the European electricity sector. *Energy Policy*, 63:1021–1031, 2013.

van der Weijde A. and Hobbs B. Locational-based coupling of electricity markets: benefits from coordinating unit commitment and balancing markets. *Journal of Regulatory Economics*, 39(3):223–251, 2011.

Van Hertem D. *The use of power flow controlling devices in the liberalized market*. PhD thesis, KU Leuven, 2009.

Van Hertem D., Verboomen J., Purchala K., Belmans R., and Kling W. Usefulness of dc power flow for active power flow analysis with flow controlling devices. In *8^{th} IEE International Conference on AC and DC Power Transmission*, pages 58–62. IET, 2006.

Vandezande L., Saguan M., Meeus L., Glachant J.-M., and Belmans R. Assessment of the implementation of cross-border balancing trade between belgium and the netherlands. In *6th International Conference on the European Energy Market*, pages 1–6. IEEE, 2009.

Vandezande L., Meeus L., Belmans R., Saguan M., and Glachant J.-M. Well-functioning balancing markets: a prerequisite for wind power integration. *Energy Policy*, 38(7):3146–3154, 2010.

Ventosa M., Baillo A., Ramos A., and Rivier M. Electricity market modeling trends. *Energy policy*, 33(7):897–913, 2005.

Ventytx Energy. Promod IV. Available at `www.ventyx.com`, 2015.

Verboomen J. *Optimisation of transmission systems by use of phase shifting transformers*. PhD thesis, TU Delft, 2008.

Vogt-Schilb A. and Hallegatte S. Marginal abatement cost curves and the optimal timing of mitigation measures. *Energy Policy*, 66:645–653, 2014.

Vukasovic M. and Skuletic S. Implementation of different methods for PTDF matrix calculation in flow-based coordinated auction. In *International Conference on Power Engineering, Energy and Electrical Drives*, pages 791–795, 2007.

Wang F. and Hedman K. Dynamic reserve zones for day-ahead unit commitment with renewable resources. *IEEE Transactions on Power Systems*, 30(2):612–620, 2015.

Waniek D., Hager U., Rehtanz C., and Handschin E. Influences of wind energy on the operation of transmission systems. In *Power and Energy Society General Meeting*, pages 1–8, 2008.

Waniek D., Rehtanz C., and Handschin E. Flow-based evaluation of congestions in the electric power transmission system. In *7th International Conference on the European Energy Market*, pages 1–6, 2010.

Ward J. Equivalent circuits for power-flow studies. *Electrical Engineering*, 68 (9):794–794, 1949.

Weber A., Graeber D., and Semmig A. Market coupling and the CWE project. *Zeitschrift für Energiewirtschaft*, 34(4):303–309, 2010.

Weigt H., Ellerman D., and Delarue E. CO_2 abatement from renewables in the German electricity sector: does a CO_2 price help? *Energy economics*, 40: 149–158, 2013.

Wolsey L. *Integer programming*, volume 42. Wiley New York, 1998.

Yamin H. Review on methods of generation scheduling in electric power systems. *Electric Power Systems Research*, 69(2):227–248, 2004.

Yamina H. and Shahidehpour S. Congestion management coordination in the deregulated power market. *Electric Power Systems Research*, 65(2):119–127, 2003.

Yang L., Jian J., Wang Y., and Dong Z. Projected mixed integer programming formulations for unit commitment problem. *International Journal of Electrical Power and Energy Systems*, 68:195–202, 2015.

Yousefi A., Nguyen T., Zareipour H., and Malik O. Congestion management using demand response and facts devices. *International Journal of Electrical Power & Energy Systems*, 37(1):78–85, 2012.

Zheng H., Jian J., Yang L., and Quan R. A deterministic method for the unit commitment problem in power systems. *Computers and Operations Research*, 2015.

Short curriculum

Kenneth Van den Bergh

Born in Lier (Belgium) on June 20, 1989.

Education:

since 2012	PhD student in Mechanical Engineering, KU Leuven. Visit to the Johns Hopkins University, spring 2015.
2013-2015	Master of Science in Management, KU Leuven. *Magna cum laude.*
2010-2012	Master of Science in Engineering: Energy, KU Leuven. *Magna cum laude.*
2007-2010	Bachelor of Science in Engineering: Mechanical Engineering, KU Leuven. *Magna cum laude.*
2001-2007	Sint-Gummarcusollege, Lier.

Publications by the author

Publications are available at `www.mech.kuleuven.be/tme/research/energy_environment`.

International peer reviewed journals

1. K. Van den Bergh, E. Delarue, and W. D'haeseleer. Impact of renewables deployment on the CO_2 price and the CO_2 emissions in the European electricity sector. Energy Policy, 63:1021-1031, 2013.

2. K. Van den Bergh and E. Delarue. Quantifying CO_2 abatement costs in the power sector. Energy Policy, 80:88-97, 2015.

3. K. Van den Bergh and E. Delarue. Cycling of conventional power plants: technical limits and actual costs. Energy Conversion Management, 97:70-77, 2015.

4. K. Bruninx, K. Van den Bergh, E. Delarue, and W. D'haeseleer. Optimization and allocation of spinning reserves in a low carbon framework. IEEE Transactions on Power Systems, 31(2):872-882, 2016.

5. K. Van den Bergh, D. Couckuyt, E. Delarue, and W. D'haeseleer. Redispatching in an interconnected electricity system with high renewables penetration. Electric Power Systems Research, 127:64-72, 2015.

6. E. Delarue and K. Van den Bergh. Carbon mitigation in the electric power sector under cap-and-trade and renewables policies. Energy Policy, 92:34-44, 2016.

7. K. Van den Bergh, J. Boury, and E. Delarue. The flow-based market coupling in Central Western Europe: concepts and definitions. The Electricity Journal, 29:24-29, 2016.

8. K. Van den Bergh and E. Delarue. An improved method to calculate injection shift keys. Electric Power Systems Research, 134:197-204, 2016.

9. K. Van den Bergh, R. Broder Hytowitz, K. Bruninx, E. Delarue, W. D'haeseleer, and B. Hobbs. Benefits of coordinating sizing, allocation and activation of reserves among market zones. Submitted for publication, 2016.

International conferences

1. K. Van den Bergh, E. Delarue, and W. D'haeseleer. The impact of renewable injections on cycling of conventional power plants. 10^{th} International Conference on the European Energy Market (EEM), Stockholm, Sweden, 2013.

2. K. Van den Bergh, E. Delarue, and W. D'haeseleer. Impact of renewables deployment on the CO_2 price and the CO_2 emissions in the European electricity sector. Annual Climate Policy Conference, European University Institute, Florence, Italy, 2013.

3. K. Van den Bergh and E. Delarue. Facilitating the integration of renewables with flexible transmission systems. Young Energy Economists and Engineers Seminar (YEEES), Dresden, Germany, 2014.

4. K. Van den Bergh and E. Delarue. Facilitating variable generation of renewables by conventional power plant cycling: costs and benefits. 9^{th} Conference on Energy Economics and Technology (ENERDAY), Dresden, Germany, 2014.

5. K. Van den Bergh and E. Delarue. Quantifying CO_2 abatement costs in the power sector. 37^{th} IAEE International Conference, New York, USA, 2014.

6. K. Van den Bergh, E. Delarue, and W. D'haeseleer. Improved zonal network models in generation scheduling. 18^{th} Power Systems Computation Conference (PSCC), Wroclaw, Poland, 2014.

7. K. Van den Bergh, D. Couckuyt, E. Delarue, and W. D'haeseleer. Redispatching in an interconnected electricity system with high penetration of offshore wind. Windfarms, Leuven, Belgium, 2015.

8. K. Van den Bergh, J. Boury, and E. Delarue. The flow-based market coupling in Central Western Europe: concepts and definitions. BAEE Research Workshop on Energy Economics, Louvain-la-Neuve, Belgium, 2015.

9. K. Van den Bergh, R. Broder Hytowitz, E. Delarue, W. D'haeseleer, and B. Hobbs. The benefits of sharing reserves between countries: a case study of the European electricity system. INFORMS Annual Meeting, Philadelphia, USA, 2015.

10. K. Van den Bergh, C. Wijsen, E. Delarue, and W. D'haeseleer. The impact of bidding zone configurations on electricity market outcomes. IEEE International Energy Conference (ENERGYCON), Leuven, Belgium, 2016.

11. K. Van den Bergh, T. Legon, E. Delarue, and W. D'haeseleer. Long-term cycling costs in short-term unit commitment models. 13^{th} International Conference on the European Energy Market (EEM), Porto, Portugal, 2016.

Others

1. K. Van den Bergh, E. Delarue, and W. D'haeseleer. DC power flow in unit commitment models. KU Leuven Working Paper, 2014.

2. K. Van den Bergh, K. Bruninx, E. Delarue, and W. D'haeseleer. LUSYM: a unit commitment model formulated as a mixed-integer linear program. KU Leuven Working Paper, 2015.

FACULTY OF ENGINEERING SCIENCE
DEPARTMENT OF MECHANICAL ENGINEERING
Celestijnenlaan 300 box 2421
B-3001 Leuven
www.mech.kuleuven.be/en/tme